ROLE OF INORGANIC COFACTORS AND SPECIES DIFFERENCES IN PHOTOSYNTHETIC WATER OXIDATION

VORGELEGT VON DIPLOM-BIOLOGE

DMITRIY SHEVELA

AUS KALUGA, RUSSLAND

VON DER FAKULTÄT II

- MATHEMATIK UND NATURWISSENSCHAFTEN -

DER TECHNISCHEN UNIVERSITÄT BERLIN ZUR ERLANGUNG

DES AKADEMISCHEN GRADES DOKTOR DER NATURWISSENSCHAFTEN

- DR. RER. NAT. -

GENEHMIGTE DISSERTATION

PROMOTIONSAUSSCHUSS:

VORSITZENDER:	PROF. DR. T. FRIEDRICH
BERICHTER:	PROF. DR. J. MESSINGER
BERICHTER:	PROF. DR. P. HILDEBRANDT
BERICHTER:	PROF. DR. W. LUBITZ
BERICHTER:	PROF. DR. V.V. KLIMOV

TAG DER WISSENSCHAFTLICHEN AUSSPRACHE: 11. MÄRZ 2008

BERLIN 2008

D 83

Role of Inorganic Cofactors and Species Differences in Photosynthetic Water Oxidation

Zusammenfassung

Shevela, Dmitriy

FUNKTION DER ANORGANISCHEN KOFAKTOREN UND ARTBEDINGTE UNTERSCHIEDE IN DER PHOTOSYNTHETISCHEN WASSEROXIDATION

Die photosynthetische Wasseroxidation ist ein fundamentaler biologischer Prozess, der im Wasserspaltungskomplex (WOC, englisch: water oxidizing complex) des Pigment-Protein-Komplexes Photosystem II (PSII) stattfindet. Der WOC setzt sich aus einem anorganischen, mit Sauerstoffbrücken verknüpften tetra-Mangan-Calcium-Komplex (Mn_4O_xCa-Komplex; $x \geq 5$) und einer hochspezifischen Proteinumgebung zusammen. Es wird erwartet, dass das Verständnis dieser Reaktion wichtige Hinweise für die Entwicklung effizienter artifizieller Systeme liefern wird, die Sonnenenergie zur Spaltung von Wasser zu O_2 und H_2 nutzen. Um die Grundlagen der photosynthetischen Wasserspaltung aufklären zu können, ist es nötig, sowohl die Energetik als auch die Struktur und Funktion aller beteiligter Komponenten in den unterschiedlichen Oxidationszuständen S_i (i = 0,...,4) des WOC zu kennen.

Der Schwerpunkt dieser Arbeit liegt in die Untersuchung der Funktionen und der Bindungsplätze der Anionen Hydrogencarbonat (HCO_3^-) und Chlorid (Cl^-) im WOC. Durch Messung von blitz-induzierten Sauerstoffoszillationsmustern (englisch kurz FIOPs), die unter streng kontrollierten Bedingungen ausgeführt wurden, wird gezeigt, dass schwach gebundenes HCO_3^- die Wasserspaltungsreaktionen im PSII nicht direkt beeinflusst. Mit massenspektrometrische Messungen (Membran-Einlass-Massenspektrometrie, MIMS) wird zudem eindeutig belegt, das CO_3^{2-}/HCO_3^- kein integraler Bestandteil des WOC ist. Somit sind die bekannten und in dieser Arbeit weitgehend bestätigten Effekte der Analoga Formiat und Acetat auf die Verdrändung von HCO_3^- von seiner Bindungsstelle am nicht-Häm-Eisen der Akzeptorseite vom PSII, sowie auf mögliche direkte Effekte dieser Anionen auf den WOC zurückzuführen.

Die mögliche direkte Bindung von Cl^- an den Mn_4O_xCa-Komplex wurde mit Hilfe von Elektronenspinresonanz (cw und gepulste EPR) und durch Röntgenabsorptions-Spektroskopie (XANES/EXAFS) untersucht. Hierzu wurde Cl^- durch Dialyse entfernt und durch den kompetitiven Inhibitor Azid (N_3^-; für Impuls-EPR, terminal ^{15}N-markiert) ersetzt. Die erzielten Ergebnisse liefern keinerlei Hinweise auf eine direkte Bindung von N_3^-, und demzufolge von Cl^-, an ein Mn-Ion des Mn_4O_xCa-Komplexes.

Ferner wird detailliert der Frage nachgegangen, in wieweit die Funktion des WOC in dem erst kürzlich entdeckten, ganz überwiegend Chlorophyll-*d*-haltigen Organismus *Acharyochloris marina* (*A. marina*) durch vermutete Unterschiede in der Energetik der primären Ladungstrennung im PSII beeinflusst wird. Mit FIOP-Messungen wird gezeigt, dass die Effizienz der Wasserspaltung und die Stabilität der S_i Zustände in *A. marina* gegenüber Chlorophyll-*a*-haltigen Spinat-Proben (*Spinacia oleracea*) praktisch unverändert sind. Eine Ausnahme davon bildet nur das Redoxpotential von Tyrosin D, E_m ($Y_D/Y_D^\bullet$).

Abstract

Shevela, Dmitriy

ROLE OF INORGANIC COFACTORS AND SPECIES DIFFERENCES IN PHOTOSYNTHETIC WATER OXIDATION

Photosynthetic water oxidation is an unique fundamental biological process that occurs in the water-oxidizing complex (WOC) of the multi-component pigment-protein complex called photosystem II (PSII). The WOC comprises an inorganic μ-oxo bridged tetra-manganese calcium cluster (Mn_4O_xCa, with $x \geq 5$) and a highly specific protein matrix. Understanding this reaction can be expected to provide essential clues for the construction of efficient artificial systems that utilize the energy of sun light to split water to O_2 and H_2. To elucidate the basics of photosynthetic water oxidation chemistry one needs to know its energetics as well as the structure and function of all the cofactors participating in the different oxidation states, S_i states (i = 0,...,4), of the WOC.

The main focus of this work is the exploration of the function and binding sites of the anions hydrogencarbonate (HCO_3^-) and chloride (Cl^-) within the WOC. Performing flash-induced oxygen evolution patterns (FIOPs) measurements under strictly controlled conditions no evidence was found for a weakly bound HCO_3^- in the water-splitting reaction of PSII. Moreover, employing membrane-inlet mass spectrometry (MIMS) it is shown that CO_3^{2-}/HCO_3^- is not a tightly bound constituent of the WOC. Therefore the previously reported and in this work largely confirmed effects of HCO_3^- analogs, such as formate and acetate, are caused by the displacement of HCO_3^- from its binding site at non-heme iron on the acceptor side of PSII and not from the WOC as suggested earlier. However, some direct effects of formate and/or acetate on the WOC cannot be fully excluded.

The possible direct Cl^- binding to the Mn_4O_xCa cluster was studied by employing both electron paramagnetic resonance (cw and pulse EPR) and X-ray absorption spectroscopy (XANES/EXAFS). In the present study Cl^- was removed from intact PSII *via* a prolonged dialysis and replaced by the competitive inhibitor azide (N_3^-; for pulse EPR, with terminally ^{15}N-labelled). The results obtained do not provide any evidences for direct binding of N_3^- and, thereby of Cl^-, to the Mn ions in the Mn_4O_xCa cluster.

Furthermore, the question was addressed whether or not the properties of the WOC in a recently discovered chlorophyll *d*-dominating cyanobacterium *Acaryochloris marina* (*A. marina*) are modified by the suspected differences in the energetics of the primary charge separation in PSII. Based on FIOPs measurements no differences are found between *A. marina* and chlorophyll *a*-containing samples from spinach (*Spinacia oleracea*) with regard to the efficiency of water splitting and the stability of the S_i states. The only exception is the redox potential of tyrosine D, E_m ($Y_D/Y_D^\bullet$).

Veröffentlichungen

TEILE DIESER ARBEIT WURDEN BEREITS PUBLIZIERT:

Peer-Reviwed Articles

(i) **D. Shevela**, A. Khorobrykh & V. Klimov (2006) Effect of bicarbonate on the water-oxidizing complex of photosystem II in the super-reduced S-states, *Biochim. Biophys. Acta* **1757**, 253-261.

(ii) **D. Shevela**, B. Nöring, H.-J. Eckert, J. Messinger & G. Renger (2006) Characterization of the water oxidizing complex of photosystem II of the Chl *d* containing cyanobacterium *Acaryochloris marina via* its reactivity towards endogenous electron donors and acceptors, *Phys. Chem. Chem. Phys.* **8**, 3460-3466.

(iii) **D. Shevela**, V. Klimov & J. Messinger (2007) Interactions of photosystem II with bicarbonate formate and acetate, *Photosynth. Res.* **94**, 247-264.

(iv) **D. Shevela**, J.-H. Su, V. Klimov & J. Messinger (2008) Hydrogencarbonate is not a tightly bound constituent of the water oxidizing complex in photosystem II, *Biochim. Biophys. Acta*, **1777**, 532-539.

(v) **D. Shevela**, V. Klimov & J. Messinger (2008) Formate-induce release of carbon dioxide/hydrogencarbonate from photosystem II. *In* J.F. Allen, E. Gantt, J.H. Golbeck, B. Osmond (eds.), *Photosynthesis. Energy from the Sun: 14th International Congress on Photosynthesis*, 497-501. *Springer*.

Conference Contributions

1. **D. Shevela**, A. Khorobrykh, S. Zharmukhamedov & V. Klimov, Bicarbonate action on photosystem II with the changing S-states of the water oxidizing complex. In the *8th International Young Scientist Conference on "Biology is the Science of XXI Century"*. Pushchino, Russia, 17-21st May 2004 (**Poster**)

2. **D. Shevela**, A. Khorobrykh, G. Ananyev & V. Klimov, An improved flash-induced technique for measurements of oxygen evolution in the preparations of photosystem II. In the *8th Latinamerican Meeting on Photochemistry and Photobiology*. La Plata, Argentina, 8-12th November 2004 (**Abstract**)

3. **D. Shevela**, A. Khorobrykh & V. Klimov, Enhancement of bicarbonate effect on the water oxidizing complex of photosystem II in the 'negative' S-states at low pH values. In the *17th Young Scientists School-Conference on "Perspective Directions of Physical-Chemical Biology and Biotechnology"*. Moscow, Russia, 7-10th February 2005 (**Poster**).

4. **D. Shevela**, A. Khorobrykh & V. Klimov, Bicarbonate effect on the distributions of the S_{-n} states of the water oxidizing complex of photosystem II. In the *9th International Young Scientist Conference on "Biology is the Science of XXI Century"*. Pushchino, Russia, 18-22nd April 2005 (**Poster**).

5. **D. Shevela**, A. Khorobrykh, D. Yanikin & V. Klimov, Enhancement of bicarbonate effect upon the transition of the water oxidizing complex of photosystem II to the 'negative' S-states. In the *XVIII Pushchino Readings on Photosynthesis & Russian Conference on "Energy Light Conversion in Photosynthesis"*. Pushchino, Russia, 19-23rd June 2005 (**Poster & Oral Presentation**).

6. **D. Shevela**, B. Nöring, H.-J. Eckert, G. Renger & J. Messinger, Flash-induced oxygen evolution measurements of *Acaryochloris marina* cells. In the *International Meeting in Honor of Prof. Barber "Photosynthesis in the Post-Genomic Era: Structure and Function of Photosystems"*. Pushchino, Russia, 20-26th August 2006 (**Poster**).

7. **D. Shevela**, V. Klimov & J. Messinger, Bicarbonate effects on the donor side of photosystem II gathered from flash-induced oxygen evolution measurements. In the *15th Photosynthesis Workshop 'Nord-West'*. Aachen, Germany, 7-8th September (**Oral presentation**).

8. **D. Shevela**, V. Klimov & J. Messinger, Interactions of bicarbonate, acetate and formate with photosystem II. In the *16th Photosynthesis Workshop 'Nord-West'*. Mülheim an der Ruhr, Germany, 3-4th May 2007 (**Poster**).

9. **D. Shevela**, V. Klimov & J. Messinger, Hydrogencarbonate binding to photosystem II. In the *14th International Congress of Photosynthesis*. Glasgow, Scotland, UK, 23-27th July 2007 (**Poster**)

Acknowledgements

Самую большую благодарность я хочу выразить моей любимой Маме, моим дорогим бабушке *Тамаре* и дедушке *Ивану*, дяде *Игорю* и брату *Никите*, за их любовь, понимание, терпение и неоценимую поддержку все эти годы.

I WISH TO EXPRESS MY SINCERE GRATITUDE TO:

- Prof. JOHANNES MESSINGER, mein Doktorvater, for giving me the possibility to do my research in his group, for outstanding guidance and explanations, for stimulation and support of my conference travels, for his patience during proofreading of this work.

- Prof. VYACHESLAV KLIMOV, my co-supervisor, for his initial supervision and for introducing me to the fascinating world of photosynthesis research, for interesting 'bicarbonate' project I was involved in, for his advices and understanding.

- Prof. WOLFGANG LUBITZ, for the opportunity to work at the *Max Planck Institute for Bioinorganic Chemistry* and continuous support, for creating a stimulating scientific atmosphere at the department.

- KATRIN BECKMANN, for the pleasure of working together during the last two years, for invaluable help and moral support, for teaching me about MIMS and other techniques, for true advices and discussions, for her never-ending enthusiasm and optimism, and, finally, for being such a great friend at work and private. Danke schön für Alles!

- Dr. JI-HU SU, for EPR studies and data interpretation, for sharing his knowledge of the EPR technique, for his highly valuable help and fruitful suggestions during the preparation of this thesis, and also for his 'morning' fruits.

- ETHEL HÜTTEL, unsere 'Labor Mutter', for her kindness, constant help and gifts, for the enjoyable time-work, and for making the every working day so much fun. Danke, liebe Ethel!

- BIRGIT NÖRING, for the excellent technical assistance and collaboration.

- MICHAEL REUS, for always being helpful and for all kinds of assistance provided.

- Prof. GERNOT RENGER and Dr. HANN-JÖRG ECKERT, for fruitful research collaboration on the '*Acaryochloris marina*' project.

- Dr. YULIA PUSHKAR, for EXAFS/XANES study and data analysis of our sample preparations, for her cooperation on the 'Azide/Chloride' project.

- Dr. ANDREW KHOROBRYKH, Dr. OLGA ZASTRIZHNAYA, KONSTANTIN TIKHONOV, and Dr. SERGEY ZHARMUKHAMEDOV, my former colleagues at the *Institute of Basic Biological Problems of Russian Academy of Sciences*, for introducing me to the basic techniques in the field of photosynthesis in the beginning of my scientific carrier.

- Dr. GENNADY ANANYEV, for valuable advices and support on the initial stages of my work.
- Dr. LIDIA KUZNETCOVA, Dr. NATALIA VORONKINA and Prof. VALERIY BEDENKO, for encouraging me to be a scientist, for their warm attitude during all these years.
- HUGUETTE SAINT-MARTIN, my 'second French mother', for her understanding and support during all these years. Merci beaucoup!
- Dr. ROMAN PISHCHALNIKOV, Dr. SAMIR ZEIN, Dr. TARAS PETRENKO, for their support and friendship.
- My old friends from Kaluga: ALEKSEY SARLEYSKIY, SERGEY KOROIDOV, ANTON SAMARIN, and others, for funny unforgettable moments and for creating a nice environment when ever I visit them.

Mülheim an der Ruhr, February 2008

Dmitriy Shevela

We must take things as we find them,
and not as we would wish them to be.
NAPOLEON

To my Mother
To my Grandparents
To Igor and Nikita

Contents

Abbreviations

A. marina	*Acaryochloris marina*
ATP	Adenosine triphosphate
CA	Carbonic anhydrase
Chl, [*Chl*]	Chlorophyll, concentration of Chl
C_i	Inorganic carbon (CO_2, HCO_3^-, CO_3^{2-})
Cyt	Cytochrome
CP43, CP47	Chlorophyll-binding proteins of PSII
CW	Continuous wave
DCBQ	2,6-dichlor-*p*-benzoquinone
DMSO	Dimethylsulfoxide
EDTA	Ethylendiaminetetraacetic acid
ENDOR	Electron nuclear double resonance
EPR	Electron paramagnetic resonance
ESEEM	Electron spin echo envelope modulation
EXAFS	Extended X-ray absorption fine structure
Fd	Ferredoxin
FeCy	$K_3[Fe(CN)_6]$
FIOPs	Flash-induced oxygen evolution patterns
FT	Fourier transform, Fourier transformation
FTIR	Fourier transform infrared spectroscopy
IR	Infrared
HC = BC	Hydrogencarbonate = bicarbonate
HC(-)	Hydrogencarbonate depleted
HC(+)	Hydrogencarbonate containing
HEPES	4-(2-hydroxyethyl)-1-piperazineethanesulfonic acid
MES	2-(*N*-morpholino)ethanesulfonic acid
MIMS	Membrane-inlet mass spectrometry
NADPH	Nicotinamide adenine dinucleotide phosphate
OEC	Oxygen evolving complex
P680	Primary electron donor chlorophyll molecule in PSII
P700	Primary electron donor chlorophyll molecule in PSI
Pheo	Primary electron acceptor pheophytin molecule in PSII
PPBQ	Phenyl-*p*-benzoquinone
PQ	Plastoquinone
PQH_2	Plastohydroquinone, reduced and protonated form of PQ
PSI	Photosystem I
PSII	Photosystem II
Q_A	Primary plastoquinone electron acceptor in PSII
Q_B	Secondary plastoquinone electron acceptor in PSII
RC	Reaction center
S_i states	Oxidation states of the Mn_4O_xCa cluster, where i is the number of stored oxidizing equivalents
T. elongatus	*Thermosynechococcus elongatus*
TMH	Transmembrane α-helices of the D1 and D2 proteins of PSII
TRIS	2-amino-2-hydroxymethyl-1,3-propanediol
UV	Ultraviolet
WOC	Water oxidizing complex
XANES	X-ray absorption near edge structure
XAS	X-ray absorption spectroscopy
XRD	X-ray diffraction crystallography
Y_D	Redox-active tyrosine 161 of the D2 protein of PSII
Y_n	Oxygen evolution yield induced by the n^{th} flash
Y_Z	Redox-active tyrosine 161 of the D1 protein of PSII
α	Miss probability during flash-induced oxygen evolution
β	Double hit parameter during flash-induced oxygen evolution

Chapter 1

Introduction to Photosynthetic Water Splitting

1.1 INTRODUCTION TO OXYGENIC PHOTOSYNTHESIS

1.1.1 WATER AND LIGHT

Evolution is cleverer than you are.
Francis Crick

The Earth was formed around 4.5 billion years ago (Nisbet & Sleep, 2001). Carbon isotope data suggest that the first autotrophic carbon fixation was taking place about 3.8–3.4 billion years ago (Cavalier-Smith *et al.*, 2006; Mojzsis *et al.*, 1996). This reaction was carried out by simple, anoxygenic photosynthetic organisms. Survival of these first photobacteria was dependent on hydrogen and/or electron donors such as H_2S, NH_3, organic acids and ferrous iron. These substances were in limited supply on the surface of the Earth in comparison to the huge water pool (Blankenship, 2001; Olson, 2006). 3.4–2.3 billion years ago (Allen & Martin, 2007; Xiong & Bauer, 2002a), some cyanobacteria-like organisms managed to utilize water as electron source for CO_2 reduction using the energy of sun light to drive this reaction (Oparin, 1965).

Already about 2.3 billion years ago, photosynthetic organisms capable of water-splitting started to be dominating and increased the O_2 level to more than 10^{-5} of its present concentration (Bekker *et al.*, 2004). The rapid development of oxygenic photosynthesis fundamentally changed the Earth by creating an aerobic atmosphere. This led to the formation of the protective ozone layer that absorbs a large part of the UV radiation from the Sun. These new conditions ultimately permitted the development of an aerobic metabolism and more-advanced life forms (Olson & Blankenship, 2004).

1.1.2 PHOTOSYNTHETIC ENERGY CONVERSION. THE LIGHT REACTIONS

Cyanobacteria, green algae, and higher plants perform the complex biological process called oxygenic photosynthesis, by which solar energy is converted into chemical energy. On a global scale about 100 Gt of carbon is fixed annually by photosynthesis resulting in the release of about 260 Gt of molecular oxygen into the atmosphere (Barber, 2004). The overall chemical reaction for the oxygenic photosynthesis is:

$$6\,CO_2 + 6\,H_2O \xrightarrow{\textit{Light energy}} C_6H_{12}O_6 + 6\,O_2 \qquad (\mathbf{1.1})$$

The atoms of molecular oxygen are derived in this process entirely from water. In algae and higher plants, the reactions of photosynthesis occur within a special cell organelle; the chloroplasts (see Fig. 1.1). The chloroplast has two outer membranes, which enclose the stroma. Inside the stroma is a closed membrane vesicle, the thylakoid,

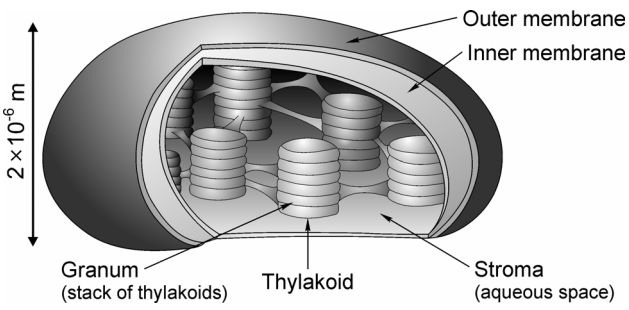

FIGURE 1.1 Three-dimensional model of chloroplast.

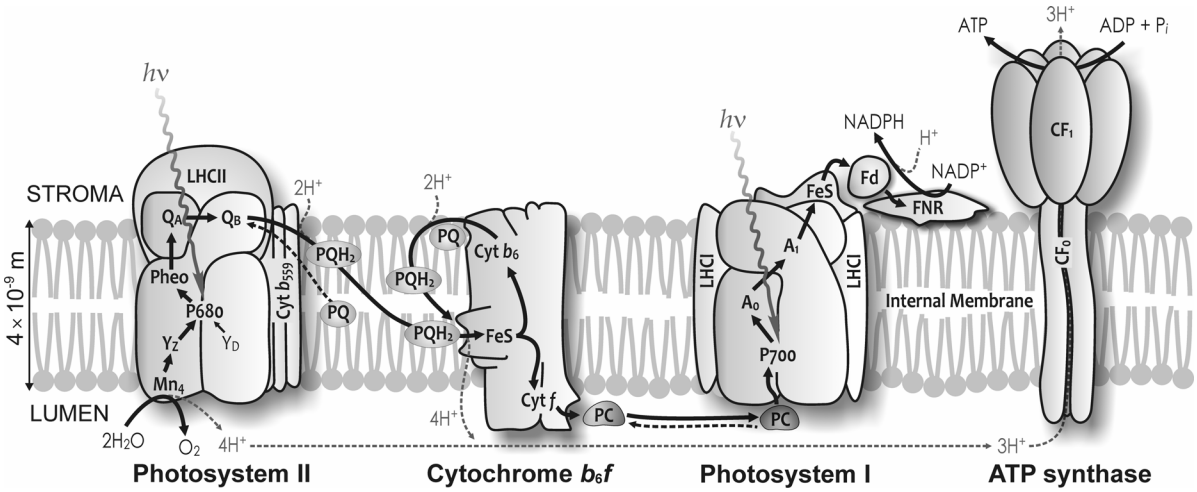

FIGURE 1.2 A schematic model representation of the protein complexes involved in the photo-induced electron and proton transfer reactions in the thylakoid membrane of photosynthetic oxygenic organisms. See text for a description.

which contains the lumen. Whereas the stroma is the site where the CO_2-fixation occurs (dark reactions), the thylakoid membrane is the site of the light reactions of energy conversion. In cyanobacteria, the thylakoid membrane is within the cytosol. The steps involved in photosynthetic energy conversion are catalysed by four protein complexes bound in the thylakoid membrane. These complexes are Photosystem II (PSII), Cytochrome b_6f (Cyt b_6f), Photosystem I (PSI) and the ATP-synthase (Fig. 1.2). PSII, Cyt b_6f and PSI contain redox active cofactors that allow the photo-induced electron transfer from water to $NADP^+$ through the thylakoid membrane. Figure 1.3 displays this linear electron transport in a way that the cofactors are arranged according to their redox potentials. This so-called Z-scheme was originally proposed by Hill and Bendall (Hill & Bendall, 1960).

The initial event in photosynthesis is the absorption of light ($h\nu$) by special light harvesting complexes (LHC) located around PSII and PSI (Nelson & Yocum, 2006). The absorbed light energy is delivered to the reaction centers chlorophylls, P680 ('monomeric' chlorophyll complex (Renger & Holzwarth, 2005)) in PSII, and P700 (chlorophyll heterodimer (Lubitz, 2006)) in PSI where a charge separation takes place.

In **photosystem II** (reviewed in (Wydrzynski & Satoh, 2005) the primary photochemical reaction is the transfer of an electron from the excited state of P680 to an electron acceptor, pheophytin (Pheo), creating $P680^{\bullet+}$ and $Pheo^{\bullet-}$. The formed $P680^{\bullet+}$ is strong enough to extract electrons from water, which is split into oxygen and protons. The electrons from water are transferred to $P680^{\bullet+}$ *via* a Mn_4O_xCa cluster and a redox-active tyrosine residue (Y_Z) (Figs. 1.2 and 1.3). Each electron passes rapidly ($\approx 10^{-10}$ s) from $Pheo^{\bullet-}$ to a permanently bound quinone, Q_A, before finally arriving to the plastoquinone pool at the Q_B site. Transfer of the second electron reduces Q_B^- to Q_B^{2-}, and the reduced Q_B^{2-} takes up two protons from the stroma side of the medium, yielding plastohydroquinone (PQH_2) (Fig. 1.2). PQH_2 then leaves the PSII complex, and diffuses in the membrane to the Cyt b_6f complex. The empty Q_B-pocket is filled by another plastoquinone molecule (PQ) from the plastoquinone pool.

The **Cytochrome b_6f complex** is a large multisubunit protein with several prosthetic groups (Berry *et al.*, 2000). It contains two *b*-type hemes (Cyt b_6), one *c*-type

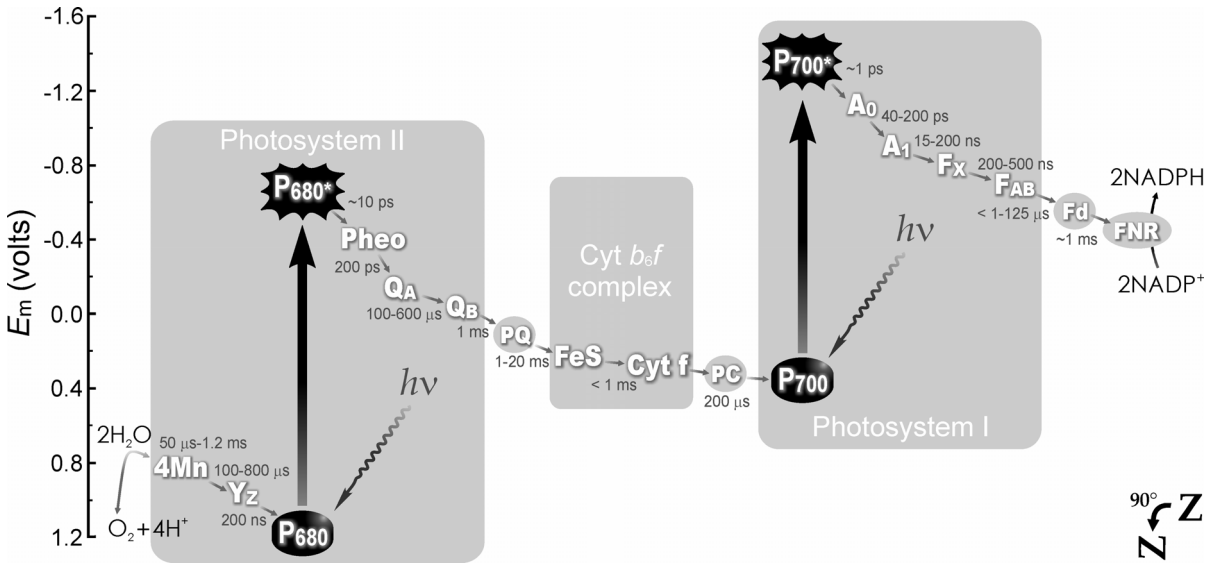

FIGURE 1.3 The Z-scheme of oxygenic photosynthesis for linear electron transfer from water to NADPH plotted on a redox potential scale.

heme (Cyt *f*) and a Rieske iron–sulfur protein (FeS_R). PQH_2 is oxidized by FeS_R under the release of protons into the lumen. One of the two electrons from PQH_2 is passed along a linear electron transport chain through Cyt *f* to a small mobile copper–protein plastocyanin (PC), which carries the electrons to PSI. The other electron goes through the two Cyt b_6 hemes and reduces another PQ, participating thereby in a cyclic process that increases the number of protons pumped across the membrane (Fig. 1.2).

Photosystem I (recently reviewed in (Golbeck, 2006)) similar to PSII also utilises light energy to drive the redox reactions of electron transfer. However, the redox potential for PSI is not high enough to extract electrons directly from water. Instead, the oxidized $P700^{\bullet+}$ is reduced by an electron provided by PC. The electron ejected from the light-excited P700* moves through PSI across the membrane to a water–soluble protein, ferredoxin (Fd). On its way to Fd, the electron passes through a number of prosthetic groups including, chlorophyll A_0, a bound phylloquinone, A_1, and the F_X and F_A/F_B iron sulfur centers (Fig. 1.3). Reduced Fd gives then one electron to the membrane–associated flavoprotein ferredoxin–NADP reductase (FNR), which reduces $NADP^+$ to NADPH, thus completing the sequence of the non-cyclic electron transport. Under certain conditions also cyclic electron flow occurs from the reducing side of PSI, through Cyt b_6f complex and back to P700. This cyclic electron flow increases proton pumping into the lumen, which can be utilized for ATP synthesis.

The accumulation of protons in the thylakoid lumen generates a proton gradient and an electrochemical potential across the membrane. The generated potential energy is utilized by **ATP–synthase** for phosphorylation of ADP to ATP. This occurs when the protons are returning to the stroma through the CF_0/CF_1 protein complexes (Fig. 1.2) of the ATP–synthase (McCarty *et al.*, 2000).

Thus, the light-driven electron transport from H_2O to $NADP^+$ catalyzed by PSII and PSI results in the formation of the energy-rich compounds NADPH and ATP, and to the evolution of O_2. The energy stored in the NADPH and ATP is subsequently used for the reduction of CO_2 to sugars. This is done by a cyclic

metabolic pathway, the so-called Calvin cycle (reviewed in (Martin *et al.*, 2000)), that occurs in the stroma of the chloroplasts and does not directly require light.

1.2 PHOTOSYNTHETIC REACTION CENTERS: EVOLUTIONARY PERSPECTIVES

1.2.1 REACTION CENTER MOTIF

In every photosynthetic organism the primary events involve the reaction center (RC) that creates the trans-membrane charge separation in response to light excitation. All photosynthetic RCs are composed of an integral membrane protein complex of homodimeric or heterodimeric nature to which pigments (carotenoids and chlorophylls) and redox–active cofactors (such as chlorophylls and quinones) are bound. Because of differences in the nature of the initial electron acceptors, the RCs can be classified into two types (for a review see (Blankenship, 1992; Olson, 2001)). The RCs of green sulfur bacteria, heliobacteria, and photosystem I belong to the iron–sulfur type (also called RC1 type), while the RCs of purple bacteria, green non–sulfur (green filamentous) bacteria, and photosystem II belong to the pheophytin–quinone type (or RC2 type) (Fig. 1.4).

There are two models for the origin of RCs (reviewed in (Olson & Blankenship, 2004; Vermaas, 2002)). In the *selective loss model* the common ancestor of all extant RCs was probably similar to the homodimeric RC1 of green sulfur bacteria (*Chlorobiaceae*) and heliobacteria. According to the *fusion model* the most recent common ancestor is postulated to have given rise to two lines, one containing RC1 and another containing RC2. A recent version of this model assumes the RC2 of purple bacteria to

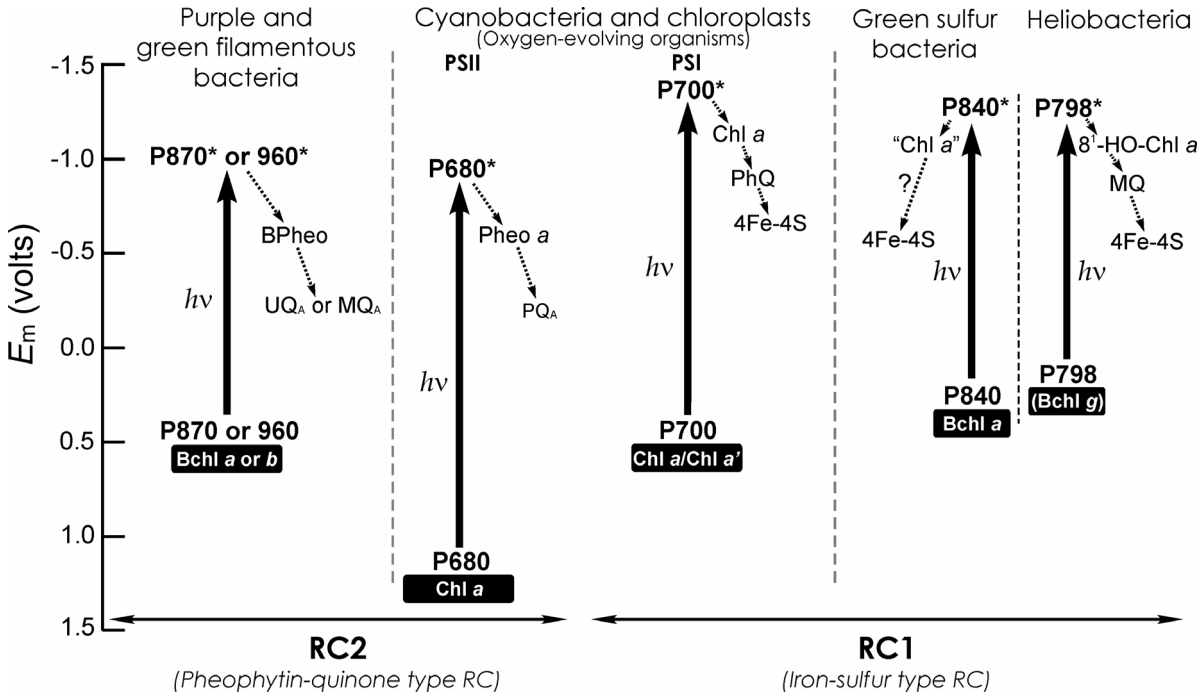

FIGURE 1.4 Photosynthetic reaction centers (RCs). For each RC the primary electron donor, initial electron acceptor, and secondary electron acceptors plotted on a redox scale are shown (adapted from (Olson, 2001; Kern, 2005). Abbreviations of some quinones: MQ – menaquinone; PhQ – phylloquinone; UQ – ubiquinone.

be more primitive and evolved from a cytochrome *b*-like protein (Xiong & Bauer, 2002a; Xiong & Bauer, 2002b).

While all known oxygen-evolving photosynthetic organisms (including cyanobacteria) contain both types of RCs (PSII and PSI) (Ort & Yocum, 1996), all anoxygenic photosynthetic bacteria have only one of these types (either RC1 or RC2) (Blankenship *et al.*, 1995). Therefore, it is generally accepted, that the origin of oxygenic photosynthesis begins with the origin of the linked RCs (PSII and PSI) in a common ancestor of oxygen-evolving organisms (for details see (Olson & Blankenship, 2004; Xiong & Bauer, 2002a)). However, to oxidize water to molecular oxygen two major changes from a more primitive non-oxygen-evolving RCs were also required: a charge-accumulating system and a RC pigment with a very high oxidizing potential.

1.2.2 THE DEVELOPMENT OF A HIGHLY OXIDIZING RC

Undoubtedly, the development of the catalytic site of water oxidation (Mn-protein complex) that is capable of collecting and storing oxidizing equivalents, formed the central stage in the transition from anoxygenic to oxygenic photosynthesis (Allen & Martin, 2007; Raymond & Blankenship, 2008). However, the development of a strongly oxidizing RC must have preceded or co-occurred with the invention of the water splitting site (Blankenship & Hartman, 1998).

Water is a very stable compound. If one considers oxidative water splitting into O_2 and four protons, the midpoint potential for this process is +0.82 V at pH 7 (Atkins & de Paula, 2006; Messinger & Renger, 2008). Therefore, a strong oxidant with redox potential greater than 0.82 V is needed to decompose water into O_2. In modern water–splitting organisms this oxidant, P, is thought to be the radical cation $P680^{\bullet+}$, the RC photoactive chlorophyll *a* (Chl *a*) (Fig. 1.5*b*) of PSII, which is part of a 'dimeric' structural motif termed P_{D1}–P_{D2} (see Section 1.3.1). $P680^{\bullet+}$ has the midpoint redox potential of about +1.25 V (Rappaport *et al.*, 2002), which is achieved by a special protein environment (Renger, 2008). This oxidizing power is about half a Volt above the special pair (P_{D1}–P_{D2}) in the RCs of all anoxygenic bacteria that contain various bacteriochlorophyll (BChl) derivatives: *a*, *b* or *g* (Fig. 1.4) (Blankenship *et al.*, 1995).

It is believed that BChl *a* (Fig. 1.5*a*) appeared before Chl *a* (Fig. 1.5*b*) in evolutionary history (Burke *et al.*, 1993; Olson & Blankenship, 2004; Raymond *et al.*, 2003). In the common ancestor of cyanobacteria ferrous iron and then hydrogen peroxide may

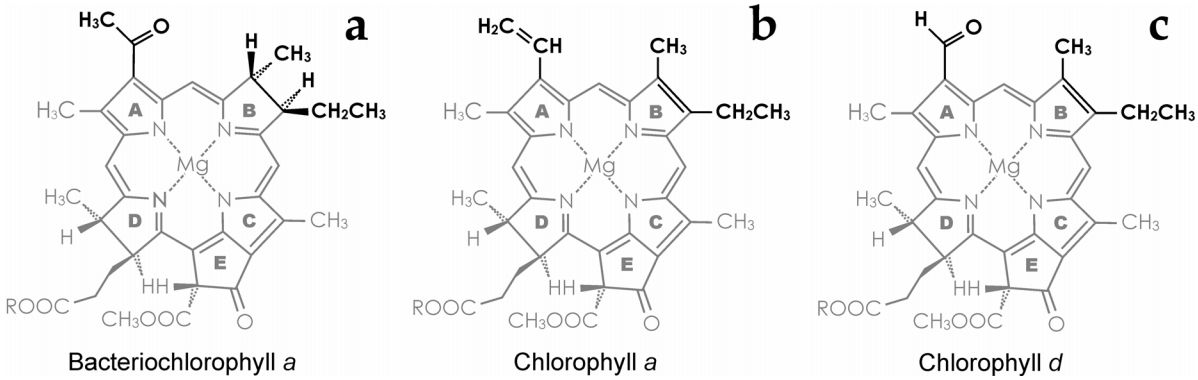

FIGURE 1.5 Chemical structures of (***a***) bacteriochlorophyll *a*, (***b***) chlorophyll *a* and (***c***) chlorophyll *d*. Differences in the structures are shown in bold. R is the phytyl tail.

have been the electron donors for photosynthetic CO_2 fixation until Chl *a* replaced BChl *a* in the RCs and the Mn-protein complex was invented (Blankenship & Hartman, 1998; Borda *et al.*, 2001; Olson, 2006; Rutherford & Nitschke, 1996).

For many years, Chl *a* had been believed to be unique and be the essential pigment among the chlorophyll species in oxygenic photosynthetic organisms. However, with the discovery of the Chl *d*–containing oxygen-evolving cyanobacterium *Acaryochloris marina* (Miyashita *et al.*, 1996) this unique role of Chl *a* for P680 became a matter of debate.

1.2.3 THE ROLE OF CHL *d* IN *Acaryochloris marina*. IS P680 ALWAYS A CHL *a* COMPLEX?

In 1996, *Acaryochloris marina* was first isolated from an extract of didemnid ascidian *Lissoclinum patella* (see Fig. 1.6) (Miyashita *et al.*, 1996), and was presumed to be a symbiont of this colonial animal (Larkum & Kühl, 2005). *A. marina* has Chl *d* (Fig. 1.5*c*) as a principal photopigment (> 95%), with a trace amount of Chl *a* (Fig. 1.5*b*) that is approximately 3% of the total Chl (Miyashita *et al.*, 1996). Such an unusual pigment composition results in a unique constitution of the photosystems of *A. marina*. Thus, Chl *d* serves as a light-harvesting pigment for both PSII and PSI (Boichenko *et al.*, 2000; Schiller *et al.*, 1997). The photoactive pigment of PSI, that represents the Chl *a*–Chl *a*′ heterodimer in all oxygen-evolving organisms, was shown to be replaced by a Chl *d*–Chl *d*′ in *A. marina* (Akiyama *et al.*, 2002). Since this pigment shows a flash-induced absorbance difference maximum at approximately 740 nm, the primary donor of PSI is named P740 (Hu *et al.*, 1998), corresponding to P700 in other oxygenic organisms. The midpoint potential of P740/P740$^{\bullet+}$ was found to be +335 mV (Hu *et al.*, 1998). This value is about 100 mV lower than the E_m of P700/P700$^{\bullet+}$ of the usual Chl *a* containing PSI, which varies between +420 mV and +470 mV for different organisms (Nakamura *et al.*, 2005; Witt *et al.*, 2002). It is still an open question whether PSII of *A. marina* uses Chl *a* or Chl *d* or both in its primary photochemistry. Chl *a* was assumed to be the constituent of the photoactive pigment of PSII (Mimuro *et al.*, 2004; Nieuwenburg *et al.*, 2003). This idea, however, is not convincing because the energetics (E_m values) and the kinetics are to a large extend tuned by the protein matrix and the chemical nature of the pigment is of minor relevance in most cases (Renger & Holzwarth, 2005). In fact, new electrochemical studies reveal that in solution

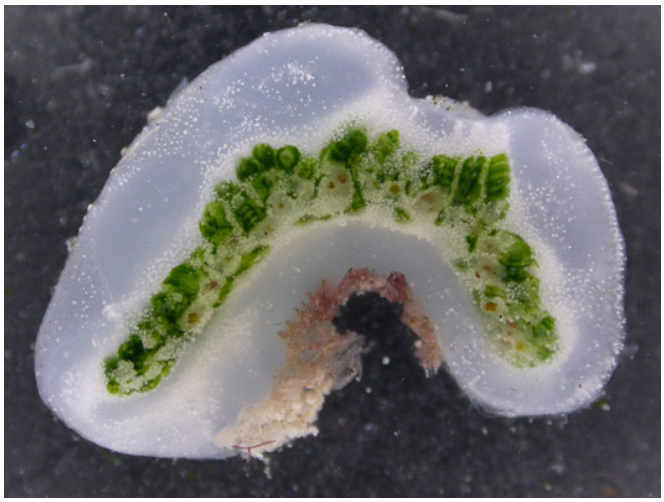

FIGURE 1.6 Vertical section through the didemnid ascidian *Lissoclinum pattela* (size about 20 mm), hosting the green exosymbiont *Prochloron* sp. in its internal cavities. Yellow-greenish colonies of *Acaryochloris marina*-like cyanobacteria are found on the lower surface of the ascidian in between patches of red–brown *Dermocapra*-like cyanobacteria. Adopted from (Kühl *et al.*, 2005).

the E_m of Chl *d*/Chl $d^{\bullet+}$ (+0.88 V in acetonitril) is even slightly higher than that of Chl *a*/Chl $a^{\bullet+}$ (+0.81 V in acetonitril) (Kobayashi *et al.*, 2007). At present three different types of models are discussed, in which the special pair (P_{D1}–P_{D2}) (Fig. 1.7) of the photoactive pigment is assigned either *i*) to a Chl *d*−Chl *d* dimer (Itoh *et al.*, 2004; Tomo *et al.*, 2007), *ii*) to a Chl *a*−Chl *a* dimer (Akimoto *et al.*, 2006; Mimuro *et al.*, 2004), or *iii*) to a Chl *d*−Chl *a* heterodimer (Kobayashi *et al.*, 2005; Kobayashi *et al.*, 2007). At the same time, the identity of the primary electron acceptor of PSII in *A. marina* has been well defined as being Pheo *a* (Chen *et al.*, 2005; Kobayashi *et al.*, 2007). If the photoactive pigment in PSII of *A. marina* is a Chl *d*−Chl *d* homodimer or a Chl *d*−Chl *a* heterodimer, our current understanding of the overall energetics of the water oxidizing system may need to be modified (depending on the actual redox potentials). The most recent findings indicate that *Acaryochloris*–like organisms may be fairly widespread (Larkum & Kühl, 2005; Miller *et al.*, 2005; Murakami *et al.*, 2004), and it is an apparent paradox that they live in environments rich in near-infrared light but show features of adaptation to strong light.

Blankenship and Hartman (Blankenship & Hartman, 1998) proposed that Chl *d* may have been a transitional evolutionary pigment between BChl *a*–containing RCs and Chl *a*–containing RCs. Alternatively, it could be a more recent adaptation to a particular light environment (Kühl *et al.*, 2005). Clearly, whatever is true, *A. marina* provides an interesting system to explore the energetics of the water splitting reaction of PSII (see Chapter 3).

1.3 PHOTOSYSTEM II: COMPOSITION AND FUNCTION

1.3.1 SUBUNITS AND COFACTORS

The essential steps of photosynthetic water-splitting take place in PSII, a large multimeric pigment-protein complex (see Fig. 1.8*a*) found in the thylakoid membranes of all oxygenic photosynthetic organisms. This complex exists as a dimer whose total weight is approx. 700 kDa. Each monomer comprises close to 30 polypeptide subunits and many cofactors (Fig. 1.7) (Barber, 2006; Shi & Schröder, 2004; Wydrzynski & Satoh, 2005).

All redox cofactors required for photochemical charge separation and for water oxidation are held by the D1 (PsbA) and D2 (PsbD) proteins (heterodimers) which have five transmembrane α-helices (TMH) each (Fig. 1.8) (Nixon *et al.*, 2005). These two proteins have sequence homology

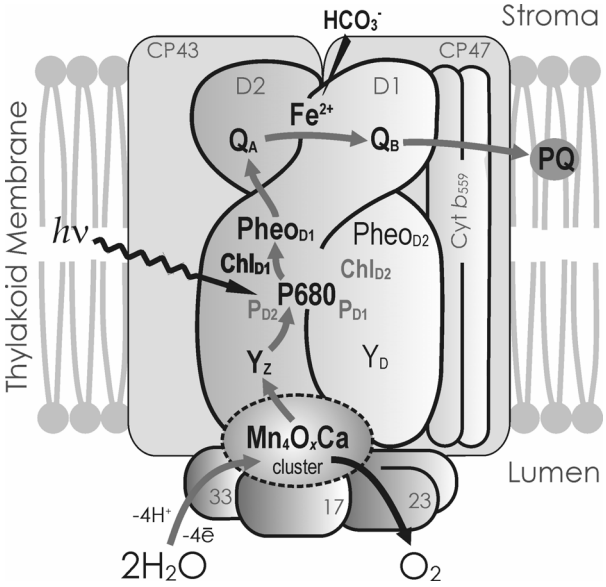

FIGURE 1.7 A schematic view of PSII RC in plants (only core proteins are included). Grey arrows show the direction of electron transfer. The labelled polypeptides and redox cofactors are described in the text. The small membrane intrinsic subunits are omitted.

with the L and M subunits of the photosynthetic RC of purple bacteria (Deisenhofer & Michel, 1989). D1 and D2 contain six Chl *a* molecules (from which two are the primary electron donor P680, P_{D1} and P_{D2}), two Pheo *a* molecules ($Pheo_{D1}$ and $Pheo_{D2}$), two quinones (Q_A on the D2 side and Q_B on the D1 side), at least one β-carotene and a non-heme iron (between Q_A and Q_B). In fact, the arrangement of the cofactors on the reducing side of the D1/D2 heterodimer is essentially identical to that of their bacterial counterparts (Feher *et al.*, 1989). The only clear exceptions is that one of the ligands for the non-heme iron of PSII is a hydrogencarbonate (discussed below) and not glutamate as in bacteria and that the Q_B site is a little larger and in closer contact with the stromal surface than in the bacterial RC. Two redox-active tyrosine residues, Y_Z (D1-Tyr161) and Y_D (D2-Tyr161) are located on the electron-donor side of D1 and D2 proteins, respectively (Fig. 1.7). The Pheo *a* molecules and the redox-active Tyr residues on D1 and D2 are homologous. However, they are not equal, since electron transfer of PSII proceeds only through the $Pheo_{D1}$ and Y_Z on D1 (Klimov, 2003; Wydrzynski & Satoh, 2005). Nevertheless, Y_D located on D2 plays an important role in the redox processes of PSII (see below). Additionally, the D1 protein also provides most of the ligands to the catalytic site of oxidative water splitting (Debus, 2005), a cluster of four Mn atoms, one Ca atom and at least five bridging oxygen's (the Mn_4O_xCa cluster).

The Mn_4O_xCa cluster forms, together with its cofactors (possibly Cl^- and HCO_3^-; discussed below) and ligands (Debus, 2005) a functional unit within PSII that is referred to as the water-oxidizing complex (WOC; also called the oxygen-evolving complex, OEC). The Mn_4O_xCa cluster is stabilized by three extrinsic proteins on the lumenal side of PSII. In the case of higher plants these extrinsic proteins are PsbO (33 kDa), PsbP (23 kDa), and PsbQ (17 kDa) (Fig. 1.7); in cyanobacteria (Fig. 1.8*a*), the two smaller proteins are substituted by cytochrome c_{550} (PsbV, 17 kDa) and PsbU (12 kDa) (reviewed in (Roose *et al.*, 2007; Seidler, 1996)). These proteins are highly important for the optimal function of water oxidation. The role of PsbO in PSII is to stabilize the Mn_4O_xCa cluster and hence the oxygen-evolving activity. Therefore, this polypeptide is often denoted "manganese stabilizing protein" (MSP). The PsbP and PsbQ polypeptides mediate/facilitate the binding of Ca^{2+} and Cl^- ions to the vicinity of the Mn_4O_xCa cluster and are essential for its function (Gregor *et al.*, 2005). In case of a removal of the extrinsic proteins, non-physiological Ca^{2+} and Cl^- concentrations are required to restore oxygen-evolving activity (van Gorkom & Yocum, 2005).

The D1-D2 heterodimer is closely associated with two internal antenna subunits, the Chl *a*-containing proteins CP43 (PsbC) and CP47 (PsbB) (Figs. 1.7 and 1.8). These two proteins are structurally homologous, each having six TMH. In addition to the TMH, both proteins contain large membrane-extrinsic loops interacting with the extrinsic subunits on the lumenal side. The large loop of CP47 is indispensable for stabilizing of the WOC (Gleiter *et al.*, 1995). The cofactors of CP43 and CP47 are chlorophylls and carotenes. They transfer captured light energy from light-harvesting antenna system to P680. Moreover, CP43 and CP47 capable to absorb light themselves (reviewed in (Bricker & Frankel, 2002)).

PsbE (or α-subunit) and PsbF (or β-subunit) proteins provide histidine ligands for the high-potential heme of cytochrome b_{559} (Cyt b_{559}) (Figs. 1.7). The Cyt b_{559} and

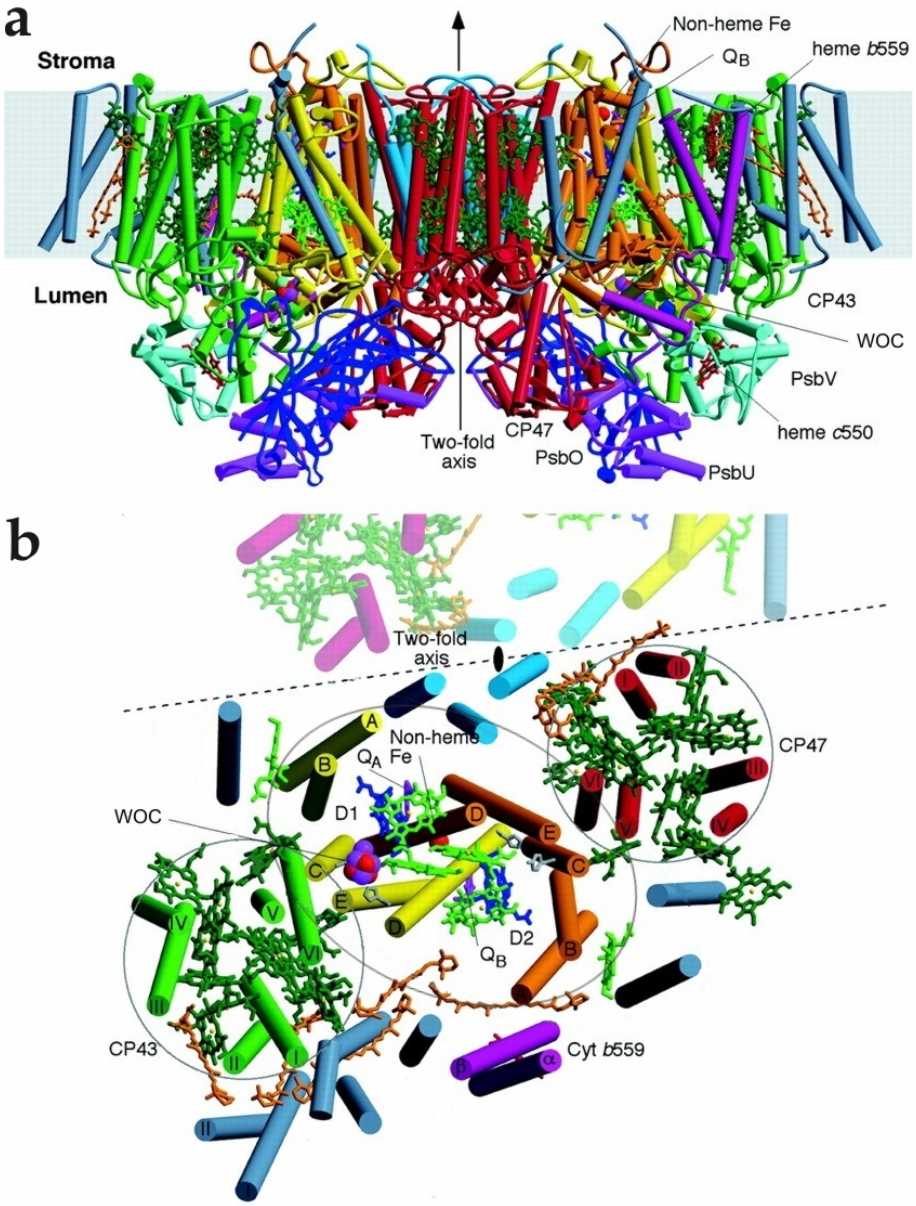

FIGURE 1.8 Overall structure of the PSII isolated from *T. elongatus* at a resolution of 3.5 Å. (***a***) View of the PSII dimer perpendicular to the membrane normal. Transmembrane α-helices (TMH) are represented as cylinders with D1 in yellow; D2 in orange; CP47 in red; CP43 in green; Cyt b_{559} in wine red. The extrinsic proteins are PsbO in dark blue, PsbU in magenta, and PsbV in cyan. All other proteins are in medium blue and in light blue. Chls of the D1/D2 RC are light green, pheophytins are blue, Chls of the antenna complexes are dark green, β-carotenes are in orange, hemes are in red, non-heme iron is red, Q_A and Q_B are purple. The WOC is shown as the red (oxygen atoms), magenta (Mn ions), and cyan (Ca^{2+}) spheres. (***b***) View of the PSII monomer along the membrane normal from the lumenal side. The pseudo-2-fold axis perpendicular to the membrane plane passing through the non-heme iron relates the TMH of the D1/D2 heterodimer. Colouring the same as in (***a***). Adopted from (Ferreira *et al.*, 2004).

the nearby β-carotene are located on the D2 side. Their function is to protect against photoinduced damage (Shi & Schröder, 2004; Stewart & Brudvig, 1998).

All foregoing subunits and cofactors of PSII have been confirmed in the latest X-ray structures at 3.5 (see Fig. 1.8) and 3.0 Å resolutions (Ferreira *et al.*, 2004; Loll *et al.*, 2005).

1.3.2 THE FUNCTION OF PSII

PSII acts as a water:plastoquinone oxidoreductase, catalysing the following reaction:

$$2\,H_2O + 2\,PQ + 4\,H^+_{stroma} \xrightarrow{4\,h\nu} O_2 + 2\,PQH_2 + 4\,H^+_{lumen} \qquad (\mathbf{1.2})$$

This process comprises three types of reaction sequences: (*i*) light-induced charge separation leading to the stabilized radical ion pair $P680^{\bullet+}PheoQ_A^{\bullet-}$ (for a review, see (Renger & Holzwarth, 2005)); (*ii*) oxidative splitting of two water molecules to molecular oxygen and four protons, with $P680^{\bullet+}$ as the driving force (recently reviewed in (Messinger & Renger, 2008)); and (*iii*) reduction of plastoquinone (PQ) to plastohydroquinone (PQH_2) under proton uptake with $Q_A^{\bullet-}$ acting as reductant (reviewed in (Petrouleas & Crofts, 2005)). Thus, in PSII the light energy is used to remove electrons from water (oxidation) and to add electrons, as well as protons, to PQ (reduction). In this regard, the role of the WOC in PSII is indispensable: it couples successive one-electron oxidations of $P680^{\bullet+}$ to the four-electron oxidation of water to dioxygen:

$$2\,H_2O \xrightarrow{4\,h\nu} O_2 + 4\,H^+ + 4\bar{e} \qquad (\mathbf{1.3})$$

1.4 OXIDATIVE WATER SPLITTING

1.4.1 PHOTOSYNTHETIC OXYGEN EVOLUTION PATTERNS AND THE KOK CYCLE

The foundation for the understanding of the mechanism of photosynthetic water oxidation was put forward almost 40 years ago. Illuminating dark-adapted algae and chloroplasts by short ('single turn-over') saturating flashes, Joliot and co-workers (Joliot *et al.*, 1969) found that O_2 was formed with a characteristic periodicity of four (Fig. 1.9*a*). The periodicity of four was readily explained by the chemistry of water oxidation, but the observation that the maximum O_2 yield occurred for the 3rd rather than the 4th flash, and that O_2 oscillation was damped after several cycles, revealed an unexpected level of complexity in the mechanism of water oxidation. Based on these findings, Kok and colleagues (Kok *et al.*, 1970) developed an elegant model of water oxidation by PSII (Fig. 1.9*b*; black symbols and arrows). It was proposed that each WOC cycles during water oxidation through five different redox states, named S_i states (i = 0, …,4), where i is the number of oxidizing equivalents stored within the WOC. The creation of the four oxidizing equivalents occurs during repeated oxidation (one electron at a time) of the WOC by $P680^{\bullet+}$ *via* a redox-active tyrosine, $Y_Z/Y_Z^{\bullet}$ (Fig. 1.9*b*; grey symbols). To account for the maximum O_2 yield after the 3rd flash the Kok model assumes that in long dark-adapted samples practically all (almost 100%) PSII centers are in the S_1 state, rather than S_0. Indeed, later studies showed that the S_0 state is slowly (tens of minutes) oxidized to the S_1 state by the oxidized form of tyrosine D, $Y_D^{\bullet}$ (also denoted as Y_D^{ox}), of polypeptide D2 (Fig. 1.9*b*; dashed grey arrows between S_0 and S_1) (Messinger, 1993; Messinger & Renger, 1993; Styring & Rutherford, 1987; Vass *et al.*, 1990a). The S_2 and S_3 states are meta-stable and are reduced within seconds to minutes into the S_1 state by the reduced tyrosine Y_D *via* a fast decay (Isgandarova *et al.*, 2003; Messinger *et al.*, 1993; Vermaas *et al.*, 1984; Vermaas *et al.*, 1988) or a slower decay due to electron donation from the reduced acceptor side quinones (symbolized by Q^{red} in Fig. 1.9*b*) (Diner, 1977; Nugent *et al.*, 1987; Rutherford & Inoue, 1984).

The S_4 state is thought to spontaneously decay into the S_0 state under the release of O_2 and the binding of one or both new substrate water molecules (review in (Hillier & Messinger, 2005; Messinger & Renger, 2008)).

To explain the damping in the O_2 oscillation patterns as the flash number increased, Kok and co-workers introduced 'miss' (α) and 'double-hit' (β) probabilities (Forbush *et al.*, 1971; Kok *et al.*, 1970). The miss probability gives the percentage of the WOCs that are in the same S state before and after flash excitation. The magnitude of the α-value is expected to depend on redox equilibria of the donor ($Y_Z P680^{\bullet+} \Leftrightarrow Y_Z^{ox} P680$) and acceptor side ($Q_A^- Q_B \Leftrightarrow Q_A Q_B^-$) of PSII (Renger & Hanssum, 1988; Shinkarev & Wraight, 1993; de Wijn & van Gorkom, 2002). Furthermore, the kinetics of $P680^{\bullet+}$ reduction by Y_Z determines the value of α (Christen *et al.*, 1999). As a consequence, the parameter α may be considered to depend on the redox state S_i of the WOC (Isgandarova *et al.*, 2003; Noguchi & Sugiura, 2002; Shinkarev & Wraight, 1993) (see Figs. 1.9 and 2.4; see also Sections 2.3.3.5, 3.3.1, 4.3.2 and, 4.4.2 of this work). However, the precise dependence of the α-values on the S_i states is difficult to measure and cannot be gathered from the FIOPs in a straight-forward manner (Hillier & Messinger, 2005; Messinger & Renger, 2008). Therefore, it is often assumed that the miss parameter is S_i state and flash number independent. The double hit probability equals the percentage of centers that have been excited twice in a single flash. It was shown that the β parameter depends (*i*) on the rate of the $Q_A^{\bullet-}$ reoxidation (Messinger *et al.*, 1993) and (*ii*) on the flash profile (Hillier & Messinger, 2005; Jursinic, 1981). Miss and double hit probabilities are strongly temperature and pH dependent (Bernat *et al.*, 2002; Messinger *et al.*, 1993; Messinger & Renger, 1994) and are also affected by H/D exchange (Christen *et al.*, 1999). For spinach thylakoids, typical Kok parameters are $\alpha \approx 6$–12% and $\beta \approx 3$–5% with xenon flash illumination (Messinger & Renger, 2008).

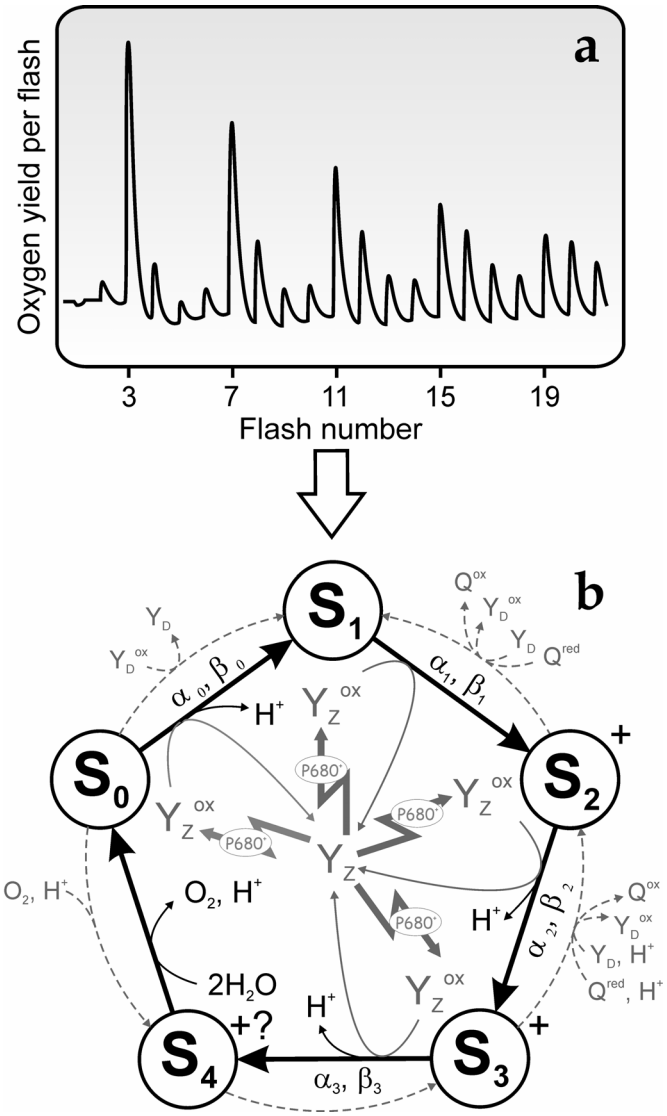

FIGURE 1.9 Flash-induced oxygen evolution pattern (FIOP) of dark-adapted spinach thylakoids induced by a train of saturating xenon flashes (2 Hz frequency) (***a***) and the extended Kok model (***b***). All symbols are explained in the main text. Adapted from (Messinger & Renger, 2008).

Today, advanced Kok models often take into account the following factors that can affect the FIOPs (described in Section 2.3.3.5; Fig. 2.4): (*i*) back reactions of S_2 and

S_3 states with Y_D during the dark time between flashes (Isgandarova *et al.*, 2003; Messinger & Renger, 1993; Vass et al., 1990a); (*ii*) a correction factor for a change of the number of active PSII centers during the flash train due to photoactivation, photoinhibition or a limited acceptor pool size (Kebekus *et al.*, 1995; Messinger *et al.*, 1997a); (*iii*) existence of so-called 'super-reduced' S_i states, which are not a part of Kok cycle and reduced below the level of the S_0 state (S_{-1}…S_{-5}) (see Section 1.4.3.1 and Fig. 1.10) (Bouges, 1971; Messinger *et al.*, 1997a; Messinger *et al.*, 2001a); and enhanced double hit on the 1st flash or on each other flash that may be caused by addition of electron acceptors (FeCy or PPBQ/DCBQ, respectively) (Jursinic, 1981; Petrouleas & Diner, 1987; Zimmermann & Rutherford, 1986).

The remarkably insightful Kok model successfully explained the main features of the flash dependence of O_2 evolution, and continues to guide research into the mechanism of water oxidation and O_2 release by PSII.

1.4.2 THE ROLE OF Y_Z AND Y_D IN WATER OXIDATION

Y_Z (situated within the D1 protein (see Section 1.3.1)) is directly involved in the light-induced electron transfer and plays a decisive role as an intermediate redox-active carrier between P680 and the Mn_4O_xCa cluster (Debus *et al.*, 1988). According to recent X-ray crystallographic results (Ferreira *et al.*, 2004; Loll *et al.*, 2005), Y_Z is close enough to the Mn_4O_xCa cluster (~5 Å to Ca) that it might be intimately involved in the chemical catalysis of water oxidation either by direct hydrogen atom transfer or by facilitating proton coupled electron transfer between substrate water and Y_Z. The rate of $Y_Z^{\bullet}$ reduction (the neutral radical) by the Mn_4O_xCa cluster is S_i state dependent and varies between ~50 μs ($S_0 \rightarrow S_1$) and ~1.5 ms ($S_3 \rightarrow S_4$) (Rappaport *et al.*, 1994; Tommos & Babcock, 2000). In many models, His190 of D1 (Debus, 2005) is proposed to be the base that accepts the proton released from Y_Z upon oxidation by $P680^{\bullet+}$ (reviewed in (Nugent *et al.*, 2004)). Thus, the electron transfer through Y_Z leads to the net reaction with Y_Z = Tyr_Z-OH···His190 and $Y_Z^{\bullet}$ = Tyr_Z-O$^{\bullet}$···$^{+}$H-His190 (for recent review see (Meyer *et al.*, 2007)).

A second redox-active tyrosine residue, Y_D (at homologous position to Y_Z in the D2 protein (Section 1.3.1)), does not have an essential role in electron flow of PSII Section 1.4.1). It is located at about the same distance to P680 as Y_Z, but its distance to the Mn_4O_xCa cluster is ~30 Å (Loll *et al.*, 2005). Therefore, Y_D is not directly involved in water splitting. Nevertheless, Y_D is able to undergo redox reactions with certain S_i states of the WOC (described in Section 1.4.1) (see also (Renger & Kühl, 2007) and references therein). Due to the oxidation by $P680^{\bullet+}$ (Faller *et al.*, 2001), Y_D has been shown to form a stable radical, $Y_D^{\bullet}$, which is slowly reduced (months at liquid nitrogen temperature) (Messinger, 1993; Vass *et al.*, 1990b). It has been suggested that the function of $Y_D^{\bullet}$ is the conversion of S_0 to S_1 in the dark in order to stabilize the Mn_4O_xCa cluster (Faller *et al.*, 2001; Styring & Rutherford, 1987) and/or increasing the redox potential of the primary donor $P680^{\bullet+}$/P680 (Diner & Rappaport, 2002). Ananyev and colleagues also proposed that $Y_D/Y_D^{\bullet}$ is involved in the photoactivation of the WOC (Ananyev *et al.*, 2002). In spite of differences in the redox kinetic of $Y_D^{\bullet}$ and $Y_Z^{\bullet}$, their x-band CW EPR spectra are similar (Miller & Brudvig, 1991).

1.4.3 WATER-OXIDIZING COMPLEX: OXIDATION STATES AND STRUCTURE

1.4.3.1 Mn Oxidations States

It is widely assumed that the oxidation state changes in the WOC are entirely manganese-based. Several spectroscopic methods, such as electron paramagnetic resonance (EPR), Fourier-transformed infra-red (FTIR), X-ray absorption spectroscopy (XAS), and UV spectroscopy, have been used to address the oxidation state of Mn in each S state (see reviews (Debus, 1992; Noguchi, 2007; Yachandra, 2005; Meyer *et al.*, 2007) and references therein). There is most agreement concerning the S_1 and S_2 states. Results obtained by EPR and X-ray absorption near edge spectroscopy (XANES) have been interpreted as favouring the oxidation-state distribution Mn_4(III,III,IV,IV) for the S_1 state of the WOC (Iuzzolino *et al.*, 1998; Yachandra *et al.*, 1996; Messinger et al., 2001b, Ono *et al.*, 1992; Roelofs *et al.*, 1996). This conclusion is in agreement with Kβ XES data (Bergmann *et al.*, 1998; Messinger *et al.*, 2001b) and with ^{55}Mn ENDOR spectra (Kulik *et al.*, 2007; Peloquin *et al.*, 2000) of PSII centers indicating Mn_4(III,IV,IV,IV) in the S_2 state. In agreement with these relatively high oxidation states of the Mn ions it was shown that the WOC can also be poised in states more reduced than the S_0 state (see Fig. 1.10) (for reviews see (Debus, 1992; Hillier & Messinger, 2005)). These S_{-i} states (i = 1,…,5) can be generated by incubation of PSII samples with small, hydrophilic reductants such as NH_2OH, NH_2NH_2 or $NO^{\bullet}$ (Bouges, 1971; Ioannidis *et al.*, 1998; Messinger *et al.*, 1991; Sarrou *et al.*, 2003). This approach with reductants aims at 'calibrating' the Mn redox states based on the reasonable assumption, that the lowest state that can be generated by these reductions is Mn_4(II,II,II,II). It is interesting to compare this reduction process with intermediates that can be observed during photoassembly of the WOC from Mn-depleted PSII samples (*apo*–PSII) and free Mn^{2+} (Ananyev *et al.*, 2001; Ono, 2001; Dismukes *et al.*, 2005), because, the reduction of the Mn_4O_xCa complex below the redox level of the S_0 state may be viewed as a reversal of the photoactivation process. EPR (Ioannidis *et al.*, 1998; Messinger *et al.*, 1997b; Messinger *et al.*, 1997c; Sarrou *et al.*, 2003) and XAS measurements on the S_{-i} states (Riggs *et al.*, 1992; Riggs-Gelasco *et al.*, 1996) proved that Mn centered reductions occur down to at least the level of the S_{-2} state, while a detailed analysis of FIOPs showed that the S_{-3} state is rather stable (hours) (Messinger *et al.*, 1997a). Moreover, indications for the existence of short-lived S_{-4} and the S_{-5} states were also presented (Messinger *et al.*, 1997a; Messinger *et al.*, 2001a). Photoactivation experiments have identified the first long-term stable

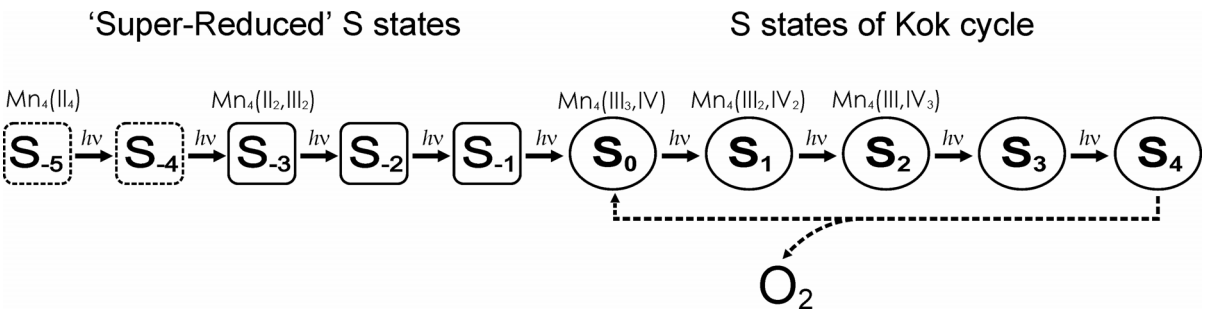

FIGURE 1.10 The Kok Model extended to so-called 'super-reduced' S_i states including the proposed oxidation states of Mn in some of the S_i states.

intermediate as being Mn_4(II,II,III,III) (Tamura & Cheniae, 1987; Tamura *et al.*, 1989). Thus, one can assume that the lowest long-tern stable state of the WOC (the S_{-3} state) has the same redox level as the first long-lived photoactivated state, *i.e.* Mn_4(II,II,III,III). All these considerations provide good evidence for the idea that the Mn oxidation states in the four electron steps more oxidized S_1 state are Mn_4(III,III,IV,IV), and not Mn_4(III,III,III,III) as proposed by some groups (Kuzek & Pace, 2001; Zheng & Dismukes, 1996). The distributions Mn_4(II,III,IV,IV) or Mn_4(III,III,III,IV) have been suggested for the S_0 state (Haumann *et al.*, 2005a; Messinger *et al.*, 2001b; Ono *et al.*, 1992; Roelofs *et al.*, 1996) and recent ^{55}Mn ENDOR results strongly favor the latter suggestion (Kulik *et al.*, 2005; Kulik *et al.*, 2007). The nature of the oxidation in the $S_2 \rightarrow S_3$ transition is hotly contested. Some XAS researchers suggest a ligand centered oxidation in this step (Messinger *et al.*, 2001b; Roelofs *et al.*, 1996; Yachandra, 2005), while others favor another Mn–based step (Dau *et al*, 2003; Haumann *et al.*, 2005b).

1.4.3.2 Structure of the Mn_4O_xCa Complex

In order to understand the mechanism of the water splitting process, numerous techniques have been applied to study the structure and oxidation states of the Mn_4O_xCa complex in the S-state cycle. Important insight about the Mn_4O_xCa complex was provided by: X-ray diffraction crystallography (XRD) and Extended X-ray Absorption Fine Structure (EXAFS) spectroscopy.

Recent **XRD** investigations on PSII at 3.0 Å (Loll *et al.*, 2005) and 3.5 Å (Ferreira *et al.*, 2004) have provided important structural information about the WOC. The XRD-derived structures of the Mn_4O_xCa cluster together with some of the suggested ligands are shown in Fig. 1.11. In both models the assignment of the amino acid ligands (Asp170, Glu189, His332, Glu333, His337, Asp342 and Ala344 of the D1 protein) of the Mn_4O_xCa complex is consistent with a wide range of mutational studies (Debus, 2001; Debus, 2005; Diner, 2001). In addition, one ligand (Glu354) from CP43 was identified (Ferreira *et al.*, 2004) (shown in Fig. 1.13). Because of limited resolution (≥ 3.0 Å), EXAFS-derived information about Mn–Mn and Mn–Ca distances has been used for the construction of these models. However, specific radiation damage to the Mn_4O_xCa cluster, *i.e.* radiation-induced structural changes,

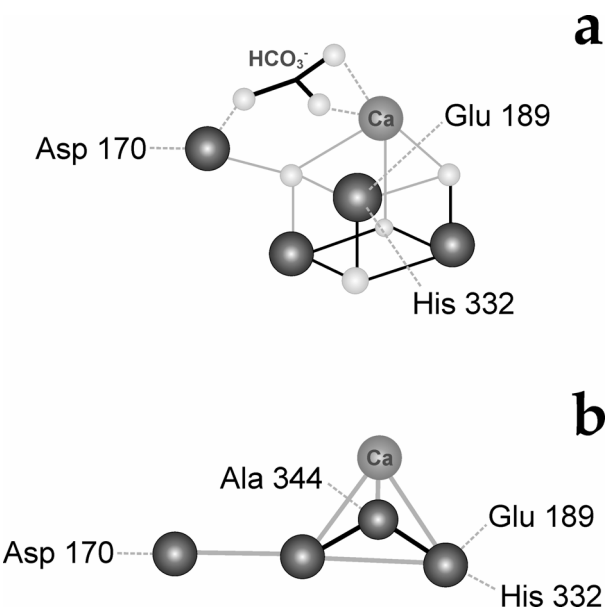

FIGURE 1.11 Proposed structures of the Mn_4O_xCa complex derived from XRD studies at (***a***) 3.5 Å (Ferreira *et al.*, 2004) and (***b***) 3.0 Å (Loll *et al.*, 2005). The black spheres represent 4 Mn ions, grey spheres stands for Ca^{2+}, while small grey spheres indicate bridging oxygen ions. Mn–Mn distances of ca. 2.7 Å are marked by black lines, and Mn–Ca distances of ~ 3.3–3.4 Å are signified by grey lines. Some of suggested ligands to the Mn_4O_xCa complex are also shown (connected by dashed grey lines). Model *b* does not contain any suggestion for the arrangement of the μ-oxo bridges. Adapted from (Messinger & Renger, 2008).

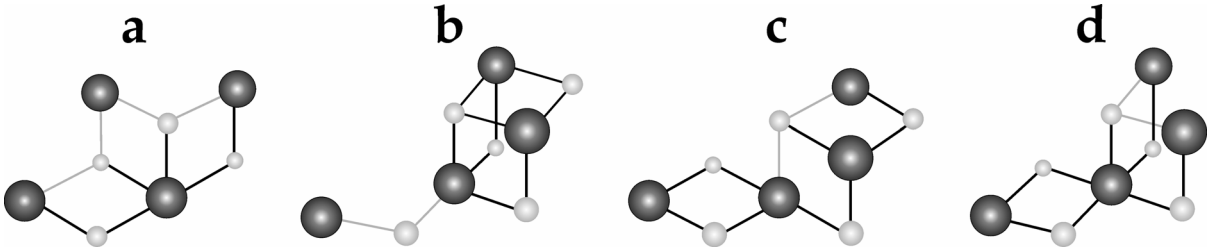

FIGURE 1.12 Proposed structures of the Mn_4O_xCa complex based on EXAPS studies (Yano *et al.*, 2005a). All ions and distances are marked as in Fig. 1.11. Adapted from (Messinger & Renger, 2008).

caused by the reduction of Mn^{III} and Mn^{IV} to Mn^{II} by X-ray generated radicals, complicate the interpretation of XRD results on the structure of the Mn_4O_xCa complex (Grabolle *et al.*, 2006; Yano *et al.*, 2005b).

EXAFS spectra provide information about the numbers, types, and distances of the backscattering atoms from the absorber (mostly Mn or Ca for PSII experiments) (Yachandra, 1995). Manganese EXAFS studies have firmly shown that two or three 2.7 Å Mn–Mn bis-μ-oxo and at least one 3.3–3.4 Å Mn–Mn mono-μ-oxo motifs are present in the Mn_4O_xCa cluster in the S_1 state. Mn–O or Mn–N vectors were also found, at a distance of 1.8–2.0 Å. Moreover, the 3.3–3.4 Å shell appeared to comprise one or two Mn–Ca contributions (for reviews see (Messinger, 2004; Robblee *et al.*, 2001; Yachandra *et al.*, 1996)). Recent results obtained from calcium EXAFS have established most convincingly that the intact WOC comprises a cluster containing both manganese and calcium (Cinco *et al.*, 2002; Cinco *et al.*, 2004). From this information several different geometries were proposed for the Mn_4O_xCa complex and some of these were considered to be likely models (DeRose *et al.*, 1994; Yachandra, 2005). A recent extended range EXAFS study revealed that the Mn_4O_xCa complex consists of three (and not two) short Mn–Mn distances: two ~2.7 Å Mn–Mn, and one ~2.8 Å Mn–Mn (Yano *et al.*, 2005a). These data significantly reduced the number of options for possible structures of the Mn_4O_xCa complex, and favoured those models shown in Fig. 1.12. Ca should be incorporated into each of the proposed structures so that 1–2 Mn–Ca vectors exist with an average angle of about 20° to the membrane normal (Cinco *et al.*, 2004).

More recently, the structure of the WOC in S_1 state was investigated by EXAFS measurements on PSII single crystals from *T. elongatus* free of radiation damage (Yano *et al.*, 2006). These data allowed identifying model *c* (Fig. 1.12*c*) as the most probable structure of the Mn_4O_x core within intact Mn_4O_xCa complex. Moreover, this model was placed in three

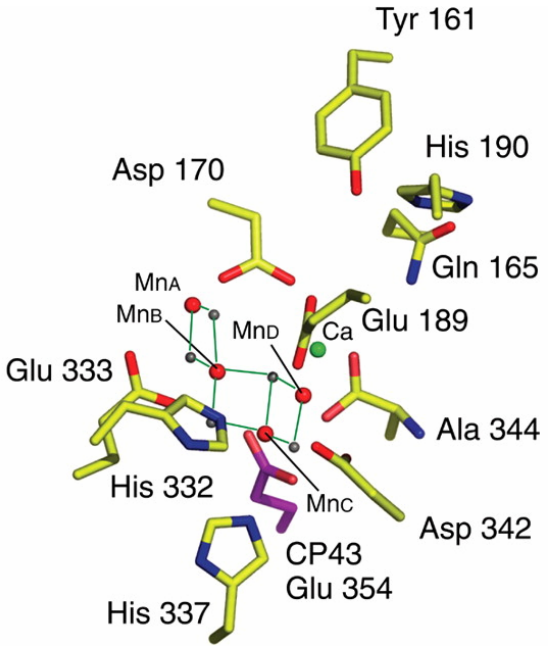

FIGURE 1.13 Placement of model ***c*** (shown in Fig. 1.11) for the Mn_4O_xCa cluster derived from polarized Mn EXAFS in relation to the putative ligands obtained from XDR at 3.0 Å (Loll *et al.*, 2005). The spheres represent Mn (red), Ca (green), and the bridging oxygen ligand atoms (grey). Adapted from (Yano *et al.*, 2006).

distinct orientations into the electron density maps obtained by XRD at 3.0 Å (Fig. 1.13), with correspondingly different positions for the Ca ion (Yano *et al.*, 2006).

The structural change as detected by EXAFS from the S_1 to S_2 state is hardly discernible (Yachandra, 2005; Yano *et al.*, 2005a). In contrast, the biggest structural changes seem to occur during the S_2 to S_3 transition, as can be observed in Mn EXAFS spectra of PSII samples. Thus, in the S_3 state, all 2.7Å Mn–Mn vectors lengthened to 2.82 Å and 2.95 Å. Moreover, the longer 3.3 Å Mn–Mn and 3.4 Å Mn–Ca vectors increased to 3.34 and 3.6 Å, respectively (Liang *et al.*, 2000). There is also direct evidence of structural changes during the S_0 to S_1 transition. Compared to S_1, one of the short Mn–Mn distances (2.7 Å) is longer by ~0.15 Å (Robblee *et al.*, 2002). Such increase was explained by assuming that one μ-oxo bridge is protonated in S_0 and loses its proton during the S_0 to S_1 transition (Baldwin *et al.*, 1994; Robblee *et al.*, 2002; Yano *et al.*, 2005a). This idea is fully consistent with the most recent EPR and ^{55}Mn ENDOR data obtained by Kulik and co-workers (Kulik *et al.*, 2007). Based on their results the authors proposed a

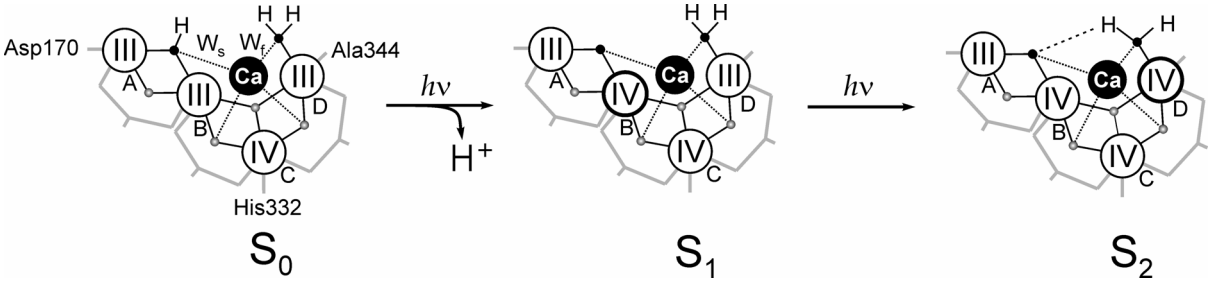

FIGURE 1.14 Molecular model of the $S_0 \rightarrow S_1$ and $S_1 \rightarrow S_2$ transitions. The Mn ions are symbolized by black circles, and their oxidation states are given in roman numbers. Ca ions are indicated by black spheres. Bridging oxygen ions are shown by grey dots, while the oxygen atoms of the slow (W_s) and fast (W_f) exchanging substrate water molecules are indicated as black dots. The grey "clamps" stand for Glu333, Glu354, and Asp342 (from left to right), which are assumed to be bidentate ligands of the Mn_4O_xCa cluster. Adapted from (Kulik *et al.*, 2007).

molecular mechanism for the first steps of the oxidation cycle ($S_0 \rightarrow S_1 \rightarrow S_2$ transition), which is shown in Fig. 1.14.

Protein ligand environment around the WOC also undergoes some structural or orientational changes during the S-state cycle as observed in the FTIR studies using site-specific mutants and isotopic labeling (Chu *et al.*, 2004; Debus *et al.*, 2005; Kimura *et al.*, 2005a; Kimura *et al.*, 2005b, Strickler *et al.*, 2006).

1.4.4 INORGANIC COFACTORS IN OXIDATIVE WATER SPLITTING

1.4.4.1 Introduction

Besides the Mn and calcium (Ca^{2+}) cations, also the anions, chloride (Cl^-) and hydrogencarbonate (HCO_3^-) have been reported to be essential for optimal oxygen evolution activity and photoactivation (van Gorkom & Yocum, 2005; van Rensen & Klimov, 2005; Ananyev *et al.*, 2001). This suggests that these inorganic ions should have an important functional role in the catalytic site and possibly in the water splitting mechanism.

In addition to the above discussed evidence for the physical proximity of Ca^{2+} to Mn, there is also biochemical support for its functional relevance in water oxidation

(recently reviewed in (Miqyass *et al.*, 2007, van Gorkom & Yocum, 2005)). Removal of Ca^{2+} blocks water oxidation chemistry at an early stage of the S-state cycle, preventing the O–O bond formation, and strontium (Sr^{2+}) is the only other divalent cation that can partially restore oxygen evolution in Ca-depleted PSII samples (Ghanotakis *et al.*, 1984). However, even in Sr^{2+}-reconstituted PSII samples all the S-state transitions are slowed (Boussac *et al.*, 1989; Westphal *et al.*, 2000). To explain these results, several possible roles (not mutually exclusive) for calcium in PSII have been suggested: (*i*) Ca may play an electrostatic role in maintaining the correct reduction potential of the WOC (Riggs-Gelasco *et al.*, 1996); (*ii*) Ca may be an important constituent of the proton relay network of the WOC, which is essential for activity (Barry *et al.*, 2005; Hillier & Messinger, 2005); and, (*iii*) Ca may be involved in formation of the O–O bond, possibly *via* substrate water binding (Hendry & Wydrzynski, 2003; Hillier & Messinger, 2005). In addition, Ca appears to be a prerequisite for the proper photoassembly of the Mn_4O_xCa cluster (Tyryshkin *et al.*, 2006).

Analysis of the roles of HCO_3^- and Cl^- for water oxidation is even more complicated. Both have been discussed as ligands of the WOC and/or as cofactors during water splitting. However, at present, firm experimental evidence for direct binding at the Mn_4O_xCa complex exists neither for HCO_3^- nor for Cl^-.

1.4.4.2 Role of Hydrogencarbonate in PSII

Many experimental results are consistent with the notion that hydrogencarbonate (HCO_3^- or HC), also known as bicarbonate, is required by PSII for both maximal activity and stability; however, the interpretation of the 'bicarbonate effect' has a history full of controversies (reviewed in (Klimov & Baranov, 2001; Stemler, 2002; van Rensen, 2002; van Rensen *et al.*, 1999; van Rensen & Klimov, 2005)).

The first report on 'HC-effects' on the electron flow in chloroplasts (Hill reaction) (see Section 1.1.2) dates back to the year 1958 (Warburg & Krippahl, 1958). However, this phenomenon was experimentally difficult to reproduce until dependable methods of HC depletion from the samples were developed (Stemler & Govindjee, 1973) (described and analyzed in detail in Sections 2.2.3 and 4.1). In particular, chemical analogs of HC, such as formate (Stemler & Radmer, 1975) or acetate (Stemler *et al.*, 1974) began to be used to replace HC its binding site(s) in PSII. In the early 1970s the stimulating effects of HC was thought to arise from interactions of HC with the WOC (Stemler *et al.*, 1974; Stemler & Govindjee, 1973) and even different models including HC as substrate for photosynthetic water oxidation were suggested (Metzner, 1978; Warburg, 1964). The latter suggestions were disproved by mass spectrometric experiments employing ^{18}O-labeled HCO_3^- or $H_2{}^{18}O$ (Clausen *et al.*, 2005; Hillier *et al.*, 2006; Radmer & Ollinger, 1980). In 1975 strong evidence for the action of HC on the electron acceptor side of PSII was presented (Wydrzynski & Govindjee, 1975). It was suggested that HC is required for fast reoxidation of $Q_A^{\bullet -}$ by $Q_B/Q_B^{\bullet -}$. This interpretation became the dominating view (for review see (van Rensen, 2002; van Rensen & Klimov, 2005; van Rensen *et al.*, 1999)), and it is also supported by two recent PSII crystal structures that display HC as a ligand of the non-heme Fe between the two acceptor side quinones Q_A and Q_B (Ferreira *et al.*, 2004; Loll *et al.*, 2005) (see also Section 1.3.1). Although, it was shown in 1980's that HC-depletion may effect both the

electron acceptor and the electron donor side of PSII (Mende & Weissner, 1985), the possible role of HC within the donor side of PSII has remained unclear for a long time (Stemler, 2002; van Rensen & Klimov, 2005).

Starting from 1995 the hypothesis for an additional role of HC at the donor side of PSII was revived by experiments showing that HC is required for both maximal activity and stability of the WOC (Allakhverdiev *et al.*, 1997; Klimov *et al.*, 1995a; Klimov *et al.*, 1995b, Klimov *et al.*, 1997a; Wincencjusz et al., 1996). The stimulating effects of HC ions are especially pronounced during reactivation (photoactivation) of the donor side of PSII with exogenous Mn^{II} ions added to Mn-depleted PSII (so-called *apo*-WOC-PSII) preparations (Baranov *et al.*, 2000; Baranov *et al.*, 2004). Electrochemical and EPR characterizations of HC complexes with Mn^{II} and Mn^{III} ions show that these ions form electroneutral complexes, and that the dissociation constant (K_d) of the Mn^{III}-HC complex is nearly 10 orders lower than the K_d of the Mn^{II}-HC complex (Kozlov *et al.*, 2004). It has been suggested that the electroneutrality of Mn^{II}-HC complexes may facilitate the photo-induced assembly of the inorganic core of the WOC (Dismukes *et al.*, 2001; Kozlov *et al.*, 2004). Furthermore, there is evidence for protective effects of HC on the WOC against photoinhibition and thermoinactivation (Klimov *et al.*, 1997b; Zharmukhamedov *et al.*, 2007), as well as against extraction of the extrinsic proteins of the WOC (Pobeguts *et al.*, 2007). However, in functionally active PSII, the 'bicarbonate effect' on the WOC is relatively small (Klimov *et al.*, 1995a; Klimov & Baranov, 2001). Currently the following explanations for the involvement of HC in the events within the WOC are considered (Klimov & Baranov, 2001; van Rensen & Klimov, 2005): (*1*) HC is required only for the process of assembly of the functionally competent WOC from *apo*-WOC-PSII and Mn^{II}, and then it leaves the site, (*2*) HC stabilize the WOC indirectly through its binding to other components in the vicinity of the Mn_4O_xCa cluster or (*3*) HC is a structural part of the WOC essential for its function and stability; it may be considered as a direct ligand to the assembled Mn_4O_xCa cluster and its removal from the WOC makes Mn_4O_xCa cluster unstable. In the recent XRD structure with 3.5 Å resolution, a HC molecule has been modeled to bind at the Mn_4O_xCa cluster (Ferreira *et al.*, 2004) (see also Fig. 1.11*a*). However, this assignment has not been confirmed in the later 3.0 Å XDR structure (Loll *et al.*, 2004) (Fig. 1.11*b*).

Thus, despite the fact that numerous data demonstrate the participation of HC in the donor side reactions of PSII, its binding sites and its role in the photosynthetic water oxidation mechanisms remain unclear.

1.4.4.3 Role of Chloride in Photosynthetic Water Oxidation

Already more then 60 years (Warburg & Lüttgens, 1946) chloride (Cl^-) was shown to be a necessary cofactor for the oxygen–evolving process. However, until now there is a lack in consensus on where and how Cl^- ions specifically interact with the water–splitting center (recently reviewed in (Popelková & Yocum, 2007; Homann, 2002; van Gorkom & Yocum, 2005)). Although chloride has not been identified in recent PSII XRD structures at 3.5 Å (Ferreira *et al.*, 2004) and 3.0 Å (Loll *et al.*, 2005), biochemical experiments with radioactively labelled $^{36}Cl^-$ demonstrated the specific binding of one Cl^- per WOC (Lindberg *et al.*, 1990; Lindberg *et al.*, 1993).

Currently two different methods are used for Cl^--depletion from the WOC: *i*) dialysis against Cl^- free medium (Olesen & Andréasson, 2003) or *ii*) removal of PSII extrinsic proteins and Cl^- by addition of sodium sulfate at high pH (Sandusky & Yocum, 1983; Wincencjusz *et al.*, 1997). Oxygen measurements of Cl^- depleted samples employing the dialysis method showed that all PSII centers are still active, but that they evolve O_2 at a reduced rate (to 30–40% of the control rate) due to slower S-state turnover (possibly at the $S_2 \rightarrow S_3$ step) (Lindberg *et al.*, 1993). Therefore, these authors suggested that chloride is not absolutely required for water splitting and that it does not bind directly to Mn (Olesen & Andréasson, 2003). In contrast, Cl^- removal by sulfate treatment completely suppresses the oxygen-evolving activity (Wincencjusz *et al.*, 1997).

Cl^- can be substituted by other anions with an order of efficiency of $Br^- \approx Cl^- >> NO_3^- > NO_2^- > I^-$ (Homann, 1988; Kelley & Izawa, 1978; Ono *et al.*, 1987; Sandusky & Yocum, 1984). Nevertheless, the $S_3 \rightarrow S_0$ transition is always slower than in the presence of chloride (Sinclair, 1984; Wincencjusz *et al.*, 1999). Recent optical studies demonstrate that chloride depletion (sulfate treatment) leads to a block of the $S_2 \rightarrow S_3$ and $S_3 \rightarrow S_0$ transitions (Wincencjusz *et al.*, 1997; Wincencjusz *et al.*, 1998). Changes in the S_2 EPR signals are associated both with Cl^- removal and with reconstitution of other anions, such as fluoride and azide, at the Cl^- site (Ono *et al.*, 1986; Haddy *et al.*, 2000; Jajoo *et al.*, 2005; Yu *et al.*, 2005). However, Cl^- replacement with these two anions inhibits activity (Kawamoto *et al.*, 1995; Haddy et al., 1999; Olesen & Andréasson, 2003). Acetate binding is also known to compete with that of Cl^- (Kühne *et al.*, 1999). Results of pulsed EPR experiments on samples, in which acetate or azide have been used to remove Cl^-, place the anion in close proximity to Mn (Clemens *et al.*, 2002; Force *et al.*, 1997; Yu *et al.*, 2005). Preliminary Mn EXAFS data are consistent with Cl^- ligation to Mn in the S_3 state (Fernandez *et al.*, 1998; Yachandra, 2005). These results are suggestive for Cl^- site located in the immediate vicinity of the Mn_4O_xCa cluster. On the other hand, there are several FTIR studies indicating that Cl^- is not a direct ligand to Mn (Hasegawa *et al.*, 2002; Hasegawa *et al.*, 2004). This idea is supported by recent X-ray spectroscopy measurements on Cl^- depleted samples that were reconstituted with bromide (Haumann *et al.*, 2006). Thus, there is no conclusive evidence for Cl^- binding to the Mn_4O_xCa complex at present.

Cl^- is currently discussed to have a role (*i*) in maintaining a hydrogen-bonding network, which facilitates proton transfer (Olesen & Andréasson, 2003), (*ii*) in tuning the redox potential of the Mn_4O_xCa cluster (Boussac & Rutherford, 1994), (*iii*) in charge balancing of the Mn_4O_xCa cluster by only binding in certain S_i states (Hasegawa *et al.*, 2004; Haumann *et al.*, 2006; Messinger, 2000), (*iv*) in preventing the binding of harder ligands such as OH^- to the Mn_4O_xCa cluster (van Gorkom & Yocum, 2005), and (*v*) in supporting functionally relevant structural changes in the protein shell during S-state cycle (Kimura et al., 2005c).

1.5 THE SCOPE OF THIS WORK

To elucidate the basics of photosynthetic water oxidation chemistry one needs to know its energetics and the structure and function of all the cofactors participating in this reaction. This thesis is focused on *1*) the exploration of the roles of the inorganic cofactors HCO_3^- and Cl^- and, *2*) on a comparative study of the energetics of the water splitting reaction of PSII in Chl *a*- and Chl *d*-containing organisms.

Chapter 2

Materials and Methods

2.1 CHEMICALS AND MATERIALS

2.1.1 REAGENTS

All chemicals used in this study were of analytical (≥ 98%) or higher grade (99.97% - 99.99%). The reagents were obtained from *Sigma*, *Aldrich*, *Fluka*, *Merck*, *Cambridge Isotope Laboratories, Isotech* etc.

For all aqueous solutions deionised and filtrated (Millipore Quality, MQ) water was used if not stated otherwise.

2.1.2 BUFFERS AND STOCK SOLUTIONS

TABLE 2.1. Buffers and stock solutions used for the experiments in this study

Abbreviation	Composition/Description	pH
Buffers used in sample preparation procedures		
G1 buffer	GRINDING BUFFER: 1 mM EDTA, 50 mM HEPES/NaOH, 4 mM $MgCl_2$, 0.4 M NaCl, 5 mM Sodium Ascorbate [A], 2 mg/mL BSA [A]	7.5
G2 buffer	400 mM Sucrose, 1 mM EDTA, 20 mM HEPES/NaOH, 35 mM NaCl, 2.5 mM Sodium Ascorbate	7.8
W1 buffer	WASH BUFFER: 8 mM $MgCl_2$, 150 mM NaCl, 50 mM MES/NaOH	6.0
W2 buffer	5 mM $MgCl_2$, 35 mM NaCl, 20 mM Tris/HCl	7.5
RI buffer	RESUSPENSION/INCUBATION BUFFER: 5 mM $CaCl_2$, 10 mM $MgCl_2$, 15 mM NaCl, 50 mM MES/NaOH	6.0
S1 buffer	SUCROSE BUFFER: 400 mM Sucrose, 5 mM $CaCl_2$, 5 mM $MgCl_2$, 15 mM NaCl, 50 mM MES/NaOH	6.0
S2 buffer	330 mM Sucrose, 35 mM NaCl, 20 mM MES/NaOH	6.5
Buffers [B] used for during various measurements		
MCMH buffer	0.4 M Mannitol, 20 mM $CaCl_2$, 10 mM $MgCl_2$, 50–80 mM HEPES/NaOH	6.8–7.4
MCMM buffer	0.4 M Mannitol, 20 mM $CaCl_2$, 10 mM $MgCl_2$, 50–150 mM MES/NaOH	5.0–6.5
*HC(+) medium**	MCMM buffer* containing 2 mM $NaHCO_3$	6.3–6.5
*HC_{air}(–) medium**	MCMM buffer* depleted of endogenous CO_2/HCO_3^- by means of 60 min flushing with air depleted of CO_2 by passage through a solution of 50% NaOH and a 20-cm layer of ascarite	6.3
*HC_{Ar}(–) medium**	MCMM buffer* depleted of endogenous CO_2/HCO_3^- by flushing with argon for 40–60 min. In some cases this procedure was combined either with brief boiling or short heating (50 °C, 10 min) of the buffer	5.0–6.5
Cl^--free buffer	0.2 M Sucrose (≤ 0.005% Cl), 20 mM MES (≤ 0.005% Cl)/NaOH	6.3
Stock Solutions		
DCBQ	20 mM DCBQ dissolved in DMSO and kept for storage at –30 °C	
Gramicidin	1 M NH_4Cl in MQ water and kept at 0 °C	
FeCy	50 mM $K_3[Fe(CN)_6]$ dissolved in MQ water and kept at –30 °C	
PPBQ	20 mM PPBQ dissolved in DMSO and kept for storage at –30 °C	
*CA**	100 μg ml^{-1} CA dissolved in HC_{Ar}(-) medium* and kept on ice	6.3

[A] Sodium Ascorbate and BSA were added to *G* buffer shortly before grinding. [B] All sample buffers were pH calibrated at the appropriate temperature. Asterisks indicate the buffers/stock solutions that were prepared shortly (couple hours) before the experiments. All other 'specific' buffers/stock solutions are described at appropriate sections of this thesis.

2.1.3 BIOLOGICAL SAMPLES

- *Spinacia oleracea* (spinach) – a specimen of higher plants. For the present study we employed thylakoid membranes and PSII membrane fragments isolated from spinach leaves. Fresh spinach was bought from the market or local farmers and the sample preparations (see below) were done at the same day. All isolation steps were performed in the cold room on ice in very dim green light.

- *Acaryochloris marina* – Chl *d*–containing cyanobacterium. *A. marina* cells were grown in the laboratory of Prof. G. Renger as described by Chen and coworkers (Chen *et al.*, 2002) in artificial seawater-based K + ESM (Erd-Schreiber modified) medium (McLachlan, 1973) at 28 °C under an illumination intensity of 20 μE m^{-2} s^{-1} (*Osram TLD 18W-25* fluorescent tubes) and continuous aeration. The sells were harvested 1-2 days before the measurements.

2.2 PREPARATIVE PROCEDURES

2.2.1 THYLAKOID MEMBRANE PREPARATION

Thylakoid membranes were isolated from spinach leaves by two different procedures.

For most experiments thylakoids were prepared as described previously (Winget *et al.*, 1965) with slight modifications (Messinger & Renger, 1993). Fresh spinach leaves were ground in *G1* buffer in a blender (*Waring Blender*, USA) for 10 s (3 times). The homogenate was then filtered through one layer of cheesecloth and immediately centrifuged for 10 min at 8.000 rpm in a *JA-10* rotor (*Avanti centrifuge*, *Beckman Coulter*™). The pellet containing thylakoid membranes was carefully resuspended in buffer *W1* and centrifuged again at 6.000 rpm for 10 min. After that the thylakoids were resuspended in buffer *S1* and washed once before being frozen in small aliquots in liquid N_2 and stored at –80 °C until used.

For some experiments that were performed in Pushchino (FIOPs measurements with a laboratory-built, Clark-type Pt/Ir electrode) thylakoid membranes were prepared according to (Robinson & Yocum, 1980; Robinson *et al.*, 1980) with some modifications (20 mM HEPES/NaOH (pH 7.8), 35 mM NaCl and 2.5 mM Sodium Ascorbate were used instead of 20 mM Tricine (pH 8.0), 2 mM $MgCl_2$ and 0.2% BSA) in *G2* buffer. After centrifugation at 5.000×*g* for 20 min, the pellet was washed twice in medium *W2* and resuspended with *S2* buffer containing 10% glycerol. The thylakoids [*c*(Chl)=2.5 mg ml^{-1}] were then frozen at –85 °C until used.

2.2.2 PREPARATION OF PSII MEMBRANE FRAGMENTS

Photosynthetic membrane fragments, *'BBY' type*, with high oxygen evolving activity were prepared from fresh thylakoid membranes according to the method of Berthold and co-workers (Berthold *et al.*, 1981) with minor modifications (Ono & Inoue, 1983). Thylakoid membranes from spinach were resuspended and homogenised in *RI* buffer at 2.5 mg Chl ml^{-1}. The total volume (*V*) of the thylakoid suspension was then diluted with *V*/4 ml of a 25% (v/v) Triton X-100 solution (made up in *RI* buffer). This was added slowly to the thylakoid suspension to solubilise the stromal thylakoid membranes. The final detergent concentration for membrane solubilisation was 5% (50 mg ml^{-1}) Triton X-100 at a concentration of 2 mg Chl ml^{-1}. The thylakoid/Triton X-100 solution was stirred in the dark at 4 °C for 5–15 min before centrifugation for 5 min at 20.000 rpm in a *JA-20* rotor (*Avanti centrifuge*, *Beckman Coulter*™) to remove starch contamination and non-solubilised material. The resulting supernatant (excluding the white starch pellet at the bottom) was then resuspended in *RI* buffer and centrifuged for 2 min at 3.000 rpm (*JA-20* rotor). The

supernatant containing the PSII membrane fragments was washed by centrifugation (20.000 rpm/12 min, *JA-20* rotor) more than three times in *S1* buffer to remove residual detergent and starch and then finally resuspended and homogenised in the same medium before being frozen as small beads in liquid N_2 and kept at –80 °C.

2.2.3 CO_2/HCO_3^- – DEPLETION PROCEDURES

2.2.3.1 Sample Washing/Incubation in C_i – free Buffers

Two procedures (Klimov *et al.*, 1995a; Klimov *et al.* 1995b; Klimov *et al.*, 1997a) were used for the reduction of the inorganic carbon (C_i) level in the samples with the following minor modifications:

(i) Sedimented thylakoids were diluted 200-fold into HC_{air}(–) medium (described in Table 2.1). The samples were subsequently incubated in this medium for 10–30 min at 4 °C in the dark (*'HC_{air}(–)thylakoids'*).

(ii) Thylakoids were 50–80-fold diluted with the HC_{Ar}(–) medium (see Table 2.1) and subsequently dark-incubated on ice for 2–10 h under argon atmosphere in sealed vials. Thereafter the thylakoids were collected by centrifugation and washed at least twice in the HC_{Ar}(–) medium (*'HC_{Ar}(–) thylakoids'*).

2.2.3.2 Sample Treatment with Formate and Acetate

Formate/acetate treatments of the samples were done according to (Stemler *et al.*, 1974; Stemler & Radmer, 1975) with some modifications described in Sections 4.2.1.3 and 5.2.1.4 (for formate), and Section 4.2.1.4 (for acetate).

2.2.4 DEPLETION OF MANGANESE FROM THE WOC

Removal of Mn from PSII samples was achieved employing several procedures: *i*) treatments with high concentrations of NH_2OH, NH_2NH_2 (Cheniae & Martin, 1971; Kretschmann & Witt, 1993), *ii*) tris-treatment (Klimov *et al.*, 1982), *iii*) heat-treatment (Messinger *et al.*, 1997b), and *iv*) HCl-treatment (Yocum *et al.*, 1981). Details of these treatments described in Section 5.2.1.3.

2.2.5 NH_2OH AND NH_2NH_2 TREATMENTS

Treatment of the samples with NH_2R (R = -OH; -NH_2) solutions was done according to (Messinger *et al.*, 1991; Messinger *et al.*, 1997a) with minor modifications described in Section 4.2.1.5.

2.2.6 CHLORIDE-DEPLETION/AZIDE TREATMENT

PSII samples were depleted of chloride by prolonged dialysis against Cl^--free buffer (see Table 2.1) (Olesen & Andréasson, 2003) and treated with azide (Haddy *et al.*, 2000; Yu *et al.*, 2005) with small changes described in detail in Sections 6.2.1.3 and 6.2.1.4.

2.3 EXPERIMENTAL TECHNIQUES AND TOOLS

2.3.1 CHLOROPHYLL DETERMINATION

Determination of the chlorophyll content in spinach thylakoids and BBY fragments was done according to (Porra *et al.*, 1989): Chlorophyll was extracted by stirring with 80% buffered acetone solution (2.5 mM $Na_2HPO_4/H_2NaPO_4 \cdot 2H_2O$, pH 7.8) (10 μl of PSII sample in 10 ml 80% acetone solution). After mixing and filtration (or centrifugation for 1 min at 10.000×*g*), the absorption spectra of the supernatant were measured against 80% buffered acetone solution at 646.6 nm, 663.6 nm and 750 nm using an *Unicam UV2-300* spectrophotometer. The obtained absorption (*A*) values were analysed using following equations:

$$\left[17.75\left(A_{646.6}-A_{750}\right)+7.34\left(A_{663.6}-A_{750}\right)\right]k \quad \textit{for } [\text{Chl } a{+}b] \qquad (\mathbf{2.1})$$

$$\left[12.25\left(A_{663.6}-A_{750}\right)+2.55\left(A_{646.6}-A_{750}\right)\right]k \quad \textit{for } [\text{Chl } a] \qquad (\mathbf{2.2})$$

$$\left[20.31\left(A_{646.6}-A_{750}\right)+4.91\left(A_{663.6}-A_{750}\right)\right]k \quad \textit{for } [\text{Chl } b] \qquad (\mathbf{2.3})$$

where *k* is dilution factor ($k = \mu l_{solution}/\mu l_{sample}$).

The chlorophyll concentration of *A. marina* cells was determined according to the methods described in (Ritchie, 2006) by using 90% acetone for chlorophyll extraction and measuring absorption spectra at 664 nm and 691 nm.

2.3.2 RATE MEASUREMENTS OF PHOTOSYNTHETIC O_2 EVOLUTION

The oxygen-evolving activity of PSII samples was measured with a Clark-type electrode (*Hansatech*) at 20–25 °C for 60 s after the start of continuous illumination (250 W halogen lamp) at the saturating intensity through a *Schott GG 455* (2 mm) and *Schott KG 3* (2 mm) filters, 8-cm water filter, and 2-cm $CuSO_4$ solution (5%) as a heat filter. Measurements were done at 10–20 μg Chl ml^{-1} in 1-ml chamber filled with designated buffers in the presence of 200 μM PPBQ (or 100 μM DCBQ) plus 500–1000 μM FeCy as artificial electron acceptors. For activity measurements of spinach thylakoids 10–100 μM gramicidin was added as uncoupler. The electrode was calibrated using air-saturated water at atmospheric pressure. The oxygen evolution rate was expressed in $\mu mol\ (O_2) \cdot mg\ (Chl)^{-1} \cdot h^{-1}$.

2.3.3 MEASUREMENTS OF FLASH-INDUCED O_2 EVOLUTION PATTERNS

2.3.3.1 Highly Sensitive-Membrane Covered Clark-Type Electrode

The laboratory-built (Pushchino), Clark-type Pt/Ir electrode (diameter 5.5 mm) was equipped with a special polymer membrane (from '*CVS*' pack) which was stretched to a thickness of about 1 μm (Ananyev *et al.*, 1992; Ananyev & Dismukes, 1996). It prevented the interaction of added electron acceptors with the polarized electrode. For each measurement 20 μl sample with a Chl concentration of 900 μg ml^{-1} was layered into a chamber (Ananyev *et al.*, 1988) of 0.3 mm thickness that was formed by the Teflon cover on top of the membrane (Fig. 2.1).

The electrode was operated at a polarization voltage of –700 mV. The measurements were performed in the presence of 0.5 mM $K_3[Fe(CN)_6]$ as electron acceptor. Before measurements were started, the samples were polarized for 6 min at

20 °C. For saturating light flashes (duration of 10 μs), a Xenon flash lamp (*ISSH-400-3*) with a repetition rate of 0.5 Hz was used (Ananyev *et al.*, 1992). The O_2 signals were amplified by a laboratory-built-low-impedance circuit and integrated over a time of 0.1–0.5 s.

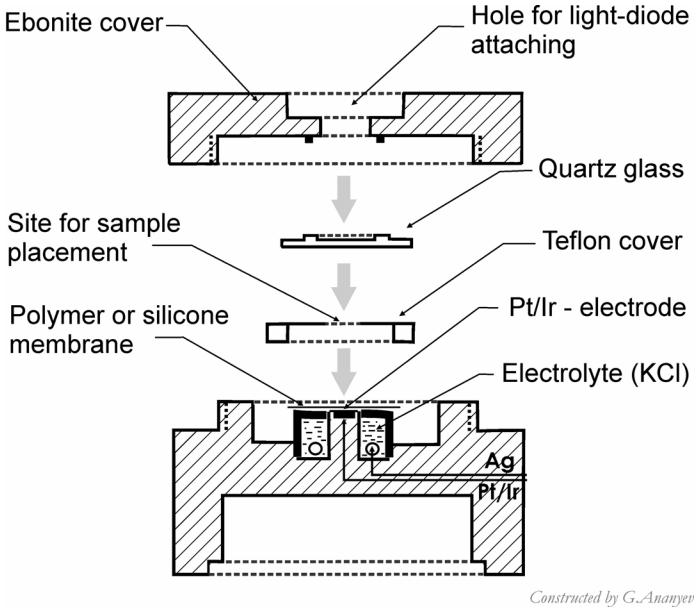

FIGURE 2.1 Schematic diagram of the laboratory-built (Pushchino) Clark-type electrode used for FIOPs measurements in the presence of artificial electron acceptors.

2.3.3.2 *Joliot-Type Electrode*

The FIOPs of PSII samples were measured in the absence of exogenous electron acceptors with a home-built Joliot-type bare platinum electrode (Joliot, 1972; Messinger, 1993), which keeps the temperature of the electrode constant within

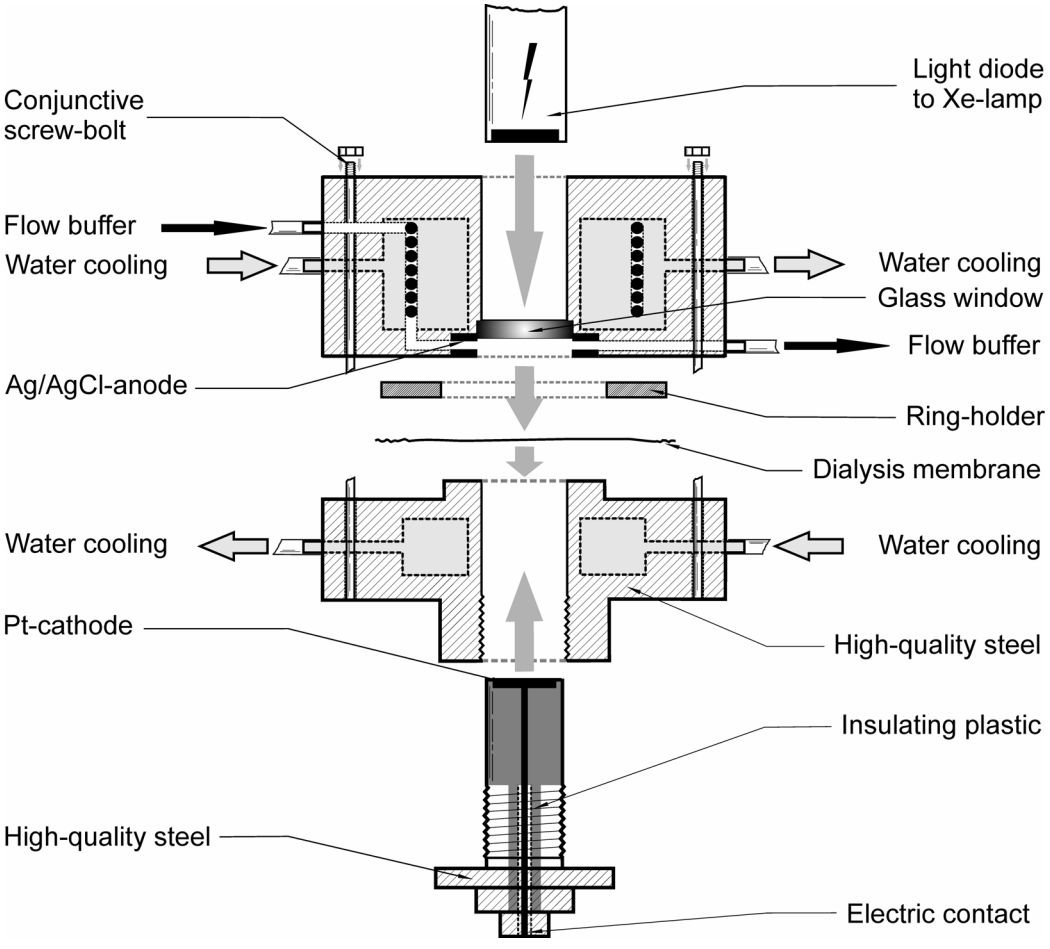

FIGURE 2.2 Schematic sketch of a home-built Joliot-type bare platinum electrode. The electrode construction is based on the device described by Joliot (Joliot, 1972) with modifications described by Messinger (Messinger, 1993).

±0.3 °C (Fig. 2.2). Sample aliquots of 10 μl were transferred to the electrode in very dim green light and kept on the Pt-electrode for 1 (or 3) min at the given temperature. The pH of the flow buffer was adjusted to the given values.

The polarization voltage of –750 mV was switched on 30 s before excitation with a train (2 Hz) of short (~5 μs half-time) saturating Xenon flashes (*EG&G*, model *PS 302*, light pack *FY-604*). The amplified amperometric signals were recorded with a personal computer at a sampling rate of 3 ms/point.

2.3.3.3 Preparation of 'S_1Y_D'- and '$S_1Y_D^{ox}$'- Samples

For FIOPs measurements two kinds of samples were prepared:

(i) *S_1Y_D samples* containing a high percentage (about 80%) of the reduced form of tyrosine D (Y_D). These preparations were obtained by long-term dark (several months) storage at –80 °C (Messinger & Renger, 1990; Messinger & Renger, 1993; Vass *et al.*, 1990b).

(ii) *$S_1Y_D^{ox}$ samples* with Y_D oxidized in about 90% of the centers were obtained by excitation of S_1Y_D samples (pH 6.3–6.5; 20 °C) with one saturating flash and subsequent 10–20 min dark-incubation as described earlier (Messinger & Renger, 1990).

2.3.3.4 S_i State Lifetime Measurements

The S_2 and S_3 state lifetimes were measured with Joliot-type electrode. Dark-adapted S_1Y_D-thylakoids were excited with one (S_2 formation) or two (S_3 formation) preflash(es) followed by the recording of the O_2-yields induced by a flash train (20 flashes at 2 Hz) that was started after various dark times, t_d (0.5 to 180 s) (see Fig. 2.3). To observe the kinetics of S_0 oxidation to S_1 by Y_D^{ox}, '$S_1Y_D^{ox}$'-thylakoids were excited with three flashes (S_0 formation) and after various dark-incubation times (from 0.5 to 60 min) FIOPs were recorded (Fig. 2.3) (Isgandarova *et al.*, 2003; Messinger & Renger, 1993).

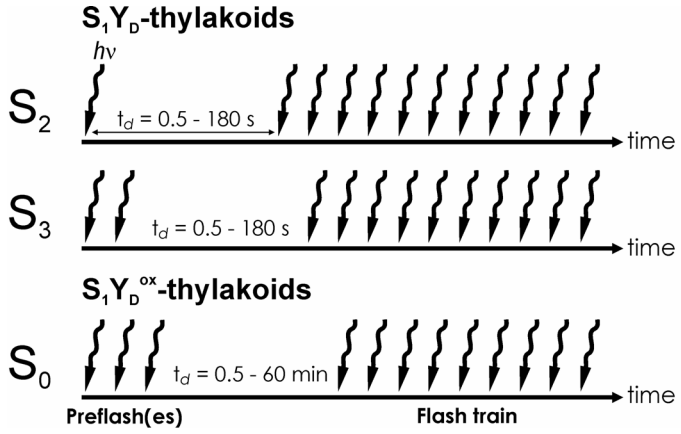

FIGURE 2.3 Schematic diagram of the S_i state lifetime measurements protocol used in the present study.

2.3.3.5 FIOP Analysis

The first 16 (or 13) flashes of each FIOP were analyzed within the framework of different extended Kok models using Excel spreadsheet programs (Messinger *et al.*, 1991; Kebekus *et al.*, 1995; Messinger *et al.*, 1997a). All fit programs are based on the formulas:

$$S_n = KS_{n-1}d \qquad (2.5)$$

and

$$Y_n^{\text{fit}} = (1-\alpha)[S_3]_{n-1} + \beta[S_2]_{n-1} \qquad (\mathbf{2.6})$$

where, S_{n-1} and S_n are vectors of the S_i state populations before and after nth flash of the train, K is the matrix containing the Kok parameters α (miss probability) and β (double hit probability), d is an activity parameter that compensates for changes in the number of active PSII centers during the flash train, Y_n^{fit} is the oxygen yield due to the nth flash, and $[S_3]_{n-1}$ and $[S_2]_{n-1}$ are the normalized S_3 and S_2 state populations immediately before the nth flash, respectively. In the most common and widely used fit procedure, misses and double hits are assumed to be the same for all S_i state transitions, the S vectors contain only redox states from S_0 to S_3 and, the matrix K expresses the univalent redox transitions $S_0 \rightarrow S_1$, $S_1 \rightarrow S_2$ *etc.*, *i.e.*

$$[S]_n = \begin{bmatrix} [S_0]_n \\ [S_1]_n \\ [S_2]_n \\ [S_3]_n \end{bmatrix} \text{ and } K = \begin{bmatrix} \alpha & 0 & \beta & \gamma \\ \gamma & \alpha & 0 & \beta \\ \beta & \gamma & \alpha & 0 \\ 0 & \beta & \gamma & \alpha \end{bmatrix} \qquad (\mathbf{2.7})$$

where, γ is the single hit probability ($\gamma = 1 - \alpha - \beta$).

The computer program minimizes the expression

$$dy_n^2 = \sum_{n=1}^{F}\left[Y_n^{\text{exp}} - Y_n^{\text{fit}}\left(\sum_{n=1}^{F} Y_n^{\text{exp}} \Big/ \sum_{n=1}^{F} Y_n^{\text{fit}} \right)\right]^2 \qquad (\mathbf{2.8})$$

where, Y_n^{exp} is the relative O_2 yield of the nth flash and F equals the number of analyzed flashes. The normalization is given by

$$\sum_{i=-1}^{3}[S_i] = 1 \qquad (\mathbf{2.9})$$

The fit quality is calculated according to Eq. 2.10:

$$fq = \frac{dy_n^2}{F - P} \qquad (\mathbf{2.10})$$

where, P is the number of free parameters used in the fit.

In a more advanced approach, the fit program also includes (*i*) a high double-hit probability in the 1st flash (β_1), (*ii*) the reduced S_{-1} state and (*iii*) S_i state dependent misses (Isgandarova *et al.*, 2003; Messinger *et al.*, 1997a; Shevela *et al.*, 2006) (Fig. 2.4). This extended Kok model is summarized in Eq. 2.11:

$$\begin{bmatrix} [S_{-1}]_n \\ [S_0]_n \\ [S_1]_n \\ [S_2]_n \\ [S_3]_n \end{bmatrix} = \begin{bmatrix} \alpha_{-1} & 0 & 0 & 0 & 0 \\ \gamma_{-1,n} & \alpha_0 & 0 & \beta_n & \gamma_{3,n} \\ \beta_n & \gamma_{0,n} & \alpha_1 & 0 & \beta_n \\ 0 & \beta_n & \gamma_{1,n} & \alpha_2 & 0 \\ 0 & 0 & \beta_n & \gamma_{2,n} & \alpha_3 \end{bmatrix} \times \begin{bmatrix} [S_{-1}]_{n-1} \\ [S_0]_{n-1} \\ [S_1]_{n-1} \\ [S_2]_{n-1} \\ [S_3]_{n-1} \end{bmatrix} \times d \qquad (\mathbf{2.11})$$

where, for example, $\gamma_{1,n} = 1 - \alpha_1 - \beta_n$ is the S_i state and flash number dependent single-hit probability. In cases where the possibility of a high-double hit in the first flash was analyzed β_n equals β_1 for the first flash ($n = 1$) and β_n equals β for $n > 1$ (in addition the restriction $\beta_1 \geq \beta$ was applied) (Shevela *et al.*, 2007). In case of S_i state dependent misses, for the sake of simplicity, the α-values for the transitions $S_0 \rightarrow S_1$ and $S_1 \rightarrow S_2$ were fixed to 0 ($\alpha_1 = \alpha_2 = 0$) since they are assumed to be insignificantly small. The α-values of $S_2 \rightarrow S_3$ and $S_3 \rightarrow S_0 + O_2 + nH^+$ were set as free running parameters. They were either varied independently or fixed to be equal, *i.e.* $\alpha_2 = \alpha_3$ (Isgandarova *et al.*, 2003; Shevela *et al.*, 2006). Accordingly, the value of Y_n^{fit} was fit using Eq. 2.12:

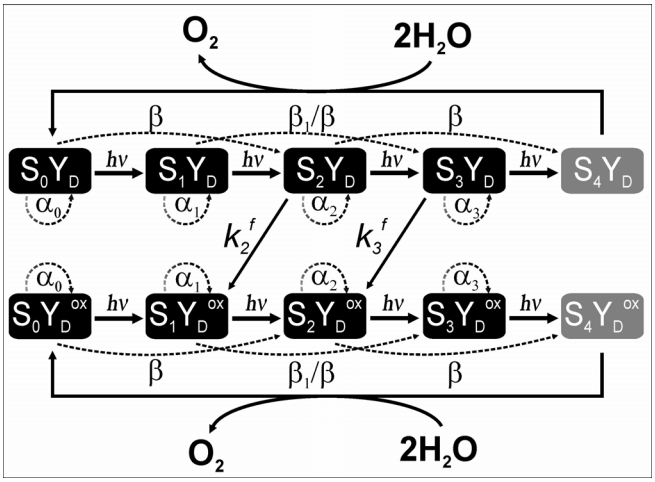

FIGURE 2.4 Extended Kok model that includes (*i*) the S_i state dependent misses, (*ii*) a high-double hit probability in the 1st flash, and (*iii*) S_i state redistributions resulting from the fast reductions (k_2^f and k_3^f) of the S_2 and S_3 states by Y_D during a flash train (see text for details). It is assumed that the miss and double hit probabilities are independent of the redox state of tyrosine D.

$$Y_n^{fit} = (1 - \alpha_3)[S_3]_{n-1} + \beta_2[S_2]_{n-1} \qquad (\mathbf{2.12})$$

For the calculation of the states more reduced than the S_0 state (the S_{-i} states), the data were analyzed using the extended Kok model, which includes, in addition to the normal S_i states ($S_0 \ldots S_3$), the $S_{-5} \ldots S_{-1}$ states. PSII samples can be found in these redox states after reduction with exogenous electron donors (Debus, 1992; Messinger *et al.*, 1997a; Hillier & Messinger, 2005). Within the model with equal miss and double hit parameters, the S state populations ($[S_i]$, $i = -5 \ldots 3$) after the nth flash are given by Eq. 2.13:

$$\begin{bmatrix} [S_{-5}]_n \\ [S_{-4}]_n \\ [S_{-3}]_n \\ [S_{-2}]_n \\ [S_{-1}]_n \\ [S_0]_n \\ [S_1]_n \\ [S_2]_n \\ [S_3]_n \end{bmatrix} = \begin{bmatrix} \alpha & 0 & 0 & 0 & 0 & 0 & 0 & 0 & 0 \\ \gamma & \alpha & 0 & 0 & 0 & 0 & 0 & 0 & 0 \\ \beta & \gamma & \alpha & 0 & 0 & 0 & 0 & 0 & 0 \\ 0 & \beta & \gamma & \alpha & 0 & 0 & 0 & 0 & 0 \\ 0 & 0 & \beta & \gamma & \alpha & 0 & 0 & 0 & 0 \\ 0 & 0 & 0 & \beta & \gamma & \alpha & 0 & \beta & \gamma \\ 0 & 0 & 0 & 0 & \beta & \gamma & \alpha & 0 & \beta \\ 0 & 0 & 0 & 0 & 0 & \beta & \gamma & \alpha & 0 \\ 0 & 0 & 0 & 0 & 0 & 0 & \beta & \gamma & \alpha \end{bmatrix} \times \begin{bmatrix} [S_{-5}]_{n-1} \\ [S_{-4}]_{n-1} \\ [S_{-3}]_{n-1} \\ [S_{-2}]_{n-1} \\ [S_{-1}]_{n-1} \\ [S_0]_{n-1} \\ [S_1]_{n-1} \\ [S_2]_{n-1} \\ [S_3]_{n-1} \end{bmatrix} \times d \qquad (\mathbf{2.13})$$

The S_i state lifetime data were analyzed by further extending the Kok model by also taking into account the fast reduction of S_2 and S_3 by Y_D that can occur during the 500 ms dark-times between flashes of a flash train (Isgandarova *et al.*, 2003; Messinger & Renger, 1993; Vass *et al.*, 1990a). The kinetic scheme is described in Fig. 2.4. The required

first order rate constants (k_2^f, k_3^f) as well as the percentage of Y_D in the samples were determined from lifetime measurements in an iterative process that is described in detail in (Isgandarova, 2004).

2.3.4 MEMBRANE-INLET MASS SPECTROMETRY MEASUREMENTS

2.3.4.1 Mass Spectrometer

The membrane-inlet mass spectrometry (MIMS) measurements were performed with an isotope ratio mass spectrometer (*ThermoFinnigan^{Plus} XP*) (the main components are presented in Fig. 2.5) that was connected *via* a cooling trap (dry ice + ethanol) to a home built membrane-inlet cell similar to that described by Messinger and co-workers (Messinger *et al.*, 1995). The volume of the cell is 150 μl and the sample was separated from the vacuum (3×10^{-8} bar) of the mass spectrometer by a silicon membrane (*MEM-213*) resting on a porous plastic support (see Fig. 2.6). The sample was stirred constantly during measurements with a magnetic stir bar. For further details on MIMS see (Konermann *et al.*, 2008).

FIGURE 2.5 Diagram of the principal components of a mass spectrometer.

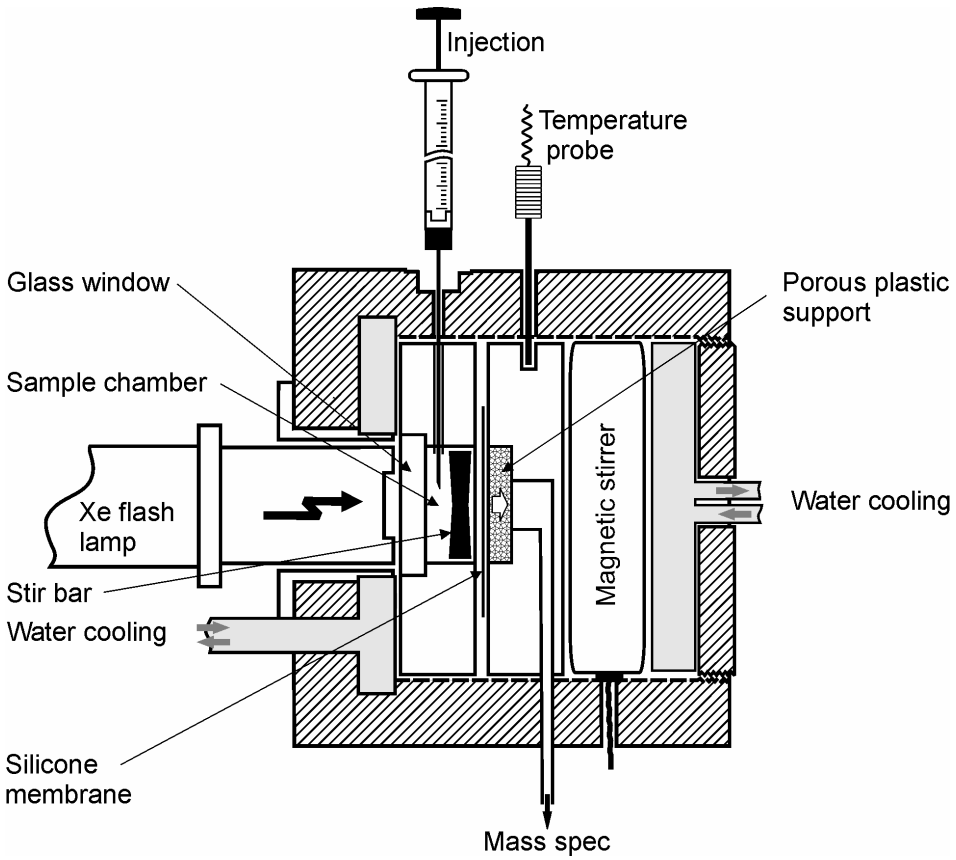

FIGURE 2.6 Experimental MIMS cell used for mass spectrometric measurements. Further details are given in the text.

2.3.4.2 ^{18}O Enrichment

$H_2{}^{18}O$ (98.5% enrichment, *Isotech*) was used to enrich PSII samples with 3–65% ^{18}O. CO_2 was detected at *m/z* = 44, *m/z* = 46 and *m/z* = 48 (*i.e.*, as the non-labelled $C^{16}O_2$, the mixed labelled $C^{16}O^{18}O$ and double labelled $C^{18}O^{18}O$ products, respectively). Similarly, N_2O was detected at *m/z* = 44, *m/z* = 46 (*i.e.*, as the non-labelled $N_2{}^{16}O$ and single-labelled $N_2{}^{18}O$, respectively). Flash-induced O_2 produced by PSII samples was measured as mixed labelled $^{16}O^{18}O$ at *m/z* = 34. For more details on the MIMS measurements see Chapter 5.

2.3.5 EPR AND EXAFS/XANES MEASUREMENTS

Details for EPR, EXAFS and XANES measurements are given in the Experimental Sections of Chapters 5 and 6.

Chapter 3

Functional Comparison of the Water-Oxidizing Complex of Photosystem II from Spinach and *Acaryochloris marina*

3.1 INTRODUCTION

Recently, a cyanobacterium, *Acaryochloris marina*, was found which contains a large fraction of Chl *d* (Fig. 1.5*c*) and only few Chl *a* molecules (Fig. 1.5*b*) (Akiyama *et al.*, 2002; Chen *et al.*, 2002; Chen *et al.*, 2005; Mimuro *et al.*, 1999; Miyashita *et al.*, 1997). In this organism, the photoactive pigment of PSI, P740 (see Section 1.2.3), was shown to be a Chl *d* – Chl *d*' dimer. The midpoint potential of P740/P740$^{\bullet+}$ was determined to be +335 mV (Hu *et al.*, 1998), compared to the typical value of about +500 mV for P700 in other cyanobacteria (Nakamura *et al.*, 2005; Witt *et al.*, 2002). The nature of the photoactive pigment of PSII in *A. marina* is a matter of controversy (Itoh *et al.*, 2001; Nieuwenburg *et al.*, 2003; Petrášek *et al.*, 2005). The special pair (P_{D1}–P_{D2}) of photoactive pigment in PSII of *A. marina* is currently discussed to be either a Chl *d*−Chl *d* homodimer (Tomo *et al.*, 2007), or a Chl *a*−Chl *d* heterodimer (Kobayashi *et al.*, 2007), or a Chl *a*−Chl *a* homodimer (Akimoto *et al.*, 2006). If one assumes the replacement of Chl *a* by Chl *d* in PSII, the actual redox potential of the reaction center maybe altered (as in case of PSI), possibly affecting the efficiency of turnover of the WOC. Apart from the particular problem of identifying the photoactive pigment and characterizing its redox properties, questions arise whether or not the properties of the WOC in Chl *d*-dominating *A. marina* are modified in comparison to the Chl *a*-containing organisms.

The present study describes investigation based on FIOPs measurements performed in whole cells of *A. marina* and thylakoids from spinach in order to unravel possible peculiarities of the WOC in the Chl *d*-containing organism. The results obtained reveal that the WOCs in both sample types are very similar, but exhibit a pronounced difference in the kinetics of S_0 oxidation and S_2/S_3 reduction by Y_D^{ox} and Y_D, respectively.

3.2 EXPERIMENTS AND ANALYSIS

3.2.1 SAMPLE PREPARATION

The cyanobacterium *A. marina* was grown as described in Section 2.1.3. Before the measurements, *A. marina* cells were diluted to about 0.4 mg Chl ml^{-1} in the growth medium containing 2.5 mM $NaHCO_3$ (pH 7.4). Since we found that O_2 yield of the long-term dark adapted (2 days after cell harvesting procedure) *A. marina* cells has virtually no oscillation (see Results and Fig. 3.1*a*), only light-activated cells were used for FIOPs measurements. Light-activation of the cells was performed by exposing them for 30 min to room light. Thereafter, they were dark-adapted for 10 min at room temperature and used for several hours. $S_1Y_D^{ox}$ samples of *A. marina* were obtained from light-activated cells by one saturating preflash directly on the Joliot electrode, followed by 10 min dark-adaptation. A similar treatment, but without light activation was use to populate the $S_1Y_D^{ox}$ state in spinach thylakoids (for details see Section 2.3.3.3).

For the measurements of spinach samples, the thylakoid beads were thawed in the dark on ice and diluted to [*Chl*] = 1 mg ml^{-1} with MCMH buffer (pH 7.4).

3.2.2 MEASUREMENTS OF FIOPS

The FIOPs of *A. marina* cells and spinach thylakoids were obtained in the absence of exogenous electron acceptors with a home-built Joliot type (bare platinum) electrode at 20 °C and pH 7.4. The samples were kept on the Pt-electrode for 1 min prior to starting the measurements and the polarization voltage (–750 mV) was switched on 30 s before excitation with a train (2 Hz) of saturating xenon flashes (for further details, see Section 2.3.3.2 and Fig. 2.2).

For S_2 and S_3 lifetime measurements (see Section 2.3.3.4 and Fig. 2.3), S_1Y_D-spinach thylakoids and activated *A. marina* cells were first sedimented on the Joliot electrode for 1 min. The samples were then illuminated by one (S_2) or two (S_3) preflashes and, after dark-incubation times of 0.5 to 180 s, by a train of 20 flashes given at 2 Hz.

For measurements of the kinetics of S_0 oxidation to S_1 by Y_D^{ox}, $S_1Y_D^{ox}$-spinach thylakoids and light activated $S_1Y_D^{ox}$ *A. marina* cells were preflashed on the Joliot electrode with three flashes and, after dark-times varying between 0.5 to 60 min, FIOPs were recorded.

All measurements were repeated at least 2-3 times.

3.2.3 ANALYSIS OF FIOPS

The O_2 yields of the first 16 flashes were analyzed using an Excel spreadsheet program based on an extended Kok model (for details, see Section 2.3.3.5; Eq. 2.11), which includes (*i*) the reduced S_{-1} state, (*ii*) an activity parameter *d*, that compensates for an increase or decrease in the number of oxygen-evolving centers during the flash train and (*iii*) the reactions of the S_2 and S_3 states with Y_D (Isgandarova *et al.*, 2003; Messinger *et al.*, 1997a). In addition, for some fits, the possibility of S_i state dependent misses was considered.

The S_i state lifetime findings were analyzed taking into account the fast reduction of S_2 and S_3 by Y_D between flashes (see Fig. 2.4 and Section 2.2.3.5) (Isgandarova *et al.*, 2003).

3.2.4 RATE CONSTANT AND HALF-TIME CALCULATIONS

The rate constants for the fast (k_i^{f}) and slow (k_i^{s}) S_2 and S_3 decay were calculated using Eq. 3.1:

$$S_i(t) = A_i e^{-k_i^{\mathrm{f}} t} + B_i e^{-k_i^{\mathrm{s}} t} \qquad \textbf{(3.1)}$$

where i = 2 or 3, and t is the dark-time between the last preflash and the first flash of the detecting flash train. A_i and B_i are the relative amplitudes of fast and slow decay, respectively.

For the reoxidation of S_0 to S_1 by Y_D^{ox}, a simple one exponential decay was assumed:

$$S_0(t) = S_0(t=0) e^{-k_0 t} \qquad \textbf{(3.2)}$$

Half-times were calculated according to

$$t_{1/2} = (\ln 2)/k \qquad \textbf{(3.3)}$$

3.3 RESULTS

3.3.1 FLASH-INDUCED OXYGEN OSCILLATION PATTERNS

Fig. 3.1 shows FIOPs measured in whole cells of *A. marina* either after long dark-adaptation (1–2 days; trace *a*) or after light activation (30 min room light) followed by 10 min dark-adaptation and preflashing (one flash plus 10 min dark-adaptation; trace

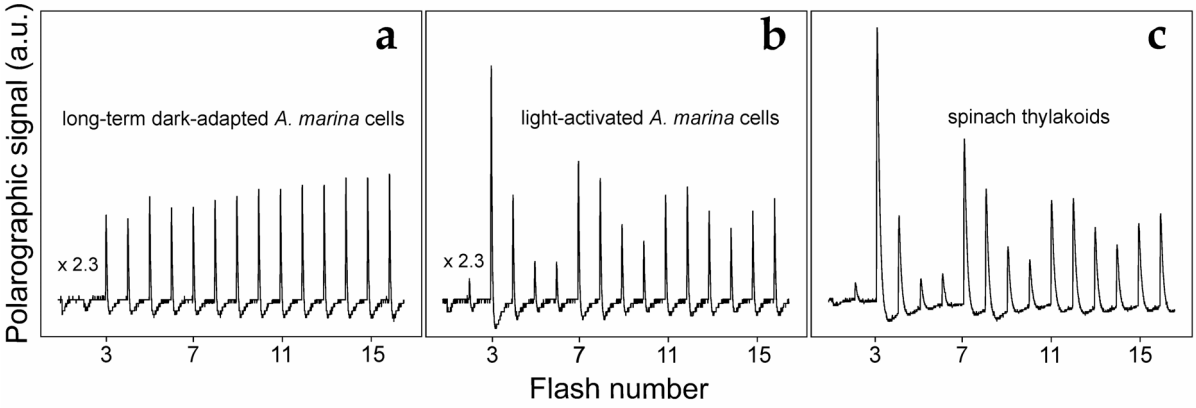

FIGURE 3.1 Original traces of the FIOPs of *A. marina* cells (***a***, ***b***) and spinach thylakoids (***c***) at 20 °C and pH 7.4. Trace ***a*** was obtained with long-term dark-adaptated (2 days) *A. marina* cells, while trace ***b*** was recorded from the same batch of cells after light activation (30 min room light plus 10 min dark-adaptation) and preflashing into the $S_1Y_D^{\mathrm{ox}}$ state (one flash plus 10 min dark-adaptation). Trace ***c*** depicts a FIOP obtained with $S_1Y_D^{\mathrm{ox}}$ thylakoids of spinach. No exogenous electron acceptors were added. The flash frequency was 2 Hz. Chlorophyll concentrations of *A. marina* and spinach thylakoids during measurements were 0.4 mg ml^{-1} and 1.0 mg ml^{-1}, respectively.

b). Trace *c* shows for comparison a FIOP of spinach thylakoids that were pre-illuminated by one flash and subsequently dark-incubated for 10 min. Inspection of this data shows that the oscillation patterns of light-activated *A. marina* cells and of thylakoids are quite similar and very pronounced, whereas *A. marina* cells after long dark-adaptation exhibit a markedly different pattern of oxygen evolution. Under these conditions, the first O_2 yield is measured after the 3rd flash and thereafter the yield increases from flash to flash with virtually no oscillation. This 'photo-activation' is reminiscent of similar features observed in several *Synechocystis* PCC 6803 mutants, where in certain regions the large lumal loop E of CP47 was truncated by deletions of 4–8 amino acids. These mutants were shown to reach an inactivated state of the WOC and full oxygen evolution could be achieved only after illumination with numerous flashes (Gleiter *et al.*, 1994; Gleiter *et al.*, 1995). In the case of *A. marina* cells, only a few flashes (~20) are required to obtain fully active systems. Therefore, the underlying mechanism seems to be different and may be related to a reduced plastoquinone pool in long-term dark-adapted samples that is oxidized during the light-activation procedure.

Light-activated and than preflashed ($S_1Y_D^{ox}$) *A. marina* cells exhibit the conventional period four oscillation (similar to that obtained in the presence of exogenous oxidants (Boichenko *et al.*, 2000)) that is characteristic for a functionally fully competent WOC (Fig. 3.1*b*). A comparison to the corresponding patterns of

TABLE 3.1. Fits of the FIOPs of light-activated ($S_1Y_D^{ox}$) *A. marina* cells and spinach thylakoids [A].

	Fit parameters (%)									
Sample	**Fit**	**α**	**α_2**	**α_3**	**β**	**S_2**	**S_1**	**S_0**	**S_{-1}**	**Y_D**	**fq×10^{-6}**
Acaryochloris marina cells	A1	14.6	–	–	3.3	–	100*	–	–	0*	7.2
	B1	13.1	–	–	3.2	–	91.1	8.9	–	0*	2.3
	C1	13.0	–	–	3.0	0.3	89.9	8.2	1.6	0*	2.4
	D1	–	26.1	21.1	2.5	–	100*	–	–	0*	1.6
	E1	–	23.7	23.7	2.5	–	100*	–	–	0*	1.5
	A2	14.3	–	–	3.3	–	100*	–	–	10*	6.7
	B2	12.8	–	–	3.2	–	90.9	9.1	–	10*	2.2
	C2	12.7	–	–	3.0	0.3	89.9	8.2	1.6	10*	2.3
	D2	–	25.7	20.7	2.5	–	100*	–	–	10*	1.5
	E2	–	23.2	23.2	2.5	–	100*	–	–	10*	1.6
Spinacia oleracea thylakoids	A3	12.3	–	–	2.4	–	100*	–	–	0*	7.0
	B3	12.1	–	–	2.4	–	98.6	1.4	–	0*	8.1
	C3	11.9	–	–	2.1	0.0	96.4	0.3	3.3	0*	7.5
	D3	–	5.9	33.1	1.6	–	100*	–	–	0*	9.1
	E3	–	19.1	19.1	1.9	–	100*	–	–	0*	10.2
	A4	11.6	–	–	2.3	–	100*	–	–	10*	6.9
	B4	11.6	–	–	2.3	–	100	0.0	–	10*	8.1
	C4	11.3	–	–	2.1	0.0	97.2	0.0	2.8	10*	8.0
	D4	–	3.8	32.9	1.6	–	100*	–	–	10*	10.7
	E4	–	19.1	19.1	1.9	–	100*	–	–	10*	11.7

[A] The FIOPs were obtained at 20 °C and pH 7.4 (Fig. 3.1***b*** and ***c***) and fit using different approaches. For fits **A–C** an extended Kok model (for details, see Chapter 2.3.3.5) with S_i state-independent miss and double hit parameters was used. In fits **D1–D4** the miss parameters of the $S_2 \rightarrow S_3$ and $S_3 \rightarrow S_0$ transitions (α_2 and α_3, respectively) were used as free parameters; in fits **E1–E4** they were forced to be equal, while those for the $S_0 \rightarrow S_1$ and $S_1 \rightarrow S_2$ transitions (α_1 and α_2, respectively) were fixed to 0. Dashes indicate that parameters were excluded from the fit, while stars mark values that were fixed during the optimization. The first 16 flash-induced oxygen yields of each FIOP were analyzed. The fit quality (*fq*) values were calculated by using Eq. 2.10 (see Chapter 2.3.3.5)

thylakoids (Fig. 3.1*c*), PSII membrane fragments and Inside-Out (ISO) vesicles from spinach reveals that the PQ-pool of *A. marina* cells is of virtually the same capacity as in the thylakoids (Messinger *et al.*, 1993; Shinkarev & Wraight, 1993) from higher plants and samples reconstituted with PQ (Seeliger *et al.*, 1997).

In order to obtain more detailed information on the properties of the WOC of *A. marina*, FIOPs of both sample types (trace *b* and *c* in Fig 3.1) were fit different versions of the extended Kok model (see Section 2.3.3.5). In the simplest and the most widely used fit procedure, the values of misses (α) and double hits (β) were set to be equal in each flash-induced S_i state transition (based on Eqs. 2.5–2.7, Chapter 2), *i.e.* independent of the S_i state and acceptor site redox equilibria (Table 3.1, fit approaches *A*–*C*).

In a more elaborate approach, the α-value depends on the S_i state (see, for details, Eq. 2.7, Chapter 2). In this case, for the sake of simplicity, the α-values for the transitions $Y_Z^{ox}S_0 \rightarrow Y_ZS_1$ and $Y_Z^{ox}S_1 \rightarrow Y_ZS_2$ are assumed to be negligibly small ($\alpha_1 = \alpha_2 = 0$) and those of $Y_Z^{ox}S_2 \rightarrow Y_ZS_3$ and $Y_Z^{ox}S_3 \rightarrow Y_ZS_0$ were free running parameters and either independent (approach D) or fixed to be equal, *i.e.* $\alpha_2 = \alpha_3$ (approach E) (Isgandarova *et al.*, 2003). Based on the obtained fit qualities, the oscillation patterns of both samples can be satisfactorily described by all these approaches (see Table 3.1).

With the simplest approach, A, the FIOPs of both sample types can be fit equally well. These fits reveal that the miss parameter is only slightly lower for spinach thylakoids (fit A3; α = 12.3%) compared to whole cells of *A. marina* (fit A1; α = 14.6%). In addition, the double hit parameter is slightly smaller (2.4%) in spinach compared to *A. marina* (3.3%). Both factors together account for the visually lower damping in the FIOP of spinach (Fig. 3.1*c*) compared to *A. marina* (Fig. 3.1*b*). For spinach thylakoids, no improvement of the fit quality was obtained with the more elaborate fit approaches (B–E). In contrast, for *A. marina* cells the best fit quality was obtained with $\alpha_2 = \alpha_3 \approx 23\%$ (fit E1). As expected for well preflashed samples, the inclusion of 10% Y_D in the fits did not improve the fit quality (fits A2–E2 and A4–E4). In spite of the differences described above, the values obtained for α, β and S_1 population can generally be considered to be similar for *A. marina* cells and spinach thylakoids.

3.3.2 DECAY RATES OF S_2 AND S_3

The kinetics of the S_2 and S_3 decay were determined by preillumination of the samples with one and two single turnover flashes, respectively, and monitoring the FIOPs at different times after the preflash(es), as described earlier (Isgandarova *et al.*, 2003; Seeliger *et al.*, 1997).

Figure 3.2 shows the calculated values of the $S_2(t)$ and $S_3(t)$ population as a function of dark-time t between the preflashes and the flash sequence for FIOPs detection for whole *A. marina* cells (closed symbols) and spinach thylakoids (open symbols). Both sample types exhibit the characteristic biphasic behaviour of the decay kinetics, which originates from the reduction of S_2 and S_3 by Y_D acting as electron donor (fast phase) and by the acceptor side (slow phase). At first glance, the data of Fig. 3.2 reveal that the decay kinetics of both S_2 and S_3 are slower for *A. marina* cells than for spinach thylakoids.

Biexponential fits lead to the results summarized in Table 3.2. A comparison of the results leads to the interesting finding that the difference between *A. marina* cells and spinach thylakoids is entirely related to the reactivity with Y_D. The half-lifetimes of the fast phase of *A. marina* are larger by a factor of 2.5–3 for both S_2 and S_3, while the rates for the slow S_2/S_3 decay are virtually identical for both organisms.

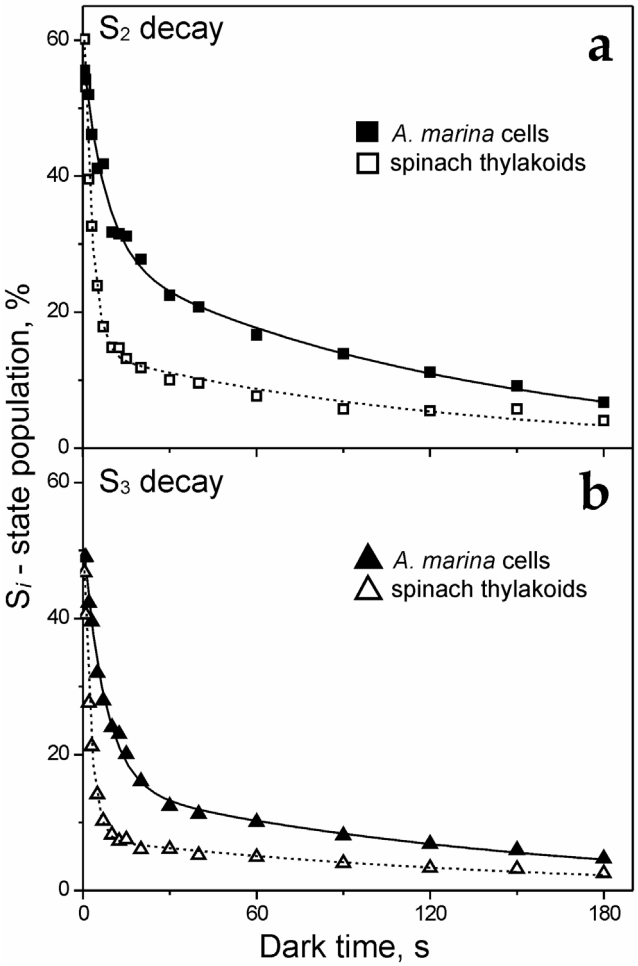

FIGURE 3.2 The kinetics of S_2 (***a***) and S_3 (***b***) state decay as a function of dark-time between the preflashe(s) (one or two, respectively) and the main flash train for light-activated *A. marina* cells (closed symbols) and spinach thylakoids (open symbols). The lines represent biexponential fits (Table 3.2). The lifetime measurements were performed at 20 °C and pH 7.4.

3.3.3 S_0 OXIDATION BY Y_D^{ox}

After repetitive excitation of PSII, the WOC attains a normalized steady state population of $[S_0] = [S_1] = [S_2] = [S_3] = 0.25$. In a following dark period, S_2 and S_3 relax *via* reduction into the S_1 state while S_0 becomes slowly oxidized to S_1 by Y_D^{ox} (for review see (Messinger, 2000). The kinetics of S_0 oxidation can be best studied by giving three flashes to activated (in case of *A. marina*) and preflashed samples and then varying the dark-time to the flash train between 1–60 min (Messinger & Renger, 1993). The results obtained for *A. marina* cells (filled circles) and spinach thylakoids (open circles) are depicted in Fig. 3.3. Inspection of this data shows that the oxidation of S_0 by Y_D^{ox} is significantly faster in *A. marina* compared to spinach thylakoids. A fit of the data results in the values shown in Table 3.2. A comparison reveals that the reaction is faster by a factor of almost five in *A. marina*.

3.4 DISCUSSION AND CONCLUSION

The results obtained in this study lead to two conclusions: (*a*) the WOC of the Chl *d*-containing *A. marina* closely resembles that of Chl *a*-containing cyanobacteria and higher plants, and (*b*) the only significant difference of the WOC properties between *A. marina* and spinach thylakoids is the interaction of the states S_2/S_3 and S_0 with the redox couple Y_D/Y_D^{ox}.

The first conclusion is based on the numerical analysis of the FIOPs, which reveals that the misses (α), double hits (β) and the dark-state population of redox state S_1 are similar for both species. A similarity of the α-values is indicative for (*i*)

similar kinetics of Y_Z^{ox} formation by the cation radical of the photoactive pigment and (*ii*) similar redox-potential differences between P680/P680$^{\bullet+}$, Y_Z/Y_Z^{ox} and the S_i states. This finding of a practically unchanged redox-potential of P680$^{\bullet+}$ does, however, not permit any straightforward conclusions on the chemical nature of the primary donor (Chl *a* and/or Chl *d* content), since changes in the protein environment that tune Chl *d* molecules to a similar potential like Chl *a* cannot be excluded.

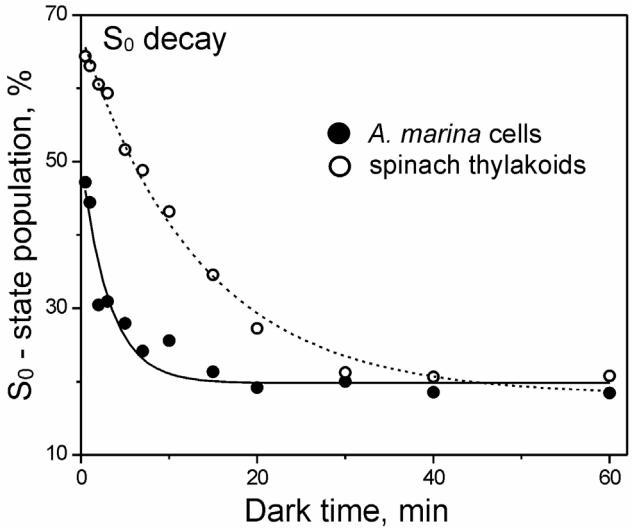

FIGURE 3.3 The kinetics of S_0 state oxidation by Y_D^{ox} as a function of dark-time between three preflashes and the main train of saturating single turnover flashes for activated *A. marina* cells (closed symbols) and spinach thylakoids (open symbols). The lines represent monoexponential fits (Table 3.2). The measurements were performed at 20 °C and pH 7.4.

The β–values of *A. marina* are somewhat higher than those of spinach thylakoids (see Table 3.1). It was recently shown that the extent of β is linearly related to the rate of $Q_A^{\bullet-}$ reoxidation (see appendix in (Messinger *et al.*, 1993)). Therefore, it can be concluded that the reoxidation of $Q_A^{\bullet-}$ is slightly faster in *A. marina* than in spinach thylakoids. A similar phenomenon was found recently for the Chl *a*-containing thermophilic cyanobacterium *T. elongatus* (Isgandarova *et al.*, 2003). Based on this finding, it is concluded that a slightly faster electron transfer from $Q_A^{\bullet-}$ to Q_B ($Q_B^{\bullet-}$) is likely to be a property of cyanobacteria rather than due to replacement of Chl *a* by Chl *d* in PSII of *A. marina*.

The most interesting finding of this study is the observation of changes in the rates of S_2 and S_3 reduction by Y_D and of S_0 oxidation by Y_D^{ox}. A retardation of the former reactions by factors of 2.5−3 and an acceleration of the latter reaction by a factor of almost 5 can be explained in a straightforward manner by the assumption of a small E_m shift of the redox couple Y_D/Y_D^{ox} relative to the values of S_0/S_1, and in the opposite direction relative to E_m of S_1/S_2 and S_2/S_3. Based on the findings that the kinetics of the slow S_2 and S_3 decay are the same in *A. marina* cells and spinach thylakoids, it appears most reasonable to assume that the energetics of the redox transitions in the WOC are virtually identical in both organisms, *i.e.* the slight E_m shift

TABLE 3.2. Rate constants (k), half-times ($t_{1/2}$) and amplitudes (A, % of total decay) for S_0 state oxidation by Y_D^{ox} and for the S_2 and S_3 state reduction by Y_D (fast phase) and the acceptor side (slow phase) for *A. marina* cells and spinach thylakoids at 20 °C and pH 7.4

		***A. marina* cells**			**Spinach thylakoids**		
		k, **s^{-1}**	$t_{1/2}$, s	**A, %**	k, **s^{-1}**	$t_{1/2}$, s	**A, %**
Slow phase	S_2	0.0079	88	49	0.0080	87	20
	S_3	0.0068	102	30	0.0068	102	14
Fast phase	S_2	0.13	5.5	51	0.35	2.0	80
	S_3	0.13	5.2	70	0.35	2.0	80
		k, **min^{-1}**	$t_{1/2}$, s		k, **min^{-1}**	$t_{1/2}$, s	
	S_0	0.330	125		0.074	580	

relates to Y_D/Y_D^{ox}. This idea is strongly supported by a recent comparative study on *T. elongatus* and spinach thylakoids. It was shown that, in this case, the S_2 and S_3 reduction by Y_D was faster by a factor of 2−3 in *T. elongatus* compared with spinach thylakoids, while the S_0 oxidation by Y_D^{ox} was slower by a factor 4 in the former organism (Isgandarova *et al.*, 2003). These are just the opposite shifts to that observed for *A. marina* cells *versus* spinach thylakoids. The phenomenon *per se* can be explained by the same mechanism, *i.e.* E_m shift of Y_D/Y_D^{ox}. However, in *T. elongatus* this E_m shift is opposite in direction.

These findings also show that the phenomenon of an E_m (Y_D/Y_D^{ox}) shift is not a unique property of Chl *d*-containing cyanobacteria, but appears to be a common feature also among Chl *a*-containing PSII. As a consequence, it is concluded that the WOC in the Chl *d*-containing *A. marina* is the same as in all the other oxygen evolving organisms. Therefore, the replacement of a large number of Chl *a* by Chl *d* in PSII has virtually no effect on the properties of the WOC.

This observation, however, is restricted to the WOC and cannot offer any straightforward conclusion on the nature of the photoactive pigment of PSII. All considerations on this point should take into account that in Chl *a*-containing organisms, P680 is a multimeric Chl a_4 $Pheo_x$ (x = 0, 1 or 2) as discussed in (Renger & Holzwarth, 2005). It is therefore difficult to assign the possible presence of only two Chl *a* molecules in PSII (Akiyama *et al.*, 2002) to a define structure of the photoactive pigment.

Chapter 4

Interactions of Photosystem II with Hydrogencarbonate, Formate and Acetate

4.1 INTRODUCTION

Hydrogencarbonate (HCO_3^-; HC) is well established to be required for maximal activity of PSII though the interpretation of its stimulating effect remains controversial (for recent reviews, see (Stemler, 2002; van Rensen, 2002; van Rensen & Klimov, 2005) and references therein) (also reviewed in Section 1.4.4.2). The problems are caused (*i*) by several different protocols for HC-depletion and (*ii*) by the absence (most of studies) of monitoring of the residual inorganic carbon levels (C_i) (CO_2, HCO_3^- and H_2CO_3). Typically three different methods were employed for HC-depletion: (*1*) Dilution of samples into buffers that were depleted of HC by bubbling with CO_2-free air, N_2 or argon (Klimov *et al.*, 1995a; Klimov *et al.*, 1995b) (see also Section 2.2.3.1). This method (Method 1) can be combined with brief boiling of the buffer (Govindjee *et al.*, 1997). (*2*) Incubation of the samples at pH 5.0 which is well below the pK_a = 6.3 of HC (Good *et al.*, 1966), induces protonation of HC and subsequent dissociation of H_2CO_3 into CO_2 and water, which facilitates HC removal (Method 2). (*3*) Addition of chemical analogs of HC, such as formate (Stemler & Radmer, 1975) or acetate (Stemler *et al.*, 1974) (see Scheme 4.1) is thought to replace HC from its binding site(s) in PSII (Method 3) (Sections 4.2.1.3 and 4.2.1.4). In this study we probe and compare the effects of these HC removals from PSII in spinach thylakoids by measuring FIOPs with a Joliot-type electrode. In addition, we carefully monitor the inorganic carbon levels in the buffers during sample incubation and under measurement conditions by MIMS.

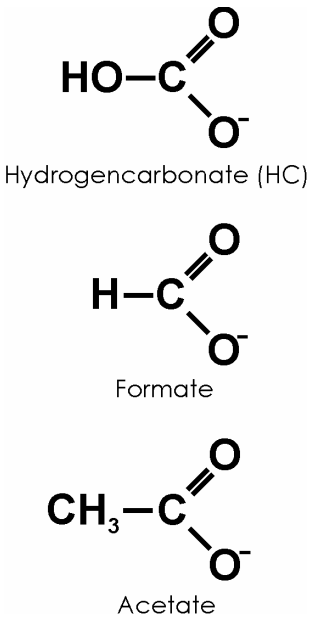

SCHEME 4.1

Intially, the donor side of PSII was considered as possible acting site for HC (Stemler & Govindjee, 1973; Stemler *et al.*, 1974). However, later, is was clearly shown that HC-depletion affects the electron transfer kinetics on the acceptor side of PSII (Wydrzynski & Govindjee, 1975). This interpretation was supported by numerous experimental data (reviewed in (van Rensen, 2002)) and confirmed by two recent XRD investigations on PSII (Ferreira *et al.*, 2004; Loll *et al.*, 2005). In contrast, the possible role of HC within the donor side of PSII is still under discussion (Stemler, 2002). Recently, it has been shown that HC ions are required for both maximal activity and stability of the WOC in PSII (Allakhverdiev *et al.*, 1997; Klimov *et al.*, 1995a; Klimov *et al.*, 1995b; Klimov *et al.*, 1997b). The stimulating effects of HC are especially pronounced during photoactivation (Baranov *et al.*, 2000; Baranov *et al.*, 2004). These and other results (discussed in Section 1.4.4.2) are consistent with several proposals (Klimov & Baranov, 2001; van Rensen & Klimov, 2005): (*1*) HC is bound to or is a structural part of the assembled Mn_4O_xCa cluster, (*2*) HC remains bound in the vicinity of the Mn_4O_xCa cluster or (*3*) HC is required during photoactivation and then leaves the site.

If HC is a direct ligand to the Mn_4O_xCa cluster it can be assumed that its removal will change the redox-potential of the WOC or may affect the accessibility of the WOC to exogenous reductants like NH_2OH and NH_2NH_2. In this study we probe these ideas by a thorough analysis of FIOPs obtained at 2 mM HC and under HC-

depleted conditions by studying (*i*) the Kok parameters in $S_1Y_D^{ox}$-thylakoids, (*ii*) the lifetimes of the S_0, S_2, and S_3 states and (*iii*) the reduction rates of the WOC by hydrazine and hydroxylamine.

4.2 EXPERIMENTS AND ANALYSIS

4.2.1 PREPARATIVE PROCEDURES

4.2.1.1 Sample Preparation

Thylakoid membranes were isolated either according to (Winget *et al.*, 1965) with some modifications (Messinger & Renger, 1993) (for FIOPs measurements by Joliot-type electrode), or according to (Robinson *et al.*, 1980; Robinson & Yocum, 1980) with slight changes (see Section 2.2.1) (for FIOPs measurements made by Clark-type Pt/Ir electrode (see Section 2.3.3.1)).

'S_1Y_D'- and '$S_1Y_D^{ox}$'-spinach thylakoids were obtained as described above in Section 2.3.3.3. Before the measurements, the thylakoids were thawed in the dark on ice and diluted to [*Chl*] = 0.9 or 1.0 mg ml^{-1} with MCMM buffer (which contained 50−150 mM MES/NaOH at pH 6.3 or 6.5).

4.2.1.2 HCO_3^-/CO_2-Depletion by Sample Washing in C_i-free Buffers

C_i depletion from the thylakoids was carried out as described in (Klimov *et al.*, 1995a; Klimov *et al.*, 1995b) by sample incubation and washing in C_i-depleted buffers (see Table 2.1 in Section 2.1.2) with some modifications (for details, see Section 2.2.3.1). We employed two types of C_i-depleted thylakoids: (*i*) *HC_{air}(–) thylakoids*, obtained by 200-fold dilution and 10-min dark incubation and washing in the HC_{air}(–) medium, and (*ii*) *HC_{Ar}(–) thylakoids*, that were obtained by 50−80-fold dilution and subsequent dark incubation on ice for 2−10 h under argon atmosphere in the HC_{Ar}(–) medium (for further details, see Sections 2.1.2 and 2.2.3.1).

4.2.1.3 Treatment of Thylakoids with Sodium Formate

Formate treatment of the $S_1Y_D^{ox}$-thylakoids was done according to the method described in (Stemler & Radmer, 1975) with some modifications. Samples were treated in the HC_{Ar}(–) medium containing 50 mM $NaHCO_2$ at 20 °C and pH 5.0 for 15 min. Then the treated samples were diluted 50-fold in HC_{Ar}(–) medium (pH 6.5) containing 50 mM $NaHCO_2$. Subsequently the thylakoids were collected by centrifugation, washed once in the same medium and finally resuspended to 1 mg Chl ml^{-1}. In reversibility experiments 10 mM $NaHCO_3$ was added to the samples ~1 min prior to the FIOP measurements, or the samples were washed in formate-free HC_{Ar}(–) buffer (pH 6.5).

4.2.1.4 Treatment of Thylakoids with Sodium Acetate

Acetate treatment of the $S_1Y_D^{ox}$-thylakoids was performed according to the method described in (Stemler *et al.*, 1974) in HC_{Ar}(–) buffer containing 40 mM CH_3COONa (30 min at 20 °C and pH 5.0 or pH 6.5). In cases, where acetate is removed prior to FIOP measurements, the treated samples were washed twice in a 50-fold excess of HC_{Ar}(–) medium (pH 6.5). Subsequently the samples were resuspended in HC_{Ar}(–) medium to 1 mg Chl ml^{-1}. In order to test the reversibility of the treatments 10 mM HC was

added to the acetate-treated samples about ~1 min before the start of the FIOP measurements.

4.2.1.5 Treatment of Thylakoids with NH_2NH_2 and NH_2OH

Hydrazine ($NH_2NH_2 \cdot H_2SO_4$) treatment of the samples was done according to the method described earlier (Messinger *et al.*, 1997a) with some modifications. Only freshly prepared and pH-adjusted NH_2NH_2 solutions were used for incubation with PSII samples. $HC_{air}(-)$ thylakoids were washed in $HC_{air}(-)$ medium (pH 6.3) and then diluted to a [*Chl*] = 0.9 mg ml^{-1} either with 3 mM NH_2NH_2 solution either dissolved in $HC_{air}(-)$ medium or in MCMM medium containing 2 mM $NaHCO_3$ (HC(+) medium). The NH_2NH_2 incubation was carried out with $S_1Y_D^{ox}$-thylakoids in the dark at pH 6.3 and 20 °C. At certain incubation times the samples (20 μl) were layered on a membrane-covered Pt/Ir cathode of a highly sensitive Clark-type-electrode.

Hydroxylamine ($NH_2OH \cdot HCl$) treatment was performed according to (Messinger *et al.*, 1991) with slight changes. $S_1Y_D^{ox}$-$HC_{Ar}(-)$ thylakoids were prepared as described above to give final concentration of 2 mg Chl ml^{-1}. The reaction was then started by the addition of NH_2OH solutions in $HC_{Ar}(-)$ or HC(+) medium. The NH_2OH solutions were prepared and adjusted to pH 6.5 shortly before the addition to PSII. The NH_2OH incubation was performed in the dark on ice. After the indicated incubation times 10 μl aliquots were taken in a very dim green light and rapidly transferred to the bare platinum cathode of the Joliot-type-electrode. In some cases NH_2OH was removed from the samples prior to taking the FIOPs. This was done by washing the NH_2OH treated samples in a 50-fold excess of MCMM medium (either $HC_{Ar}(-)$ or HC(+)).

4.2.2 FIOPs MEASUREMENTS

4.2.2.1 Clark-Type Membrane-Covered Pt/Ir Electrode

FIOPs measurements with the laboratory-built Clark-type membrane-covered Pt/Ir electrode (for details, see Section 2.3.3.1 and Fig. 2.1 therein) were performed in the presence of 0.5 mM FeCy as electron acceptor at pH 6.3 and 20 °C. 20 μl of $S_1Y_D^{ox}$-thylakoids ([*Chl*] = 0.9 mg ml^{-1}) were rapidly transferred (~15 s of transfer time, is the time when direct exposure of the samples to air could occur) and immediately hermetically covered by quartz glass (see Fig. 2.1). Then the samples were polarized in the dark on a membrane-covered electrode for 6 min prior to starting the FIOPs. For sample excitation 13 saturating Xenon flashes were given at a flash frequency of 0.5 Hz (see Section 2.3.3.1).

4.2.2.2 Joliot-Type Bare Pt Electrode

The FIOPs measured with a home-built Joliot-type bare Pt electrode (see, however, Section 2.3.3.2 and Fig. 2.2 therein) were obtained in the absence of exogenous electron acceptors at pH 6.5 and 20 °C. Chlorophyll concentration during the measurements was 1 mg ml^{-1}. For HC-depleted samples only freshly prepared $HC_{Ar}(-)$ buffer (MCMM, pH 6.5) was used as flow buffer, while for control

measurements HC(+) medium was used that contained 2 mM $NaHCO_3$. Since, it was impractical to operate the Joliot electrode inside a glove box, we flushed for HC(–) measurements the airspace above the flow buffer in the reservoir constantly with argon. Tubing between the reservoir and the electrode was kept to a minimum. Direct exposure of the samples to air was only possible during the ~40 s transfer time, required for the application of the 10 μl aliquots onto the electrode surface and for electrode assembly. For some experiments this transfer was done under an open nitrogen 'tent' to further reduce CO_2 contamination. However, the obtained FIOPs were indistinguishable between the two procedures. All other measuring conditions are the same as described in Section 2.3.3.2.

The kinetics of the S_2 and S_3 decay were determinated by exciting the S_1Y_D-thylakoids with one and two single turnover flashes, respectively, and monitoring the FIOPs at various dark-times t_d (from 0.5 to 90 s) after the preflash(es). The kinetics of S_2 oxidation was studied by giving three flashes to the $S_1Y_D^{ox}$-thylakoids and then varying t_d between 0.5–60 min (for further details on the S_i state lifetime measurements see Section 2.3.3.4 and references therein).

All FIOPs measurements were repeated at least 2–3 times.

4.2.3 FIOPs Analysis

The first 16 flashes (in some cases 13) of each FIOP were analyzed within extended Kok model as described in Section 2.3.3.5. In addition to the normal Kok parameters, the following parameters were included in this analysis: (*i*) S_{-1}…S_{-5} states that can be found after the reduction of the WOC with exogenous electron donors (see Eq. 2.13 in Section 2.3.3.5), (*ii*) a high-double-hit probability in the 1st flash (β_1), and (*iii*) S_i state-dependent miss parameters (see Eqs. 2.11, Section 2.3.3.5 and references therein). The theoretical O_2-yield of the *n*th flash (Y_n^{fit}) (see Eq. 2.6 and 2.12) and the fit quality (*fq*) (see Eq. 2.10) were calculated as described in Section 2.3.3.5.

For analysis of the S_i state lifetime data, the fast reductions $S_2Y_D \rightarrow S_1Y_D^{ox}$ and $S_3Y_D \rightarrow S_2Y_D^{ox}$ (Fig. 2.4) were taken into account (Section 2.3.3.5). Biphasic decay is assumed for the least square analysis of the S_2 and S_3 state population (see Eq. 3.1). In contrast, the dark-oxidation of S_0 to S_1 by Y_D^{ox} was modeled by a mono exponential decay (Eq. 3.2) as discussed in Section 3.2.4 (Isgandarova *et al.*, 2003).

4.2.4 MIMS Measurements

MIMS measurements (Fig. 2.5) of the inorganic carbon content (CO_2, HCO_3^-, H_2CO_3) of buffers used in this study were performed with an isotope ratio mass spectrometer described in Section 2.3.4.1. 25 μl of studied buffer (pH 6.4) was injected into 150 μl MCMM medium (pH 6.4) that was thoroughly degassed for 20 min in the MS cell (Fig. 2.6).

4.3 Results

4.3.1 Inorganic Carbon Levels in HC-Depleted Buffers

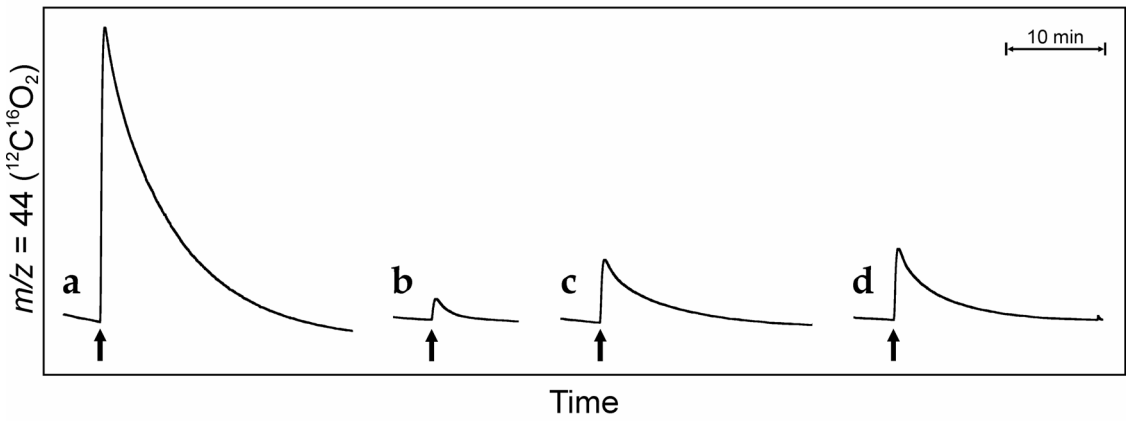

FIGURE 4.1 Membrane-inlet mass spectrometry measurements of the inorganic carbon content (CO_2, HCO_3^-, H_2CO_3) of buffers used in this study. 25 μl aliquots each were injected into 150 μl MCMM medium (pH 6.4) that was thoroughly degassed in the MIMS cell. The time of injection is marked by arrows. Samples: MCMM buffer (pH 6.4) before (***a***) and after (***b***) CO_2-depletion by Ar-bubbling (HC_{Ar}(–) medium). Curves ***c*** and ***d*** show the CO_2 release in HC_{Ar}(–) medium (same as curve ***b***), but after exposure to air on a Joliot-type electrode (for 40 s), and in flow buffer tube (for 5 min).

For most experiments presented in this study HC was removed from the media by argon bubbling and the samples were subsequently assayed on a Joliot-type electrode. Despite extreme care, it cannot be excluded that some CO_2 may diffuse back into the samples during the quick sample transfer and measurements (total time < 2 min). Therefore, the actual C_i levels during the experiments were measured as described below.

The level of HC-depletion from the media can be determined using MIMS (see Fig. 4.1) by monitoring the CO_2 level in depleted buffers compared to air-saturated media at given pH. For this 25 μl of these media were injected into the mass spectrometric cell (150 μl volume) that was filled with degassed buffer (pH 6.4). Comparison of trace *a* (non-depleted buffer) and trace *b* (argon bubbled buffer) shows that our HC-depletion method leads to an about 50-fold reduction of CO_2-levels in the buffer. After a 40 s exposure to air (on the surface of the electrode), which simulates the application of the sample onto the Joliot electrode, this level rises to about 5-fold below ambient (Fig. 4.1 and Table 4.1).

TABLE 4.1. Average amount of CO_2 (measured by area) in different samples of MMCM buffer (pH 6.4) shown in Fig. 4.1 [A].

Buffer samples	CO_2 (%)
(a) *MCMM buffer before HC-depletion*	100.0 ± 1.5
(b) *Fresh HC_{Ar}(–) buffer*	2.3 ± 0.3
(c) *HC_{Ar}(-) buffer (after 40 sec on electrode)*	14.3 ± 2.6
(d) *HC_{Ar}(-) buffer in flow buffer tube (for 5 min)*	20.9 ± 4.7

[A] Values for each buffer samples are mean ± s.e., $n \geq 3$. All measuring conditions are the same as described in Fig. 4.1.

4.3.2 EFFECT OF HYDROGENCARBONATE ON THE KOK PARAMETERS IN $S_1Y_D^{ox}$-THYLAKOIDS

In order to analyze the effect of hydrogencarbonate (HC) on the parameters of the Kok cycle, FIOPs of dark-adapted $S_1Y_D^{ox}$-thylakoids were measured after depletion of HC from the PSII sample (Fig. 4.2). The HC-depletion of PSII was achieved by repeated washing of the thylakoids with pH 6.5 buffer, which had a reduced HC/CO_2 content due to extensive bubbling with argon ('HC_{Ar}(–) buffer'). Fig. 4.2*b* displays a FIOP of thylakoids that were treated as above, but to which subsequently

2 mM $NaHCO_3$ was added. For both samples typical period four oscillations with maxima of O_2 evolution after the 3rd, 7th, and 11th flashes are observed. This indicates the overall miss and double-hit parameters are unaffected by our HC depletion, HC(–), procedure. A close inspection of the data shows, however, that the O_2-yield induced after the 2nd flash, Y_2, is rather large in HC_{Ar}(–) samples (Fig. 4.2*a*). Y_2 is reversed to normal control levels by addition of 2 mM $NaHCO_3$ (Fig. 1*b*). Since both samples were preflashed once prior to the measurement in order to oxidize Y_D at least two mechanism may be responsible for the high O_2-yield induced by the second flash in HC-depleted samples: (*i*) the S_2 decay is significantly slower in HC_{Ar}(–) samples or (*ii*) in HC_{Ar}(–) samples the 1st flash is coupled with a high-double-hit probability, β_1. High β_1 values are known, for example, from FeCy treated PSII samples (Jursinic, 1981) and high-double hits on every second flash were reported earlier for the measurements in the presence of PPBQ (Zimmermann &

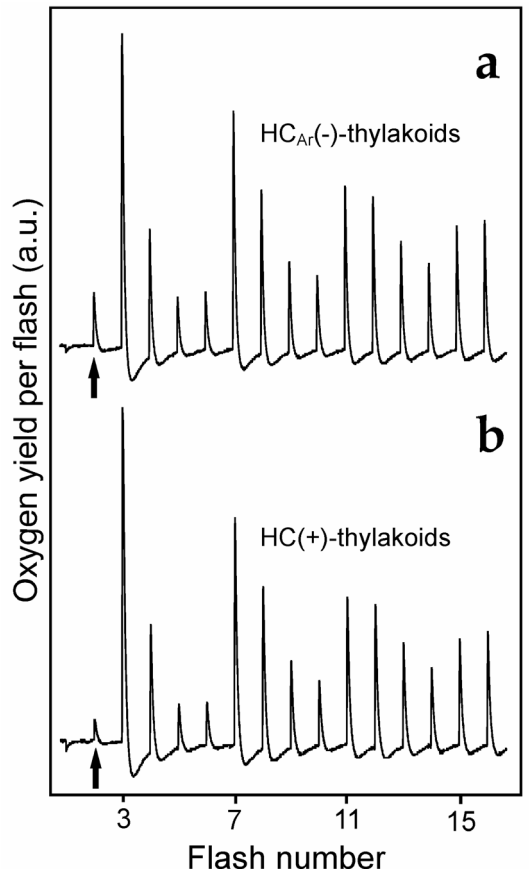

FIGURE 4.2 Original, unnormalized FIOPs of dark-adapted spinach thylakoids ($S_1Y_D^{ox}$) that were incubated and washed in CO_2/HCO_3^- depleted buffer (FIOP ***a***, HC_{Ar}(–) sample). FIOP ***b*** (HC(+) sample) was obtained after readdition of 2 mM $NaHCO_3$ to the HC_{Ar}(–) sample. FIOPs were recorded with a flash frequency of 2 Hz at pH 6.5 and 20 °C. No exogenous electron acceptors were added.

TABLE 4.2. Fits of the FIOPs of preflashed ($S_1Y_D^{ox}$) spinach thylakoids after hydrogencarbonate depletion and readdition of 2 mM $NaHCO_3$ obtained in the absence of exogenous acceptors (displayed in Fig. 4.2) [A].

	Fit parameters (%)								
Sample	**Fit**	**α**	**α_2**	**α_3**	**β**	**β_1**	**S_1**	**S_0**	**fq**
HC_{Ar}-depleted thylakoids (FIOP ***a***)	A_1	12.4	–	–	4.1	–	(100)	–	0.000063
	B_1	12.1	–	–	2.3	10.5	(100)	–	0.000046
	C_1	10.1	–	–	2.4	10.4	86.5	13.5	0.000035
	D_1	–	20.6	20.5	1.7	10.5	(100)	–	0.000028
HC(+) thylakoids (FIOP ***b***)	A_2	12.2	–	–	2.6	–	(100)	–	0.000034
	B_2	12.2	–	–	2.4	3.4	(100)	–	0.000036
	C_2	10.7	–	–	2.5	2.9	90.1	9.9	0.000031
	D_2	–	20.4	20.2	1.9	2.9	(100)	–	0.000023

[A] The FIOPs were obtained at 20 °C and pH 6.5 (Fig. 4.2***a***, ***b***). For fit approaches **A-C** an extended Kok model (for details, see Section 2.3.3.5) with S_i state independent miss (α) and double-hit (β) was used. In fits **D** the miss parameter of the $S_2 \rightarrow S_3$ and $S_3 \rightarrow S_0$ transitions (α_2 and α_3, respectively) were used as free parameters while those for the $S_0 \rightarrow S_1$ and $S_1 \rightarrow S_2$ transitions (α_1 and α_2, respectively) were fixed to 0 (see Sections 2.3.3.5 and 3.3.1). β_1 is the double-hit probability of the first flash. The quality of a fit is represented by the *fq* parameter. Smaller *fq* values indicate a better fit. Dashes denote parameters that were excluded from the fit, while numbers in parentheses give values, which were fixed during optimization. The first 16 flash-induced O_2-yields of each oscillation pattern were analyzed.

Rutherford, 1986). In both cases the non-heme iron (Fe^{2+}) on the acceptor side of PSII is eventually oxidized by the artificial acceptor to Fe^{3+}, which then allows a fast oxidation of Q_A^- within the duration of following xenon flash and thus opens PSII for a second turnover within the same flash. Since, the difference in the 2nd flash O_2 yields persist even after extended dark-times (several hours) between pre-flash and recording of the FIOPs, explanation (*i*) appears rather unlikely (see also S_2 lifetime measurements below). We, therefore, strongly favor option (*ii*).

These qualitative observations are confirmed by a detailed analysis of these FIOPs (see Table 4.2) employing the extended Kok model described in the Experimental Section (see Section 2.3.3.5). The fits in Table 4.2 show that inclusion of the β_1 parameter (fits B and C) leads to a significant improvement of the fit quality for the FIOP obtained with the HC_{Ar}(–) sample; in contrast, the inclusion of this extra parameter does not lead to an improvement of the fit of the FIOP recorded after readdition of hydrogencarbonate (HC(+) sample). We tested several combinations of S_i state-dependent miss parameter (see, for instance fits D in Table 4.2). However, this did not lead to any new insights, and therefore, only one of these approaches is shown in Table 4.2.

Our data differ from previous reports (Jursinic & Stemler, 1984; Stemler *et al.*, 1974; Stemler & Lavergne, 1997). In these earlier publications effects of HC depletion on the miss parameter, but not on β_1 were observed (unless FeCy was added (Jursinic & Stemler, 1984)). A detailed comparison of the HC depletion and measuring conditions

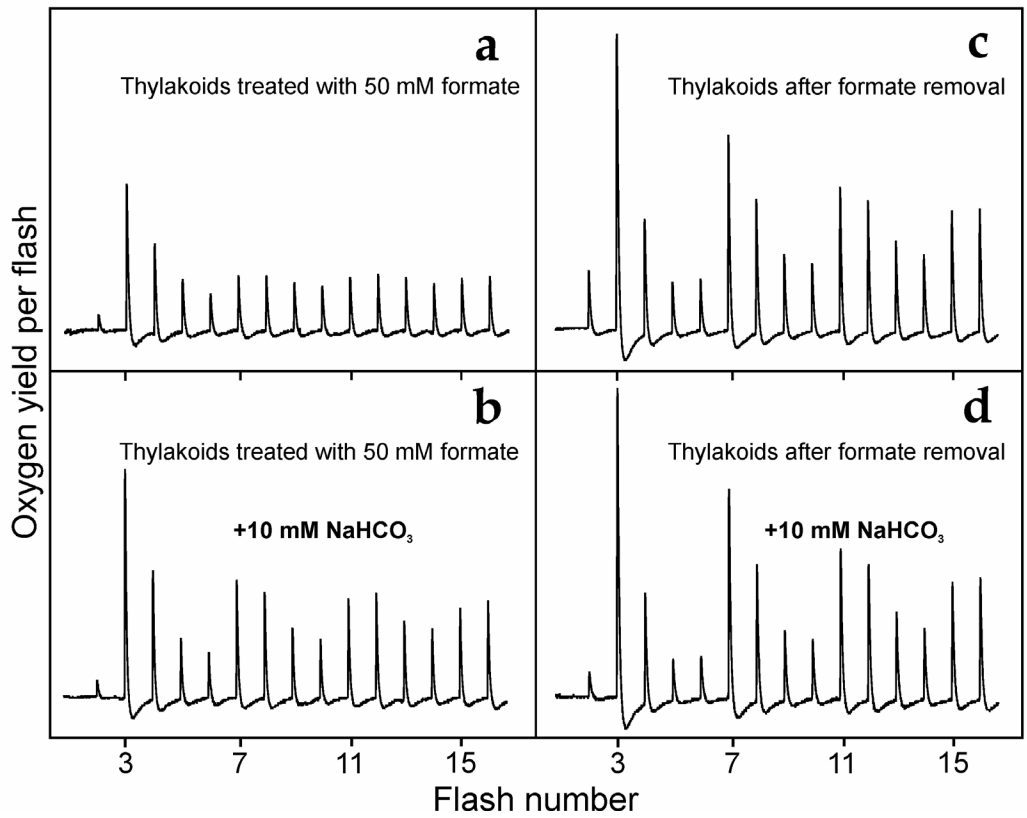

FIGURE 4.3 Original unnormalized FIOPs of dark-adapted spinach thylakoids ($S_1Y_D^{ox}$) that were incubated at pH 5.0 with 50 mM formate (FIOP ***a***). FIOP ***b*** was obtained after addition of 10 mM $NaHCO_3$ to sample ***a***. Washing of sample ***a*** in HC- and formate-free buffer yields FIOP ***c***. FIOP ***d*** was recorded after addition of 10 mM HC to sample ***c***. All FIOPs were recorded with a flash-frequency of 2 Hz at pH 6.5 and 20 °C. No exogenous electron acceptors were added.

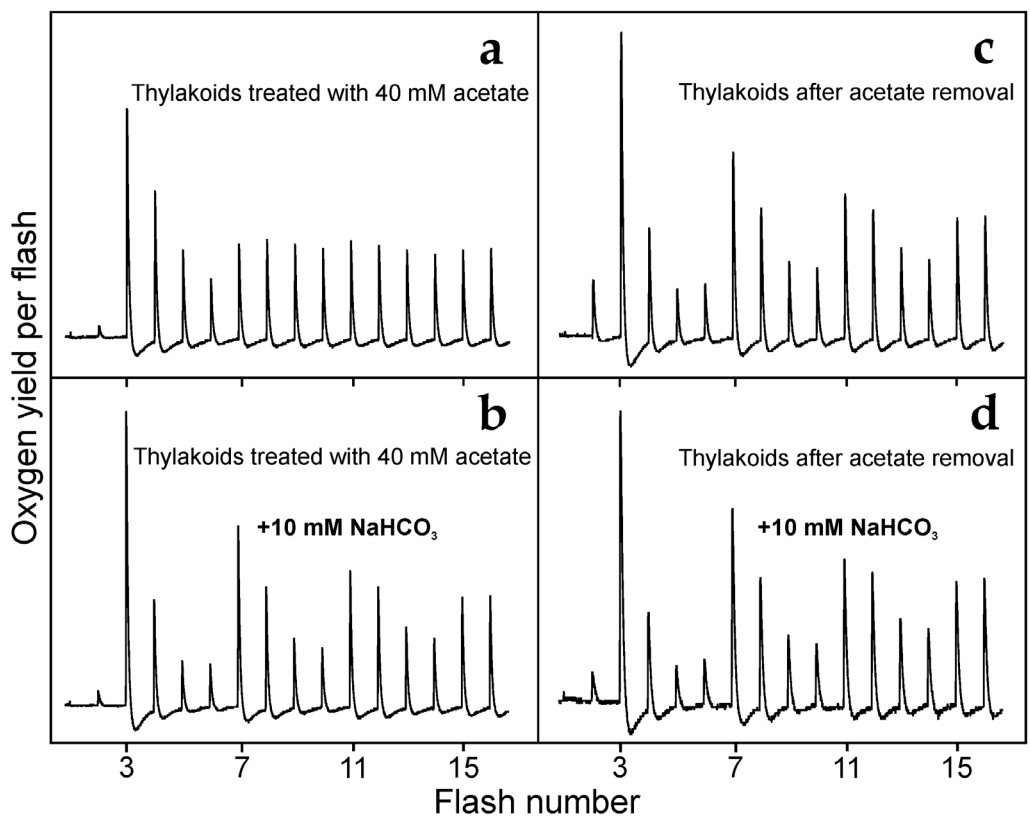

FIGURE 4.4 Original, unnormalized FIOPs of dark-adapted spinach thylakoids ($S_1Y_D^{ox}$) that were incubated for 30 min at pH 5.0 with 40 mM acetate (FIOP ***a***). FIOP ***b*** was obtained after addition of 10 mM $NaHCO_3$ to sample ***a***. Washing of sample ***a*** in HC- and acetate-free buffer yields FIOP ***c***. FIOP ***d*** was recorded after addition of 10 mM HC to sample ***c***. All FIOPs were recorded with a flash-frequency of 2 Hz at pH 6.5 and 20 °C. No exogenous electron acceptors were added.

shows that the most significant difference between the conditions appears to be the presence of either 100 mM formate (Stemler & Lavergne, 1997) or 40 mM acetate (Stemler *et al.*, 1974) during depletion at pH 5.0 and also during the FIOP measurements at pH 6.8. We, therefore, added 50 mM formate (Fig. 4.3) or 40 mM acetate (Fig. 4.4) to our buffer and pre-treated the samples at pH 5.0 as described in the previous publications (Stemler *et al.*, 1974; Stemler & Radmer, 1975) (see also Sections 4.2.1.3 and 4.2.1.4). Figure 4.3*a* and 4.4*a* show that under these conditions, indeed high miss parameters are observed that could be reduced to almost normal values by addition of 10 mM $NaHCO_3$ (Figs. 4.3*b*, 4.4*b*, and Table 4.3). Interestingly, in contrast to our HC depletion procedure neither the addition of formate nor that of acetate leads to an increased β_1 parameter (Figs. 4.3*a*, 4.4*a*, and Table 4.3). While the increase in the miss parameter is similar for formate and acetate (Table 4.3), formate leads under our conditions to an inhibition of ~50% of the PSII centers, while acetate leads only to a decrease of ~10–20% (on the basis of the steady state O_2 yields). Fits employing S_i state-dependent misses gave qualitatively similar results and are, therefore, not presented. These results are in agreement with previous observations (Stemler *et al.*, 1974; Stemler & Lavergne, 1997). It should be remarked that we obtained an only slightly smaller increase of the miss parameter if pH 5.0 treatment was omitted and formate or acetate were added directly to the sample at pH 6.5 (data not shown).

The above experiments demonstrate that the information gathered about the function of hydrogencarbonate in PSII is critically dependent on the choice of the HC

TABLE 4.3. Fits of the flash-induced oxygen evolution patterns (FIOPs) of $S_1Y_D^{ox}$-thylakoids isolated from spinach after incubation with 50 mM $NaHCO_2$ or 40 mM $NaCH_3CO_2$ at pH 5.0 (see Figs. 4.3 and 4.4) [A].

Samples		Fit parameters (%)					fq
		Fit	α	β	β_1	S_1	
Formate-treated thylakoids (Fig. 4.3)	FIOP ***a***	A_1	24.1	6.0	–	(100)	0.000069
		B_1	24.1	4.3	4.3	(100)	0.000087
	FIOP ***b***	A_2	17.6	5.4	–	(100)	0.000054
		B_2	17.2	4.0	4.0	(100)	0.000069
	FIOP ***c***	A_3	12.1	4.0	–	(100)	0.000045
		B_3	11.9	2.8	10.7	(100)	0.000026
	FIOP ***d***	A_4	10.9	2.9	–	(100)	0.000022
		B_4	10.9	2.6	4.3	(100)	0.000023
Acetate-treated thylakoids (Fig. 4.4)	FIOP ***a***	A_5	26.2	5.6	–	(100)	0.000033
		B_5	26.2	3.3	3.3	(100)	0.000055
	FIOP ***b***	A_6	11.7	3.9	–	(100)	0.000029
		B_6	11.6	3.2	3.2	(100)	0.000034
	FIOP ***c***	A_7	12.4	5.5	–	(100)	0.000057
		B_7	12.0	3.4	9.1	(100)	0.000024
	FIOP ***d***	A_8	11.2	4.1	–	(100)	0.000037
		B_8	10.9	2.9	5.9	(100)	0.000022

[A] The FIOPs were obtained at 20 °C in presence of acetate or formate (Patterns ***a***, ***b***), while patterns ***c***, ***d*** were obtained after removal of acetate/formate from the samples. Patterns ***b***, ***d*** were recorded after addition of 10 mM $NaHCO_3$. The FIOPs were fit using two different approaches (**A, B**) within an extended Kok model. Parameter: α, S_i state independent miss parameter; β, S_i state independent double-hit parameter and β_1, double-hit probability of the first flash. The quality of a fit is represented by the *fq* parameter. Smaller *fq* values indicate a better fit. Dashes denote parameters that were excluded from the fit, while numbers in brackets give values that were fixed during optimization.

depletion procedure. To investigate this further, we washed formate or acetate treated thylakoids with HC_{Ar}(–) buffer (pH 6.5). This procedure removes these additives from the samples, while simultaneously minimizing the rebinding of HC to PSII. The FIOPs obtained under these conditions are shown in Figs. 4.3*c* and 4.4*c*, respectively. Interestingly, these FIOPs are almost identical to that in Fig. 4.2*a*, *i.e.*, they show normal miss parameters and an increased oxygen yield in the second flash. Remarkably, also the formate induced block of PSII centers is fully removed during this washing step. This finding is in agreement with two previous studies (Feyziev *et al.*, 2000; Wiessner *et al.*, 1992). The high β_1 value (Figs. 4.3*c*, 4.4*c*) can be reversed by addition of $NaHCO_3$ (Figs. 4.3*d*, 4.4*d*).

It is important to note, that in above-described measurements our samples did not contain any exogenous electron acceptors. Therefore, we also employed the measurements of FIOPs in the presence of FeCy (as exogenous electron acceptor) in order to check, whether the effect of HC depletion on β_1 disappear in the samples with oxidized non-heme iron. For these measurements we used a highly sensitive membrane-covered (Clark-type) electrode described in Experimental Sections 2.3.3.1 and 4.2.2.1. Figure 4.5*a* shows the FIOPs with typical period four oscillations with maxima on the 3rd and 7th flashes obtained in $S_1Y_D^{ox}$-HC_{air}(–) thylakoids (Section 4.2.1.2) that were pre-treated with 0.5 mM FeCy before flash illumination in the absence (curve *1*) and presence (curve *2*) of 2 mM $NaHCO_3$. There is no significant differences between these two FIOPs except the amplitudes of all flashes are slightly higher in the presence of HC. As visually seen from the original (Fig. 4.5*a*) and

normalized FIOPs (Fig. 4.5*b*), the overall miss and double-hit parameters seem to be unaffected by the HC depletion procedure as in previous case (Fig. 4.2, Table 4.2). Furthermore, a rather high Y_2, (that corresponds to a high value of β_1) is seen for both sample types due to the presence of FeCy (Fig. 4.5*a*, *b*).

Detailed analysis of these oscillation patterns was performed using an extended Kok model (Section 4.2.3). The results are presented in Table 4.4. In both fits (A and B) the very high value of β_1 (~22%) was unaffected by our HC depletion and/or HC re-addition procedures. Fits A (which assume S_1 state population equal to 100%), reveal that the miss parameter is only slightly lower for HC(+)-thylakoids (fit A_1; α = 6.9%) compared to HC_{air}(–)-thylakoids (fit A_2; α = 8.1%), while in fits B (where S_1 and S_0 state populations were set as free parameters), these α-values are practically the same (Table 4.4). Thus, the presence of FeCy during the FIOPs measurements eliminates HC effect on β_1 parameter observed in the absence of exogenous acceptors (Fig. 4.2, Table 4.2).

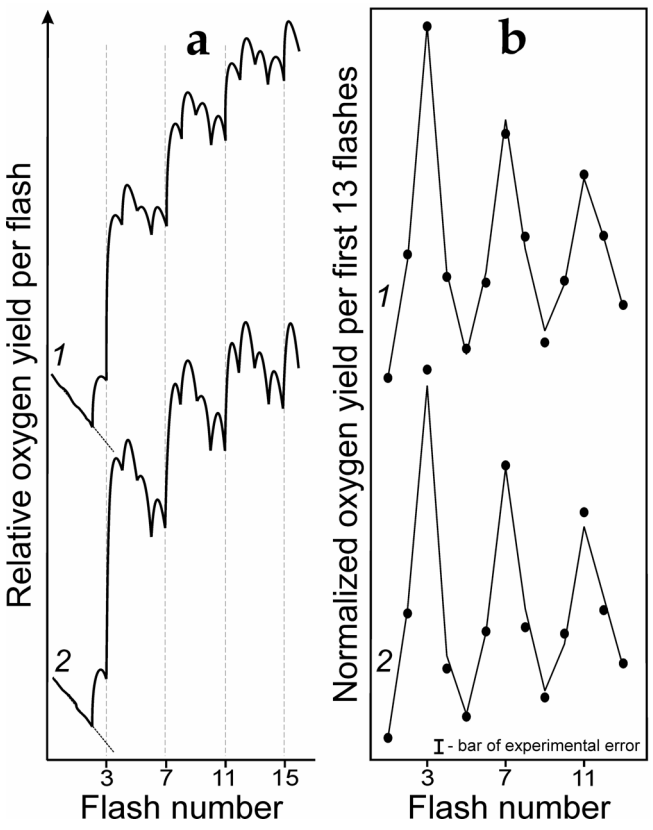

FIGURE 4.5 Original traces of FIOPs (***a***) and their calculated normalized O_2 yields per flash (***b***) of dark-adapted $S_1Y_D^{ox}$- thylakoids that were incubated and washed in HC_{air}(–) medium (pH 6.3) in the absence (traces ***1***) and presence of 2 mM $NaHCO_3$ (traces ***2***) at 20 °C. Solid lines on ***b*** show the fits in accordance with the extended Kok model (see fits B in Table 4.4) described in Section 2.3.3.5. Experimental data on ***b*** are represented by circles. Bar shows maximal possible experimental error which could be caused by noise level and it spreads on all flashes. The flash frequency was 0.5 Hz. All measurements were carried out at [*Chl*] = 0.9 mg ml^{-1} in the presence of 0.5 mM FeCy as electron acceptor.

TABLE 4.4. Fits of the FIOPs of $S_1Y_D^{ox}$ spinach thylakoids after hydrogencarbonate depletion and readdition of 2 mM $NaHCO_3$ obtained in the presence of 0.5 mM FeCy as electron acceptor (shown in Fig. 4.5) [A].

	Fit parameters (%)						
Sample	**Fit**	**α**	**β**	**β_1**	**S_1**	**S_0**	**fq**
HC_{air}-depleted thylakoids	A_1	8.1	1.8	21.5	(100)	–	0.000036
(FIOP ***1***)	B_1	7.0	1.6	22.3	92.1	7.9	0.000034
HC(+) thylakoids	A_2	6.9	2.0	22.0	(100)	–	0.000024
(FIOP **2**)	B_2	6.7	1.8	21.9	98.3	1.7	0.000038

[A] The FIOPs were obtained at 20 °C and pH 6.3 (Fig. 4.5, traces ***1*** and **2**). For both fit approaches (**A**, **B**) an extended Kok model (see Section 2.3.3.5) with S_i state independent miss (α), double-hit (β), and high double-hit probability after the first flash (β_1). The first 13 flash-induced O_2 yields of each oscillation pattern have been analyzed. Numbers in parenthesis give values, which were fixed during optimization. Dashes indicate that parameters were excluded from the fit. The *fq* parameter gives the quality of a fit.

4.3.3 S_0, S_2 AND S_3 LIFETIME MEASUREMENTS

For testing the effect of hydrogencarbonate depletion on the redox potential of the Mn_4O_xCa cluster we explored the effect of HC depletion on the rates of S_2 and S_3 state reduction by endogenous electron donors. The expectation is that removal of HC from a putative binding site at the Mn_4O_xCa cluster should modify the redox potential of the cluster and thereby, alter the stability of the higher S_i states. The S_2 and S_3 lifetimes were determined in the traditional way by giving one (S_2 state) or two (S_3 state) preflashes and varying the dark-time to the FIOP measurements (for details, see Section 2.3.3.4 and Fig. 2.3). The obtained FIOPs were then deconvoluted into S_i state populations taking the back reactions of Y_D with S_2 and S_3 into account (see Fig. 2.4). The obtained S_2 and S_3 populations are plotted for HC(+) (closed symbols) and HC_{Ar}(–) thylakoids (open symbols) as a function of dark-time in Fig. 4.6. Lines represent for both sample types biexponential fits. The two phases in the reduction of S_2 and S_3 originate from electron donation by Y_D (fast kinetics) and by the acceptor side of

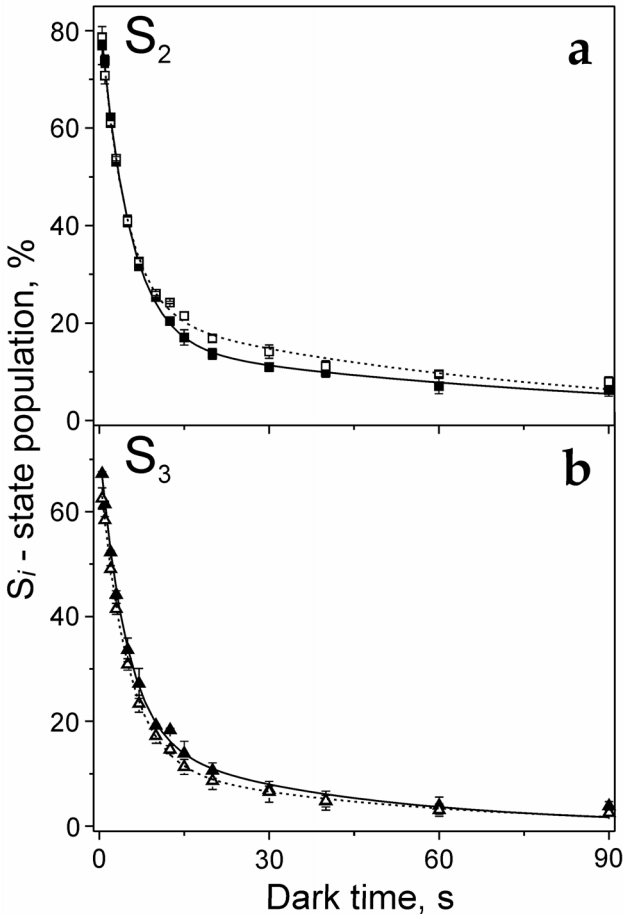

FIGURE 4.6 Relative S_2 (top, ***a***) and S_3 (bottom, ***b***) state populations of spinach thylakoids (S_1Y_D) as a function of dark-time between one or two preflash(es), respectively, and the main train of saturating single turnover flashes. Closed symbols: thylakoids were incubated over night in HC_{Ar}(–) buffer. Open symbols: treated as above, but after addition of 2 mM $NaHCO_3$. Symbols and error bars represent the average of 2 or 3 independent measurements. The lines represent biexponential fits (Table 4.5). The lifetime measurements were performed at 20 °C and pH 6.5.

TABLE 4.5. S_i state decay in HC(+) and HC_{Ar}(–) thylakoids [A].

		CO_2/HCO_3^- depleted medium			In presence of 2 mM $NaHCO_3$		
		***k*, s^{-1}**	***t*$_{1/2}$, s**	**A, %**	***k*, s^{-1}**	***t*$_{1/2}$, s**	**A, %**
Slow phase	S_2	0.014	51	26	0.011	59	19
	S_3	0.022	32	18	0.026	27	23
Fast phase	S_2	0.22	3.1	74	0.19	3.6	81
	S_3	0.21	3.3	82	0.21	3.3	77
		***k*, min^{-1}**	***t*$_{1/2}$, s**		***k*, min^{-1}**	***t*$_{1/2}$, s**	
	S_0	0.060	690		0.053	780	

[A] Rate constants (*k*), half-times ($t_{1/2}$) and amplitudes (A, % of total decay) for S_0 state oxidation by $S_1Y_D^{ox}$ and for the S_2 and S_3 state reduction by Y_D (fast phase) and the acceptor side (slow phase) in spinach thylakoids after over-night dark-incubation (on ice) in HC_{Ar}(–) medium. The measurements were performed at 20 °C and pH 6.5 either in the absence or presence of 2 mM $NaHCO_3$. The fit error for the values is ~10%.

PSII (slow kinetics).

It is clear from Fig. 4.6 that our HC depletion (method 1) and measuring conditions (see below) do not affect the stability of the S_2 and S_3 states. Within an estimated fit error of about 10% the derived kinetics for the fast and slow decays of these S_i states are found to be independent of the presence or absence of HC (Table 4.5). Despite the above-discussed significant differences in sample treatment, this result is in agreement with the earlier publication of (Stemler *et al.*, 1974), where the slow S_3 state decay was shown to be independent of the HC concentration in a medium containing acetate. It may be remarked, however, that the present data give more direct information, because (*i*) the complication with acetate is avoided and (*ii*) the possible mixing of donor and acceptor side effects of HC during S_2 and S_3 state decay is avoided by studying the interaction of Y_D with the Mn_4O_xCa cluster.

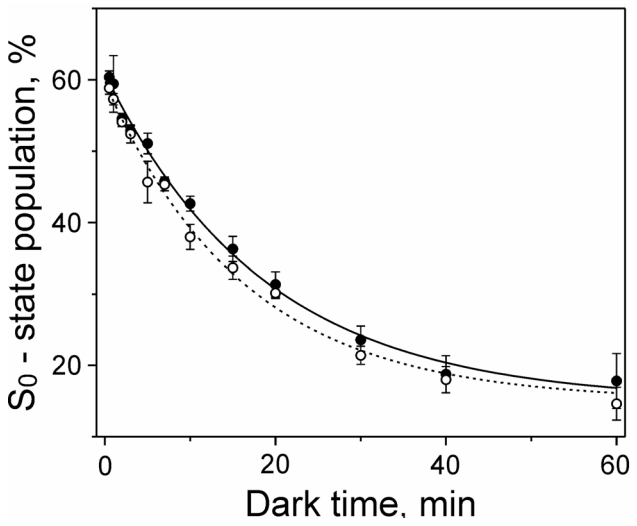

FIGURE 4.7 Relative S_0 state populations of spinach thylakoids ($S_1Y_D^{ox}$) as a function of dark-time between three preflashes and a train of saturating single turnover flashes. Closed symbols: thylakoids were incubated over night in HC_{Ar}(–) buffer. Open symbols: treated as above, but after addition of 2 mM $NaHCO_3$ shortly before the measurement. Symbols and error bars represent the results of three measurements. The lines show monoexponential fits (see Table 4.5). The measurements were performed at 20 °C and pH 6.5.

These lifetime measurements were completed by measuring the kinetics of S_0 oxidation to S_1 by Y_D^{ox}. In this case, three preflashes are used to excite $S_1Y_D^{ox}$-thylakoids. Then again the dark-time is varied to the recording of the FIOPs. The results obtained for HC(+) (closed symbols) and HC_{Ar}(–) thylakoids (open symbols) are shown in Fig. 4.7. Within the fit error of 10% practically no differences exist between the two sample types (Table 4.5). Therefore, HC does not affect the redox potential of the S_0 state under our conditions.

4.3.4 HYDROGENCARBONATE EFFECTS IN CHEMICALLY REDUCED STATES OF THE WOC

4.3.4.1 Reduction of the WOC by NH_2OH and NH_2NH_2

The HC was shown to be a cofactor during photoactivation of PSII and to form complexes with Mn^{2+} (Baranov *et al.*, 2004; Dismukes *et al.*, 2001; Kozlov *et al.*, 2004). It is, therefore, possible that HCO_3^- binds to the Mn_4O_xCa cluster in the chemically reduced S_{-i} states, because most of the S_{-i} states contain at least one Mn^{2+} ion (except S_{-1}, which may contain only Mn^{3+} ions). Similar to the S_i state lifetime measurements above we assume that binding of HC to the Mn_4O_xCa cluster in the S_{-i} states would modify the redox potential of the reduced states and/or alter their accessibility for NH_2OH, and thereby slow down a possible further reduction.

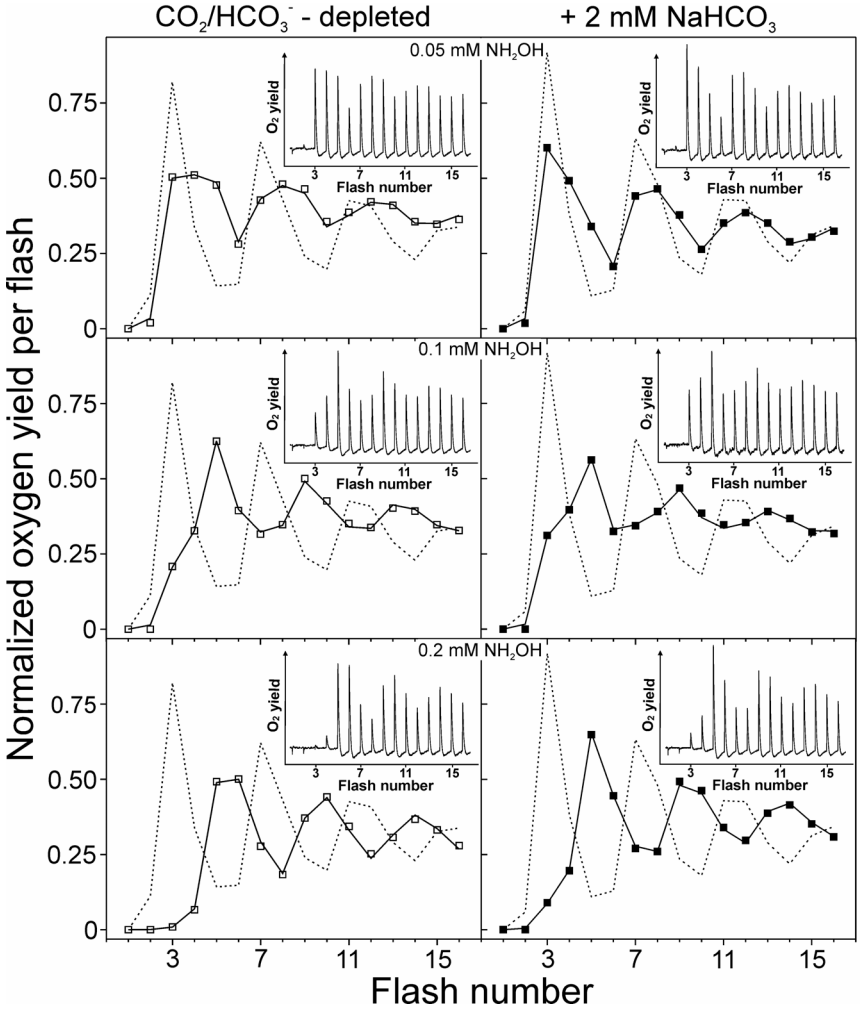

FIGURE 4.8 Normalized FIOPs of spinach thylakoids ($S_1Y_D^{ox}$) measured after 1 min treatments with 0.05 mM (top), 0.1 mM (middle) and 0.2 mM (bottom) NH_2OH on ice at pH 6.5. HC_{Ar}(–) samples (left side, open symbols) were obtained by washing with CO_2/HCO_3^-depleted buffer prior to NH_2OH incubation. For HC(+) samples (right side, closed symbols) 2 mM $NaHCO_3$ was added to HC_{Ar}(–) samples about 1 min before the addition of NH_2OH. FIOP measurements were performed without removal of NH_2OH from the samples. Solid lines show fits with the extended Kok model described in the Experimental Section 4.2.3 (see Eq. 2.13). Broken lines represent FIOPs of HC_{Ar}(–) and HC(+) thylakoids, respectively, prior to the addition of NH_2OH. The inserts show the original, unnormalized FIOPs. FIOPs were recorded with a flash-frequency of 2 Hz at pH 6.5 and 20 °C. No exogenous electron acceptors were added. Normalization of the FIOPs was performed by dividing each flash-induced O_2-yield by the average of the O_2-yields induced by flashes 4–7.

Figure 4.8 presents original (insets) and normalized FIOPs (symbols) that were obtained with spinach thylakoids after 1 min of dark incubation with the indicated concentrations of NH_2OH in HC_{Ar}(–) medium (left) and HC(+) medium (right). The dotted lines show for comparison the respective FIOP of the $S_1Y_D^{ox}$ thylakoids prior to NH_2OH addition. An inspection of the data shows that independent of the presence of HC a progressive shift of the 1st maximum of oxygen evolution towards higher-flash numbers is observes as a function NH_2OH concentration. However, the extent of this shift at all concentrations smaller in the presence of HC samples (right side) as compared to those obtained with HC_{Ar}(–) thylakoids (left side of Fig. 4.8). Employing the extended Kok model (see Section 4.2.3) we calculated the S_i/S_{-i} state distribution of the WOC for FIOPs shown in Fig. 4.8. Indeed, as seen in Table 4.6, the shift of the WOC to the reduced S_{-i} states (by NH_2OH) is retarded by the presence of 2 mM $NaHCO_3$ in the HC_{Ar}(–) medium.

TABLE 4.6. S_i state distribution of flash-induced oxygen evolution patterns displayed in Fig. 4.8 [A].

Sample	[NH_2OH] (mM)	Fit parameters (%)					fq
		S_1	S_0	S_{-1}	S_{-2}	S_{-3}	
HC_{Ar}-depleted thylakoids	**0.05**	34.1	27.9	30.3	4.5	3.2	0.000003
	0.1	14.2	18.2	51.1	11.0	5.6	0.000003
	0.2	0.6	1.3	52.5	36.5	9.2	0.000006
HC(+) thylakoids	**0.05**	46.0	28.3	20.9	1.9	2.9	0.000005
	0.1	21.8	22.8	43.8	6.7	5.0	0.000003
	0.2	6.4	9.6	61.3	16.7	6.0	0.000003

[A] The extended Kok model described in Section 4.2.3 was used to fit FIOPs of $S_1Y_D^{ox}$-HC_{Ar}(–)- and $S_1Y_D^{ox}$-HC(+)- thylakoids measured after 1 min dark treatments with 0.05 mM, 0.1 mM and 0.2 mM NH_2OH on ice at pH 6.5. Fixed parameters: misses 10.0%, double hits 2.4%, other S_i states 0.0%. The values of double hit probability of the first flash were set to be equal to 2.4% for both sample types, since, the inclusion of its high value into the fit (~10%) for HC_{Ar}(–) thylakoids significantly decreased quality of the fit (*fq*) (not shown). Smaller *fq* values indicate a better fit. The first 16 flash induced O_2-yields of each FIOP were analyzed.

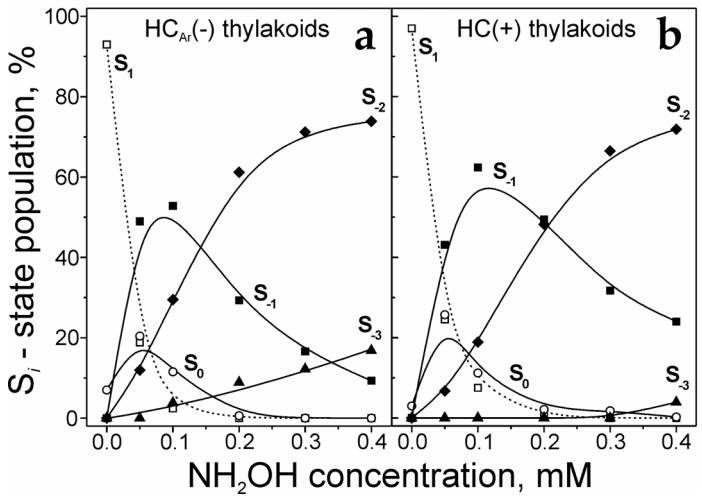

FIGURE 4.9 Normalized S_i state population of spinach thylakoids ($S_1Y_D^{ox}$) as a function of NH_2OH concentration. The FIOPs measurements were carried out with HC_{Ar}(–) (*a*) and HC(+) (*b*) thylakoids. The samples were incubated with NH_2OH for 5 min on ice at pH 6.5. All other conditions are as described in Fig. 4.8.

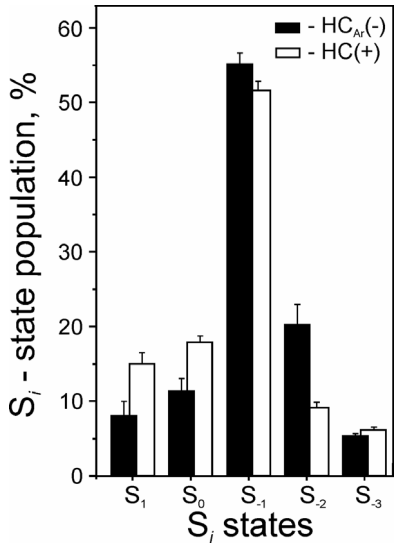

FIGURE 4.10 Normalized S_i state population of HC_{Ar}(–) (black columns) and HC(+) (white columns) $S_1Y_D^{ox}$-thylakoids after incubation with 50 μM NH_2OH for 10 min on ice at pH 6.5. For other conditions see Fig. 4.8.

Figure 4.9 displays the calculated normalized S_i state populations as a function of NH_2OH concentration in thylakoids after dark-incubation during 5 min in C_i-depleted medium without (a, left side) and after re-addition of hydrogencarbonate (b, right side). Again, an apparent retardation in the reduction of all S_i states is observed. The above-discussed differences are still present even after more prolonged (10 min) dark-incubation of the samples with NH_2OH (see Fig. 4.10).

In addition, we employed NH_2NH_2 treatment for the reduction of the WOC. The advantage is that in contrast to the one-electron NH_2OH (see, for instance, Table 4.6) NH_2NH_2 is a two-electron reductant ($S_1 \rightarrow S_{-1} \rightarrow S_{-3}$). This allows to reach a higher population of the S_{-3} state for further probing of HC effect on the reduced S states of the WOC. In this case FIOPs were obtained using a highly sensitive Clark-type electrode covered with a very thin polymer membrane. The measurements were performed in the presence of FeCy.

The visible shift of the first maximum of O_2 evolution from flash 3 (broken lines in Fig. 4.11*b*) to flashes 6/7 that appears after a 20-min dark incubation at 20 °C of $S_1Y_D^{ox}$-thylakoids in the presence of 3 mM NH_2NH_2 in the HC_{air}(–) medium (pH 6.3) is shown in Fig. 4.11 (traces *1*). The same NH_2NH_2-treatment in the presence of 2 mM $NaHCO_3$ leads to the shift of the first O_2 evolution maximum to flashes 5/6 (traces *2*).

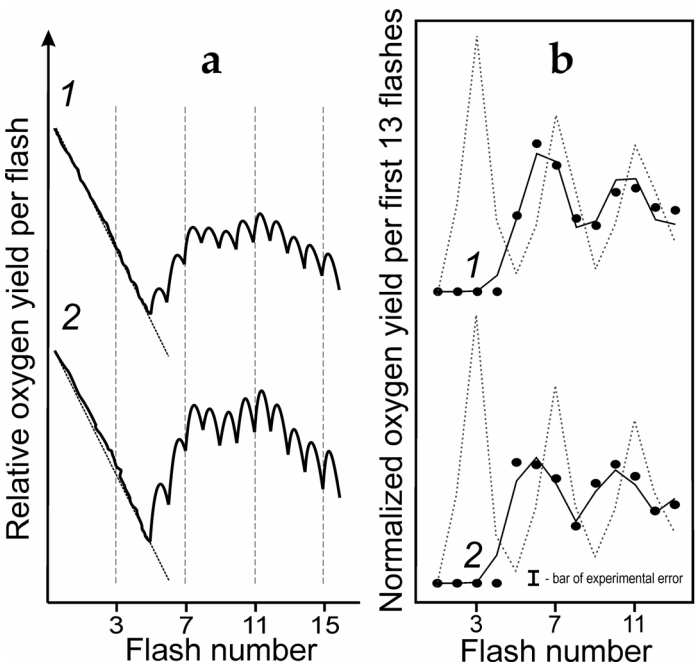

FIGURE 4.11 Original, unnormalized FIOPs (***a***) and the respective normalized O_2 yields per flashes (***b***) of dark-adapted HC_{air}(–) $S_1Y_D^{ox}$-thylakoids (broken lines) obtained after a 20-min incubation with 3 mM NH_2N_2H (dissolved in HC_{air}(–) medium) in the dark at 20 °C and pH 6.3 in the absence (traces ***1***) and presence (traces ***2***) of 2 mM $NaHCO_3$. The measurements were done without removal of NH_2NH_2 from the treated samples. The corresponding fits on ***b*** (solid curves) are given in Table 4.7. Experimental data on ***b*** are represented by circles. Bar shows maximal possible experimental error which could be caused by noise level and it spreads an all flashes. FIOPs were recorded with a flash-frequency of 0.5 Hz at pH 6.3 and 20 °C. All measurements were carried out at [*Chl*] = 0.9 mg ml^{-1} in the presence of 0.5 mM $K_3[Fe(CN)_6]$ as exogenous electron acceptor.

Two strategies within an extended Kok model (see Experimental Section 4.2.3) were undertaken to analyze these FIOPs shown in Fig. 4.11*a* (traces *1* and *2*): (*i*) assuming that S_{-3} state is the lowest possible oxidation state of the WOC (fits A in Table 4.7) and (*ii*) assuming S_{-5} is the lowest oxidation state of the WOC (fits B in Table 4.7) because preliminary evidence for the existence of labile S_{-4} and S_{-5} states has been obtained from the analysis of FIOPs on *T. elongatus* thylakoids (Messinger *et al.*, 2001a). Thus, S_1–S_{-3} and S_1–S_{-5} states populations were varied (see Table 4.7) but α, β and β_1-probabilities were fixed to the values found in 'control' $S_1Y_D^{ox}$-thylakoids as shown in Table 4.4.

The presence of 2 mM $NaHCO_3$ during NH_2NH_2-treatment, as seen Fig. 4.11*b* and in Table 4.7 (compare fits A and A_1) obviously changes the S_{-i} state distribution of the reduced WOC. Normalized S_i state populations in the presence of 2 mM $NaHCO_3$ were following: 32% of S_{-1}, 36% of S_{-2} and 31% of S_{-3}. In the absence of HC in HC_{air}(–) medium, only 16% of S_{-1} state still remains while S_{-2} and S_{-3} states dominated (40% and 44%, respectively). Remarkably, if we evaluate the S_i state populations assuming that S_{-5} is the lowest S state of the WOC then S_{-i} state distribution in the presence of HC remains unchanged (fits A_1 and B_1 in Table 4.7), while in the absence of HC, a quite different S_{-i} state distribution corresponding to 10% of S_{-1}, 45% of S_{-2}, 34% of S_{-3} and ~11% of formal S_{-4} is obtained (fits A and A_1 in Table 4.7). In spite of the not ideal fit quality, these two approaches make clear that the shift to the lowest S_{-i} states is higher in the samples treated with NH_2NH_2 in the absence of HC in HC_{air}(–) medium.

TABLE 4.7. S_i state distribution of FIOPs displayed in Fig. 4.11 [A].

Sample	Fit	Fit parameters (%) S_1	S_0	S_{-1}	S_{-2}	S_{-3}	S_{-4}	S_{-5}	fq
HC_{air}(–) depleted	A	0.0	0.0	15.5	40.2	44.3	–	–	0.000207
thylakoids	B	0.0	0.0	9.9	45.0	34.4	10.7	0.0	0.000194
HC(+)- thylakoids	A_1	0.0	0.0	31.8	36.0	31.2	–	–	0.000269
	B_1	0.0	0.0	31.8	36.0	31.2	0.0	0.0	0.000376

[A] The extended Kok model described in Section 4.2.3 was used to fit FIOPs of $S_1Y_D^{ox}$-HC_{air}(–)- and $S_1Y_D^{ox}$-HC(+)- thylakoids measured after 20 min dark incubation with 3 mM NH_2NH_2 at 20 °C and pH 6.3. Fixed parameters that were found in 'control' $S_1Y_D^{ox}$-thylakoids (for details, see Table 4.4): miss probability 6.9%, double hit probability 1.8% and, double hit probability of the first flash 22.0% (for both sample types, since, the FIOPs were obtained in the presence of $K_3[Fe(CN)_6]$). Smaller *fq* values indicate a better fit. Dashes denote parameters excluded from the fit. The first 13 flash induced O_2-yields of each FIOP were analyzed.

Figure 4.12 displays the calculated normalized S_{-i} state populations assuming that S_{-3} (*a*, *b*) or S_{-5} (*c*, *d*) states are the lowest reduced states of the WOC as a function of incubation time of HC_{air}(–)-$S_1Y_D^{ox}$-thylakoids with 3 mM NH_2NH_2 at 20 °C and pH 6.3 in the absence (*a*, *c*) and in the presence (*b*, *d*) of 2 mM $NaHCO_3$. As seen in Fig. 4.12*a* and *b*, the addition of 2 mM $NaHCO_3$ into the HC_{air}(–) thylakoids obviously changes the S_i/S_{-i} state distributions in the same direction as observed with NH_2OH-treated thylakoids to which no exogenous electron acceptors were added.

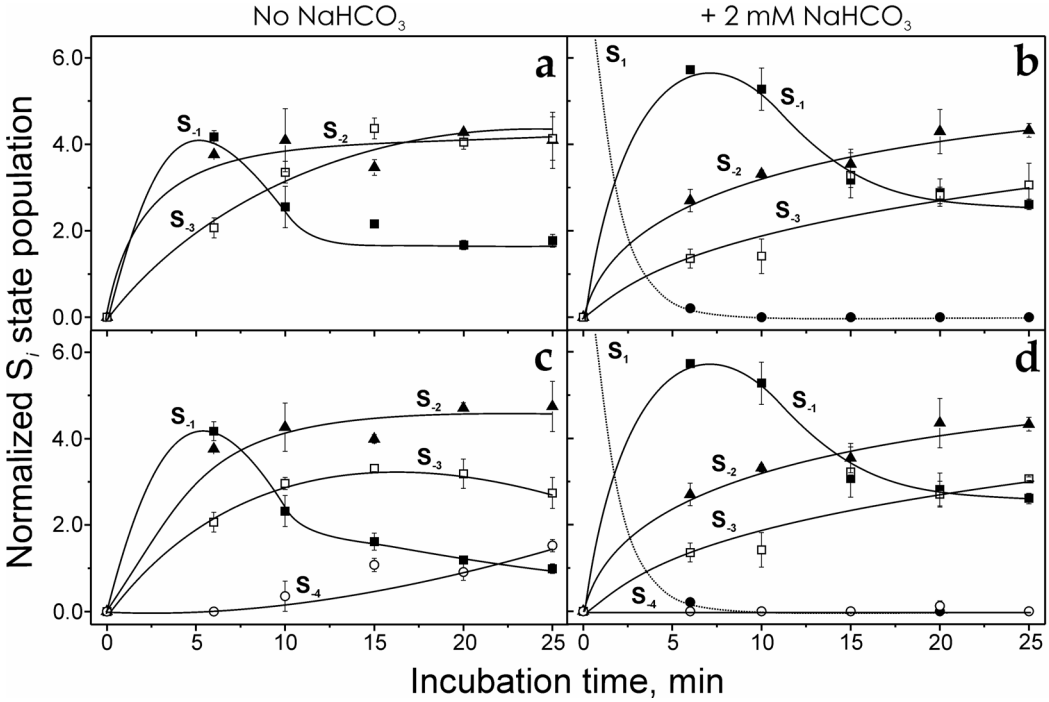

FIGURE 4.12 Normalized S_i state population of spinach thylakoids ($S_1Y_D^{ox}$) as a function of dark incubation time with 3 mM NH_2NH_2 in HC_{air}(–) medium at pH 6.3 and 20 °C. Incubations were carried out in the absence (***a***, ***c***) and in the presence (***b***, ***d***) of 2 mM $NaHCO_3$. The obtained data were calculated assuming that the lowest redox states of the WOC are S_{-3} (***a***, ***b***) or S_{-5} (***c***, ***d***) states. For the sake of clarity, the S_{-5} state is not shown as no population of this state was obtained. In the case of incubation in HC_{air}(–) medium containing 2 mM $NaHCO_3$ (***b***, ***d***) the fast decay of the S_1 population is also shown since after 6-min incubation some population of this state still remains while in HC_{air}(–) medium without added $NaHCO_3$ (***a***, ***c***) no population of S_1 state was obtained. The O_2 yields of the first 13 flashes were included in the fits. Misses (α), double hits (β) and high double hits in the first flash were kept at the values determined for the 'control' $S_1Y_D^{ox}$-thylakoids. The results are the average of 3 experiments. All measurements were done in the presence of 0.5 mM $K_3[Fe(CN)_6]$.

Computation under the speculation that S_{-5} is the lowest oxidation state of the WOC does not result in significant changes in the S_{-i} state distributions obtained in the in the presence of HC (Fig. 4.12, compare *b* and *d*). In contrast, clear deviations are obtained under this assumption (compare *a* and *c*) in the case of the absence of HC during NH_2NH_2 treatment. These differences are mainly characterized by the appearance and slow increase of a formal S_{-4} state population (up to 15% at 25 min of incubation) along with the decrease of the S_{-3} and, partially, the S_{-1} state populations. Thus, the results obtained by two ways of calculation do not contradict each other and show that the shift of the WOC to the lowest reduced S_i states (by NH_2NH_2) is 'retarded' by the addition of HC in HC_{air}(–) medium. This finding is in agreement with the results presented above, where a similar observation was made with NH_2OH as reductant. On the other hand, we found that effect of HC (see Section 4.3.2) on the double hit probability of the first flash (β_1) was eliminated in the case, when we used the electron acceptor FeCy during the measurements of $S_1Y_D^{ox}$ samples (compare data in Tables 4.2 and 4.4). However, FeCy used in present measurements did not 'remove' the HC effect on the S_i/S_{-i} state distribution of the reduced WOC, that is indicative for the donor side origin of this HC effect.

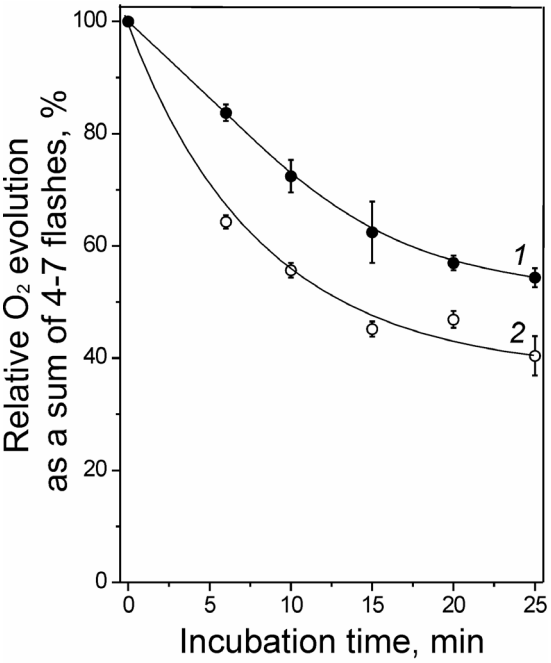

FIGURE 4.13 Summarized O_2-yields for flashes 4–7 as a function of dark incubation time of $S_1Y_D^{ox}$-thylakoids in the presence of 3 mM NH_2NH_2 (pH 6.3, 20 °C) in HC_{air}(–) medium. Incubation of samples was done with (***1***) and without (***2***) addition of 2 mM $NaHCO_3$. 100% is the O_2-yields due to flashes 4–7 taken from dark-adapted untreated (control) $S_1Y_D^{ox}$-thylakoids. Other experimental conditions are the same as described in Fig. 4.11.

Figure 4.13 represents the evaluation of an inactivation (which is known to be caused by NH_2R treatments (Bouges, 1971; Cheniae & Martin, 1971)) of the obtained FIOPs (as in Fig. 4.11*a*) in thylakoid membranes in HC_{air}(–) medium in the presence (curve *1*) and in the absence (curve *2*) of 2 mM HC, where as criterion of relative O_2-evolving activity the sum of O_2-yields resulting from flashes 4–7 was used. Relevant sums of O_2-yields (4–7 flashes) obtained in 'control' $S_1Y_D^{ox}$-thylakoids were taken as 100%. It is seen that the addition of HC during dark treatment with 3 mM NH_2NH_2 prevents (for about 15%) the loss of relative O_2-evolving activity throughout the NH_2NH_2 incubation times. Presumably, this effect of HC is coupled somehow with the use of FeCy, since in previous study, where we did not use any exogenous acceptors during the measurements, no significant differences in steady state of O_2 evolution per flashes were found (see, for instance, insets in Fig. 4.8).

4.3.4.2 Does HCO_3^- Affect the Reduction of the WOC by NH_2R?

The apparent S_i/S_{-i} state distributions after NH_2R incubation result from a complex sequence of reactions: (*i*) diffusion of NH_2R toward the WOC, (*ii*) the reduction of the

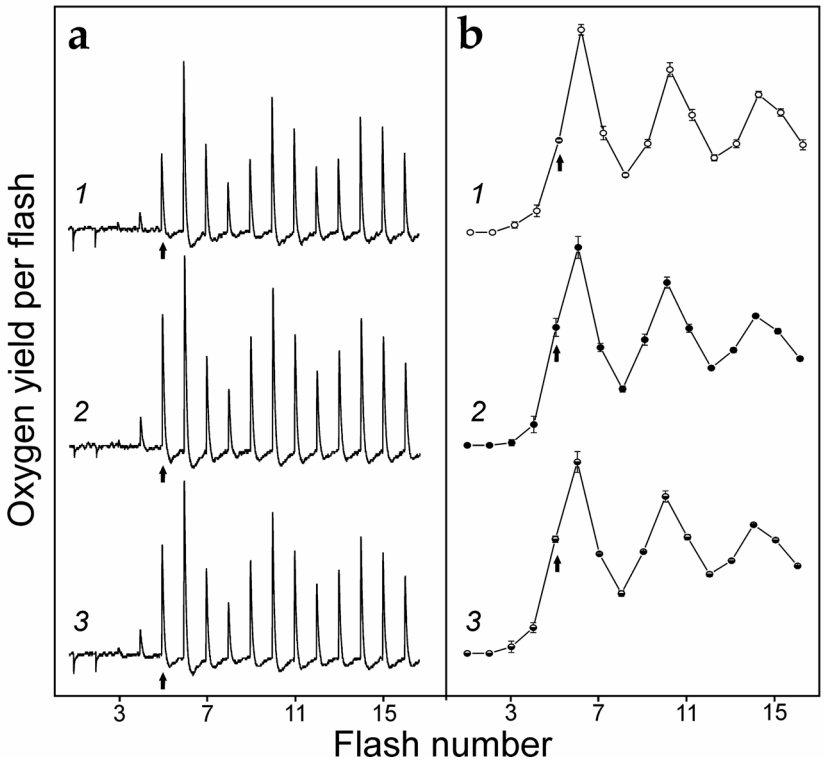

FIGURE 4.14 Original, unnormalized FIOPs (***a***) and the respective normalized O_2 yields per flashes (***b***) of dark-adapted HC_{Ar}(–) spinach thylakoids ($S_1Y_D^{ox}$) obtained after 10-min incubation with 0.2 mM NH_2OH on ice at pH 6.5. In contrast to Fig. 4.8 all samples were washed after NH_2OH-incubation once in NH_2OH-free medium before the FIOPs were recorded. For FIOP ***1*** the sample was incubated and measured in the absence of HC, while for FIOP ***2*** hydrogencarbonate (2 mM) was present throughout the procedure. FIOP ***3*** was obtained by performing the NH_2OH incubation in the absence of HC, while 2 mM HC was added ~1 min before the measurement. Circles and bars (right side, ***b***) show the mean values and standard deviations of three measurements. The corresponding fits are given in Table 4.8. FIOPs were recorded with a flash-frequency of 2 Hz at pH 6.5 and 20 °C. No exogenous electron acceptors were added. Normalization of the FIOPs was performed by dividing each flash-induced oxygen yield by the average of the O_2-yields induced by flashes 4–7.

TABLE 4.8. Fits of the flash-induced oxygen evolution patterns displayed in Fig. 4.14 [A].

Sample	Fit parameters (%)									fq
	Fit	S_1	S_0	S_{-1}	S_{-2}	S_{-3}	α	β	β_1	
FIOP ***1***	A	0.3	3.8	25.1	70.8	0.0	(10.0)	(2.2)	–	0.000004
	B	0.0	2.2	20.0	77.8	0.0	(10.0)	(2.2)	(10.0)	0.000004
	C	0.6	3.4	22.2	70.6	3.2	9.2	2.3	4.1	0.000003
FIOP ***2***	A_1	0.1	5.4	39.4	55.2	0.0	(10.0)	(2.2)	–	0.000007
	B_1	0.0	2.0	37.7	60.3	0.0	(10.0)	(2.2)	(10.0)	0.000007
	C_1	0.5	4.1	36.0	57.5	1.9	9.1	2.8	2.8	0.000006
FIOP ***3***	A_1	0.5	5.3	35.2	59.0	0.0	(10.0)	(2.2)	–	0.000005
	B_1	0.2	2.7	32.5	64.6	0.0	(10.0)	(2.2)	(10.0)	0.000005
	C_1	0.7	4.2	31.9	59.6	3.7	9.0	2.7	2.7	0.000003

[A] The extended Kok model described in Experimental Section (Section 4.2.3) was used to fit FIOPs of spinach thylakoids. The samples were incubated in the dark for 10 min on ice with 0.2 mM NH_2OH and then washed once in NH_2OH-free medium. For FIOP ***1*** all steps were performed in HC_{Ar}(–) medium, while for FIOP ***2*** hydrogencarbonate (2 mM) was added before NH_2OH incubation and during washing steps. FIOP ***3*** was obtained from a sample that was treated as described for FIOP ***1***, but 2 mM HC was added prior to the measurement. Fit parameters: S_1–S_{-3}, normalized S-state populations; α, miss probability; β, double-hit probability and β_1, double-hit probability of the first flash. Smaller fit quality (*fq*) values indicate a better fit. Dashes denote parameters that were excluded from the fit, while numbers in parentheses give values, which were fixed during optimization. The first 16 flash induced O_2-yields of each FIOP were analyzed.

Mn_4O_xCa cluster, and (*iii*) the efficiency of light-induced oxidations during the flash train. In addition, back reactions of the formed S_{-i} states with Y_D^{ox} (Messinger & Renger, 1993) or other electron acceptors need to be considered.

In order to address the question at which point of the above-described chain of events HC modifies the apparent S_i/S_{-i} state populations, we compare in Fig. 4.14 FIOPs that were obtained as follows: (*1*) $HC_{Ar}(-)$ thylakoids were incubated for 10 min with 0.2 mM NH_2OH and then washed and measured in $HC_{Ar}(-)$ medium; (*2*) HC(+) thylakoids were incubated with NH_2OH and then washed and measured in HC(+) medium, and (*3*) $HC_{Ar}(-)$ thylakoids were incubated with NH_2OH, but then washed and measured in HC(+) medium. The effect of the washing was 2-fold: firstly it allows changing the HC concentration after the NH_2OH incubation and secondly it stops the reduction process by removing the reductant, thus allowing to study the point of action of HC.

The original FIOPs presented in Fig. 4.14 (left) reveal that a 10-min incubation of $S_1Y_D^{ox}$-thylakoids with 0.2 mM NH_2OH leads to the first maximum of O_2 evolution after the 6th flash, *i.e.*, most centers are shifted into the S_{-2} state. A comparison of patterns *1* and *2* in Fig. 4.14 and Table 4.8 reveals that the subtle, yet highly reproducible difference (see below) in the shift between $HC_{Ar}(-)$ and HC(+) samples can be observed again, despite the fact that NH_2OH was removed prior to measuring the FIOPs. FIOP *3* in Fig. 4.14 was obtained with a sample that was reduced with NH_2OH in $HC_{Ar}(-)$ buffer (like FIOP *1*, Fig. 4.14), but measured after washing with HC(+) medium (like FIOP *2*, Fig. 4.14). It is obvious that pattern *3* more closely resembles FIOP *2* than FIOP *1* in Fig. 4.14. This indicates that HC does not affect the reaction sequence during NH_2OH reduction, but leads to an apparent shift of the S_i states before or during the measurements. To test, if the differences in apparent S_i/S_{-i}

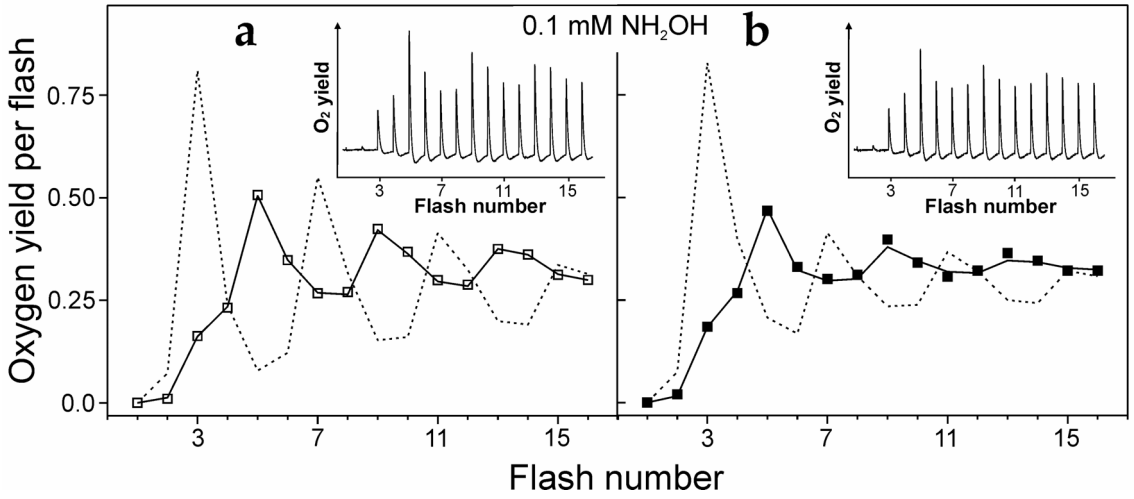

FIGURE 4.15 Normalized FIOPs after 1-min treatments of spinach thylakoids ($S_1Y_D^{ox}$) with 0.1 mM NH_2OH on ice at pH 6.4. $HC_{Ar}(-)$ samples (***a***, open symbols) were obtained by washing with $HC_{Ar}(-)$ buffer medium prior to NH_2OH incubation. Acetate treated samples (***b***, closed symbols) were obtained as described in Chapter 5 by 30-min incubation with 40 mM acetate at pH 6.4. FIOP measurements were performed without removal of NH_2OH from the samples. Broken lines represent FIOPs of $HC_{Ar}(-)$ and acetate thylakoids, respectively, prior to the addition of NH_2OH. The inserts show the original, unnormalized FIOPs at the respective conditions. FIOPs were recorded with a flash-frequency of 2 Hz at pH 6.4 and 20 °C. No exogenous electron acceptors were added. Normalization of the FIOPs was performed by dividing each flash-induced O_2-yield by the average of the O_2-yields induced by flashes 4–7.

state populations are simply the consequence of the effect of HC on the β_1 parameter, we included this parameter in our fits that are presented in Table 4.8. Three different scenarios are tested in Table 4.8: (*A*) the β_1 parameter is not considered ($\beta_1 = \beta$), (*B*) β_1 is fixed to 10% as found for HC_{Ar}(–) samples in Table 4.2 and (*C*) β_1 is allowed to vary freely. These fits show that observed differences in S_i/S_{-i} state distribution after NH_2OH incubation of HC_{Ar}(–) and HC(+) thylakoids do not vanish after including the β_1 in the fits. The right side of Fig. 4.14 displays a summary of three repeats of each experiment. The small error bars show that the experimental error is well below the above-discussed differences.

On the basis of ESEEM measurements it was shown that acetate binds in the vicinity or at Mn_4O_xCa cluster (Clemens *et al.*, 2002). We, therefore, tested if acetate slows down the reduction of the Mn by NH_2OH. Figure 4.15 shows that no significant slowing of the reduction of the S_1, S_0 and S_{-1} states is observed in presence of 40 mM acetate at pH 6.4. The small differences between the patterns are well explained by the increase in miss parameter caused by acetate addition (compare dashed lines in Fig. 4.15a, b).

4.4 DISCUSSION

4.4.1 BINDING OF HYDROGENCARBONATE WITHIN THE WOC

With the HC-depletion levels reached in this study (~50-times during incubation and ~5-times during measurements) no evidence was found that HC binds to the Mn_4O_xCa cluster. Neither the miss parameter, nor the stabilities of the S_0, (S_1), S_2 and S_3 states during the reaction with endogenous electron donors and acceptors were found to be affected by washing thylakoids in HC(–) buffer obtained by extensive bubbling with argon or CO_2-free air. In addition, although a small (about 15%) reproducible shift in the S_i/S_{-i} state distribution was observed in this study after the reduction of the WOC by NH_2OH or NH_2NH_2, HC, apparently did not change the rate of the reduction caused by these external reductants. The observed effects are rather related to HC interaction with the WOC after the reduction with NH_2OH (or NH_2NH_2), or they may occur during the light-induced transitions in the flash train (Fig. 4.14). Our data are consistent with earlier reports (Baranov *et al.*, 2000; Baranov *et al.*, 2004), where the dependence of HC interaction to Mn on the Mn valency is evidently responsible for a much better effect of HC on the donor side of PSII when Mn^{II} is used as an electron donor to Mn-depleted PSII (compared to the effect of HC on the functionally competent WOC when Mn is mainly in the valency Mn^{III} and Mn^{IV}). Unfortunately, we are presently unable to provide a conclusive explanation for the above described phenomenon. At any case, both the effect on the S_i/S_{-i} state distribution (see, for example, Figs. 4.8, 4.12 and 4.14), and the effect on the prevention of a loss of O_2-evolving activity (Fig. 4.13) appear to be too small to allow the conclusion that HCO_3^- is bound at or near the Mn_4O_xCa cluster.

To further test this question, we examined, whether the HC analog acetate affects the reaction of NH_2OH with the Mn_4O_xCa cluster. The reasoning behind this experiment is that acetate was shown by ESEEM spectroscopy to bind near or possibly even at the Mn_4O_xCa cluster (Clemens *et al.*, 2002). The data of Fig. 4.15 show

that acetate, at the concentration used in this study (40 mM), does not affect the interaction of NH_2OH with the Mn_4O_xCa cluster, despite the fact that this concentration is high enough to significantly increase the miss parameter. This suggests that the increased miss parameter is a consequence of the interaction of acetate with the acceptor side, and/or that the acetate (or HC) and NH_2OH interact at independent sites at the donor side (or WOC).

Although our NH_2OH (and NH_2NH_2) incubations were performed outside the electrode, *i.e.*, at about ~50-fold decreased HC-levels, they cannot fully exclude very tight HC binding, which might be present if HC was for example a structural component of the WOC.

4.4.2 HYDROGENCARBONATE BINDING AT THE NON-HEME IRON

This study demonstrates for the first time that an increased β_1 parameter is found in HC(–) samples (see Section 4.3.2) in the absence of exogenous electron acceptors. This effect can be suggested to be coupled to the redox state of the non-heme iron on the acceptor side of PSII. The HC binding to the non-heme iron is suggested by crystallography (Ferreira *et al.*, 2004; Loll *et al.*, 2005) and previous studies (involving mostly formate treatments, see below) have established that the 'bicarbonate' effect on the acceptor side involves binding of formate or acetate at the non-heme iron (for review see (van Rensen, 2002; van Rensen & Klimov, 2005; van Rensen *et al.*, 1999)). Most likely, our HC removal procedure is able (at least in some RC) to extract the HC molecule bound to the non-heme iron (Fe^{2+}) in a way that it is not replaced by a similar ligand. This appears to alter the redox potential of the non-heme iron so that it can be oxidized to Fe^{3+} by the ambient redox potential. If xenon flashes of a few μs half-width are used for excitation this situation causes a high-double hit only in the first flash, because Fe^{3+} accepts after the first flash very rapidly an electron from Q_A^- and a second turnover can take place in such centers within the same flash. Thereafter, the non-heme iron remains in oxidation state Fe^{2+} for the rest of the flash train and the double hit returns to normal values (Jursinic, 1981).

In previous studies, an altered value of β_1 was not found for HC depleted samples (Jursinic & Stemler, 1984; Stemler *et al.*, 1974; Stemler & Lavergne, 1997). The same results were also observed in our study, when ferricyanide was used as electron acceptor during the flash experiments (see Table 4.4). The differences are straight forwardly explained. In our case, the non-heme iron was oxidized by ferricyanide in all samples and, therefore, no difference was noted between HC(+) and HC(–) thylakoids. In two studies of Stemler HC depletion was achieved by addition of either acetate (Stemler *et al.*, 1974) or formate (Stemler & Lavergne, 1997) and in both cases this did not lead to an increase of β_1. These earlier observations are confirmed by the experiments presented in Figs. 4.3 and 4.4. We propose that in presence of these carboxylic acids HC is replaced at the non-heme iron by acetate/formate, which prevents its oxidation to Fe^{3+} at ambient redox-potentials. Consistent with this idea it was shown in two previous studies that it is much harder to oxidize the non-heme iron by ferricyanide in the presence of formate (Jursinic & Stemler, 1984; Radmer & Ollinger, 1980). These findings indicate that the redox potential of the non-heme iron dependents on its ligands: it is most easily oxidized to Fe^{3+} in absence of HC, while

formate or acetate appear to stabilizes the Fe^{2+} oxidation level as compared to the natural HC ligand.

While the above suggestion gives a coherent explanation for the observed data of this study, we have to remark that we neither directly observed HC binding to PSII (the non-heme iron) nor did we obtain direct information about the redox-state of the non-heme iron. Given the fact that the CO_2/HCO_3^- levels very quickly rise from ~50-fold depletion to a ~5-fold depletion during sample transfer to the Joliot – electrode, it is also possible that we are unable to observe an increase of the miss parameter similar to that observed with acetate or formate, because of a very rapid (< 2 min) rebinding of HC to the non-heme iron during the transfer. This scenario would also be consistent with the above-suggested oxidation of the non-heme iron, because the oxidation of the non-heme iron would in any case occur during the incubation in the sealed vials outside the electrode.

4.4.3 EFFECTS OF FORMATE AND ACETATE

Formate and acetate have been added in the past to PSII samples in order to replace HC that may be bound to PSII. This approach is supported by the similar structures of these carboxylic acids as compared to HC (Scheme 4.1). Consistent with previous studies we find significantly increased miss parameters under these conditions. This raises the question about the mechanistic basis for this effect.

Extensive experimental work by many laboratories has established that there are at least two binding sites for these carboxylic acids within PSII: one at the non-heme iron (Deligiannakis *et al.*, 1994; Diner & Petrouleas, 1990; Jajoo *et al.*, 2005; Kühne *et al.*, 1999; Nugent *et al.*, 1992; Wydrzynski & Govindjee, 1975; Xiong *et al.*, 1997; Xiong *et al.*, 1998) and one between Y_Z and the Mn_4O_xCa cluster (Bock *et al.*, 1988; Clemens *et al.*, 2002; Dorlet *et al.*, 1999; Dorlet *et al.*, 1998; Feyziev *et al.*, 2000; Force *et al.*, 1997; Govindjee *et al.*, 1997; Jajoo *et al.*, 2005; Jajoo *et al.*, 2006; Klimov *et al.*, 1995a; Klimov *et al.*, 1995b; Lakshmi *et al.*, 1999; Mende & Wiessner, 1985; Saygin *et al.*, 1986; Szalai & Brudvig, 1996; Wincencjusz *et al.*, 1996). However, it is unclear if formate and acetate indeed replace HC at both binding sites. While on the basis of the cited literature HC replacement appears to be well established for the binding site at the non-heme iron, binding within the WOC is often reported to occur in competition with Cl^- rather than HC. It was attempted in two previous MIMS studies to quantify the number of bound HC molecules to PSII. While in the first study no evidence was found for CO_2 release after formate injection (Stemler, 1989), the subsequent report was able to detect the slow release of 0.4−1.2 CO_2 per PSII complex after formate injection at pH 6.5 (Govindjee *et al.*, 1991) (for details see Chapter 5).

Formate (and acetate) binding to the non-heme iron have been reported to slow the Q_A^- to Q_B^- electron transfer, possibly by disrupting the protonation pathway for Q_B^{2-} (Govindjee *et al.*, 1997; van Rensen & Klimov, 2005). Binding of acetate (and formate) within the WOC was shown to slow the $Y_Z^\bullet$ reduction kinetics. Especially the $S_2Y_Z^\bullet \rightarrow S_3Y_Z$ transition is slowed significantly at room temperature so that the $S_2Y_Z^\bullet$ state can be traped (Bock *et al.*, 1988; Dorlet *et al.*, 1999; Dorlet *et al.*, 1998; Feyziev *et al.*, 2000; Force *et al.*, 1997; Kühne *et al.*, 1999; Lakshmi *et al.*, 1999; Lydakis-Simantiris *et al.*, 1998; Szalai & Brudvig, 1996; Wincencjusz *et al.*, 1996; Wincencjusz *et al.*, 1999). Both phenomena can give rise to higher miss parameters and the current study does not allow deciding which effect is

dominating under our conditions. It also remains to be established, whether the high miss parameters are caused by the absence of HC or the presence of acetate or formate. Our current data appear to favor the latter, but due to the relatively low depletion levels during the FIOP measurements they are not fully conclusive in this regard.

4.4.4 MIMS MEASUREMENTS

Our MIMS data show that argon bubbling of buffers leads to a significant reduction of the inorganic carbon levels, in our hands ~50-fold. They also show that CO_2 is diffusing back into the depleted solutions very quickly if small aliquots are handled. This may be one reason for the discrepancies in the literature, and monitoring of the CO_2/HCO_3^- level should be part of any future study.

4.5 CONCLUSION

The present study shows that reducing the HCO_3^- concentration in the samples ~5-fold relative to air saturated buffers does not affect the redox potential of the WOC in PSII as shown by unchanged S_0, S_2, and S_3 life-times. Even at ~50-fold reduced HCO_3^- level the rate of reduction of the WOC by NH_2OH was unchanged. Therefore, it appears likely that HC, after its probable involvement in the assembly of the Mn_4O_xCa cluster, leaves the WOC. Alternatively HCO_3^- could remain so tightly bound to the WOC that we were unable to remove it by washing with HCO_3^-/CO_2-depleted buffer. This question is addressed in MIMS studies presented in Chapter 5.

Chapter 5

Hydrogencarbonate Binding to Photosystem II

5.1 INTRODUCTION

Since the 1970s, the donor and acceptor sides of PSII are considered as possible sites for hydrogencarbonate (HCO_3^-; HC) interactions with PSII (reviewed in (Stemler, 2002; van Rensen, 2002; van Rensen & Klimov, 2005)) (see also Section 1.4.4.2 of this work). The idea of HCO_3^- binding on the acceptor side of PSII as a ligand of the non-heme iron between two quinones Q_A and Q_B (Wydrzynski & Govindjee, 1975; Govindjee *et al.*, 1976; van Rensen & Vermaas, 1981), was recently supported by PSII crystal structures (Ferreira *et al.*, 2004; Loll *et al.*, 2005). This acceptor side effect complicates the search for specific effects of HC on the donor side of PSII. Thus, it is still under discussion if HC also binds at the donor side of PSII, where the Mn_4O_xCa cluster is considered as a possible binding site (Klimov *et al.*, 1997a; van Rensen & Klimov, 2005). In particular, in a recent publication on the X-ray structure of PSII core complex from *T. elongatus* (at resolution of 3.5 Å), one HC molecule has been tentatively included as a non-protein ligand of the WOC between Ca^{2+} and Mn (Ferreira *et al.*, 2004). On the other hand, HC is not seen as a ligand to the Mn_4O_xCa cluster in a more recent PSII crystal structure obtained with a resolution of 3.0 Å (Loll *et al.*, 2005).

In the literature formate and acetate have been concluded to bind both at the acceptor and donor sides of PSII by replacing HCO_3^- from its binding sites due to the similar structures (discussed in Section 4.4.3; see also Scheme 4.1) (for recent reports see (Clemens *et al.*, 2002; Feyziev *et al.*, 2000; Jajoo *et al.*, 2006; Kühne *et al.*, 1999). Moreover, a slow release of CO_2 after formate addition into thylakoid membrane suspensious was detected by Govindjee and co-workers (Govindjee *et al.*, 1991; Govindjee *et al.*, 1997), while in another study no evidence was found for formate-induced release of CO_2 (Stemler, 1989). Here we revisit these mass spectroscopic measurements to specifically probe the binding of inorganic carbon, C_i (H_2CO_3, HCO_3^-, CO_3^{2-}), to the Mn_4O_xCa cluster at the donor side of PSII by injections of formate and hydroxylamine. The latter compound is known to specifically reduce (low concentrations) (Bouges, 1971; Messinger *et al.*, 1991) or destroy (high concentrations) (Cheniae & Martin, 1971; Yocum *et al.*, 1981) the Mn_4O_xCa cluster.

5.2 EXPERIMENTS AND ANALYSIS

5.2.1 PREPARATIVE PROCEDURES

5.2.1.1 Sample Preparation

The PSII membrane fragments, (BBY-particles), were thawed in the dark on ice and diluted to a certain chlorophyll concentration (from 0.3 to 5.5 mg ml^{-1}) with MCMM buffer of the following composition: 400 mM mannitol, 20 mM $CaCl_2$, 10 mM $MgCl_2$, and 100 mM MES/NaOH, pH 6.0–6.4 (adjusted at 20 °C).

Typical rates of oxygen evolution of studied samples were 360–500 μmol (O_2) mg (Chl)$^{-1}$ h^{-1}.

5.2.1.2 Depletion of C_i

If not stated otherwise, all solutions destined for injections into the mass MIMS cell were depleted of inorganic carbon (C_i) by intensive flushing with argon in septum vials for 10–20 min. In accordance with data presented in Section 4.3.1, our C_i-depletion procedure leads to an about 50-fold reduction of C_i-levels in the medium. In some cases, this depletion method was combined with heating of the injection solution to 50 °C for 10 min before flushing with argon. To avoid CO_2 contamination when handling samples, all transfers into MIMS cell were made with gas tight syringes that had been pre-flushed with argon.

5.2.1.3 Mn-depletion Procedures from the WOCs

- ***Hydroxylamine–treatments*** were performed either (*i*) in 1.5-ml Eppendorf tubes similar to the protocol described in Section 4.2.1.5 or (*ii*) directly inside of the MIMS cell (reaction vessel). In the first case, after 30 min of dark incubation on ice with NH_2OH, the treated PSII samples (2 mg ml^{-1}) were washed twice in NH_2OH-free MCMM medium (pH 6.4). The pellet was then resuspended to 2 mg Chl ml^{-1} in the same buffer and transferred in the MIMS cell followed by thorough degassation of the samples for 40–45 min. In the latter case, the MIMS cell was filled with the non-treated PSII samples and immediately after that NH_2OH was injected into the cell. Incubation of the samples (final [Chl] = 2 mg ml^{-1}) with NH_2OH in the cell (at 20 °C) was limited by degassation time of 40–45 min. In both cases, hydroxylamine was added to PSII samples from a freshly prepared and pH adjusted $NH_2OH \cdot HCl$ stock solution (120 mM, pH 6.3–6.4, 20 °C) in MCMM buffer to a final concentration of 7.5 mM. This concentration was shown to be enough for full extraction of Mn from the WOCs (see Results section).
- ***Hydrazine-treatment*** was carried out based on a method described in Section 4.2.1.5 with slight changes. Thawed PSII membrane fragments were ~3-fold diluted to a [Chl] = 2.25 mg ml^{-1} with freshly prepared MCMM buffer solution containing 120 mM NH_2NH_2 (pH 6.3, adjusted at 20 °C) and incubated for 30 min in the dark on ice. NH_2NH_2-treated samples (without washing from NH_2NH_2) were then transferred into the MIMS cell. Immediately after their transfer, the samples were diluted by the injection (10 μl) of the same (NH_2NH_2-containing)

MCMM buffer and subsequent additions of CA and $H_2{}^{18}O$ to give final chlorophyll concentration in the cell of 2 mg ml^{-1} and final NH_2NH_2 concentration of ~80 mM. Then the samples were further incubated in the MIMS cell at 20 °C for 45 min degassation.

- ***Tris-treatment*** was done according to the method described earlier (Klimov *et al.*, 1982) with some modifications. PSII samples at 100 μg *Chl* ml^{-1} were incubated for 1 h on ice under room light in medium containing 1 M Tris/HCl (pH 8.0) and 0.5 M $MgCl_2$. Then PSII particles were washed twice in MCMM buffer (pH 6.4) and the pellet was resuspended to 2 mg *Chl* ml^{-1} with the same buffer. Tris-treated samples were kept on ice until transfer into the MIMS cell.
- ***Heat-treatment*** of PSII membrane fragments was performed at 2 mg *Chl* ml^{-1} for 5–20 min at 50–70 °C in a water bath in darkness (precise conditions are noted in figure legends). After the heat treatment, the samples were immediately transferred to an ice bath and then assayed or frozen in liquid N_2 (in EPR tubes).
- ***HCl-treatment*** was done according to (Yocum *et al.*, 1981) with slight modifications. HCl was added to PSII samples ([*Chl*] ≈ 4–5 mg ml^{-1}) directly in EPR tubes to give final HCl concentration of 0.3–0.5 M.

5.2.1.4 Formate Treatment

Formate treatment of PSII membrane fragments was done directly in the MIMS cell. PSII samples diluted to a [*Chl*] = 2.25 mg with MCMM buffer (pH 6.3–6.4) were transferred into the MIMS cell and further diluted by the injection of MCMM buffer containing 1.6 M $NaHCO_2$ (pH 6.3–6.4, 20 °C) to give a final formate concentration in the cell of 100 mM. After all other additions (CA and $H_2{}^{18}O$) the final *Chl* concentration of the samples in the cell was 2 mg ml^{-1}. Before the measurements started the samples were incubated with formate in MIMS cell (at 20 °C) in the dark for 40–45 min (degassation time).

5.2.2 MIMS EXPERIMENTS

MIMS measurements of formate/NH_2OH-induced release of CO_2/N_2O and the flash-induced O_2 evolved by PSII membrane fragments were carried out in a 150-μl home-built sample chamber (MIMS cell) (for further details, see Fig. 2.5 and Section 2.3.4) at 20 °C. After filling the chamber with PSII sample, $H_2{}^{18}O$ was injected to give a final ^{18}O enrichment of 3% to 65%. Due to the enrichment we were able to monitor a variety of labeled products (such as CO_2, N_2O and O_2) at the respective *m/z* values.

TABLE 5.1. The diversity of differently labeled CO_2, N_2O and O_2 detected at the given *m/z* values

Studied products	**Isotopic Species**		
	***m/z* = 44**	***m/z* = 46**	***m/z* = 48**
CO_2	$^{12}C^{16}O^{16}O$	$^{12}C^{16}O^{18}O$	$^{12}C^{18}O^{18}O$
$^{14}N_2O$ [A]	$^{14}N_2{}^{16}O$	$^{14}N_2{}^{18}O$	–
$^{15}N_2O$	–	$^{15}N_2{}^{16}O$	$^{15}N_2{}^{18}O$

[A] $^{14}N_2O$ release corresponds to oxidation of the non-labeled $^{14}NH_2OH \cdot HCl$ (provided by '*Fluka*' with assay ≥ 98.0%) by the Mn_4O_xCa cluster, while the release of $^{15}N_2O$ coincides with $^{15}NH_2OH \cdot HCl$ (provided by '*Isotec*' with assay of ^{15}N atom ≥ 98.0%) oxidation (Kretschmann & Witt, 1993).

The differently labeled products are summarized in Table 5.1. In some cases, in order to facilitate equilibration between CO_2 and HCO_3^-, carbonic anhydrase (CA; *Sigma C3934*, from bovine erythrocytes, 2699 W-A units/mg protein) was added to the PSII samples before measurements to a final concentration of 3 μg ml^{-1}. Depending on the ^{18}O enrichment level in the MIMS cell the samples were degassed for 30–100 min before the measurements until an only slightly sloping baseline was reached. Except for the CO_2 calibration experiments (see Experimental section), all injections performed during the measurements were done with thoroughly C_i-depleted solutions (see Section 5.2.1.2) using gas tight syringes.

5.2.3 EPR MEASUREMENTS

CW-EPR measurements were performed using a *Bruker ELEXYS E500* X-band spectrometer with a standard cavity *Bruker ST4102*. An *Oxford 900* liquid helium cryostat and *ITC-503* temperature controller (*Oxford Instruments Ltd.*) were used to regulate the sample temperature to 7.0 K. Other instrumental conditions are given in the figure legends.

5.2.4 MEASUREMENTS OF O_2 EVOLUTION ACTIVITY

Rates of O_2 evolution of PSII-enriched membranes were measured using a Clark-type electrode (see Section 2.3.2) at 25 °C under continuous actinic illumination. 200 μM of PPBQ and 500 μM $K_3[Fe(CN)_6]$ were used as electron acceptors during measurements. In some cases FIOPs measurements (Section 2.3.3.2) were used for the estimation of O_2-evolving activity. Further details are given in the corresponding figure legends.

The measurements of O_2-evolving activity of PSII membranes that were performed directly in the MIMS cell are described in Section 5.3.2.4 (see also the legend of Fig. 5.11).

5.3 RESULTS

5.3.1 PROBING HCO_3^- BINDING TO PSII BY NH_2OH ADDITION

5.3.1.1 Release of Masses 44 and 46 from the WOC Induced by NH_2OH

At high (mM) concentration, NH_2OH is well known to specifically destroy the WOC by simultaneously releasing free Mn^{2+}, and this is coupled with irreversible deactivation of oxygen evolution (Cheniae & Martin, 1971; Sivaraja & Dismukes, 1988a; Yocum *et al.*, 1981). If hydrogencarbonate is a tightly bound ligand to the Mn_4O_xCa cluster, as was suggested earlier (for recent reviews, see (Klimov & Baranov, 2001; van Rensen & Klimov, 2005)), the known destruction of the Mn_4O_xCa cluster by addition of large NH_2OH concentrations should also release CO_2/HCO_3^- together with Mn^{2+} and Ca^{2+}.

Injection of NH_2OH (to final concentration 10 mM) into PSII samples induces a rapid release of mass 44 (short dashed traces) measured by MIMS at 20 °C and pH

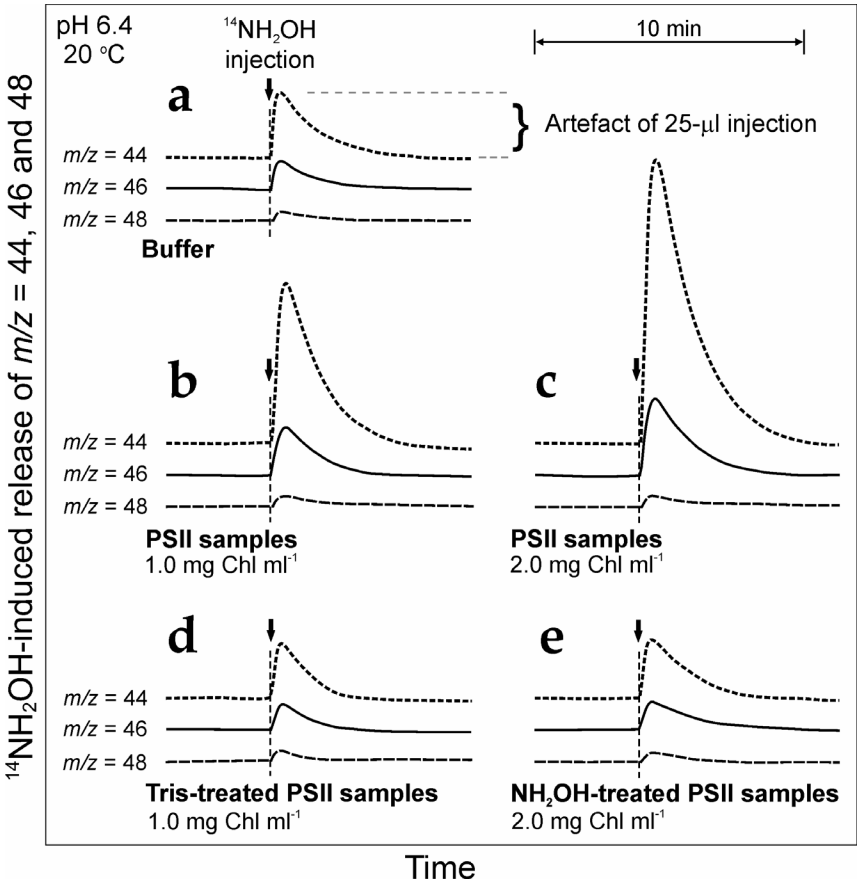

FIGURE 5.1 *m/z* = 44 (short dash traces), *m/z* = 46 (solid traces) and *m/z* = 48 (dash traces) release measured by MIMS upon the injection of $^{14}NH_2OH$ (to final concentration 10 mM) into the spinach BBY particles at [*Chl*] = 1.0 mg ml^{-1} (***b***) and [*Chl*] = 2.0 mg ml^{-1} (***c***) that were degassed in the MIMS cell for 40 min. Traces ***a*** displays the injection of $^{14}NH_2OH$ into the MMCM buffer, while the traces ***d*** and ***e*** show the $^{14}NH_2OH$ injection into the Tris- (1 M) and NH_2OH-pre-treated (10 mM) BBY particles, respectively (see text for treatment details). All measurements were carried out in the absence of CA at pH 6.4 and 20 °C. In all cases only C_i–depleted $^{14}NH_2OH$ solution was used for the injection of 25 µl aliquots into the 150-µl MIMS cells filled with the samples. The amplification of the Faraday cups for the detection of *m/z* = 46 and 48 was 100 and 1000, respectively. The time of injection is marked by arrows. One representative result each out of 3–4 repeat experiments is presented.

6.4 (Fig. 5.1*b*). As seen in Fig. 5.1*b* and *c*, the release is dependent on the chlorophyll concentration of the samples in the MIMS cell. Figure 5.1*a* shows that the artifact caused by 25-µl injections of NH_2OH into MCMM buffer (pH 6.4) is significantly smaller than the observed release in PSII samples. Simultaneously, we monitored also masses 46 (solid traces) and 48 (dash traces). A close inspection of these spectra shows that, although, mass 46 is less affected by NH_2OH addition, it is also dependent on the concentration of chlorophyll in the cell. While, the mass 48 is not influenced by NH_2OH addition into PSII samples, and has almost identical increase in all cases. NH_2OH-induced increase of masses 44 and 46 was fully completed within 5–7 min.

In the late 1980s, NH_2OH was shown to interact both with electron-donor and electron-acceptor side of PSII (Beck & Brudvig, 1987; Sivaraja & Dismukes, 1988a; Sivaraja & Dismukes, 1988b), and, therefore, it is not clear, if the observed release originates from both sides or only from one of the side of PSII. To test this question we employed Tris-treated samples for NH_2OH injection, since Tris has also (as NH_2OH) been observed to cause irreversible inhibition of O_2 evolution and loss of the Mn_4O_xCa cluster as Mn^{2+} (Cheniae & Martin, 1978; Frasch & Cheniae, 1980), but no reports were found

for Tris interactions with the acceptor side of PSII. The samples pre-treated with 1 M Tris (Fig. 5.1*d*) or 10 mM NH_2OH (Fig. 5.1*e*) (for treatment details see Section 5.2.1.3) do not release any gas (at *m/z* = 44, 46 and 48), because the same injection artifact is observed as in Fig. 5.1*a*. Our Tris- and NH_2OH-treatments led to a total suppression of O_2-evolving activity in PSII (Fig. 5.2). This indicates the complete loss of the Mn_4O_xCa cluster (Blankenship & Sauer, 1974; Cheniae & Martin, 1971; Kuntzleman & Yocum, 2005; Rickert *et al.*, 1991). Thus, the latter experiments clearly show that observed gas (*m/z* = 44, 46) (Fig. 5.1*b*, *c*) is released as a result of the interaction of NH_2OH with the Mn_4O_xCa cluster.

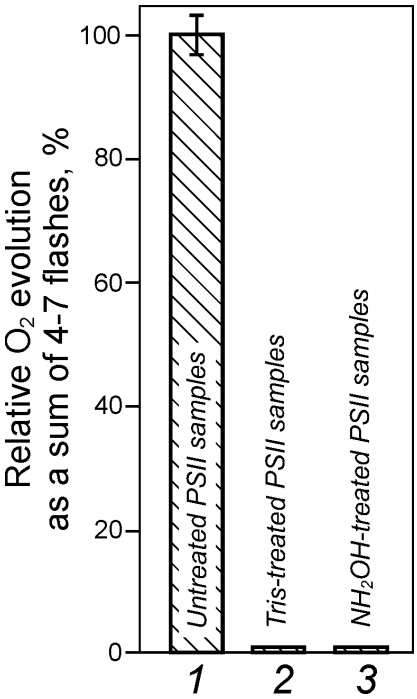

FIGURE 5.2 Inhibition of oxygen evolution activity measured as the sum of O_2-yields of flashes 4–7 in PSII membrane fragments caused by 1-h incubation (under the room light conditions) ice with 1 M Tris (pH 8.0) (**2**) and 30-min dark-incubation with 10 mM NH_2OH (pH 6.3, on ice) (**3**). Before the FIOPs were measured, all treated samples were washed twice in MCMM medium (pH 6.3). 100% is the O_2-yields due to flashes 4-7 taken from dark-adapted untreated (control) BBY particles (**1**). FIOPs measurements were performed with a flash-frequency of 2 Hz at pH 6.3 and 20 °C. The rate of O_2 evolution of the 'control' PSII samples was ~360 μmol (O_2) mg (Chl)$^{-1}$ h^{-1}.

5.3.1.2 CO_2 or N_2O?

An important question arises from the above data: what gas is detected at *m/z* = 44 and 46 after injection of NH_2OH into PSII membrane fragments? Typically CO_2 is measured at these masses, but there is a very high probability that NH_2OH may induce release of N_2O, which has almost identical molar masses as CO_2: M ($^{12}C^{16}O_2$) = M ($^{14}N_2{}^{16}O$) ≈ 44.01 (Wieser, 2006). Consequently, N_2O can also be detected at *m/z* = 44 (as $^{14}N_2{}^{16}O$) and 46 (as $^{14}N_2{}^{18}O$) (see Table 5.1). Indeed, together with expected CO_2 (that could be released in case if HC is a ligand to the Mn_4O_xCa cluster), N_2O may be also released as one of the products of NH_2OH oxidation by the Mn_4O_xCa cluster:

$$2\ NH_2OH + 2\ Mn^{3+}/Mn^{4+}{}_{(cluster)} \rightarrow N_2O + H_2O + 4\ Mn^{2+}{}_{(free)} + 4\ H^+ \qquad (\mathbf{5.1})$$

Kretschmann and Witt (Kretschmann & Witt, 1993) presented mass spectrometric evidence that NH_2OH is oxidized in the dark simultaneously with the reduction of the Mn_4O_xCa cluster. In their experiments the oxidation of ^{15}N-labeled NH_2OH was recognized by a $^{15}N_2$ and $^{15}N_2O$ evolution (see also Table 5.1). Studies of the kinetics of the NH_2OH oxidation by Mn^{III}-complexes *in vitro* also showed that the most common oxidation products of NH_2OH are N_2O and N_2 (Panja *et al.*, 2003; Salem, 1995). Moreover, N_2O was shown to be a product of the NH_2OH oxidation by Fe^{III} ions (Butler & Gordon, 1986; Kolasa & Wardencki, 1974). The latter possibility for NH_2OH oxidation by non-heme iron on the acceptor side of PSII as source for N_2O can be excluded since, (*i*) we did not use any artificial acceptors in our MIMS measurements

that would oxidized non-heme iron Fe^{2+} to Fe^{3+} in PSII samples (Petrouleas & Diner, 1986; Zimmermann & Rutherford, 1986), and (*ii*) the Tris- and NH_2OH-treated samples do not evolve any gas at *m/z* = 44 and 46 above the injection background (see Section 5.3.1.1; Fig. 5.1*d*).

In addition, one should consider that this gas product may consist of both proposed gases, *i.e.*, CO_2 + N_2O. Below we present evidence showing that the observed gas product in PSII samples is only N_2O and no CO_2 is released by NH_2OH addition.

5.3.1.3 Natural Isotopic Abundances of Released Gas

Assuming the natural abundance of stable isotopes for each element (Kaltashov & Eyles, 2005) we compared calculated theoretical molecular isotopic distributions for CO_2 and N_2O with experimental isotopic distributions of gas released in PSII samples at various chlorophyll concentrations. The values of these isotopic distributions given in Table 5.2 indicate that experimental isotopic abundances of 'unknown' NH_2OH-induced gas product in PSII samples are very similar to the natural isotopic distribution of N_2O and differ from CO_2. The very small experimental error is well below than the differences in theoretical isotopic distributions for CO_2 and N_2O.

TABLE 5.2. Relative theoretical molecular distribution of natural isotopes of CO_2 and N_2O compared to experimental isotope distribution of released gas (*m/z* = 44 and 46) in PSII samples at [*Chl*] = 2 mg ml^{-1} (Fig. 5.1*c*)

	Theoretical (%) [A]		**Experimental (%)** [B]
m/z	**for CO_2**	**for N_2O**	**PSII samples** (2 mg *Chl* ml^{-1})
44	99.60	99.80	99.80 ± 0.02
46	0.40	0.20	0.20 ± 0.02

[A] Isotopic distributions of the molecules were calculated using on-line *Molecular Isotopic Distribution Calculator Program* (for description see (http://www2.sisweb.com/mstools/isotope.htm)). Mass 48 was not taken into account since our MIMS measurements were done without ^{18}O enrichment (see Fig. 5.1). [B] Factual values for released gas product in PSII samples (pH 6.4) were obtained by subtracting artifact caused by injection of NH_2OH into MCMM buffer (pH 6.4) shown on Fig. 5.1*a*. Values of calculated isotopic distributions are mean ± s.e., $n \geq 3$.

5.3.1.4 Release of $^{15}N_2O$ Induced by ^{15}N-labeled NH_2OH

It has been reported earlier (Kretschmann & Witt, 1993) that the oxidation of ^{15}N-labelled NH_2OH by the Mn_4O_xCa cluster is coupled with the evolution of $^{15}N_2O$ as well as $^{15}N_2$. Therefore, if the gas that we observed upon the addition of non-labelled NH_2OH to PSII samples at mass 44 (see Fig. 5.1) is only N_2O (and not CO_2), then the injection of ^{15}N-labelled NH_2OH must shift the detection of labelled gas product ($^{15}N_2O$) from mass 44 to mass 46. At this point, unless CO_2 is also present in the released gas, the mass signal 44 should be fully removed by such injection. Fig. 5.3*e* shows that the injection of $^{15}NH_2OH$ into PSII samples induces only the release of $^{15}N_2O$ monitored at mass 46 and no CO_2 was observed by mass signal 44. Thus, the injection of $^{15}NH_2OH$ into 'active' PSII samples (Fig. 5.3*e*) causes exactly the same injection artifact affecting mass 44 as in buffer (Fig. 5.3*a*), heat-treated (Fig. 5.3*b*) and NH_2OH-treated (Fig. 5.3*c*) BBY particles (conditions of treatments are in figure legend). While the $^{15}NH_2OH$ injection into 'active' PSII samples induces the release both mass 46 and mass 48 (Fig. 5.3*e*), the heat-treated as well as NH_2OH-treated PSII

samples do not release any (compare *m/z* = 46, *m/z* = 48 in Fig. 5.3*b*, and *c*, respectively). Since we performed our MIMS measurements without ^{18}O-enrichment, the $^{15}NH_2OH$-induced release of mass 48 in non-treated PSII samples (Fig. 5.3*e*) may represent only natural molecular isotope $^{15}N_2{}^{18}O$ and, in no circumstances, the double-labelled $C^{18}O_2$. The latter statement is supported also by the calculated isotopic distribution. The values of distributions obtained for mass 46 and mass 48 (99.79 ± 0.02% and 0.22 ± 0.02%, respectively) are in a good agreement with theoretical distributions of stable isotopes: 99.80% for $^{15}N_2{}^{16}O$ and 0.2% for $^{15}N_2{}^{18}O$, respectively. And *vice versa*, the injection of non-labeled $^{14}NH_2OH$ into PSII samples induces the release of only $^{14}N_2{}^{16}O$ (*m/z* = 44) (Fig. 5.3*d*) with its natural isotope $^{14}N_2{}^{18}O$ as shown above (see sections 5.3.1.2 and 5.3.1.3).

Thus, the results obtained clearly indicate that not CO_2, but N_2O is released upon the destruction of Mn_4O_xCa cluster by NH_2OH. However, one can assume that

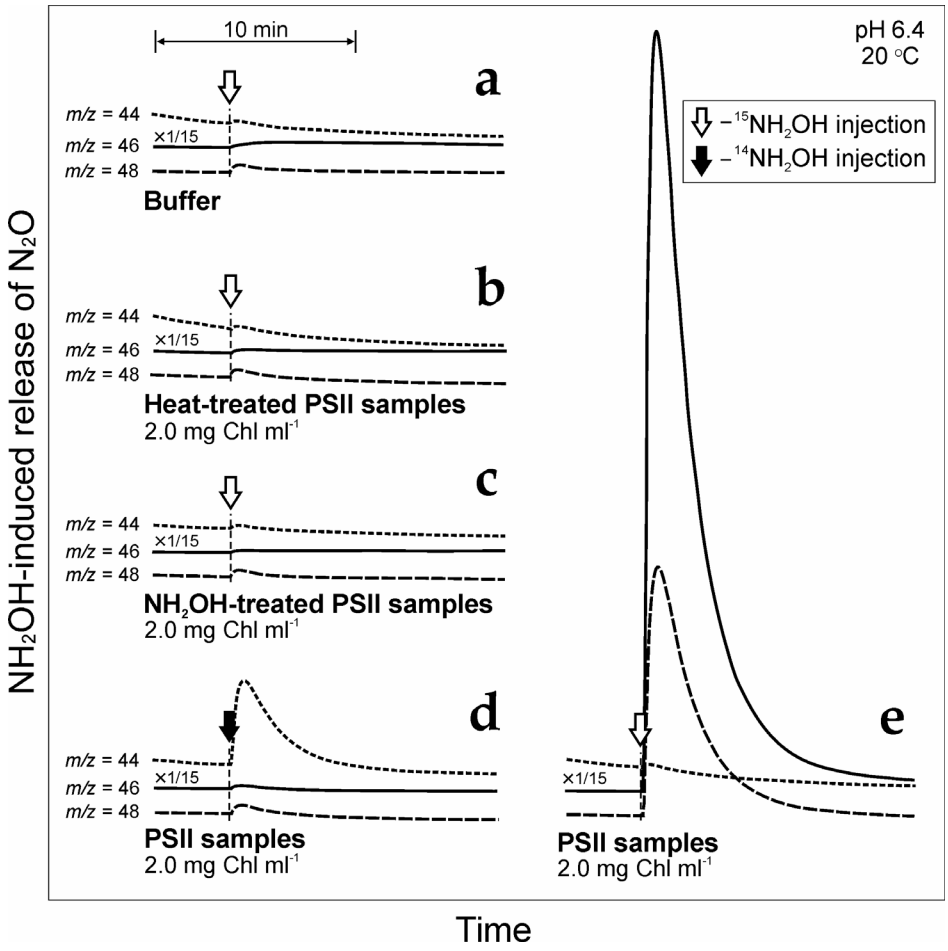

FIGURE 5.3 MIMS measurements of $^{15}N_2{}^{16}O$ and $^{15}N_2{}^{18}O$ evolution induced by the addition of labelled $^{15}NH_2OH$ to PSII samples ([*Chl*] = 2 mg ml^{-1}) monitored at *m/z* = 46 (solid lines) and *m/z* = 48 (dash lines), respectively (***e***), and compared to that the release of $^{14}N_2{}^{16}O$ monitored at *m/z* = 44 (short dash lines) upon the injection of non-labelled $^{14}NH_2OH$ to PSII (***d***). Traces ***a***, ***b*** and ***c*** - the absence of $^{15}NH_2OH$-induced N_2O release measured as 'controls' in MCMM buffer (pH 6.4), heat-pre-treated PSII samples (70 °C, 5 min), and in PSII samples that were pre-incubated with 7.5 mM $^{14}NH_2OH$ for 15 min, respectively. Only C_i-depleted $^{15}NH_2OH/^{14}NH_2OH$ solutions were used for the 10-μl injections into the samples that were preliminarily degassed for 25 min in the 150-μl MIMS cell. The time of injections of $^{15}NH_2OH$ and $^{14}NH_2OH$ (to 7.5 mM in both cases) is marked by open and closed arrows, respectively. The amplification of the Faraday cups for the detection of *m/z* = 46 and 48 was 100 and 1000, respectively. The measurements were performed in the presence of CA (3 μg ml^{-1}) at pH 6.4 and 20 °C.

the absence of the NH_2OH-induced release of CO_2 in our PSII samples may be caused by a possible suppression of CO_2 evolution due to the presence of the NH_2OH. On the other hand, we found that the amount of the released CO_2 upon the injections of air-saturated H_2O into the MIMS cell filled with MCMM medium (pH 6.3) (see Section 5.3.2.3 and Fig. 5.10) is not affected by the presence of NH_2OH (7.5 mM) in the medium (data not shown), and therefore, the latter suggestion should be rejected.

5.3.1.5 Deactivation of the WOC and Mn Depletion by NH_2OH: Examination by EPR and MIMS

It has been suggested that upon the NH_2OH addition N_2O evolution is only observed when the Mn^{2+} ions are released into the solution (Kretschmann & Witt, 1993). In the present study we found that NH_2OH-pretreated PSII samples which lost all their O_2 evolving activity (Fig. 5.2) do not evolve any N_2O (see Figs. 5.1*e*, 5.3*c*). These data may signify full deactivation of the WOC. However, at the same time, the data do not prove full extraction of Mn from the Mn_4O_xCa cluster by the used NH_2OH concentration (Sivaraja & Dismukes, 1988b; Yocum *et al.*, 1981). Consequently, one can explain the absence of CO_2 signal after the injection of NH_2OH into PSII samples by the possibility that our presumptive HCO_3^- is still tightly bound with the non-extracted Mn in the WOC. Thus, an important question arises: was the final concentration of NH_2OH (7.5–10 mM) used for injections in our MIMS study high enough for the extraction of all Mn from the Mn_4O_xCa cluster?

Our EPR results obtained provide evidence that after the NH_2OH-treatment the PSII samples do not contain any residual Mn in the WOC (Fig. 5.4). Thus, the six-line EPR signal of hexaaquo Mn^{2+} (reviewed in (Miller & Brudvig, 1991)), shown as spectrum *a*, corresponds to the total Mn content (that can be released by heat treatment) in our PSII samples. Spectrum *b* was obtained in NH_2OH-treated PSII sample (for details of treatment, see the legend of Fig. 5.4 and Section 5.2.1.3), where free Mn^{2+} (released from the WOC) was removed by thorough washing prior the measurement and, therefore, no

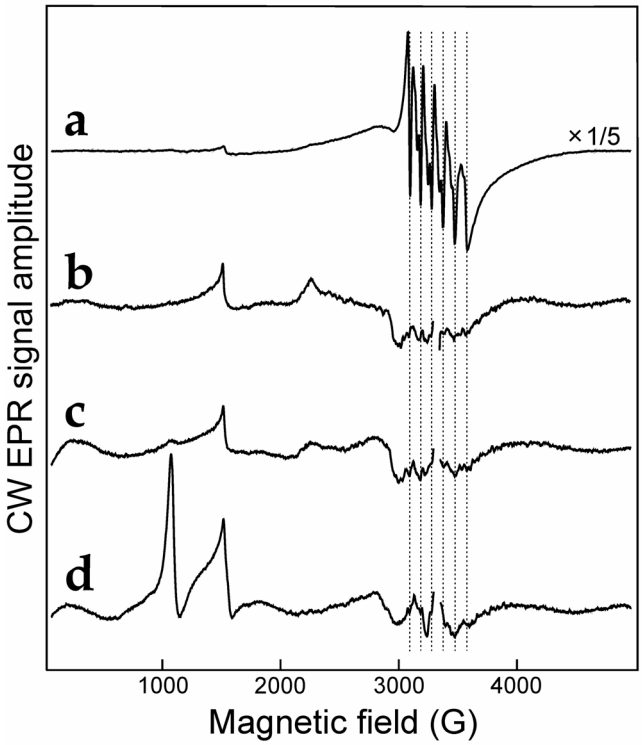

FIGURE 5.4 CW-EPR spectra from BBY samples ([*Chl*] = 5.5 mg ml^{-1}) at 7 K: spectrum ***a***, dark adapted samples after 20–min heat treatment in water bath at 57 °C; spectrum ***b***, samples that were incubated for 15 min with 7.3 mM NH_2OH on ice at pH 6.3 and then washed three times in NH_2OH-free MCMM medium (pH 6.3); spectrum ***c***, as in spectrum ***b***, but after 20–min heat treatment in water bath at 57 °C; spectrum ***d***, as in spectrum ***c***, but after addition of ~0.3 M HCl (final concentration) to the samples. EPR settings: microwave frequency, 9.41 GHz; microwave power, 20 mW; modulation amplitude, 15.0 G; modulation frequency, 100 kHz. Each spectrum is the average of 8 scans.

Mn^{2+} signal is observed. The Mn removal was necessary for easier detection of extra release of Mn^{2+} (if any) that could be caused by further (heat- and HCl-) treatments of our NH_2OH-pre-treated PSII sample. However, the employment of the sample both for the heat- (spectrum *c*) and the HCl-treatment (spectrum *d*) does not induce any extra release of Mn^{2+} and, thus, clearly demonstrates that all Mn has been released by previous NH_2OH-treatment. Consequently, the concentration of NH_2OH (7.5 mM) used in our MIMS measurements for an injection into PSII samples is sufficient to remove all Mn from the WOC.

Using MIMS we compared the release of N_2O induced by the injection of 7.5 mM NH_2OH (that as shown removes all Mn from the WOC) into PSII samples (at 1.0 mg *Chl* ml^{-1}) with N_2O evolutions caused by the additions of NH_2OH in range from 0.05 to 15 mM. As seen from Fig. 5.5*a*, the kinetics of N_2O evolutions induced by the additions of 5 mM and 15 mM NH_2OH are almost identical to that observed after the injection of 7.5 mM NH_2OH (compare traces *1–3*). The injection of low NH_2OH concentrations into PSII samples (from ≤ 1.0 mM) slows down N_2O evolution rates (traces *4–8*). Most probably this retardation observed in N_2O evolution corresponds to more slow release of Mn^{2+} from the WOC (Kretschmann & Witt, 1993) compared to the injection of higher NH_2OH concentrations (5–15 mM) into PSII samples. However, in spite of different rates of N_2O release, according to the normalized evolution of N_2O (measured by signal area) plotted in Fig. 5.5*b* as a function of injected NH_2OH concentration, the addition of NH_2OH from 0.25 mM to 15 mM induces approximately the same amount of N_2O. Only the injections of very small NH_2OH concentrations (till 0.1 mM) induce about 2-fold reduced release of N_2O.

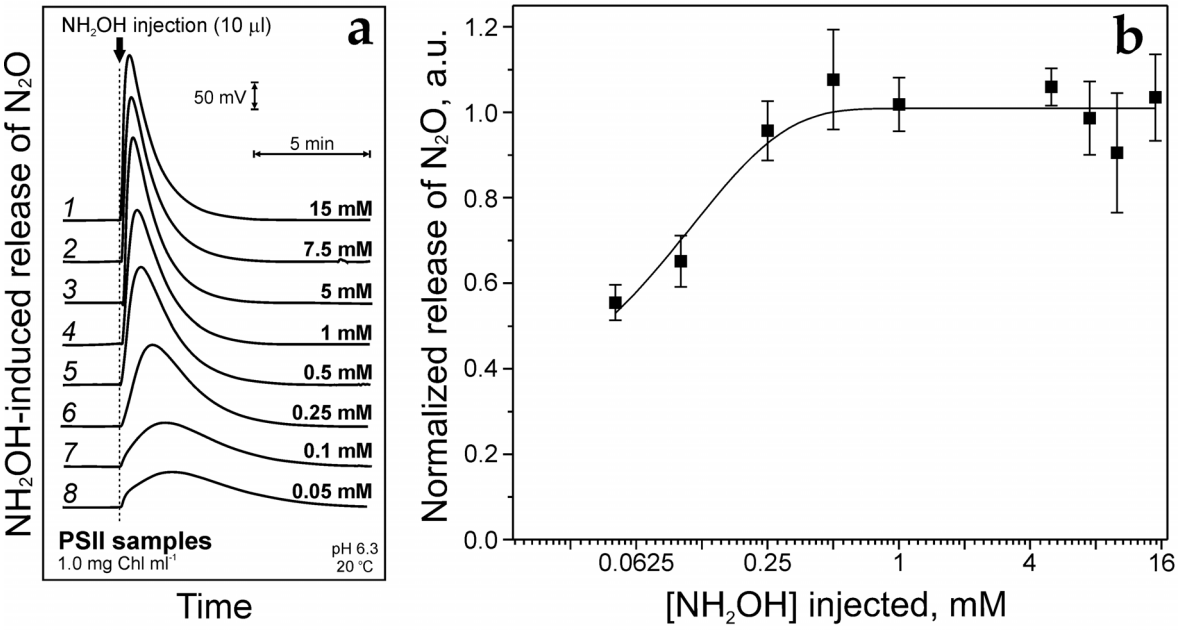

FIGURE 5.5 MIMS measurements of N_2O release (measured at *m/z* = 44) in BBY particles ([*Chl*] = 1 mg ml^{-1}) induced by the injections of C_i-depleted NH_2OH to final concentrations from 15 mM to 0.05 mM (traces ***1-8***) (***a***) and normalized yields of N_2O as a function of NH_2OH concentration injected in the MIMS cell (***b***). Before the addition of NH_2OH, PSII samples were degassed in the MIMS cell for 20-25 min. The measurements were performed at pH 6.3 and 20 °C in the presence of CA (3 μg ml^{-1}). The time of injections is marked by arrow and dot line. The N_2O yields obtained by the subtraction of injection artifacts from the signal area are plotted normalized to the average N_2O release induced by the injection of 15 mM NH_2OH.

Since low concentrations of NH_2OH are known to cause the reduction of the Mn_4O_xCa cluster (Bouges, 1971; Messinger *et al.*, 1991) (see also Chapter 4) coupled with only partial release of Mn^{2+} from the WOC (Kuntzleman & Yocum, 2005), our results support the correlation of the amount of Mn^{2+} released with N_2O evolution proposed earlier (Kretschmann & Witt, 1993). However, this correlation is not fully conclusive and, therefore, has to be checked in the future in a detailed study. Nevertheless, combining the results obtained (EPR and MIMS) it can be concluded that NH_2OH concentration (7.5–10 mM) chosen for injections into PSII samples in the MIMS cell (see Figs. 5.1 and 5.3) is high enough for full (Fig. 5.4) and fast (see Fig. 5.5) release of all Mn from the WOC. Moreover, the absence of N_2O evolution upon the injection of high NH_2OH concentrations into PSII samples may be used as additional test for the Mn-content of PSII samples.

5.3.2 PROBING HCO_3^- BINDING TO PSII BY FORMATE ADDITION

5.3.2.1 Formate-Induced Release of CO_2 from PSII

The data presented above strongly indicate that HCO_3^- is not an integral part of the Mn_4O_xCa cluster. In order to further test this conclusion we performed also the approach of formate addition to PSII samples since formate has already been shown to cause the release of CO_2 from PSII (Govindjee *et al.*, 1991).

Figure 5.6*b*, *d* displays that the injection of formate (final concentration 100 mM)

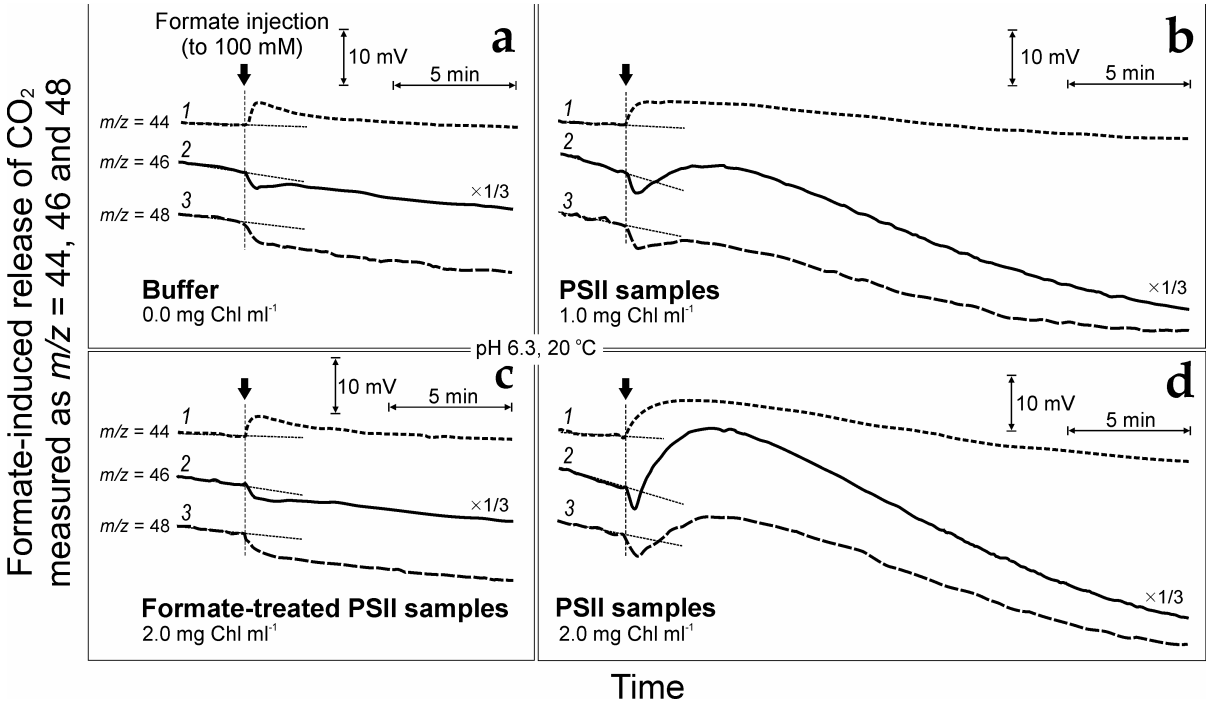

FIGURE 5.6 MIMS measurements of the C_i release measured as CO_2 at masses 44 (traces ***1***), 46 (traces **2**) and 48 (traces ***3***) upon the addition of C_i-depleted formate (to final concentration 100 mM) into the spinach BBY particles with concentration of 1.0 mg *Chl* ml^{-1} (***b***) and 2.0 mg *Chl* ml^{-1} (***d***) in the dark at pH 6.3 and 20 °C. (***a***) - the C_i release after formate addition into the MCMM buffer (pH 6.3), while (***c***) displays the release of C_i in BBY samples pre-treated with 100 mM formate directly in the MIMS cell. Before the 10-μl injection of formate all samples were thoroughly degassed in the 150-μl MIMS cell during 45 min. The $H_2{}^{18}O$ enrichment was ~6%, [CA] = 3 μg ml^{-1}. For all cases one representative result out of 2–3 repeat measurements is presented.

into BBY samples induces a slow release of CO_2 that can be detected by MIMS at 20 °C and pH 6.3. This confirms previous data presented by Govindjee and co-workers (Govindjee *et al.*, 1991; Govindjee *et al.*, 1997). However, for better sensitivity we monitored, in contrast to the previous works, the release of CO_2 not only at mass 44 (*i.e.* $C^{16}O_2$) (traces *1*), but also at mass 46 (*i.e.* $C^{16}O^{18}O$) (traces *2*) and mass 48 (*i.e.* $C^{18}O_2$) (traces *3*), employing an ~6-% $H_2{}^{18}O$ enrichment. This enrichment caused a high signal intensity for CO_2 at mass 46 (singly labelled), and much smaller (by ~4 times) at masses 44 and 48. The observed formate-induced release of CO_2 was complete within 15–20 min.

Comparison of the traces presented in Figs. 5.6*b* and *d* shows that the amount of released CO_2 depends on the concentration of PSII samples in the mass spectrometric cell. Additionally, traces in Fig. 5.6*a* demonstrate the 'injection' artifact caused by the addition of 100 mM C_i-depleted formate into the MIMS cell filled with MCMM buffer (pH 6.3). This injection causes a rapid increase in the mass 44 signal (trace *1*) followed by a slower decrease. While, for signals of masses 46 (trace *2*) and 48 (trace *3*), the 'injection' artifact is characterized by only a rapid decrease. In all cases, this artifact is significantly smaller than the observed CO_2 release (Fig. 5.6*b* or *d*). Figure 5.6*c* indicates that the samples pre-treated with 100 mM formate for 45 min in the MIMS

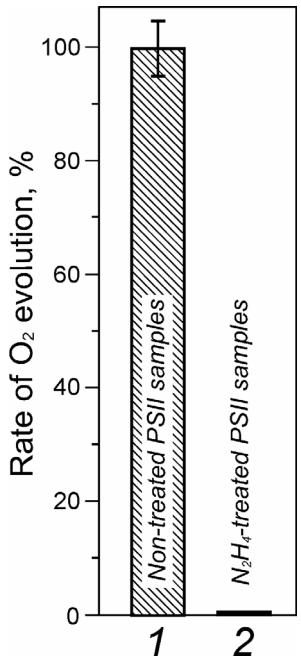

FIGURE 5.7 The oxygen-evolving activity of PSII membranes before (column ***1***) and after (column **2**) the treatment with 80 mM NH_2NH_2 for 75 min. The O_2 rates were measured at pH 6.3 and 25 °C. Before the measurements the samples were washed 3 times in NH_2NH_2-free medium (pH 6.3). The rate of O_2 evolution of the non-treated (control) samples was ~360 μmol (O_2) mg (*Chl*)$^{-1}$ h^{-1}. For NH_2NH_2 treatment details, see section 5.2.1.3.

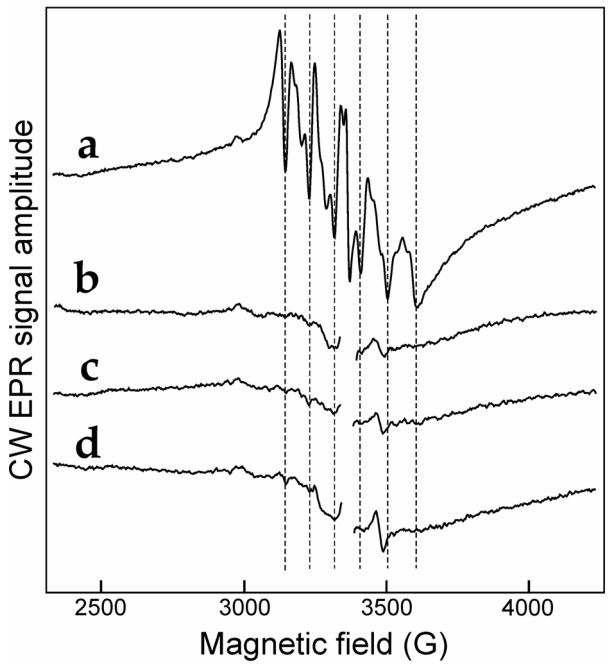

FIGURE 5.8 CW-EPR assays of Mn bound to PSII membranes before (***a***) and after (***b***-***d***) NH_2NH_2 treatment at pH 6.3. Spectrum ***a***, dark adapted samples ([*Chl*] ≈ 4 mg ml^{-1}) after 10–min heat treatment in water bath at 56 °C; spectrum ***b***, samples that were incubated for 75 min with 80 mM NH_2NH_2 (as described in section 5.2.1.3) and then washed three times in NH_2NH_2-free MCMM medium (pH 6.3); spectrum ***c***, as in spectrum ***b***, but after 10–min heat treatment in water bath at 56 °C; spectrum ***d***, as in spectrum ***c***, but after addition of ~0.5 M HCl (final concentration) to the samples. EPR settings: microwave frequency, 9.41 GHz; microwave power, 20 mW; modulation amplitude, 10.0 G; modulation frequency, 100 kHz; sample temperature, 7 K.

cell (for details, see Section 5.2.1.4) do not release any CO_2, because almost the same injection artifact is observed as in Fig. 5.6*c*. The latter experiment also confirms that 100 mM formate is sufficient for the full effect.

5.3.2.2 From which Binding Side(s) in PSII does Formate Release C_i?

Since formate was reported to bind both at the acceptor and donor sides of PSII (Feyziev *et al.*, 2000; Jajoo *et al.*, 2006), it is unclear, from which binding side(s) in PSII (acceptor and/or donor) the released C_i originates. In order to check the possibility that the released C_i comes from the Mn_4O_xCa cluster of the WOC, we compared the C_i evolution in PSII membranes before and after inactivation/removal of the WOC by NH_2NH_2. Similar to hydroxylamine, NH_2NH_2 at high concentrations (several tens of mM), has been shown to irreversibly inactivate O_2 evolution and to destroy the WOC by releasing Mn^{2+} (Cheniae & Martin, 1972; Kretschmann & Witt, 1993; Messinger *et al.*, 1997b; Schansker *et al.*, 2002).

As seen in Fig. 5.7, the treatment of PSII membranes with 80 mM NH_2NH_2 under our conditions (for details, see section 5.2.1.3) leads to a complete loss of O_2 evolving activity, indicating deactivation of the WOC. Moreover, according to EPR data presented in Fig. 5.8, it is clear that such NH_2NH_2–treatment causes the removal of the total manganese (as Mn^{2+}) from the WOC that can be released by heat and/or HCl treatments (for details, see figure legend). This is seen from the absence of Mn^{2+} six line signal in NH_2NH_2–treated samples (that were thoroughly washed in NH_2NH_2-free medium) before (spectrum *b*) and after heat (spectrum *c*) and HCl (spectrum *d*) treatments.

Figure 5.9*a* displays the formate–induced release of $^{12}C^{16}O^{18}O$ (*m/z* = 46) in

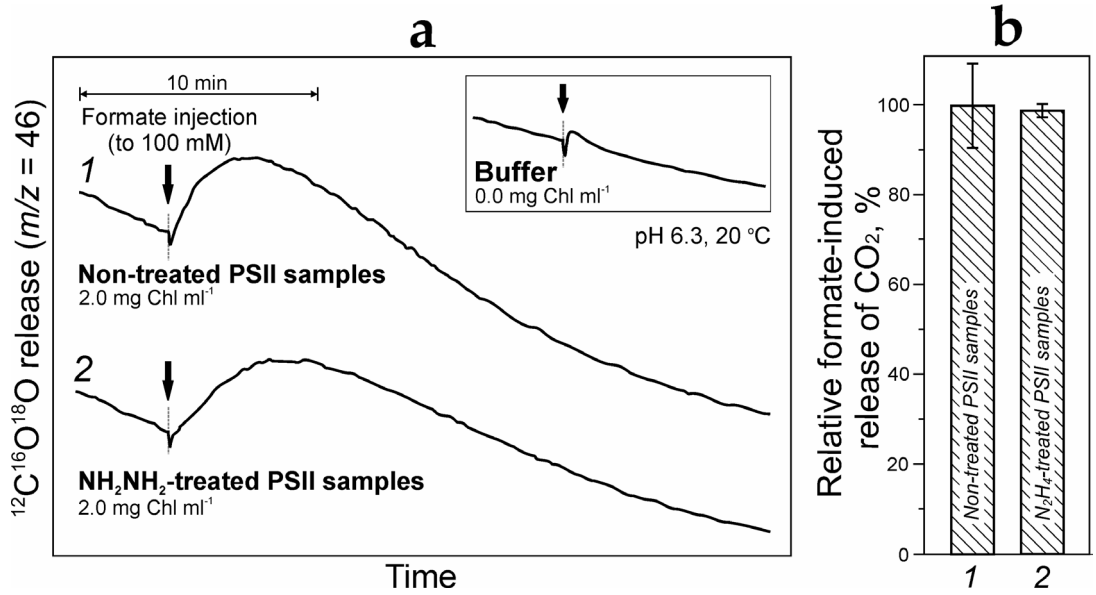

FIGURE 5.9 ***a,*** C_i release measured by MIMS (at pH 6.3; 20 °C) as $^{12}C^{16}O^{18}O$ (*m/z* = 46) upon the addition of formate to 100 mM (marked by closed arrows) into the non-treated 'control' PSII membranes (trace ***1***) and PSII membranes pre–incubated with 80 mM NH_2NH_2 for 75 min (trace ***2***) (for treatment details see section 5.2.1.3). The inset shows the artifact caused by the injection of formate into the MCMM buffer (pH 6.3) at 20 °C. The $H_2{}^{18}O$ enrichment was ~3%. All other measuring conditions are the same as on Fig. 5.6. ***b***, a comparison of relative formate-induced release of CO_2 (estimated by signal intensity area) in the non-treated PSII membranes (column ***1***) and in PSII membranes pre-incubated with NH_2NH_2 (column ***2***).

hydrazine–pre-treated PSII membranes (trace *2*) compared to control (non–hydrazine–treated) PSII samples (trace *1*). In spite of the slightly different kinetics of observed CO_2 release in both sample types, it is clear from Fig. 5.9*b*, that the hydrazine–treated PSII membranes (column *2*) release practically the same amount of CO_2 as control PSII membranes (column *1*). The amount of the released CO_2 was determined by signal area after formate additions into PSII samples (Fig. 5.9*a*). The results obtained indicate that C_i released by formate addition (see Figs. 5.6 and Fig. 5.9) does not originate from the electron donor side of PSII (namely from the Mn_4O_xCa cluster), but comes from a different binding site, *i.e.* most likely from the electron acceptor side.

5.3.2.3 Quantification of the Released CO_2

For quantification of the released CO_2, both, the CO_2 calibration measurements and formate addition experiments were performed with an $H_2{}^{18}O$ enrichment of 3%. The released CO_2 was quantified by baseline subtraction and subsequent integration of the $^{12}C^{16}O^{18}O$ signal (*m/z* = 46) within *OriginPro* software. The calibration of the CO_2 signals was performed by injecting various volumes of air-saturated water samples (kept for several hours at 20 °C) into the MIMS chamber filled with degassed MCMM buffer (pH 6.3) (Fig. 5.10). CO_2 solubility/concentration determination in water was done using a thermodynamic model (Diamond & Akinfiev, 2003) based on Henry's law and on recent high-accuracy Henry's law constants reported by (Carroll *et al.*, 1991; Crovetto *et al.*, 1991) for low pressures.

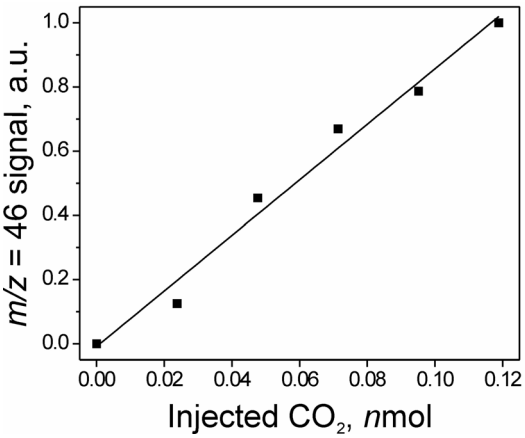

FIGURE 5.10 Calibration curve relating the CO_2 concentration in injected air-saturated H_2O (20 °C, 0.1 MPa) with relative release of CO_2 measured at mass 46 by MIMS at 20 °C. MIMS cell filled with MCMM buffer (pH 6.3) was degassed during 30 min before the measurements. Final $H_2{}^{18}O$ enrichment in the cell was 3%.

As shown above (Fig. 5.1*a*, *c*), the artifact caused by the injection of 100 mM sodium formate is the initial rapid decrease in CO_2 signal detected as mass 46 (traces *2*). Subtraction of this 'formate' injection artifact from the formate-induced release of CO_2/HCO_3^- results in the detection of 0.34 ± 0.01 nmol dissolved C_i (n = 6) per 0.15 ml PSII sample or a concentration of 2.3 ± 0.1 μM CO_2.

After the injection (10 μl) of formate into the MIMS cell with PSII samples, the real chlorophyll concentration in the cell becomes equal to ~2000 μg *Chl* ml^{-1}. Assuming that 1 CO_2/HCO_3^- binds per 1 PSII RC, which contains ~250 *Chls*, we estimated that the 3.0 × 10^{-4} g *Chl* in our 0.15 ml sample should contain ~1.2 nmol of CO_2/HCO_3^-. Thus, the concentration of predicted CO_2/HCO_3^- is ~8.0 μM. Thereby, the release of 2.2 ± 0.1 μM CO_2 detected at pH 6.3 concludes that formate releases ~0.3 HCO_3^- per PSII RC. This value is very close to data reported earlier by Govindjee and co-workers (Govindjee *et al.*, 1991; Govindjee *et al.*, 1997), where from 0.4 to 1.2 HCO_3^-/CO_2 per reaction center were detected by mass spectrometry and infrared

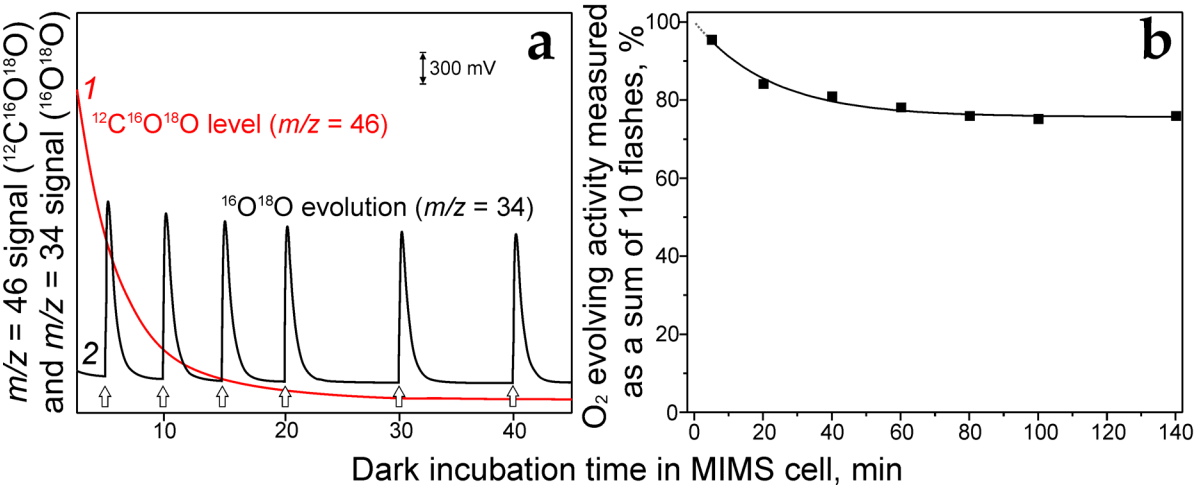

FIGURE 5.11 ***a***, level of $^{12}C^{16}O^{18}O$ (*m/z* = 46; ***1***, red trace) and O_2 yields induced by a series of 10 saturating Xe flashes (2 Hz) and measured as $^{16}O^{18}O$ (*m/z* = 46; **2**, black trace) as a function of dark incubation time of PSII membrane fragments in the MIMS cell at pH 6.3 and 20 °C. The $H_2{}^{18}O$ enrichment was 3%. The onsets of flash illumination are marked by arrows. ***b***, the same as ***a***, but with an $H_2{}^{18}O$ enrichment of 6%. Squares represent the integrated and normalized (to projected value at the time of injection) *m/z* = 34 ($^{16}O^{18}O$) signal intensities that were induced by 10 saturating Xe flashes as described above. All measurements were carried out with a *Chl* concentration of 0.4 mg ml^{-1} in presence of 1.5 mM $K_3[Fe(CN)_6]$ as electron acceptor and [CA] = 3 μg ml^{-1}. The rate of O_2 evolution of the studied BBY samples (measured by Clark-type electrode) was ~360 μmol (O_2) mg (*Chl*)$^{-1}$ ml^{-1} h^{-1}.

gas analyzer at pH 6.0–6.5. However, ~0.7 HCO_3^- is missing to be 1 HCO_3^-/1 PSII RC.

5.3.2.4 Activity of PSII Samples in the MIMS Cell during Degassation

One of the possible explanations for the missing HCO_3^- may be a loss of some HCO_3^- in PSII samples during the degassation procedure of the MIMS cell that is essential condition to be able to monitor the released gases (CO_2, N_2O) in our study. Since such involuntary depletion of 'structural' HCO_3^- from PSII (~0.7 per RC) due to degassation may significantly affect the activity of PSII samples, it can not be excluded that we detect formate-induced release of CO_2 in functionally 'impaired' PSII samples. To check this possibility we measured O_2–evolving activity of PSII membranes directly in the MIMS cell during its degassation with simultaneous monitoring CO_2 level. It should be mentioned that due to a very fast drift of O_2 during the first minutes of degassation of the MIMS cell, we were unable to detect O_2 evolution immediately after the placement of the samples into the MIMS cell. 5 min was found to be the minimal degassation time needed for the detection of flash-induced O_2 yield. Therefore, for initial O_2-evoliting activity we considered the activity of the samples after 5-min degassation of the MIMS cell.

As seen in Fig. 5.11*a*, the degassation/incubation of the samples in the MIMS cell during 40 min is coupled with significant reduction of CO_2 level (trace *1*). While the loss of the O_2–evolving activity of PSII membranes measured as O_2 yields (trace 2) resulting from 10 flashes (see figure legend for details) was estimated to be about 20% for the first 40 min of degassation. Further degassation of the MIMS cell during almost 2 h just insignificantly (~5%) decreases the relative O_2-evolving activity of the samples (Fig. 5.11*b*). Thus, the major loss of the activity (~15%) is observed within the first 20 min of the degassation where most of the CO_2 is removed (Fig. 5.11*a*).

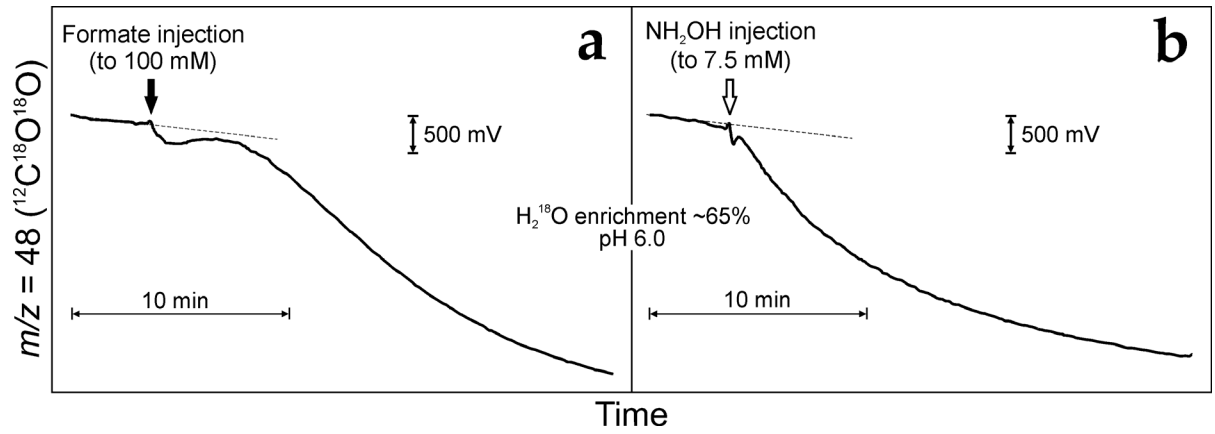

FIGURE 5.12 Formate-induced release of CO_2 (***a***) compared with the absence of CO_2 release upon the injection of NH_2OH (***b***) measured by MIMS at masses 48 in spinach BBY particles ([*Chl*] = 2 mg ml^{-1}) at pH 6.0 and 20 °C. Before the 10-μl injections of C_i-depleted formate to final concentration 100 mM (closed arrows) and C_i-depleted $^{14}NH_2OH$ to final concentration 7.5 mM (open arrows), PSII samples were degassed in the MIMS cell for 100 min. The measurements were performed in the presence of carbonic anhydrase [CA] = 3 μg ml^{-1}. The $H_2{}^{18}O$ enrichment was ~65%.

Although, it is difficult to judge whether the inhibition of O_2-evolving activity of the sample occurs due to the reduction of CO_2 level in the cell or is due to other factors, the loss of the activity (maximum 15%) during sample degassation is in any case not dramatic. Thereby our data clearly indicate that the measurements of CO_2 release induced by formate addition (Fig. 5.6*b, c*) were carried out with functionally active PSII membranes.

5.3.2.5 *Distinctions between Formate–Induced Released of CO_2 and NH_2OH–Induced Release of N_2O at High ^{18}O Enrichment*

Figure 5.12 represents additional evidence for the absence of NH_2OH-induced release of CO_2 from PSII samples. Since only CO_2 can be monitored at mass 48 (as double-labeled $^{12}C^{18}O_2$) and no N_2O, we performed formate (trace *a*) and NH_2OH (trace *b*) injections into PSII samples at high ^{18}O enrichment (~65%). While the injection of formate induces a slow release of $^{12}C^{18}O_2$, no $^{12}C^{18}O_2$ is observed upon the injection of NH_2OH into PSII samples. In both cases the injection artifacts are characterized by the decreasing in $^{12}C^{18}O_2$ level that corresponds to dilution effect of ^{18}O in the MIMS cell by non-^{18}O-labeled aqueous solutions of formate and NH_2OH. The results obtained confirm the conclusion that not CO_2, but only N_2O is released upon the injection of NH_2OH into PSII samples.

5.4 DISCUSSION AND CONCLUSION

5.4.1. PROBING HCO_3^- BINDING WITHIN THE WOC BY NH_2OH

In contrast to the acceptor side of PSII, where HC was shown to be a ligand to the non-heme iron (Blubaugh & Govindjee, 1988; Ferreira *et al.*, 2004; Loll *et al.*, 2005; van Rensen, 2002), it is still under discussion if HCO_3^- also binds at the WOC of PSII, where, for example, the Mn_4O_xCa cluster is considered as possible binding site (reviewed in (Klimov & Baranov, 2001; van Rensen & Klimov, 2005)). If HC is a structural part of the Mn_4O_xCa cluster or an integral cofactor of the WOC, then the destruction of the WOC

should cause the release of free C_i ($HCO_3^-/CO_3^{2-}/CO_2$) into the solution. Independent of the initial form of C_i, this release can be detected by MIMS as CO_2 because of the pH-dependent equilibria between all these species (see, for instance, (Govindjee *et al.*, 1991)). We checked this idea by employing hydroxylamine which is widely used for irreversible inactivation of PSII by releasing Mn^{2+} and extrinsic polypeptides (17, 23 and 33 kDa) from the WOC (Kuntzleman & Yocum, 2005; Tamura & Cheniae, 1985; Yocum *et al.*, 1981). The injections of high concentrations (7.5–10 mM) of NH_2OH into the MIMS cell filled with PSII samples cause extraction of all Mn from the WOC (Fig. 5.4). While NH_2OH is the most appropriate reductant performing very fast and full destruction of the WOC, one has to take into account that together with the possible release of CO_2 (if HCO_3^- indeed a ligand to the Mn_4O_xCa cluster), N_2O which has the same molecular mass as CO_2 (m/z = 44) can be released due the reaction of NH_2OH with the Mn_4O_xCa cluster (see Eq. 5.1). It has been reported earlier that the oxidation of NH_2OH to N_2O and N_2 is catalyzed by such ions as Cu^{II} (Anderson, 1964), Fe^{III} (Butler & Gordon, 1986; Kolasa & Wardencki, 1974) and, even by mononuclear Mn^{III}-complexes (Panja *et al.*, 2003; Salem, 1995). Moreover, in a previous study, $^{15}N_2O$ has been detected as one of the products of ^{15}N-labelled NH_2OH oxidation by the Mn_4O_xCa cluster of PSII (Kretschmann & Witt, 1993).

In spite of the same m/z value (44) for detection of CO_2 and N_2O, our MIMS data clearly show that N_2O is the only gas released upon the injection of NH_2OH into PSII samples. The absence of CO_2 in the NH_2OH-induced release of N_2O in PSII samples is demonstrated by (*i*) the full shift of mass signal 44 ($^{14}N_2{}^{16}O$) to mass signal 46 ($^{15}N_2{}^{16}O$), when instead of non-labelled NH_2OH, ^{15}N-labelled NH_2OH was used (see Figs. 5.1 and 5.3), (*ii*) the absence of mass signal 48 ($^{12}C^{18}O_2$), upon the injection of NH_2OH into PSII samples that were highly (~65%) enriched with ^{18}O (Fig. 5.12) and (*iii*) the calculated experimental values of natural isotopic distributions of the released gas, which fit the natural isotopic distribution of N_2O rather than of CO_2 (see Table 5.2). Thus, complete destruction of the WOC by hydroxylamine does not lead to any release of C_i. This shows that HCO_3^- is not a tightly bound ligand of the Mn_4O_xCa cluster or of the extrinsic polypeptides of PSII.

5.4.2. PROBING HCO_3^- BINDING TO PSII BY FORMATE

We also probed binding of HCO_3^- to the WOC by formate additions, since formate is commonly used for the removal of HCO_3^- from its binding sites in PSII (Feyziev *et al.*, 2000; Jajoo *et al.*, 2005; Klimov *et al.*, 1995a). Our MIMS data (Fig. 5.6) confirm that the injection of formate induces a slow release of C_i from PSII (Govindjee *et al.*, 1991, Govindjee *et al.*, 1997) and, thereby, demonstrate that hydrogencarbonate is bound to PSII.

Assuming that formate induces the removal of HCO_3^- not only from the non-heme iron (electron acceptor side), but also from the Mn_4O_xCa cluster (electron donor side), removal of the Mn_4O_xCa cluster from PSII prior to formate injection should reduce the amount of CO_2 released by formate. Since the same amount of CO_2 was observed for both sample types, the data in Fig. 5.9 indicate that the released CO_2 originates solely from the acceptor side of PSII. This confirms that C_i is not a ligand of the Mn_4O_xCa cluster.

The amount of HCO_3^-/CO_2 released by formate per PSII reaction center (pH 6.3) has been found to be ~0.3 (see section 5.3.2.3) and, therefore ~0.7 HCO_3^-/CO_2 is missing to have 1 HCO_3^-/1 PSII RC. There are three possible explanations for missing hydrogencarbonate: (*1*) Formate is unable to remove all 'structural' HCO_3^-/CO_3^- from PSII. (*2*) The value of ~0.3 HCO_3^-/1 PSII RC is within the 'norm' for our spinach PSII membranes (at pH 6.3). Govindjee and co–workers (Govindjee *et al.*, 1991, Govindjee *et al.*, 1997) detected in their studies 0.4 to 1.25 HCO_3^-/CO_2 per reaction center, depending on the sample types (less in maize thylakoids, more in pea thylakoids) and pH values (minimal at pH 6.0, maximal at pH 6.5). Therefore, the different number of CO_2 released per PSII RC has been suggested to have physiological significance. (*3*) Some of HCO_3^- can be already released during degasation of the samples in the MIMS cell prior to formate injection.

Thus, the results presented in this study clearly show that HCO_3^- is not a ligand to the Mn_4O_xCa cluster. Therefore, HCO_3^- is probably required only for the process of the assembly of the functionally competent WOC from the cofactor-depleted *apo*-WOC-PSII centers, that appear as a result of disassembling of the WOC under stress conditions or when newly synthesized (Allakhverdiev *et al.*, 1997; Baranov *et al.*, 2000; Baranov *et a.*, 2004; Klimov *et al.*, 1997a; Klimov & Baranov, 2001; van Rensen & Klimov, 2005). After its participation in photo-assembly process, HCO_3^- appears to leave the WOC. However, it can not be excluded, that HCO_3^- can be involved indirectly in water reactions, *e.g.* as a proton transfer mediator (Ananyev *et al.*, 2005; Shutova *et al.*, 2008).

5.4.3. CONCLUSION

In this study, we provide strong evidence that HC is neither a tightly bound ligand to the Mn_4O_xCa cluster nor a cofactor strongly coupled with the WOC. This is demonstrated by performing NH_2OH addition into PSII samples and simultaneously monitoring the released gaseous products by MIMS. We cannot exclude by these experiments the presence of a weak HCO_3^- ligand to the Mn_4O_xCa cluster that is already removed during degassation of the sample in the MIMS cell. However, as shown in Chapter 4 (see also (Shevela *et al.*, 2007)) we did not find any evidence for a weakly bound HCO_3^- ligand to the WOC on the basis of flash-induced oxygen evolution measurements on a Joliot-type electrode. Therefore, most probably, hydrogencarbonate plays the role of a transient ligand during the assembly of the Mn_4O_xCa cluster (Allakhverdiev *et al.*, 1997; Baranov *et al.*, 2000; Baranov *et al.*, 2004; Dasgupta *et al.*, 2007; Dismukes *et al.*, 2001) and stabilizes the WOC indirectly through binding to other components on the donor side of PSII (Klimov et al., 1995a; Klimov *et al.*, 1995b; Pobeguts *et al.*, 2007).

Chapter 6

Azide and Chloride Interactions with the Mn_4O_xCa Cluster of Photosystem II

6.1 INTRODUCTION

Chloride (Cl^-) has long been known to affect photosynthetic oxygen evolution in PSII, but its functional role in the water splitting process is not established, and there is no firm evidence that Cl^- is bound to the Mn_4O_xCa cluster (recently reviewed in (Popelková & Yocum, 2007; Homann, 2002; van Gorkom & Yocum, 2005)). From the observation that chloride, primary amines, and other Lewis bases compete for the same binding site it has been proposed that chloride binds directly to manganese or to a site very close to the manganese, affecting the redox properties of the Mn_4O_xCa cluster (Sandusky & Yocum, 1984). This assumption was supported by the fact that Cl-depleted PSII membranes exhibit altered S_2 state EPR signals (Ono *et al.*, 1986). It has been also shown that the presence of chloride is necessary only for the $S_2 \rightarrow S_3$ and $S_3 \rightarrow S_0$ transitions of the WOC, while the earlier steps of the cycle can proceed in its absence (Wincencjusz *et al.*, 1997; Wincencjusz *et al.*, 1998). However, it has been suggested that the Cl^- dependence of O_2 evolution may be a consequence of the treatments used to remove the anion (Wydrzynski *et al.*, 1990; Olesen & Andréasson, 2003). Thus, in some cases, (see for example (Wincencjusz *et al.*, 1998)) the Cl^- requirement is determined after extrinsic proteins (16 and 23 kDa) have been purposely removed. This treatment is known to be coupled with severe inhibition of the oxygen-evolving activity, which may be recovered by the addition of Cl^- (Miyao & Murata, 1984; Ono et al., 1986; Homann, 1988). On the other hand, it has been reported that all PSII centers remain active if Cl^- is removed from intact PSII by prolonged dialysis under conditions that avoid dissociation of the extrinsic protein (Lindberg *et al.*, 1993; Lindberg & Andréasson, 1996). This finding called in question the above proposal that Cl^- is an integral constituent of the WOC (Olesen & Andréasson, 2003). In addition, none of the recent XRD models of PSII (Ferreira *et al.*, 2004; Loll *et al.*, 2005) includes Cl^- in the WOC.

In previous studies azide (N_3^-) was found to be an inhibitor of oxygen evolution of PSII, however, its inhibitory mechanism remains unclear (Katoh, 1972; Stemler & Murphy, 1985). It has been suggested that azide inhibits oxygen evolution by acting primarily as chloride competitor and that it prevents the WOC from undergoing the normal progression to the S_2 state. Recently, the effect of N_3^- on the S_2 state multiline EPR signal has been studied and a weak magnetic interactions between ^{14}N in the azide and the Mn ion(s) in the Mn_4O_xCa cluster was proposed (Haddy *et al.*, 1999; Haddy *et al.*, 2000; Yu *et al.*, 2005). However, these interactions were not resolved by the advanced pulse EPR techniques such as electron spin–echo envelope modulation (ESEEM). In a previous report (Yu *et al.*, 2005), a broad signal was detected by two-pulse ESEEM in Cl^--depleted/$^{15}N_3^-$-treated PSII samples and, this signal was interpreted as originating from the magnetic interaction between the ^{15}N-labeled azide and the Mn ion(s).

Recently, it has been observed (Messinger *et al.*, unpublished) in a Mn^{III}-N_3 model complex (Weyhermüller & Wieghardt, unpublished) that under X-ray illumination N_2 was released from the complex and that $Mn^V{\equiv}N$ was formed (see Fig. 6.1), which was easily detectable by a transient increase in the pre-edge peak of Mn XANES spectra. Therefore, if a similar effect can be observed in azide-treated PSII samples, this would prove that N_3^- (Cl^-) is bound to the only remaining Mn^{III} in the S_2 state. In the present study in order to prove (or to disprove) N_3^- binding (and, therefore, Cl^-

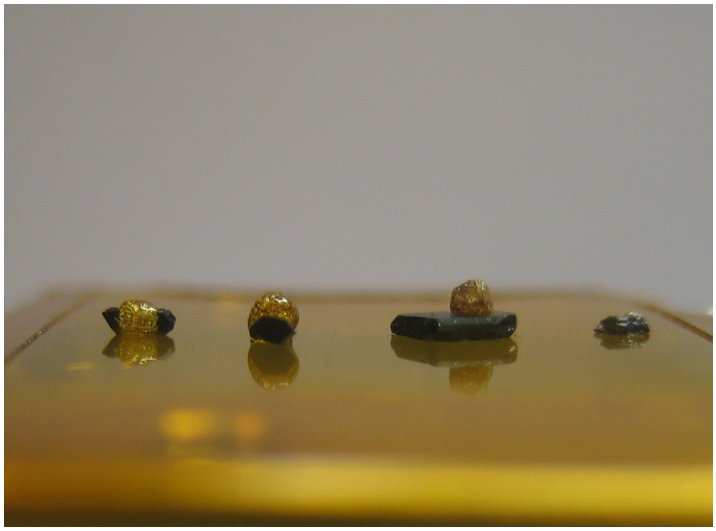

FIGURE 6.1 Formation of $Mn^{V}{\equiv}N$ from $Mn^{III}–N_3$ model complex under high doses of X-ray radiation. N_2 release led to the formation of bubbles on top of the black $Mn^{III}–N_3$ crystals.

binding) to Mn ions within the Mn_4O_xCa cluster we employed both EPR and EXAFS/XANES measurements of Cl^--depleted/N_3^--treated PSII samples. To avoid destruction of the extrinsic proteins, a prolonged dialysis (Lindberg *et al.*, 1993) has been chosen as a procedure for Cl^- removal from intact PSII.

6.2 EXPERIMENTS AND ANALYSIS

6.2.1 PREPARATIVE PROCEDURES

6.2.1.1 Chemicals

NaN_3 (^{15}N single terminal labeled, $^{15}N^{14}N^{14}N^-$ ≥ 99.0%) was purchased from *Cambridge Isotope Laboratories*. Cl^--'free' buffer, was prepared using 200 mM Sucrose (≤ 0.005% Cl) and 20 mM MES/NaOH, pH 6.3. For further details see Sections 2.1.1 and 2.1.2.

6.2.1.2 Sample Preparation

PSII-enriched (BBY) membranes isolated from spinach as described in Section 2.2.2. The oxygen-evolving activity of the PSII preparations at saturating light intensities was about 500 μmol (O_2) mg (*Chl*)$^{-1}$ h^{-1}. The samples (~6.5 mg *Chl* ml^{-1}), were thawed in the dark on ice.

6.2.1.3 Chloride Removal

Cl^- removal was carried out by repetitive washing followed by dialysis according to the method described earlier in (Lindberg *et al.*, 1993; Yu *et al.*, 2005) with some modifications. PSII membranes were suspended in Cl^--free buffer to a concentration of about 1 mg *Chl* ml^{-1} and then concentrated by centrifugation. The pellet was washed twice to ensure complete replacement of the buffer medium. Then the samples were placed in dialysis tubing (*Visking Code DTV*, approx. 12–14 kDa) and dialyzed in the dark cold room (4 °C) for 19–20 hours against Cl^--free buffer (pH 6.3) (changed twice during the dialysis). These PSII membranes will in the following be referred to as Cl^--depleted.

6.2.1.4 Azide Treatment/Anion Repletion

Azide treatment/anion repletion was performed with Cl^--depleted PSII membranes. After sedimentation, the pellets prepared from the dialyzed PSII samples were resuspended and diluted to about 0.4 mg Chl ml^{-1} in a Cl^--free buffer containing NaN_3 at the desired concentrations (natural abundance or ^{15}N terminal labeled). In some cases, the dialyzed Cl^--depleted samples were split up into three parts. Then one part was treated with Cl^--free buffer (no additions), while the rests were treated either with NaN_3 (40–50 mM) or NaCl (40 mM) dissolved in Cl^--free buffer.

After incubation on ice in the dark for about 50 min, PSII samples were collected by centrifugation at 4 °C (30.000 ×*g*, 90 min) and the supernatant was discarded. The centrifuge tubes with pellets were kept upside down in cold room for 10 min, and then small amount of buffer inside the tubes was wiped away. About 30–50% (v/v) of glycerol was added to each pellet and carefully mixed with the PSII sample in small glass dishes. The final sample paste was then either transferred with a palette-knife into Lexan sample holders (22 × 3.2 × 0.8 mm inner dimensions) designed to fit for both the EPR cavity and the X-ray cryostat. Alternatively, some of the pellets were diluted with final buffer and loaded into quartz EPR tubes. Afterwards, the

samples were concentrated to about 20–30 mg Chl ml^{-1} by centrifugation in the EPR tubes (Kulik *et al.*, 2007; Messinger *et al.*, 1997c; Su *et al.*, 2008). The samples were stored in liquid nitrogen until used. All procedures were carried out under dim green light at 4 °C.

The PSII samples in the S_1 state were advanced to the S_2 state by 10–20 min continuous illumination using a 2 × 250 W (double sided) halogen lamps from which the IR and UV contributions were largely removed by the following filters: 8 cm water, 2 cm $CuSO_4$ solution (5% w/v), *Schott KG 3* (2 mm) and *Schott GG 445*. The final light intensity at sample level was ~0.5 W/cm^2. Samples were places in a tall test tube which was suspended in a 200 K dry ice/ethanol bath in an unsilvered glass dewar.

6.2.2 EPR MEASUREMENTS

CW-EPR spectra were recorded as described in Section 5.2.3. Electron spin echo (ESE) field sweeps and ESE envelope modulation (ESEEM) spectra were collected at 4.2 K using a *Bruker ESP-580* X-band pulse EPR spectrometer equipped with *superXFT* bridges, *Oxford-900* liquid helium cryostat, and *ITC-503* temperature controller. The corresponding pulse sequences and other EPR settings are given in the figure legends.

6.2.3 XAS SPECTROSCOPY

EXAFS Data Collection. X-ray absorption spectra were collected at SSRL (Stanford Synchrotron Radiation Laboratory) on beamline 7–3 at an electron energy of 3.0 GeV and an average current 70–100 mA (described in (DeRose *et al.*, 1994; Latimer *et al.*, 1995)). The intensity of the incident X-rays was monitored by a N_2-filled ion chamber (I_0) in front of the sample. The radiation was monochromatized by a by a Si(220) double-crystal monochromator. To reduce the sample damage by X-ray radiation, the incident X-ray beam was defocused at the sample position. The samples were protected from the beam during spectrometer movements between different energy positions by a shutter synchronized with the scan program. The total photon flux on the sample was limited to 1×10^7 photons per μm^2, which was determined to be non-damaging on the basis of detailed radiation-damage studies of PSII solution samples (Yano *et al.*, 2005b). The samples were kept at 9 ± 1 K in a He atmosphere at ambient pressure using an *Oxford CF-1208* continuous-flow liquid He cryostat. Data were recorded as fluorescence excitation spectra using a germanium 30-element energy-resolving detector (*Canberra Electronics*). For Mn XAS, energy was calibrated by the pre-edge peak of $KMnO_4$ (6543.3 eV) which was placed between two N_2-filled ionization chambers (I_1 and I_2) after the sample.

EXAFS Data Analysis. Data reduction of the EXAFS spectra was performed essentially as described in (DeRose *et al.*, 1994; Robblee *et al.*, 2002). After conversion of background-corrected spectra from energy space to photoelectron wave vector (k) space, and weighted by k^3, a four-domain spline was subtracted for a final background removal. The k-space data were then truncated near the zero crossing (k = 3.5–11.5 $Å^{-1}$ in Mn EXAFS) before Fourier transformation.

6.3 RESULTS

6.3.1 INHIBITION INDUCED BY AZIDE FOR PSII SAMPLES IN THE ABSENCE OF CHLORIDE

Cl^--depletion or replacement of Cl^- with N_3^- or other anions (*e.g.* F^-) is known to result in a suppression of the S_2 state multiline signal and an increase in the g = 4.1 signal (DeRose *et al.*, 1995; Haddy *et al.*, 2000; Olesen & Andréasson, 2003; Ono *et al.*, 1987; Yu *et al.*, 2005). Moreover, the replacement of Cl^- with N_3^- is characterized by a complete absence of water-splitting activity (Haddy *et al.*, 2000; Kawamoto *et al.*, 1995). We therefore examinated our Cl^--depleted and N_3^--treated samples (see Sections 6.2.1.3 and 6.2.1.4) by EPR spectrometry and Clark-type O_2 evolution assays.

EPR spectra shown in Fig. 6.2 represent difference spectra made by subtracting the spectra of dark-adapted samples from those obtained after 200 K illumination. As seen in the Fig. 6.2, only a very weak S_2 state EPR multiline signal was detected in Cl^--depleted PSII samples (spectrum *a*). The addition of N_3^- (40 mM) to these samples (in S_1 state) resulted in almost complete suppression the formation of the S_2 multiline signal (spectrum *b*). On the contrary, Cl^--depleted PSII membranes to which Cl^- (40 mM) had been added revealed normal formation of the g = 2 multiline signal (spectrum *c*). In addition, the S_2 state EPR spectrum of dialyzed and N_3^--treated PSII membranes was characterized by a stronger g = 4.1 signal than that observed in Cl^--repleted samples. These results are in good agreement with earlier studies (Olesen & Andréasson, 2003; Haddy *et al.*, 2000; Yu *et al.*, 2005). O_2 evolution assays of the same PSII samples (in the final suspension buffers) showed about 35% activity for the Cl^--depleted sample, whereas the N_3^--containing sample revealed essentially no activity at all (see Table 6.1). These observations are in full agreement with previous reports on the partial inhibition of PSII upon the Cl^--depletion (by prolonged dialysis) (Haddy *et al.*, 2000; Lindberg & Andréasson, 1996; Olesen & Andréasson, 2003) and complete inhibition of PSII that occurs when catalytic turnovers take place in the presence of N_3^- (Haddy *et al.*, 1999; Haddy *et al.*, 2000; Kawamoto *et al.*, 1995).

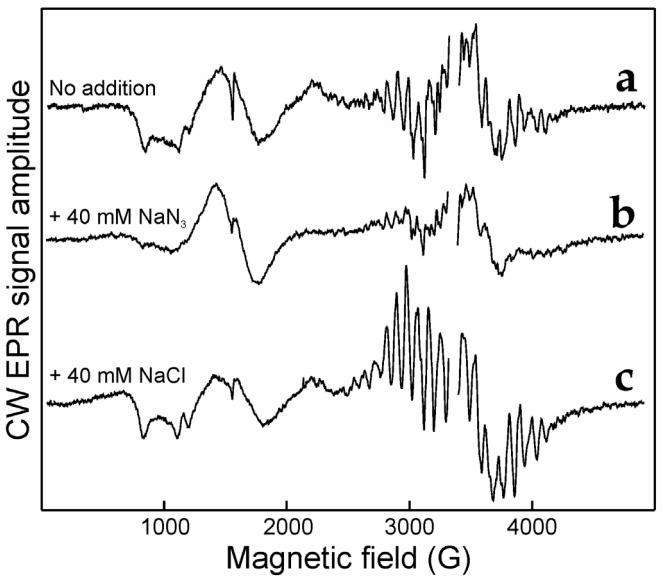

FIGURE 6.2 200 K illuminated-minus-dark difference EPR spectra of PSII membrane fragments after Cl^- depletion (see Section 6.2.1.3): spectrum ***a***, no addition; spectrum ***b***, with 40 mM NaN_3; and spectrum ***c***, with 40 mM NaCl. EPR settings: microwave frequency, 9.43 GHz; microwave power, 10 mW; modulation amplitude, 15.0 G; sample temperature, 7 K. Each spectrum is the average of 8 scans. The absorption of the Tyr D radical was removed for the presentation.

Thus, the experimental characteristics of our Cl^--depleted/ N_3^--treated samples are identical to those described in the literature, where azide was suggested to replace chloride in

its binding site near the Mn_4O_xCa cluster (Britt *et al.*, 2000; Haddy *et al.*, 1999; Haddy *et al.*, 2000; Yu *et al.*, 2005). Using the same protocol for sample preparation (described in Sections 6.2.1.3 and 6.2.1.4) we further investigated the possibility of N_3^- and/or Cl^- binding to the Mn_4O_xCa cluster by pulse EPR (with ^{15}N terminally labeled azide).

TABLE 6.1. Rates of oxygen evolution with normalized values as measured before and after Cl^- depletion (long dialysis described in Section 6.2.1.3) and azide treatment (see Section 6.2.1.4) of PSII membranes

Samples	**O_2 evolution rates (μmol (O_2) mg (*Chl*)$^{-1}$ h^{-1})**	**% activity**
Control (containing 35 mM Cl^-)	510 ± 20	100
Cl^--depleted	180 ± 15	35
Cl^--depleted + 40 mM NaN_3	0 ± 0 [A]	0

[A] Small oxygen uptake (~30 μmol (O_2) mg (*Chl*)$^{-1}$ h^{-1}) was observed in Cl^--depleted/NaN_3-treated samples

6.3.2 PULSE EPR MEASUREMENTS

Cl^--depleted PSII membranes were treated with ^{15}N terminal labeled NaN_3 (50 mM), these samples were employed for the pulsed EPR measurements. Figure 6.3 displays the result of the two-pulse ESE-detected field-swept EPR measurement. The spectrum shows that there is some absorption in the region of g = 2.0, corresponding to the S_2 state multiline signal in Fig. 6.2*b*.

The two-pulse ESEEM measurement was conducted at the magnetic field position of 3550 G (indicated by the arrow in Fig. 6.3). At this field position nitrogen coupling should be visible at the Larmor frequencies 1.093 and 1.553 MHz for ^{14}N and ^{15}N, respectively. Figure 6.4 shows the Fourier transformation (FT) of the frequency domain ESEEM spectrum obtained on the Cl^--depleted and azide-repleted sample (^{15}N terminally labeled). It is seen that none of the proposed signals for ^{14}N and ^{15}N with weak hyperfine coupling is observed at the indicated Larmor frequencies (compared, for example with the ^1H signals centered around 15.15 MHz). The result obtained differs from a recent report (Yu *et al.*, 2005), in which the a new peak was detected at about 1.9 MHz in Cl^--depleted/^{15}N-terminally labeled NaN_3-treated samples compared to that of untreated PSII membranes. Although this peak

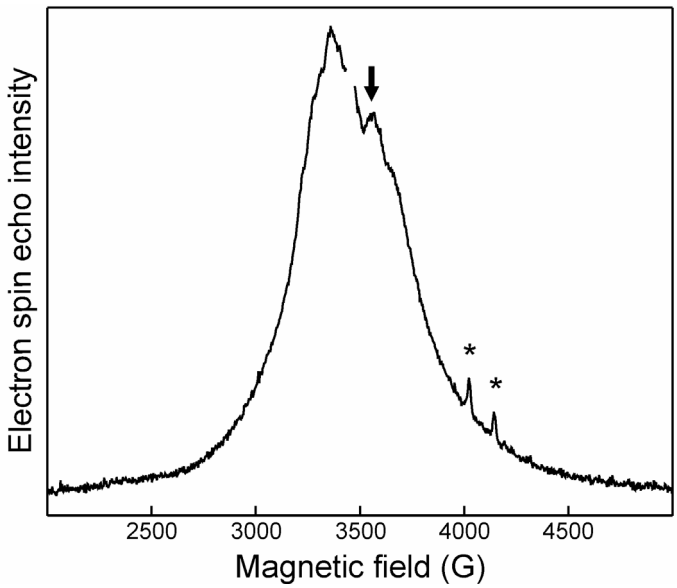

FIGURE 6.3 ESE field-swept EPR spectrum of the S_2 state in Cl^- depleted BBY samples treated with 50 mM ^{15}N terminally labeled NaN_3. The pulse sequence employed is $\pi/2$-τ-π-τ-echo, where $\pi/2$ = 12 ns, τ = 128 ns, 100 shots/point, and shot repetitive time 10 ms. Other EPR settings: microwave frequency = 9.70 GHz; temperature = 4.2 K. The arrow shows the field position used for experiment displayed in Fig. 6.4 and Fig. 6.5. The stars indicate instrumental artifacts. The absorption of the Tyr D radical was removed for presentation.

was 0.4 MHz higher than the 1.5 MHz ^{15}N Larmor frequency, the authors suggested that the 1.9 MHz ESEEM feature arises from the terminal azide ^{15}N label.

In order to improve resolution we performed a three-pulse ESEEM measurement (Deligiannakis *et al.*, 2000). The two-dimensional three-pulse ESEEM spectrum of Cl^--depleted PSII samples treated with ^{15}N terminal labeled azide is displayed in Fig. 6.5. Again, neither the signal centered at ^{14}N-Larmor frequency (shown as blue short dash) nor at ^{15}N-Larmor frequency (shown as red short dash) was observed under conditions when time intervals, τ (pulse sequence given in legend of Fig. 6.5) was increased from 120 to 312 ns.

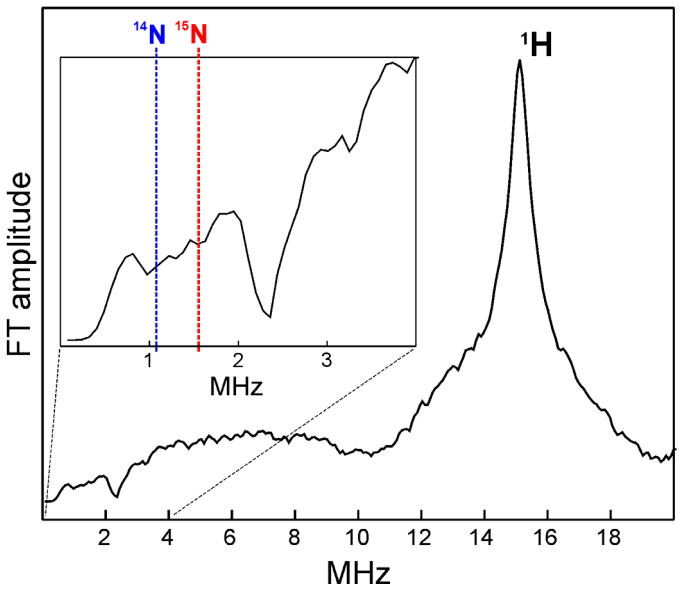

FIGURE 6.4 FT of the two-pulse ESEEM of Cl^- depleted PSII samples treated with 50 mM [^{15}N]azide. The pulse sequence employed is π/2-τ-π-τ-echo, where π/2 = 12 ns, τ varies from 120 to 6260 ns in 12 ns-steps, shot repetitive time 10 ms and 100 shots/point. Experimental parameters: microwave frequency = 9.70 GHz; B_0 = 3550 G; temperature = 4.2 K. The Larmor frequencies of ^1H, ^{14}N, and ^{15}N are 15.15, 1.093, and 1.553 MHz, respectively. The inset panel is amplifying the region from 0 to 4 MHz.

Thus, no evidence from both two- and three-pulse ESEEM could be obtained for the magnetic interaction between the $^{14}N/^{15}N$ and Mn ion(s).

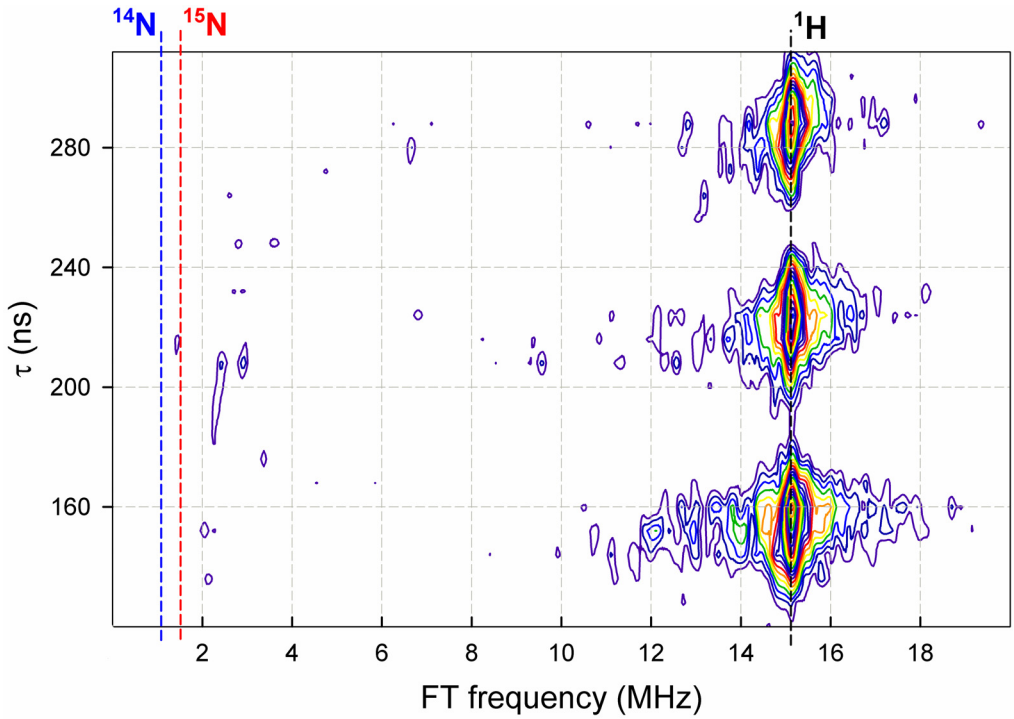

FIGURE 6.5 FT of two-dimensional 3-pulse ESEEM of Cl^- depleted PSII samples treated with 50 mM [^{15}N]azide. The pulse sequence is π/2-τ-π/2-T-π/2-τ-echo, where π/2 = 24 ns, τ starts from 120 to 312 ns in 8 ns-step s, and T varies from 48 to 6192 ns in 24 ns-steps, four-phase cycling, 50 shots/point, shot repetitive time 10 ms, B_0 = 3550 G. The Larmor frequencies of ^1H, ^{14}N, and ^{15}N are 15.15 (black dashes), 1.093 (blue dashes), and 1.553 (red dashes) MHz, respectively.

6.3.3 XANES/EXAFS SPECTROSCOPY DATA

The same Cl^--depleted/N_3^--treated PSII samples as for CW-EPR (Fig. 6.2*b*) and O_2 evolution activity (Table 6.1) measurements were employed for the EXAFS/XANES study.

Upon advancement of the WOC from the S_1 to the S_2 state by 200 K illumination the Mn K-edge XANES of PSII shifts by 1.6–1.8 eV, which has been interpreted as evidence for direct Mn oxidation (Goodin *et al.*, 1984). If azide indeed prevents the WOC from undergoing the normal progression to the S_2 state due to binding to the Mn_4O_xCa cluster at the chloride binding site, as proposed earlier (Haddy *et al.*, 2000; Yu *et al.*, 2005), then illumination of the Cl^--depleted/N_3^--treated PSII samples should not cause a shift of the Mn K-edge XANES. Figure 6.6 represents a comparison of K-edge XANES spectra shifts for the S_1 (in black) and S_2 states (in red) obtained in PSII samples before (spectra *a*) and after Cl^--depletion and treatment with 40 mM NaN_3 (spectra *b*). It is seen that the edge shifts even in Cl^--depleted/N_3^--treated PSII samples, although to a smaller extend than in Cl^--containing 'control' samples. The data indicates that at least in some PSII centers treated with N_3^- the S_2 state can be formed.

It should be mentioned that the edges for Cl^--depleted/N_3^--treated samples are slightly shifted to a lower energy due to the presence of Mn^{2+}. Indeed, from the appearance of the typical hexaquo Mn^{2+} EPR signal PSII samples (data not shown) we found that PSII centers loose some Mn during the Cl^--depletion depletion

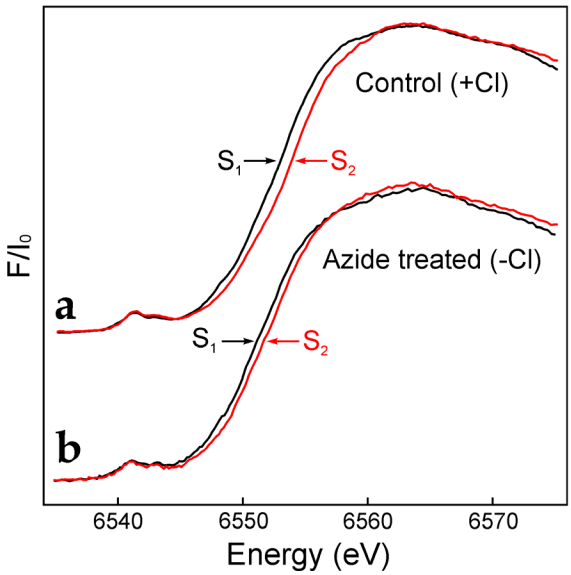

FIGURE 6.6 Normalized Mn K-edge XANES spectra for the S_1 (black) and S_2 states (red) obtained from Cl^--depleted PSII membranes repleted with 40 mM NaN_3 (*b*) and compared with PSII control samples (prior to Cl^--depletion and NaN_3 treatment) (***a***). A linear scatter background was subtracted, and the spectra were normalized at the energy of maximal absorption.

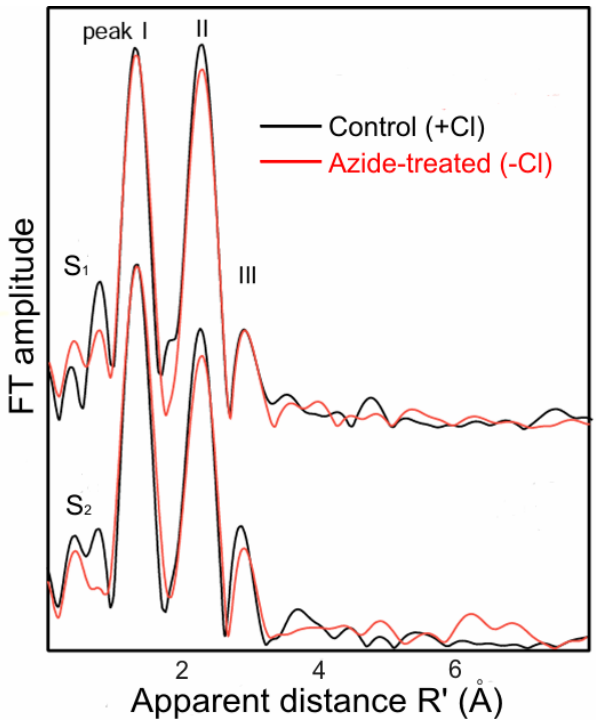

FIGURE 6.7 The Fourier transforms (FTs) of the k^3-weighted Mn-EXAFS spectra (3.5–11.5 $Å^{-1}$) obtained from Cl^--depleted PSII membranes repleted with 50 mM NaN_3 (red spectra) and compared to PSII controls (black spectra) in the S_1 state (top) and S_2 state (bottom). The main FTs peaks are labeled I, II and III. FT peak I is from Mn-ligand backscattering; FT peal II is from three Mn-Mn distances at 2.7 to 2.8 Å; and FT peak III is from one Mn-Mn and two Mn-Ca distances at 3.3 and 3.4 Å, respectively.

procedure. We calculated that about 5% of Mn^{2+} was left in the pellet after all preparative procedures.

Recently, Mn^{III}–N_3 model complex has been shown to form $Mn^{V}\equiv N$ under X-ray illumination (Fig. 6.1). $Mn^{V}\equiv N$ can be easily detected on the basis of its sharp pre-edge peak (see Introduction). Therefore, some of the PSII-azide samples were exposed to high X-ray fluxes, but the expected change in pre-edge XANES spectra was not observed in N_3^--treated PSII during X-ray illumination. This indicates that no $Mn^{V}\equiv N$ formation occurs in our Cl^--depleted/N_3^--repleted samples and that it is therefore very unlikely that azide is bound to the Mn^{III} ion in the S_2 state.

In addition, Mn-EXAFS of N_3^--repleted PSII was measured since in case of N_3^- binding to Mn a multiple scattering peak may be displayed due to linear arrangement of N's in N_3^-. However, as shown in Fig. 6.7, such peak is not seen in Cl^--depleted/N_3^--repleted PSII membranes (red spectra) neither in S_1 nor in S_2 state. The FT-EXAFS spectra are very similar for Cl^--contained 'control' PSII samples and azide-treated PSII.

Thus, the presented results do not provide any indications for N_3^- binding to Mn within the Mn.

6.4 DISCUSSION AND CONCLUSION

No evidence for N_3^-(Cl^-) binding to the Mn_4O_xCa cluster was found in the present study by performing both two- and three-pulse ESEEM and XANES/EXAFS measurements, despite the fact that the samples displayed the known changes in the CW-EPR S_2 multiline signal and in O_2 evolution rates. This finding is in direct contrast to a previous 2 pulse ESEEM report (Yu *et al.*, 2005), in which it was concluded that azide binds at or in close visinity of the Mn_4O_xCa cluster. This raises two questions: (*i*) did we carefully deplete our samples of Cl^-? and (*ii*) is the previously reported signal reliable?

It was previously shown that using dialysis it is possible to deplete PSII of Cl^- without disturbing the composition of extrinsic proteins (23 and 17 kDa), but there remains significant residual oxygen evolution activity (25–40%) in the absence of Cl^- (Lindberg & Andréasson, 1996; Olesen & Andréasson, 2003; Wydrzynski *et al.*, 1990). Moreover, such depletion is characterized by the alteration the S_2 state multiline EPR signal and, the small increase of g = 4.1 signal (Lindberg & Andréasson, 1996; Olesen & Andréasson, 2003; Ono *et al.*, 1987). In our study chloride was likely depleted to the same extend as in these former studies, because our Cl^--depletion procedure caused the decrease of O_2 activity to ~35% of the control (Table 6.1) and the significant suppression of the g = 2 multiline signal (Fig. 6.2) with some modification of g = 4.1 signal.

The broad signal detected recently by two-pulse ESEEM in Cl^--depleted/$^{15}N_3^-$-treated PSII samples (Yu *et al.*, 2005) was interpreted as reflecting the magnetic interaction between the ^{15}N in the ^{15}N terminally labeled azide with the Mn ion(s) of the WOC in the S_2 state. This signal was not observed by the same authors if Cl^- was not removed from PSII samples prior to azide addtion. These results suggested that azide might inhibit water oxidation on the donor side of PSII and that the azide effects occur from the chloride competitive site. However, this signal was found at about 1.9 MHz rather then at 1.5 MHz as expected from the ^{15}N Larmor frequency.

This raises questions about the origin of this peak. Our data presented in Table 6.1 and Fig.6.1 clearly show that the azide addition to the Cl^--depleted samples lead to a total inhibition of O_2 evolution activity and almost complete suppression of the S_2 state multiline signal. However, performing the Cl^--depleted/[^{15}N] azide-treated samples for both two- and three-pulse ESEEM measurements no signal indication for a weak or strong hyperfine coupling between the S_2 state and the spin I = ½ of ^{15}N was found. We also did not observe any signal centered at 1.9 MHz. It should be noted that in this study a much higher concentration of ^{15}N–NaN_3 (50 mM) was used than in the previous study (8 mM).

Our XANES data indicate that some percentage of the N_3^--treated PSII centers advances from S_1 to S_2 state. This is shown by the small modified S_2 multiline signal and the generation of the g = 4.1 signal during 200 K illumination (Fig. 6.2*b*) also observed in earlier studies for N_3^--repleted PSII (Haddy *et al.*, 2000; Yu *et al.*, 2005). An important result obtained by XANES was the absence of the predicted change in pre-edge under X-ray illumination in our N_3^--treated samples (see Section 6.1). This indicates that N_3^- (Cl^-) is not bound to the only Mn^{III} in the S_2 state. In addition, employing Mn-EXAFS spectra we did not observe a multiple scattering peak that would be indicative for azide binding. Therefore, it seems that azide does not bind to Mn in the Mn_4O_xCa cluster neither in S_1 nor in the S_2 state.

Thus, azide appears to inhibit PSII without direct ligation to the to the Mn_4O_xCa cluster. However, Cl^- still may be a ligand if Yocum and co-workers (Popelková & Yocum, 2007) are right that the extrinsic (16 and 23 kDa) proteins must be removed to release the functional Cl^- bound to the Mn_4O_xCa cluster. It is possible that Yu and co-authors (Yu *et al.*, 2005) lost some of these extrinsic proteins during their Cl^- depletion procedure (by dialysis) and thereby were able to detect a ^{15}N-coupling to Mn. Future pulse EPR and EXAFS/XANES measurements of the samples that were Cl^--depleted by the removal of extrinsic proteins and treated with N_3^- should clarify this question.

Alternatively, azide (and, consequently Cl^-) may bind not to the Mn, but to Ca within the Mn_4O_xCa cluster. In addition, it cannot be excluded that after the removal of Cl^- from the WOC by dialysis, azide may occupy not the chloride binding site but another site within the WOC without direct interaction between this anion and the Mn_4O_xCa cluster. However, in case that azide is indeed a competitor of chloride, our data may indicate that Cl^- is not direct ligand to the Mn ions in the Mn_4O_xCa cluster. Such an interpretation is consistent with a recent Br^--EXAFS study that concluded that Br^- (Cl^-) is at least 5 Å away from the closest Mn ion (Haumann *et al.*, 2006). Thus, our data support the idea that chloride participates in establishing a proton relay network by interacting with charged amino acid residues rather than being an integral constituent of the WOC (Olesen & Andréasson, 2003). In this model, releasing chloride from PSII disrupts the normal proton-relay network and retards the release of protons from the water-splitting reaction, which would block the WOC in the S_2 state. Thus, recent MIMS data clearly indicate that Cl^- has an effect on a slow phase of water exchange (Beckmann, 2008).

Bibliography

Akimoto S, Murakami A, Yokono M, Koyama K, Tsuchiya T, Miyashita H, Yamazaki I, Mimuro M (2006) Fluorescence properties of the chlorophyll *d*-dominated cyanobacterium *Acaryochloris* sp. strain Awaji. *J. Photochem. Photobiol. A* **178:** 122-129

Akiyama M, Miyashita H, Kise H, Watanabe T, Mimuro M, Miyachi S, Kobayashi M (2002) Quest for minor but key chlorophyll molecules in photosynthetic reaction centers - unusual pigment composition in the reaction centers of the chlorophyll *d*-dominated cyanobacterium *Acaryochloris marina*. *Photosynth. Res.* **74:** 97-107

Allakhverdiev SI, Yruela I, Picorel R, Klimov VV (1997) Bicarbonate is an essential constituent of the water-oxidizing complex of photosystem II. *Proc. Natl. Acad. Sci. USA* **94:** 5050-5054

Allen JF, Martin W (2007) Evolutionary biology - Out of thin air. *Nature* **445:** 610-612

Ananyev G, Nguyen T, Putnam-Evans C, Dismukes GC (2005) Mutagenesis of CP43-arginine-357 to serine reveals new evidence for (bi)carbonate functioning in the water oxidizing complex of Photosystem II. *Photochem. Photobiol. Sci.* **4:** 991-998

Ananyev G, Wydrzynski T, Renger G, Klimov V (1992) Transient Peroxide Formation by the Manganese-Containing, Redox-Active Donor Side of Photosystem-II upon Inhibition of O_2 Evolution with Lauroylcholine Chloride. *Biochim. Biophys. Acta* **1100:** 303-311

Ananyev GA, Sakiyan I, Diner BA, Dismukes GC (2002) A functional role for tyrosine-D in assembly of the inorganic core of the water oxidase complex of photosystem II and the kinetics of water oxidation. *Biochemistry* **41:** 974-980

Ananyev GM, Dismukes GC (1996) Assembly of the tetra-Mn site of photosynthetic water oxidation by photoactivation: Mn stoichiometry and detection of a new intermediate. *Biochemistry* **35:** 4102-4109

Ananyev GM, Shafiev MA, Klimov VV (1988) Flash-Induced Photoactivation of Oxygen Evolution by PSII Particles Deficient in Water-Soluble Proteins. *Biofizika* **33:** 594-599

Anderson JH (1964) Copper-Catalysed Oxidation of Hydroxylamine. *Analyst* **89:** 357-362

Atkins PW, de Paula J (2006) *Physical Chemistry*, Ed 8th. Oxford University Press, Oxford

Baldwin MJ, Stemmler TL, Riggs-Gelasco PJ, Kirk ML, Penner-Hahn JE, Pecoraro VL (1994) Structural and magnetic effects of successive protonations of oxo bridges in high-valent manganese dimers. *J. Am. Chem. Soc.* **116:** 11349-11356

Baranov SV, Ananyev GM, Klimov VV, Dismukes GC (2000) Bicarbonate accelerates assembly of the inorganic core of the water-oxidizing complex in manganese depleted photosystem II: a proposed biogeochemical role for atmospheric carbon dioxide in oxygenic photosynthesis. *Biochemistry* **39:** 6060 -6065

Baranov SV, Tyryshkin AM, Katz D, Dismukes GC, Ananyev GM, Klimov VV (2004) Bicarbonate is a native cofactor for assembly of the manganese cluster of the photosynthetic water oxidizing complex. Kinetics of reconstitution of O_2 evolution by photoactivation. *Biochemistry* **43:** 2070-2079

Barber J (2004) Water, water everywhere, and its remarkable chemistry. *Biochim. Biophys. Acta* **1655:** 123-132

Barber J (2006) Photosystem II: an enzyme of global significance. *Biochem. Soc. Trans.* **34:** 619-631

Barry BA, Hicks C, De Riso A, Jenson DL (2005) Calcium ligation in photosystem II under inhibiting conditions. *Biophys. J.* **89:** 393-401

Beck WF, Brudvig GW (1987) Reactions of Hydroxylamine with the Electron-Donor Side of Photosystem II. *Biochemistry* **26:** 8285-8295

Beckmann K (2008) *Membrane-Intel Mass Spectrometry Studies of Natural and Artificial Photosynthesis.* Ph.D. TU Berlin, Berlin

Bekker A, Holland HD, Wang PL, Rumble D, Stein HJ, Hannah JL, Coetzee LL, Beukes NJ (2004) Dating the rise of atmospheric oxygen. *Nature* **427:** 117-120

Bergmann U, Grush MM, Horne CR, DeMarois P, Penner-Hahn JE, Yocum CF, Wright DW, Dubé CE, Armstrong WH, Christou G, Eppley HJ, Cramer SP (1998) Characterization of the Mn oxidation states in photosystem II by Kβ X-ray fluorescence spectroscopy. *J. Phys. Chem. B* **102:** 8350-8352

Bernat G, Morvaridi F, Feyziyev Y, Styring S (2002) pH dependence of the four individual transitions in the catalytic S-cycle during photosynthetic oxygen evolution. *Biochemistry* **41:** 5830-5843

Berry EA, Guergova-Kuras M, Huang LS, Crofts AR (2000) Structure and function of cytochrome bc complexes. *Annu. Rev. Biochem.* **69:** 1005-1075

Berthold DA, Babcock GT, Yocum CF (1981) A highly resolved, oxygen-evolving photosystem II preparation from spinach thylakoid membranes. *FEBS Lett.* **134:** 231-234

Blankenship RE (1992) Origin and Early Evolution of Photosynthesis. *Photosynth. Res.* **33:** 91-111

Blankenship RE (2001) Molecular evidence for the evolution of photosynthesis. *Trends Plant Sci.* **6:** 4-6

Blankenship RE, Hartman H (1998) The origin and evolution of oxygenic photosynthesis. *Trends Biochem. Sci.* **23:** 94-97

Blankenship RE, Madigan MT, Bauer CE, eds (1995) *Anoxygenic Photosynthetic Bacteria*, Vol 2. Kluwer Academic Publishers, Dordrecht

Blankenship RE, Sauer K (1974) Manganese in Photosynthetic Oxygen Evolution. 1. Electron-Paramagnetic Resonance Study of Environment of Manganese in Tris-Washed Chloroplasts. *Biochim. Biophys. Acta* **357:** 252-266

Blubaugh DJ, Govindjee (1988) Kinetics of the Bicarbonate Effect and the Number of Bicarbonate-Binding Sites in Thylakoid Membranes. *Biochim. Biophys. Acta* **936:** 208-214

Bock CH, Gerken S, Stehlik D, Witt HT (1988) Time resolved EPR on photosystem II particles after irreversible and reversible inhibition of water cleavage with high concentrations of acetate. *FEBS Lett.* **227:** 141-146

Boichenko VA, Klimov VV, Miyashita H, Miyachi S (2000) Functional characteristics of chlorophyll *d*-predominating photosynthetic apparatus in intact cells of *Acaryochloris marina*. *Photosynth. Res.* **65:** 269-277

Borda MJ, Elsetinow AR, Schoonen MA, Strongin DR (2001) Pyrite-induced hydrogen peroxide formation as a driving force in the evolution of photosynthetic organisms on an early Earth. *Astrobiology* **1:** 283-288

Bouges B (1971) Action de faibles concentrations d'hydroxylamine sur l'emission d'oxygene des algues chlorella et des chloroplastes d'epinards. *Biochim. Biophys. Acta* **936:** 228-235

Boussac A, Rutherford AW (1994) The oxygen-evolving enzyme: effects of calcium and chloride ions. *Biochem. Soc. Trans.* **22:** 352-358

Boussac A, Zimmermann J-L, Rutherford AW (1989) EPR signals from modified charge accumulation states of the oxygen evolving enzyme in Ca^{2+}-deficient photosystem II. *Biochemistry* **28:** 8984-8989

Bricker TM, Frankel LK (2002) The structure and function of CP47 and CP43 in Photosystem II. *Photosynth. Res.* **72:** 131-146

Britt RD, Peloquin JM, Campbell KA (2000) Pulsed and parallel-polarization EPR characterization of the photosystem II oxygen evolving complex. *Annu. Rev. Biophys. Biomol. Struct.* **29:** 463-495

Burke DH, Hearst JE, Sidow A (1993) Early Evolution of Photosynthesis - Clues from Nitrogenase and Chlorophyll Iron Proteins. *Proc. Natl. Acad. Sci. USA* **90:** 7134-7138

Butler JH, Gordon LI (1986) Rates of Nitrous-Oxide Production in the Oxidation of Hydroxylamine by Iron(III). *Inorg. Chem.* **25:** 4573-4577

Carroll JJ, Slupsky JD, Mather AE (1991) The Solubility of Carbon-Dioxide in Water at Low-Pressure. *J. Phys. Chem. Ref. Data* **20:** 1201-1209

Cavalier-Smith T, Brasier M, Embley TM (2006) Introduction: how and when did microbes change the world? *Philos. Trans. R. Soc. London B* **361:** 845-850

Chen M, Bibby TS, Nield J, Larkum AWD, Barber J (2005) Structure of a large photosystem II supercomplex from *Acaryochloris marina*. *FEBS Lett.* **579:** 1306-1310

Chen M, Quinnell RG, Larkum AWD (2002) The major light-harvesting pigment protein of *Acaryochloris marina*. *FEBS Lett.* **514:** 149-152

Cheniae GM, Martin IF (1971) Effects of Hydroxylamine on Photosystem II. 1. Factors Affecting Decay of O_2 Evolution. *Plant Physiol.* **47:** 568-575

Cheniae GM, Martin IF (1972) Effects of Hydroxylamine on Photosystem II. 2. Photoreversal of NH_2OH Destruction of O_2 Evolution. *Plant Physiol.* **50:** 87-94

Cheniae GM, Martin IF (1978) Studies on Mechanism of Tris-Induced Inactivation of Oxygen Evolution. *Biochim. Biophys. Acta* **502:** 321-344

Christen G, Renger G (1999) The role of hydrogen bonds for the multiphasic $P680^{+\bullet}$ reduction by Y_Z in photosystem II with intact oxygen evolution capacity. Analysis of kinetic H/D isotope exchange effects. *Biochemistry* **38:** 2068-2077

Chu HA, Hillier W, Debus RJ (2004) Evidence that the C-terminus of the D1 polypeptide of photosystem II is ligated to the manganese ion that undergoes oxidation during the S_1 to S_2 transition: An isotope-edited FTIR study. *Biochemistry* **43:** 3152-3166

Cinco RM, McFarlane Holman KL, Robblee JH, Yano J, Pizarro SA, Bellacchio E, Sauer K, Yachandra VK (2002) Calcium EXAFS establishes the Mn-Ca cluster in the oxygen evolving complex of photosystem II. *Biochemistry* **41:** 12928-12933

Cinco RM, Robblee JH, Messinger J, Fernandez C, Holman KLM, Sauer K, Yachandra VK (2004) Orientation of calcium in the Mn_4Ca cluster of the oxygen-evolving complex determined using polarized strontium EXAFS of photosystem II membranes. *Biochemistry* **43:** 13271-13282

Clausen J, Beckmann K, Junge W, Messinger J (2005) Evidence that bicarbonate is not the substrate in photosynthetic oxygen evolution. *Plant Physiol.* **139:** 1444-1450

Clemens KL, Force DA, Britt RD (2002) Acetate binding at the photosystem II oxygen evolving complex: An S_2 state multiline signal ESEEM study. *J. Am. Chem. Soc.* **124:** 10921-10933

Crovetto R (1991) Evaluation of Solubility Data of the System CO_2-H_2O from 273-K to the Critical-Point of Water. *J. Phys. Chem. Ref. Data* **20:** 575-589

Dasgupta J, Tyryshkin AM, Dismukes GC (2007) ESEEM spectroscopy reveals carbonate and an N-donor protein-ligand binding to Mn^{2+} in the photoassembly reaction of the Mn_4Ca cluster in photosystem II. *Angew. Chem. Int. Ed.* **46:** 8028-8031

Dau H, Liebisch P, Haumann M (2003) X-ray absorption spectroscopy to analyze nuclear geometry and electronic structure of biological metal centers - Potential and questions

examined with special focus on the tetra-nuclear manganese complex of oxygenic photosynthesis. *Anal. Bioanal. Chem.* **376:** 562-583

de Wijn R, van Gorkom HJ (2002) S-state dependence of the miss probability in photosystem II. *Photosynth. Res.* **72:** 217-222

Debus R (2005) The catalytic manganese cluster: protein ligation. *In* T Wydrzynski, K Satoh, eds, Photosystem II. The Light Driven Water:Plastiquinone Oxidoreductase, Vol 22. Springer, Dordrecht, pp 261-284

Debus RJ (1992) The manganese and calcium ions of photosynthetic oxygen evolution. *Biochim. Biophys. Acta* **1102:** 269-352

Debus RJ (2001) Amino acid residues that modulate the properties of tyrosine Y_Z and the manganese cluster in the water oxidizing complex of photosystem II. *Biochim. Biophys. Acta* **1503:** 164-186

Debus RJ, Barry BA, Sithole I, Babcock GT, Mcintosh L (1988) Directed mutagenesis indicates that the donor to $P680^+$ in photosystem II is tyrosine-161 of the D1 polypeptide. *Biochemistry* **27:** 9071-9074

Debus RJ, Strickler MA, Walker LM, Hillier W (2005) No evidence from FTIR difference spectroscopy that aspartate-170 of the D1 polypeptide ligates a manganese ion that undergoes oxidation during the S_0 to S_1, S_1 to S_2, or S_2 to S_3 transitions in photosystem II. *Biochemistry* **44:** 1367-1374

Deisenhofer J, Michel H (1989) The Photosynthetic Reaction Center from the Purple Bacterium *Rhodopseudomonas viridis*. *Science* **245:** 1463-1473

Deligiannakis Y, Louloudi M, Hadjiliadis N (2000) Electron spin echo envelope modulation (ESEEM) spectroscopy as a tool to investigate the coordination environment of metal centers. *Coord. Chem. Rev.* **204:** 1-112

Deligiannakis Y, Petrouleas V, Diner BA (1994) Binding of carboxylate anions at the non-heme Fe(II) of PS II. 1. Effects on the Q_A-Fe^{2+} and Q_AFe^{3+} EPR spectra and the redox properties of the iron. *Biochim. Biophys. Acta* **1188:** 260-270

DeRose VJ, Latimer MJ, Zimmermann J-L, Mukerji I, Yachandra VK, Sauer K, Klein MP (1995) Fluoride substitution in the Mn cluster from Photosystem II: EPR and X-ray absorption studies. *Chem. Phys.* **194:** 443-459

DeRose VJ, Mukerji I, Latimer MJ, Yachandra VK, Sauer K, Klein MP (1994) Comparison of the manganese oxygen-evolving complex in photosystem II of spinach and *Synechococcus* sp. with multinuclear manganese model compounds by X-ray absorption spectroscopy. *J. Am. Chem. Soc.* **116:** 5239-5249

Diamond LW, Akinfiev NN (2003) Solubility of CO_2 in water from -1.5 to 100 °C and from 0.1 to 100 MPa: evaluation of literature data and thermodynamic modelling. *Fluid Phase Equilib.* **208:** 265-290

Diner BA (1977) Dependence of deactivation reactions of photosystem II on redox state of plastoquinone pool A varied under anaerobic conditions. Equilibria on the acceptor side of photosystem II. *Biochim. Biophys. Acta* **460:** 247-258

Diner BA (2001) Amino acid residues involved in the coordination and assembly of the manganese cluster of photosystem II. Proton-coupled electron transport of the redox active tyrosines and its relationship to water oxidation. *Biochim. Biophys. Acta* **1503:** 147-163

Diner BA, Petrouleas V (1990) Formation by NO of nitrosyl adducts of redox components of the photosystem II reaction center. 2. Evidence that HCO_3^-/CO_2 binds to the acceptor-side non-heme iron. *Biochim. Biophys. Acta* **1015:** 141-149

Diner BA, Rappaport F (2002) Structure, dynamics, and energetics of the primary photochemistry of photosystem II of oxygenic photosynthesis. *Annu. Rev. Plant Biol.* **53:** 551-580

Dismukes C, Ananyev GM, Watt R (2005) Photo-assembly of the catalytic manganese cluster. *In* T Wydrzynski, K Satoh, eds, Photosystem II. The Light-Driven Water:Plastoquinone Oxidoredutase, Vol 22. Springer, Dordrecht, pp 609-626

Dismukes GC, Klimov VV, Baranov SV, Kozlov YN, DasGupta J, Tyryshkin A (2001) The origin of atmospheric oxygen on earth: The innovation of oxygenic photosynthesis. *Proc. Natl. Acad. Sci. USA* **98:** 2170-2175

Dorlet P, Boussac A, Rutherford AW, Un S (1999) Multifrequency high-field EPR study of the interaction between the tyrosyl Z radical and the manganese cluster in plant photosystem II. *J. Phys. Chem. B* **103:** 10945-10954

Dorlet P, Di Valentin M, Babcock GT, McCracken JL (1998) Interaction of $Y_Z^{\bullet}$ with its environment in acetate-treated photosystem II membranes and reaction center cores. *J. Phys. Chem. B* **102:** 8239-8247

Faller P, Debus RJ, Brettel K, Sugiura M, Rutherford AW, Boussac A (2001) Rapid formation of the stable tyrosyl radical in photosystem II. *Proc. Natl. Acad. Sci. USA* **98:** 14368-14373

Feher G, Allen JP, Okamura MY, Rees DC (1989) Structure and Function of Bacterial Photosynthetic Reaction Centers. *Nature* **339:** 111-116

Fernandez C, Cinco RM, Robblee JH, Messinger J, Pizarro SA, Sauer K, Yachandra VK, Klein MP (1998) Calcium and chloride cofactors of the oxygen evolving complex: X-ray absorption spectroscopy evidence for a Mn/Ca/Cl heteronuclear cluster. *In* G Garab, ed, Photosynthesis: Mechanisms and Effects. Kluwer Academic Publishers, Dordrecht, pp 1399-1402

Ferreira KN, Iverson TM, Maghlaoui K, Barber J, Iwata S (2004) Architecture of the photosynthetic oxygen-evolving center. *Science* **303:** 1831-1838

Feyziev YM, Yoneda D, Yoshii T, Katsuta N, Kawamori A, Watanabe Y (2000) Formate-induced inhibition of the water-oxidizing complex of photosystem II studied by EPR. *Biochemistry* **39:** 3848-3855

Forbush B, Kok B, McGloin MP (1971) Cooperation of charges in photosynthetic oxygen evolution. II. Damping of flash yield oscillation, deactivation. *Photochem. Photobiol.* **14:** 307-321

Force DA, Randall DW, Britt RD (1997) Proximity of acetate, manganese, and exchangeable deuterons to tyrosine $Y_Z^{\bullet}$ in acetate-inhibited photosystem II membranes: Implications for the direct involvement of $Y_Z^{\bullet}$ in water-splitting. *Biochemistry* **36:** 12062-12070

Frasch WD, Cheniae GM (1980) Flash Inactivation of Oxygen Evolution - Identification of S_2 as the Target of Inactivation by Tris. *Plant Physiol.* **65:** 735-745

Ghanotakis DF, Babcock GT, Yocum CF (1984) Calcium reconstitutes high rates of oxygen evolution in polypeptide depleted Photosystem II preparations. *FEBS Lett.* **167:** 127-130

Gleiter HM, Haag E, Shen J-R, Eaton-Rye JJ, Seeliger AG, Inoue Y, Vermaas WFJ, Renger G (1995) Involvement of the CP47 protein in stabilization and photoactivation of a functional water oxidizing complex in the cyanobacterium *Synechocystis sp* PCC 6803. *Biochemistry* **34:** 6847-6856

Gleiter HM, Haag E, Shen JR, Eaton-Rye JJ, Inoue Y, Vermaas WFJ, Renger G (1994) Functional-Characterization of Mutant Strains of the Cyanobacterium *Synechocystis sp* PCC 6803 Lacking Short Domains within the Large, Lumen-Exposed Loop of the Chlorophyll-Protein CP47 in Photosystem II. *Biochemistry* **33:** 12063-12071

Golbeck JH, ed (2006) *Photosystem I. The Light-Driven Plastocyanin:Ferredoxin Oxidoreductase*, Vol 24. Springer, Dordrecht

Good NE, Winget GD, Winter W, Connolly TN, Izawa S, Singh RMM (1966) Hydrogen ion buffers for biological research. *Biochemistry* **5:** 467-477

Goodin DB, Yachandra VK, Britt RD, Sauer K, Klein MP (1984) The state of manganese in the photosynthetic apparatus. 3. Light-induced changes in x-ray absorption (K-edge) energies of manganese in photosynthetic membranes. *Biochim. Biophys. Acta* **767:** 209-216

Govindjee, Pulles MPJ, Govindjee R, Vangorkom HJ, Duysens LNM (1976) Inhibition of Reoxidation of Secondary-Electron Acceptor of Photosystem II by Bicarbonate Depletion. B*iochim. Biophys. Acta* **449:** 602-605

Govindjee, Weger HG, Turpin DH, van Rensen JJS, Devos OJ, Snel JFH (1991) Formate releases carbon dioxide/bicarbonate from thylakoid membranes - measurements by mass spectroscopy and infrared gas analyzer. *Naturwissenschaften* **78:** 168-170

Govindjee, Xu C, van Rensen JJS (1997) On the requirement of bound bicarbonate for photosystem II activity. *Z. Naturforsch.* **52:** 24-32

Grabolle M, Haumann M, Müller C, Liebisch P, Dau H (2006) Rapid loss of structural motifs in the manganese complex of oxygenic photosynthesis by x-ray irradiation at 10-300 K. *J. Biolog. Chem.* **281:** 4580-4588

Gregor WG, Cinco RM, Yu H, Yachandra VK, Britt RD (2005) Influence of the 33 kDa manganese-stabilizing protein on the structure and substrate accessibility of the oxygen-evolving complex of photosystem II. *Biochemistry* **44:** 8817-8825

Haddy A, Hatchell JA, Kimel RA, Thomas R (1999) Azide as a competitor of chloride in oxygen evolution by photosystem II. *Biochemistry* **38:** 6104-6110

Haddy A, Kimel RA, Thomas R (2000) Effects of azide on the S_2 state EPR signals from Photosystem II. *Photosynth. Res.* **63:** 35-45

Hasegawa K, Kimura Y, Ono T (2004) Oxidation of the Mn cluster induces structural changes of NO_3^- functionally bound to the Cl^- site in the oxygen-evolving complex of photosystem II. *Biophys. J.* **86:** 1042-1050

Hasegawa K, Kimura Y, Ono TA (2002) Chloride cofactor in the photosynthetic oxygen-evolving complex studied by Fourier transform infrared spectroscopy. *Biochemistry* **41:** 13839-13850

Haumann M, Barra M, Loja P, Loscher S, Krivanek R, Grundmeier A, Andreasson LE, Dau H (2006) Bromide does not bind to the Mn_4Ca complex in its S_1 state in Cl^--depleted and Br^--reconstituted oxygen-evolving photosystem II: Evidence from X-ray absorption spectroscopy at the Br K-edge. *Biochemistry* **45:** 13101-13107

Haumann M, Liebisch P, Müller C, Barra M, Grabolle M, Dau H (2005a) Photosynthetic O_2 formation tracked by time-resolved X-ray experiments. *Science* **310:** 1019-1021

Haumann M, Müller C, Liebisch P, Iuzzolino L, Dittmer J, Grabolle M, Neisius T, Meyer-Klaucke W, Dau H (2005b) Structural and oxidation state changes of the photosystem II manganese complex in four transitions of the water oxidation cycle ($S_0 \rightarrow S_1$, $S_1 \rightarrow S_2$, $S_2 \rightarrow S_3$, and S_3, $S_4 \rightarrow S_0$) characterized by X-ray absorption spectroscopy at 20 K and room temperature. *Biochemistry* **44:** 1894-1908

Hendry G, Wydrzynski T (2003) ^{18}O isotope exchange measurements reveal that calcium is involved in the binding of one substrate-water molecule to the oxygen-evolving complex in photosystem II. *Biochemistry* **42:** 6209-6217

Hill R, Bendall F (1960) Function of the 2 Cytochrome Components in Chloroplasts - Working Hypothesis. *Nature* **186:** 136-137

Hillier W, McConnell I, Badger MR, Boussac A, Klimov VV, Dismukes GC, Wydrzynski T (2006) Quantitative assessment of intrinsic carbonic anhydrase activity and the capacity for bicarbonate oxidation in photosystem II. *Biochemistry* **45:** 2094-2102

Hillier W, Messinger J (2005) Mechanism of photosynthetic oxygen production. *In* T Wydrzynski, K Satoh, eds, Photosystem II. The Light-Driven Water:Plastoquinone Oxidoredutase, Vol 22. Springer, Dordrecht, pp 567-608

Homann PH (1988) The chloride and calcium requirement of photosynthetic water oxidation: effects of pH. *Biochim. Biophys. Acta* **934:** 1-13

Homann PH (2002) Chloride and calcium in Photosystem II: from effects to enigma. *Photosynth. Res.* **73:** 169-175

Hu Q, Miyashita H, Iwasaki I, Kurano N, Miyachi S, Iwaki M, Itoh S (1998) A photosystem I reaction center driven by chlorophyll *d* in oxygenic photosynthesis. *Proc. Natl. Acad. Sci. USA* **95:** 13319-13323

Ioannidis N, Sarrou J, Schansker G, Petrouleas V (1998) NO reversibly reduces the water oxidizing complex of photosystem II through S_0 and S_1 to the state characterized by the Mn(II)-Mn(III) multiline EPR signal. *Biochemistry* **37:** 16445-16451

Isgandarova S (2004) *Untersuchungen zum Mechanismus der photosynthetischen Wasseroxidation im thermophilen Cyanobakterium Thermosynechococcus elongatus und Spinat.* Ph.D. TU Berlin, Berlin

Isgandarova S, Renger G, Messinger J (2003) Functional differences of photosystem II from *Synechococcus elongatus* and spinach characterized by flash-induced oxygen evolution patterns. *Biochemistry* **42:** 8929-8938

Itoh S, Fukushima Y, Tomi T, Shigenaga T, Mino H (2004) Photosystem II of A*caryochloris marina* that uses Chl *d*. *Plant Cell Physiol.* **45:** S14-S14

Itoh S, Iwaki M, Noguchi T, Kawamori A, Mino Q, Hu Q, Iwasaki I, Miyashita H, Kurano N, Miyachi S, Shen R (2001) Photosystem I and II reaction centers of a new oxygenic organism Acaryochloris marina that use chlorophyll d. *In* Proceedings of the 12th International Congress on Photosynthesis. CSIRO Publishing, Collingwood, Australia, pp S6-028

Iuzzolino L, Dittmer J, Dörner W, Meyer-Klaucke W, Dau H (1998) X-ray absorption spectroscopy on layered photosystem II membrane particles suggests manganese centered oxidation of the oxygen evolving complex for the S_0-S_1, S_1-S_2, and S_2-S_3 transitions of the water oxidation cycle. *Biochemistry* **37:** 17112-17119

Jajoo A, Bharti S, Kawamori A (2005) EPR characteristics of chloride-depleted photosystem II membranes in the presence of other anions. *Photochem. Photobiol. Sci.* **4:** 459-462

Jajoo A, Katsuta N, Kawamori A (2006) An EPR study of the pH dependence of formate effects on Photosystem II. *Plant Physiol. Biochem.* **44:** 186-192

Joliot P (1972) Modulated light source use with the oxygen electrode. *In* A San Pietro, ed, Photosynthesis and Nitrogen Fixation, Vol 24 B. Academic Press, New York, pp 123-134

Joliot P, Barbieri G, Chabaud R (1969) Un nouveau modele des centres photochimiques du systeme II. *Photochem. Photobiol.* **10:** 309-329

Jursinic P (1981) Investigation of double turnovers in photosystem II charge separation and oxygen evolution with excitation flashes of different duration. *Biochim. Biophys. Acta* **635:** 38-52

Jursinic PA, Stemler A (1984) Effects of bicarbonate depletion on secondary acceptors of photosystem II. *Biochim. Biophys. Acta* **764:** 170-178

Kaltashov IA, Eyles SJ (2005) *Mass Spectrometry in Biophysics. Conformation and Dynamics of Biomolecules.* John Wiley & Sons, Inc., Hoboken

Katoh S (1972) Inhibitors of Electron-Transport Associated with Photosystem II in Chloroplasts. *Plant Cell Physiol.* **13:** 273-286

Kawamoto K, Mano J, Asada K (1995) Photoproduction of the Azidyl Radical from the Azide Anion on the Oxidizing Side of Photosystem II and Suppression of Photooxidation of Tyrosine-Z by the Azidyl Radical. *Plant Cell Physiol.* **36:** 1121-1129

Kebekus U, Messinger J, Renger G (1995) Structural changes in the water oxidizing complex monitored via the pH dependence of the reduction rate of redox state S_1 by hydrazine and hydroxylamine in isolated spinach thylakoids. *Biochemistry* **34:** 6175-6182

Keller MD, Selvin RC, Claus W, Guillard RRL (1987) Media for the culture of oceanic ultraphytoplankton. *J. Phycol.* **23:** 633-638

Kelley PM, Izawa S (1978) The role of chloride ion in Photosystem II: effects of chloride ion on Photosystem II electron transport and hydroxylamine inhibition. *Biochim. Biophys. Acta* **502:** 198-210

Kern J (2005) *Structural and functional investigations of photosystem II from Thermosynechococcus elongatus.* Ph.D. TU Berlin, Berlin

Kimura Y, Mizusawa N, Ishii A, Ono T (2005a) FTIR detection of structural changes in a histidine ligand during S-state cycling of photosynthetic oxygen-evolving complex. *Biochemistry* **44:** 16072-16078

Kimura Y, Yamanari T, Ishii A, Ono T (2005b) FTIR detection of water-sensitive low-frequency vibrational modes during photosynthetic water oxidation in photosystem II. *Plant Cell Physiol.* **46:** S26-S26

Kimura Y, Hasegawa K, Yamanari T, Ono T (2005c) Studies on photosynthetic oxygen-evolving complex by means of Fourier transform infrared spectroscopy: calcium and chloride cofactors. *Photosynth. Res.* **84:** 245-250

Klimov VV, Allakhverdiev SI, Shuvalov VA, Krasnovsky AA (1982) Effect of Extraction and Re-Addition of Manganese on Light Reactions of Photosystem II Preparations. *FEBS Lett.* **148:** 307-312

Klimov VV, Baranov SV (2001) Bicarbonate requirement for the water-oxidizing complex of photosystem II. *Biochim. Biophys. Acta* **1503:** 187-196

Klimov VV, Allakhverdiev SI, Baranov SV, Feyziev YM (1995a) Effects of bicarbonate and formate on the donor side of photosystem 2. *Photosynth. Res.* **46:** 219-225

Klimov VV, Allakhverdiev SI, Feyziev YM, Baranov SV (1995b) Bicarbonate requirement for the donor side of photosystem II. *FEBS Lett.* **363:** 251-255

Klimov VV, Hulsebosch RJ, Allakhverdiev SI, Wincencjusz H, van Gorkom HJ, Hoff AJ (1997a) Bicarbonate may be required for ligation of manganese in the oxygen-evolving complex of photosystem II. *Biochemistry* **36:** 16277-16281

Klimov VV, Baranov SV, Allakhverdiev SI (1997b) Bicarbonate protects the donor side of photosystem II against photoinhibition and thermoinactivation. *FEBS Lett.* **418:** 243-246

Klimov VV (2003) Discovery of pheophytin function in the photosynthetic energy conversion as the primary electron acceptor of Photosystem II. *Photosynth. Res.* **76:** 247-253

Kobayashi M, Ohashi S, Iwamoto K, Shiraiwa Y, Kato Y, Watanabe T (2007) Redox potential of chlorophyll *d* in vitro. *Biochim. Biophys. Acta* **1767:** 596-602

Kobayashi M, Watanabe S, Gotoh T, Koizumi H, Itoh Y, Akiyama M, Shiraiwa Y, Tsuchiya T, Miyashita H, Mimuro M, Yamashita T, Watanabe T (2005) Minor but key chlorophylls in photosystem II. *Photosynth. Res.* **84:** 201-207

Kok B, Forbush B, McGloin M (1970) Cooperation of charges in photosynthetic O_2 evolution. *Photochem. Photobiol.* **11:** 457-476

Kolasa T, Wardencki W (1974) Quantitative-Determination of Hydroxylamine. *Talanta* **21:** 845-857

Konermann L, Messinger J, Hillier W (2008) Mass spectrometry based methods for studying kinetics and dynamics in biological systems. *In* TJ Aartsma, J Matysik, eds, Biophysical Techniques in Photosynthesis (Volume II), Vol 26. Springer, Dordrecht, pp 167-190

Kozlov YN, Zharmukhamedov SK, Tikhonov KG, Dasgupta J, Kazakova AA, Dismukes GC, Klimov VV (2004) Oxidation potentials and electron donation to photosystem II of manganese complexes containing bicarbonate and carboxylate ligands. *Phys. Chem. Chem. Phys.* **6:** 4905-4911

Kretschmann H, Witt HT (1993) Chemical reduction of the water splitting enzyme system of photosynthesis and its light-induced reoxidation characterized by optical and mass spectrometric measurements: a basis for the estimation of the states of the redox active manganese and of water in the quaternary oxygen evolving S-state cycle. *Biochim. Biophys. Acta* **1144:** 331-345

Kühl M, Chen M, Ralph PJ, Schreiber U, Larkum AWD (2005) A niche for cyanobacteria containing chlorophyll *d*. *Nature* **433:** 820-820

Kühne H, Szalai VA, Brudvig GW (1999) Competitive binding of acetate and chloride in photosystem II. *Biochemistry* **38:** 6604-6613

Kulik LV, Epel B, Lubitz W, Messinger J (2005) ^{55}Mn pulse ENDOR at 34 GHz of the S_0 and S_2 states of the oxygen-evolving complex in photosystem II. *J. Am. Chem. Soc.* **127:** 2392-2393

Kulik LV, Epel B, Lubitz W, Messinger J (2007) Electronic structure of the Mn_4O_xCa cluster in the S_0 and S_2 states of the oxygen-evolving complex of photosystem II based on pulse ^{55}Mn-ENDOR and EPR Spectroscopy. *J. Am. Chem. Soc.* **129:** 13421-13435

Kuntzleman T, Yocum CF (2005) Reduction-induced inhibition and Mn(II) release from the photosystem II oxygen-evolving complex by hydroquinone or NH_2OH are consistent with a Mn(III)/Mn(III)/Mn(IV)/Mn(IV) oxidation state for the dark-adapted enzyme. *Biochemistry* **44:** 2129-2142

Kuzek D, Pace RJ (2001) Probing the Mn oxidation states in the OEC. Insights from spectroscopic, computational and kinetic data. *Biochim. Biophys. Acta* **1503:** 123-137

Lakshmi KV, Eaton SS, Eaton GR, Brudvig GW (1999) Orientation of the tetranuclear manganese cluster and tyrosine Z in the O_2-evolving complex of photosystem II: An EPR study of the $S_2Y_Z^{\bullet}$ state in oriented acetate-inhibited photosystem II membranes. *Biochemistry* **38:** 12758-12767

Larkum AWD, Kühl M (2005) Chlorophyll *d*: the puzzle resolved. *Trends Plant Sci.* **10:** 355-357

Latimer MJ, DeRose VJ, Mukerji I, Yachandra VK, Sauer K, Klein MP (1995) Evidence for the proximity of calcium to the manganese cluster of photosystem II: determination by x-ray absorption spectroscopy. *Biochemistry* **34:** 10898-10909

Liang W, Roelofs TA, Cinco RM, Rompel A, Latimer MJ, Yu WO, Sauer K, Klein MP, Yachandra VK (2000) Structural change of the Mn cluster during the S_2 to S_3 state transition of the oxygen evolving complex of photosystem II. Does it reflect the onset of water/substrate oxidation? Determination by Mn x-ray absorption spectroscopy. *J. Am. Chem. Soc.* **122:** 3399-3412

Lindberg K, Vänngård T, Andréasson L-E (1993) Studies of the slowly exchanging chloride in photosystem II of higher plants. *Photosynth. Res.* **38:** 401-408

Lindberg K, Andréasson L-E (1996) A one-site, two-state model for the binding of anions in photosystem II. *Biochemistry* **35:** 14259-14267

Lindberg K, Wydrzynski T, Vänngård T, Andréasson L-E (1990) Slow release of chloride from ^{36}Cl-labeled photosystem II membranes. *FEBS Lett.* **264:** 153-155

Loll B, Kern J, Saenger W, Zouni A, Biesiadka J (2005) Towards complete cofactor arrangement in the 3.0 Å resolution structure of photosystem II. *Nature* **438:** 1040-1044

Lubitz W (2006) EPR Studies of the Primary Electron Donor P700 in Photosystem I. *In* JH Golbeck, ed, Photosystem I. The Light-Driven Plastocyanin:Ferredoxin Oxidoreductase, Vol 24. Springer, Dordrecht, pp 245-269

Lydakis-Simantiris N, Dorlet P, Ghanotakis DF, Babcock GT (1998) Kinetic and spectroscopic properties of the $Y_Z^{\bullet}$ radical in Ca^{2+}- and Cl^{-}-depleted photosystem II preparations. *Biochemistry* **37:** 6427-6435

Martin W, Scheibe R, Schnarrenberger C (2000) The Calvin Cycle and Its Regulation. *In* RC Leegood, TD Shakey, S von Caemmerer, eds, Photosynthesis: Physiology and Metabolism, Vol 9. Kluwer Academic Publishers, Dordrecht, pp 9-51

McCarty RE, Evron Y, Johnson EA (2000) The chloroplast ATP synthase: A rotary enzyme? *Annu. Rev. Plant Physiol. Plant Mol. Biol.* **51:** 83-109

McLachlan (1973) Handbook of Phycological Methods: Culture Methods and Growth Measurements. *In* JR Stein, ed. University Press, Cambridge, pp 25-51

Mende D, Wiessner W (1985) Bicarbonate *in vivo* requirement of photosystem II in the green alga *Chlamydobotrys stellata*. *J. Plant Physiol.* **118:** 259-266

Messinger J (1993) *Untersuchungen über die reaktiven Eigenschaften der verschiedenen Redoxzustände der Wasseroxidase Höherer Pflanzen.* Ph.D. TU Berlin, Berlin

Messinger J (2000) Towards understanding the chemistry of photosynthetic oxygen evolution: dynamic structural changes, redox states and substrate water binding of the Mn cluster in photosystem II. *Biochim. Biophys. Acta* **1459:** 481-488

Messinger J (2004) Evaluation of different mechanistic proposals for water oxidation in photosynthesis on the basis of Mn_4O_xCa structures for the catalytic site and spectroscopic data. *Phys. Chem. Chem. Phys.* **6:** 4764 - 4771

Messinger J, Badger M, Wydrzynski T (1995) Detection of *one* slowly exchanging substrate water molecule in the S_3 state of photosystem II. *Proc. Natl. Acad. Sci. USA* **92:** 3209-3213

Messinger J, Renger G (1990) The reactivity of hydrazine with PS II strongly depends on the redox state of the water oxidizing system. *FEBS Lett.* **277:** 141 - 146

Messinger J, Renger G (1993) Generation, oxidation by the oxidized form of the tyrosine of polypeptide D2, and possible electronic configuration of the redox States S_0, S_{-1} and S_{-2} of the water oxidase in isolated spinach thylakoids. *Biochemistry* **32:** 9379-9386

Messinger J, Renger G (1994) Analysis of pH-induced modifications of the period four oscillation of the flash induced oxygen evolution reveal distinct structural changes of the photosystem II donor side at characteristic pH values. *Biochemistry* **33:** 10896-10905

Messinger J, Renger G (2008) Photosynthetic Water Splitting. *In* G Renger, ed, Primary Processes of Photosynthesis, Part 2 Principles and Apparatus, Vol 9. RSC Publishing, Cambridge, pp 291-351

Messinger J, Robblee JH, Bergmann U, Fernandez C, Glatzel P, Isgandarova S, Hanssum B, Renger G, Cramer SP, Sauer K, Yachandra VK, eds (2001a) Manganese oxidation states in photosystem II. CSIRO Publishing, Collingwood, Australia, pp S10-019

Messinger J, Robblee JH, Bergmann U, Fernandez C, Glatzel P, Visser H, Cinco RM, McFarlane KL, Bellacchio E, Pizarro SA, Cramer SP, Sauer K, Klein MP, Yachandra VK (2001b) Absence of Mn centered oxidation in the S_2 to S_3 transition: implications for the mechanism of photosynthetic water oxidation. *J. Am. Chem. Soc.* **123:** 7804-7820

Messinger J, Schröder WP, Renger G (1993) Structure-function relations in photosystem II. Effects of temperature and chaotropic agents on the period four oscillation of flash induced oxygen evolution. *Biochemistry* **32:** 7658-7668

Messinger J, Seaton G, Wydrzynski T, Wacker U, Renger G (1997a) S_{-3} state of the water oxidase in photosystem II. *Biochemistry* **36:** 6862-6873

Messinger J, Nugent JHA, Evans MCW (1997b) Detection of an EPR Multiline Signal for the S_0^* State in Photosystem II. *Biochemistry* **36:** 11055-11060

Messinger J, Robblee JH, Yu WO, Sauer K, Yachandra VK, Klein MP (1997c) The S_0 state of the oxygen evolving complex in photosystem II is paramagnetic: detection of an EPR multiline signal. *J. Am. Chem. Soc.* **119:** 11349-11350

Messinger J, Wacker U, Renger G (1991) Unusual low reactivity of the water oxidase in the redox state S_3 toward exogenous reductants. Analysis of the NH_2OH and NH_2NH_2 induced modifications of flash induced oxygen evolution in isolated spinach thylakoids. *Biochemistry* **30:** 7852-7862

Metzner H (1978) *Photosynthetic Oxygen Evolution.* Academic Press, London

Meyer TJ, Huynh MHV, Thorp HH (2007) The possible role of proton-coupled electron transfer (PCET) in water oxidation by photosystem II. *Angew. Chem. Int. Ed.* **46:** 5284-5304

Miller A-F, Brudvig GW (1991) A guide to electron paramagnetic resonance spectroscopy of Photosystem II membranes. *Biochim. Biophys. Acta* **1056:** 1-18

Miller SR, Augustine S, Le Olson T, Blankenship RE, Selker J, Wood AM (2005) Discovery of a free-living chlorophyll *d*-producing cyanobacterium with a hybrid proteobacterial/cyanobacterial small-subunit rRNA gene. *Proc. Natl. Acad. Sci. USA* **102:** 850-855

Mimuro M, Akimoto S, Gotoh T, Yokono M, Akiyama M, Tsuchiya T, Miyashita H, Kobayashi M, Yamazaki I (2004) Identification of the primary electron donor in PSII of the Chl *d*-dominated cyanobacterium *Acaryochloris marina*. *FEBS Lett.* **556:** 95-98

Mimuro M, Akimoto S, Yamazaki I, Miyashita H, Miyachi S (1999) Fluorescence properties of chlorophyll *d*-dominating prokaryotic alga, *Acaryochloris marina*: studies using time-resolved fluorescence spectroscopy on intact cells. *Biochim. Biophys. Acta* **1412:** 37-46

Miqyass M, van Gorkom HJ, Yocum CF (2007) The PSII calcium site revisited. *Photosynth. Res.* **92:** 275-287

Miyao M, Murata N (1984) Role of the 33-kDa polypeptide in preserving Mn in the photosynthetic oxygen-evolution system and its replacement by chloride ions. *FEBS Lett.* **170:** 350-354

Miyashita H, Adachi K, Kurano N, Ikemoto H, Chihara M, Miyachi S (1997) Pigment composition of a novel oxygenic photosynthetic prokaryote containing chlorophyll *d* as the major chlorophyll. *Plant Cell Physiol.* **38:** 274-281

Miyashita H, Ikemoto H, Kurano N, Adachi K, Chihara M, Miyachi S (1996) Chlorophyll *d* as a major pigment. *Nature* **383:** 402-402

Mojzsis SJ, Arrhenius G, McKeegan KD, Harrison TM, Nutman AP, Friend CRL (1996) Evidence for life on Earth before 3,800 million years ago. *Nature* **384:** 55-59

Mukerji I, Andrews JC, DeRose VJ, Latimer MJ, Yachandra VK, Sauer K, Klein MP (1994) Orientation of the oxygen-evolving manganese complex in a photosystem II membrane preparation: an X-ray absorption spectroscopy study. *Biochemistry* **33:** 9712-9721

Murakami A, Miyashita H, Iseki M, Adachi K, Mimuro M (2004) Chlorophyll *d* in an epiphytic cyanobacterium of red algae. *Science* **303:** 1633-1633

Nakamura A, Suzawa T, Kato Y, Watanabe T (2005) Significant species-dependence of P700 redox potential as verified by spectroelectrochemistry: Comparison of spinach and *Theromosynechococcus elongatus*. *FEBS Lett.* **579:** 2273-2276

Nelson N, Yocum CF (2006) Structure and function of photosystems I and II. *Annu. Rev. Plant Biol.* **57:** 521-565

Nieuwenburg P, Clarke RJ, Cai ZL, Chen M, Larkum AWD, Cabral NM, Ghiggino KP, Reimers JR (2003) Examination of the photophysical processes of chlorophyll *d* leading to a clarification of proposed uphill energy transfer processes in cells of *Acaryochloris marina*. *Photochem. Photobiol.* **77:** 628-637

Nisbet EG, Sleep NH (2001) The habitat and nature of early life. *Nature* **409:** 1083-1091

Nixon PJ, Barker M, Boehm M, de Vries R, Komenda J (2005) FtsH-mediated repair of the photosystem II complex in response to light stress. *J. Exp. Bot.* **56:** 357-363

Noguchi T (2007) Light-induced FTIR difference spectroscopy as a powerful tool toward understanding the molecular mechanism of photosynthetic oxygen evolution. *Photosynth. Res.* **91:** 59-69

Noguchi T, Sugiura M (2002) FTIR detection of water reactions during the flash-induced S-state cycle of the photosynthetic water oxidizing complex. *Biochemistry* **41:** 15706-15712

Nugent JHA, Ball RJ, Evans MCW (2004) Photosynthetic water oxidation: the role of tyrosine radicals. *Biochim. Biophys. Acta* **1655:** 217-221

Nugent JHA, Demetriou C, Lockett CJ (1987) Electron donation in photosystem II. *Biochim. Biophys. Acta* **894:** 534-542

Nugent JHA, Doetschman DC, Maclachlan DJ (1992) Characterization of the multiple EPR line shapes of iron semiquinones in photosystem 2. *Biochemistry* **31:** 2935-2941

Olesen K, Andréasson L-E (2003) The function of the chloride ion in photosynthetic oxygen evolution. *Biochemistry* **42:** 2025-2035

Olson JM (2001) 'Evolution of Photosynthesis' (1970), re-examined thirty years later. *Photosynth. Res.* **68:** 95-112

Olson JM (2006) Photosynthesis in the Archean Era. *Photosynth. Res.* **88:** 109-117

Olson JM, Blankenship RE (2004) Thinking about the evolution of photosynthesis. *Photosynth. Res.* **80:** 373-386

Ono T-A (2001) Metallo-radical hypothesis for photoassembly of Mn_4 cluster of photosynthetic oxygen evolving complex. *Biochim. Biophys. Acta* **1503:** 40-51

Ono T-A, Inoue Y (1983) Mn-preserving extraction of 33-, 24- and 16-kDa Proteins from O_2-evolving PS II particles by divalent salt-washing. *FEBS Lett.* **164:** 255-260

Ono T-A, Noguchi T, Inoue Y, Kusunoki M, Matsushita T, Oyanagi H (1992) X-ray detection of the period-four cycling of the manganese cluster in the photosynthetic water oxidizing enzyme. *Science* **258:** 1335-1337

Ono T-A, Zimmermann J-L, Inoue Y, Rutherford AW (1986) EPR evidence for a modified S-state transition in chloride depleted photosystem II. *Biochim. Biophys. Acta* **851:** 193-201

Ono TA, Nakayama H, Gleiter H, Inoue Y, Kawamori A (1987) Modification of the Properties of S_2 State in Photosynthetic O_2-Evolving Center by Replacement of Chloride with Other Anions. *Arch. Biochem. Biophys.* **256:** 618-624

Oparin IA (1965) The Origin of Life and the Origin of Enzymes. *In* FF Nord, ed, Advances in Enzymology and Related Areas of Molecular Biology, Vol 27. Interscience Publishers, New York, pp 347-380

Ort DR, Yocum CF, eds (1996) *Oxygenic Photosynthesis: The Light Reactions*, Ed Vol 4. Kluwer Academic Publishers, Dordrecht

Panja A, Shaikh N, Gupta S, Butcher RJ, Banerjee P (2003) New mononuclear manganese(III) complexes with hexadentate (N_4O_2) Schiff base ligands: Synthesis, crystal structures, electrochemistry, and electron-transfer reactivity towards hydroxylamine. *Eur. J. Inorg. Chem.***:** 1540-1547

Peloquin JM, Campbell KA, Randall DW, Evanchik MA, Pecoraro VL, Armstrong WH, Britt RD (2000) ^{55}Mn ENDOR of the S_2-State multiline EPR signal of photosystem II: implications on the structure of the tetranuclear Mn cluster. *J. Am. Chem. Soc.* **122:** 10926-10942

Petrasek Z, Schmitt F, Theiss C, Huyer J, Chen M, Larkum A, Eichler HJ, Kemnitz K, Eckert H (2005) Excitation energy transfer from phycobiliprotein to chlorophyll *d* in intact cells of *Acaryochloris marina* studied by time- and wavelength-resolved fluorescence spectroscopy. *Photochem. Photobiol. Sci.* **4:** 1016-1022

Petrouleas V, Crofts AR (2005) The Iron-Quinone Acceptor Complex *In* T Wydrzynski, K Satoh, eds, Photosystem II. The Light-Driven Water:Plastoquinone Oxidoreductase, Vol 22. Springer, Dordrecht, pp 177-206

Petrouleas V, Diner BA (1986) Identification of Q_{400}, a high potential electron acceptor of photosystem II, with the iron of the quinone-iron acceptor complex. *Biochim. Biophys. Acta* **849:** 264-275

Petrouleas V, Diner BA (1987) Light-induced oxidation of the acceptor side Fe^{II} of photosystem II by exogenous quinones acting through the Q_B binding site. 1. Quinones, kinetics and pH-dependence. *Biochim. Biophys. Acta* **893:** 126-137

Pobeguts OV, Smolova TN, Zastrizhnaya OM, Klimov VV (2007) Protective effect of bicarbonate against extraction of the extrinsic proteins of the water-oxidizing complex from Photosystem II membrane fragments. *Biochim. Biophys. Acta* **1767:** 624-632

Popelkova H, Yocum CF (2007) Current status of the role of Cl^- ion in the oxygen-evolving complex. *Photosynth. Res.* **93:** 111-121

Porra RJ, Thompson WA, Kriedemann PE (1989) Determination Of Accurate Extinction Coefficients and Simultaneous Equations For Assaying Chlorophyll-*a* and Chlorophyll-*b* Extracted With 4 Different Solvents - Verification Of the Concentration Of Chlorophyll Standards By Atomic Absorption Spectroscopy. *Biochim. Biophys. Acta* **975:** 384-394

Radmer R, Ollinger O (1980) Isotopic composition of photosynthetic O_2 flash yields in the presence of $H_2{}^{18}O$ and $HC^{18}O_3^-$. *FEBS Lett.* **110:** 57-61

Rappaport F, Blanchard-Desce M, Lavergne J (1994) Kinetics of electron transfer and electrochromic change during the redox transitions of the photosynthetic oxygen evolving complex. *Biochim. Biophys. Acta* **1184:** 178-192

Rappaport F, Guergova-Kuras M, Nixon PJ, Diner BA, Lavergne J (2002) Kinetics and pathways of charge recombination in photosystem II. Biochemistry **41:** 8518-8527

Raymond J, Blankenship RE (2008) The Origin of the Oxygen-evolving Complex. *Coord. Chem. Rev.* **252:** 377-383

Raymond J, Zhaxybayeva O, Gogarten JP, Blankenship RE (2003) Evolution of photosynthetic prokaryotes: a maximum-likelihood mapping approach. *Philos. Trans. R. Soc. London B* **358:** 223-230

Renger G (2008) Functional Pattern of Photosystem II. *In* G Renger, ed, Primary Processes of Photosynthesis, Part 2 Principles and Apparatus, Vol 9. RSCPublishing, Cambridge, pp 237-291

Renger G, Hanssum B (1988) Studies on the deconvolution of flash induced absorption changes into the difference spectra of individual redox steps within the water oxidizing enzyme system. *Photosynth. Res.* **16:** 243-259

Renger G, Holzwarth AR (2005) Primary electron transfer. *In* TJ Wydrzynski, K Satoh, eds, Photosystem II. The Light-Driven Water:Plastoquinone Oxidoreductase, Vol 22. Springer, Dordrecht, pp 139-175

Renger G, Kuhn P (2007) Reaction pattern and mechanism of light induced oxidative water splitting in photosynthesis. *Biochim. Biophys. Acta* **1767:** 458-471

Rickert KW, Sears J, Beck WF, Brudvig GW (1991) Mechanism of Irreversible Inhibition of O_2 Evolution in Photosystem II by Tris(Hydroxymethyl)Aminomethane. *Biochemistry* **30:** 7888-7894

Riggs-Gelasco PJ, Mei R, Ghanotakis DF, Yocum CF, Penner-Hahn JE (1996) X-ray absorption spectroscopy of calcium substituted derivatives of the oxygen evolving complex of photosystem II. *J. Am. Chem. Soc.* **118:** 2400-2410

Ritchie RJ (2006) Consistent sets of spectrophotometric chlorophyll equations for acetone, methanol and ethanol solvents. *Photosynth. Res.* **89:** 27-41

Robblee JH, Cinco RM, Yachandra VK (2001) X-ray spectroscopy based structure of the Mn cluster and mechanism of photosynthetic oxygen evolution. *Biochim. Biophys. Acta* **1503:** 7-23

Robblee JH, Messinger J, Cinco RM, McFarlane KL, Fernandez C, Pizarro SA, Sauer K, Yachandra VK (2002) The Mn cluster in the S_0 State of the oxygen evolving complex of photosystem II studied by EXAFS spectroscopy: are there three di-μ-oxo-bridged Mn_2 moieties in the tetranuclear Mn complex? *J. Am. Chem. Soc.* **124:** 7459-7471

Robinson HH, Sharpa RR, Yocum CF (1980) Effect of Manganese on the Nuclear Magnetic Relaxivity of Water Protons in Chloroplast Suspensions. *Biochem. Biophys. Res. Commun.* **93:** 755-761

Robinson HH, Yocum CF (1980) Cyclic Photophosphorylation Reactions Catalyzed by Ferredoxin, Methyl Viologen and Anthraquinone Sulfonate - Use of Photochemical-Reactions to Optimize Redox Poising. *Biochim. Biophys. Acta* **590:** 97-106

Roelofs TA, Liang W, Latimer MJ, Cinco RM, Rompel A, Andrews JC, Sauer K, Yachandra VK, Klein MP (1996) Oxidation states of the manganese cluster during the flash-induced S-state cycle of the photosynthetic oxygen evolving complex. *Proc. Natl. Acad. Sci. USA* **93:** 3335-3340

Roose JL, Wegener KM, Pakrasi HB (2007) The extrinsic proteins of photosystem II. *Photosynth. Res.* **92:** 369-387

Rutherford AW, Inoue Y (1984) Oscillation of delayed luminescence from PS II: recombination of $S_2Q_B^-$ and $S_3Q_B^-$. *FEBS Lett.* **165:** 163-170

Rutherford AW, Nitschke W (1996) Photosystem II and the Quinone-Iron-Containing Reaction Centers: Comparison and Evolutionary Perspectives. *In* H Batscheffky, ed, Origin and Evolution of Biological Energy Conversion. VCH, New York, pp 143-174

Salem IA (1995) A Kinetic-Study of the Homogeneous Oxidation of Hydroxylamine by Manganese(III)-Bis(Salicylaldimine) Complexes. *Transition Met. Chem.* **20:** 312-315

Sandusky PO, Yocum CF (1983) The Mechanism of Amine Inhibition of the Photosynthetic Oxygen Evolving Complex - Amines Displace Functional Chloride from a Ligand Site on Manganese. *FEBS Lett.* **162:** 339-343

Sandusky PO, Yocum CF (1984) The chloride requirement for photosynthetic oxygen evolution: analysis of the effects of chloride and other anions on amine inhibition of the oxygen evolving complex. *Biochim. Biophys. Acta* **766:** 603-611

Sarrou J, Isgandarova S, Kern J, Zouni A, Renger G, Lubitz W, Messinger J (2003) Nitric oxide induced formation of the S_{-2} state in the oxygen evolving complex of photosystem II from *Synechococcus elongatus*. *Biochemistry* **42:** 1016-1023

Saygin Ö, Gerken S, Meyer B, Witt HT (1986) Total recovery of O_2 evolution and nanosecond reduction kinetics of chlorophyll$_a$II$^+$ (P680$^+$) after Inhibition of water cleavage with acetate. *Photosynth. Res.* **9:** 71-78

Schansker G, Goussias C, Petrouleas V, Rutherford AW (2002) Reduction of the Mn cluster of the water oxidizing enzyme by nitric oxide: formation of an S_{-2} State. *Biochemistry* **41:** 3057-3064

Schiller H, Senger H, Miyashita H, Miyachi S, Dau H (1997) Light-harvesting in *Acaryochloris marina* - Spectroscopic characterization of a chlorophyll *d*-dominated photosynthetic antenna system. *FEBS Lett.* **410:** 433-436

Schlodder E, Cetin M, Eckert H, Schmitt F, Barber J, Telfer A (2007) Both chlorophylls *a* and *d* are essential for the photochemistry in photosystem II of the cyanobacteria, *Acaryochloris marina*. *Biochim. Biophys. Acta* **1767:** 589-595

Seeliger AG, Kurreck J, Renger G (1997) Kinetics of S_2 and S_3 Reduction by Tyrosine Y_D and Other Endogenous Donors as a Function of Temperature in Spinach PS II Membrane Fragments with a Reconstituted Plastoquinone Pool. *Biochemistry* **36:** 2459-2464

Seidler A (1996) The extrinsic polypeptides of photosystem II. *Biochim. Biophys. Acta* **1277:** 35-60

Shevela D, Klimov V, Messinger J (2007) Interactions of photosystem II with bicarbonate, formate and acetate. *Photosynth. Res.* **94:** 247–264

Shevela D, Nöring B, Eckert HJ, Messinger J, Renger G (2006) Characterization of the water oxidizing complex of photosystem II of the Chl *d*-containing cyanobacterium *Acaryochloris marina via* its reactivity towards endogenous electron donors and acceptors. *Phys. Chem. Chem. Phys.* **8:** 3460-3466

Shi LX, Schröder WP (2004) The low molecular mass subunits of the photosynthetic supracomplex, photosystem II. *Biochim. Biophys. Acta* **1608:** 75-96

Shinkarev V, Wraight CA (1993) Oxygen evolution in photosynthesis: from unicycle to bicycle. *Proc. Natl. Acad. Sci. USA* **90:** 1834-1838

Shutova T, Kenneweg H, Buchta J, Nikitina J, Terentyev V, Chernyshov S, Andersson B, Allakhverdiev SI, Klimov VV, Dau H, Junge W, Samuelsson G (2008) The photosystem II-associated Cah3 in *Chlamydomonas* enhances the O_2 evolution rate by proton removal. *EMBO J.* **27:** 782-791

Sinclair J (1984) The Influence of Anions on Oxygen Evolution by Isolated Spinach-Chloroplasts. *Biochim. Biophys. Acta* **764:** 247-252

Sivaraja M, Dismukes GC (1988a) Inhibition of Electron-Transport in Photosystem-II by NH_2OH - Further Evidence for 2 Binding-Sites. *Biochemistry* **27:** 6297-6306

Sivaraja M, Dismukes GC (1988b) Binding of Hydroxylamine to the Water-Oxidizing Complex and the Ferroquinone Electron-Acceptor of Spinach Photosystem II. *Biochemistry* **27:** 3467-3475

Stemler A (1989) Absence of a formate-induced release of bicarbonate from photosystem 2. *Plant Physiol.* **91:** 287-290

Stemler A, Babcock GT, Govindjee (1974) Effect of bicarbonate on photosynthetic oxygen evolution in flashing light in chloroplast fragments. *Proc. Natl. Acad. Sci. USA* **71:** 4679-4683

Stemler A, Govindjee (1973) Bicarbonate ion as a critical factor in photosynthetic oxygen evolution. *Plant Physiol.* **52:** 119-123

Stemler A, Murphy JB (1985) Bicarbonate-Reversible and Irreversible Inhibition of Photosystem II by Mono-Valent Anions. *Plant Physiol.* **77:** 974-977

Stemler A, Radmer R (1975) Source of photosynthetic oxygen in bicarbonate-stimulated Hill reaction. *Science* **190:** 457-458

Stemler AJ (2002) The bicarbonate effect, oxygen evolution, and the shadow of Otto Warburg. *Photosynth. Res.* **73:** 177-183

Stemler AJ, Lavergne J (1997) Evidence that formate destabilizes the S_{-1} state of the oxygen-evolving mechanism in Photosystem II. *Photosynth. Res.* **51:** 83-92

Stewart DH, Brudvig GW (1998) Cytochrome *b*(559) of photosystem II. *Biochim. Biophys. Acta* **1367:** 63-87

Strickler MA, Hillier W, Debus RJ (2006) No evidence from FTIR difference spectroscopy that glutamate-189 of the D1 polypeptide ligates a Mn ion that undergoes oxidation during the S_0 to S_1, S_1 to S_2, or S_2 to S_3 transitions in photosystem II. *Biochemistry* **45:** 8801-8811

Styring S, Rutherford AW (1987) In the oxygen evolving complex of photosystem II the S_0 state is oxidized to the S_1 State by Y_D^+ (Signal II_{slow}). *Biochemistry* **26:** 2401-2405

Su J-H, Lubitz W, Messinger J (2008) Probing Mode and Site of Substrate Water Binding to the Oxygen-Evolving Complex in the S_2 State of Photosystem II by ^{17}O-HYSCORE Spectroscopy. *J. Am. Chem. Soc.* **130:** 786-787

Szalai VA, Brudvig GW (1996) Reversible binding of nitric oxide to tyrosyl radicals in photosystem II. Nitric oxide quenches formation of the S_3 EPR signal species in acetate-inhibited photosystem II. *Biochemistry* **35:** 15080-15087

Tamura N, Cheniae GM (1987) Photoactivation of the water-oxidizing complex in Photosystem II membranes depleted of Mn and extrinsic proteins. I. Biochemical and kinetic characterization. *Biochim. Biophys. Acta* **890:** 179-194

Tamura N, Inoue Y, Cheniae GM (1989) Photoactivation of the water oxidizing complex in photosystem II membranes depleted of Mn, Ca and extrinsic proteins. II. Studies on the functions of Ca^{2+}. *Biochim. Biophys. Acta* **976:** 173-181

Tommos C, Babcock GT (2000) Proton and hydrogen currents in photosynthetic water oxidation. *Biochim. Biophys. Acta* **1458:** 199-219

Tomo T, Okubo T, Akimoto S, Yokono M, Miyashita H, Tsuchiya T, Noguchi T, Mimuro M (2007) Identification of the special pair of photosystem II in a chlorophyll *d*-dominated cyanobacterium. *Proc. Natl. Acad. Sci. USA* **104:** 7283-7288

Tyryshkin AM, Watt RK, Baranov SV, Dasgupta J, Hendrich MP, Dismukes GC (2006) Spectroscopic evidence for Ca^{2+} involvement in the assembly of the Mn_4Ca cluster in the photosynthetic water-oxidizing complex. *Biochemistry* **45:** 12876-12889

van Gorkom HJ, Yocum CF (2005) The calcium and chloride cofactors. *In* T Wydrzynski, K Satoh, eds, Photosystem II. The Light-Driven Water:Plastoquinone Oxidoreductase, Vol 22. Springer, Dordrecht, pp 307-328

van Rensen JJS (2002) Role of bicarbonate at the acceptor side of Photosystem II. *Photosynth. Res.* **73:** 185-192

van Rensen JJS, Klimov VV (2005) Bicarbonate interactions. *In* T Wydrzynski, K Satoh, eds, Photosystem II. The Light-Driven Water:Plastoquinone Oxidoreductase, Vol 22. Springer, Dordrecht, pp 329-346

van Rensen JJS, Xu C, Govindjee (1999) Role of bicarbonate in photosystem II, the water-plastoquinone oxido-reductase of plant photosynthesis. *Physiol. Plant.* **105:** 585-592

van Rensen JJS, Vermaas WFJ (1981) Action of Bicarbonate and Photosystem-2 Inhibiting Herbicides on Electron-Transport in Pea Grana and in Thylakoids of a Blue-Green-Alga. *Physiol. Plant.* **51:** 106-110

Vass I, Deak Z, Hideg E (1990a) Charge equilibrium between the water oxidizing complex and the electron donor tyrosine D in photosystem II. *Biochim. Biophys. Acta* **1017:** 63-69

Vass I, Deak Z, Jegerschold C, Styring S (1990b) The accessory electron-donor tyrosine D of photosystem II is slowly reduced in the dark during low-temperature storage of isolated thylakoids. *Biochim. Biophys. Acta* **1018:** 41-46

Vermaas WEJ, Renger G, Dohnt G (1984) The reduction of the oxygen evolving system in chloroplasts by thylakoid components. *Biochim. Biophys. Acta* **764:** 194-202

Vermaas WFJ (2002) Evolution of Photosynthesis. *In* Encyclopedia of Life Sciences. Nature Publishing Group, London (http://www.els.net), pp 1-18

Vermaas WFJ, Rutherford AW, Hansson O (1988) Site directed mutagenesis in photosystem II of the cyanobacterium *Synechocystis sp.* PCC 6803: donor D is a tyrosine residue in the D2 protein. *Proc. Natl. Acad. Sci. USA* **85:** 8477-8481

Warburg O (1964) Prefactory Chapter. *Annu. Rev. Biochem.* **33:** 1-18

Warburg O, Krippahl G (1958) Hill-Reaktionen. *Z. Naturforsch.* **13:** 509-514

Warburg O, Lüttgens W (1946) [Photochemical reduction of quinone in green granules]. *Biokhimiya* **11:** 301-322

Westphal KL, Lydakis-Simantiris N, Cukier RI, Babcock GT (2000) Effects of Sr^{2+} substitution on the reduction rates of $Y_Z^{\cdot}$ in PSII membranes: evidence for concerted hydrogen atom transfer in oxygen evolution. *Biochemistry* **39:** 16220-16229

Wieser ME (2006) Atomic weights of the elements 2005 - (IUPAC technical report). *Pure Appl. Chem.* **78:** 2051-2066

Wiessner W, Mende D, Demeter S (1992) Thermoluminescence study of the *in vivo* effects of bicarbonate depletion and acetate formate presence in the 2 algae *Chlamydobotrys stellata* and *Chlamydomonas reinhardtii*. *Photosynth. Res.* **34:** 279-285

Wincencjusz H, Allakhverdiev SI, Klimov VV, van Gorkom HJ (1996) Bicarbonate-reversible formate inhibition at the donor side of Photosystem II. *Biochim. Biophys. Acta* **1273:** 1-3

Wincencjusz H, van Gorkom HJ, Yocum CF (1997) The Photosynthetic Oxygen Evolving Complex Requires Chloride for Its Redox State S_2–S_3 and S_3-S_0 Transitions But Not for S_0-S_1 or S_1-S_2 Transitions. *Biochemistry* **36:** 3663-3670

Wincencjusz H, Yocum CF, van Gorkom HJ (1998) S-state dependence of chloride binding affinities and exchange dynamics in the intact and polypeptide-depleted O_2 evolving complex of photosystem II. *Biochemistry* **37:** 8595-8604

Wincencjusz H, Yocum CF, van Gorkom HJ (1999) Activating anions that replace Cl^- in the O_2 evolving complex of photosystem II slow the kinetics of the terminal step in water oxidation and destabilize the S_2 and S_3 states. *Biochemistry* **38:** 3719-3725

Winget GD, Izawa S, Good NE (1965) Stoichiometry of photophosphorylation. *Biochem. Biophys. Res. Commun.* **21:** 438-441

Witt H, Schlodder E, Teutloff C, Niklas J, Bordignon E, Carbonera D, Kohler S, Labahn A, Lubitz W (2002) Hydrogen bonding to P700: Site-directed mutagenesis of threonine A739 of photosystem I in *Chlamydomonas reinhardtii*. *Biochemistry* **41:** 8557-8569

Wydrzynski T, Baumgart F, MacMillan F, Renger G (1990) Is there a direct chloride cofactor requirement in the oxygen evolving reactions of photosystem II? *Photosynth. Res.* **25:** 59-72

Wydrzynski T, Govindjee (1975) New site of bicarbonate effect in photosystem II of photosynthesis - Evidence from chlorophyll fluorescence transients in spinach-chloroplasts. *Biochim. Biophys. Acta* **387:** 403-408

Wydrzynski T, Satoh K, eds (2005) *Photosystem II. The Light-Driven Water:Plastoquinone Oxidoreductase*, Vol 22. Springer, Dordrecht

Xiong J, Bauer CE (2002) Complex evolution of photosynthesis. *Annu. Rev. Plant Biol.* **53:** 503-521

Xiong J, Bauer CE (2002) A cytochrome *b* origin of photosynthetic reaction centers: an evolutionary link between respiration and photosynthesis. *J. Mol. Biol.* **322:** 1025-1037

Xiong J, Hutchison RS, Sayre RT, Govindjee (1997) Modification of the photosystem II acceptor side function in a D1 mutant (arginine-269-glycine) of *Chlamydomonas reinhardtii*. *Biochim. Biophys. Acta* **1322:** 60-76

Xiong J, Minagawa J, Crofts A, Govindjee (1998) Loss of inhibition by formate in newly constructed photosystem II D1 mutants, D1-R257E and D1-R257M, of *Chlamydomonas reinhardtii*. *Biochim. Biophys. Acta* **1365:** 473-491

Yachandra VK (1995) X-ray absorption spectroscopy and applications in structural biology. *Methods in Enzymology* **246:** 638-675

Yachandra VK (2005) The catalytic manganese cluster: organization of the metal ions. *In* T Wydrzynski, K Satoh, eds, Photosystem II. The Light-Driven Water:Plastoquinone Oxidoreductase, Vol 22. Springer, Dordrecht, pp 235-260

Yachandra VK, Sauer K, Klein MP (1996) Manganese cluster in photosynthesis: where plants oxidize water to dioxygen. *Chem. Rev.* **96:** 2927-2950

Yano J, Pushkar Y, Glatzel P, Lewis A, Sauer K, Messinger J, Bergmann U, Yachandra VK (2005a) High-resolution Mn EXAFS of the oxygen-evolving complex in photosystem II: structural implications for the Mn_4Ca cluster. *J. Am. Chem. Soc.* **127:** 14974-14975

Yano J, Kern J, Irrgang KD, Latimer MJ, Bergmann U, Glatzel P, Pushkar Y, Biesiadka J, Loll B, Sauer K, Messinger J, Zouni A, Yachandra VK (2005b) X-ray damage to the Mn_4Ca complex in single crystals of photosystem II: a case study for metalloprotein crystallography. *Proc. Natl. Acad. Sci. USA* **102:** 12047-12052

Yano J, Kern J, Sauer K, Latimer MJ, Pushkar Y, Biesiadka J, Loll B, Saenger W, Messinger J, Zouni A, Yachandra VK (2006) Where water is oxidized to dioxygen: structure of the photosynthetic Mn_4Ca cluster. *Science* **314:** 821-825

Yocum CF, Yerkes CT, Sharp RR, Blankenship RE, Babcock GT (1981) Stoichiometry, Inhibitor Sensitivity, and Organization of Manganese Associated with Photosynthetic Oxygen Evolution. *Proc. Natl. Acad. Sci. USA* **78:** 7507-7511

Yu H, Aznar CP, Xu XZ, Britt RD (2005) Evidence that azide occupies the chloride binding site near the manganese cluster in photosystem II. *Biochemistry* **44:** 12022-12029

Zharmukhamedov SK, Shirshikova GN, Maevskaya ZV, Antropova TM, Klimov VV (2007) Bicarbonate protects the water-oxidizing complex of photosystem II against thermoinactivation in intact *Chlamydomonas reinhardtii* cells. *Russ. J. Plant Phys.* **54:** 302-308

Zheng M, Dismukes GC (1996) Orbital configuration of the valence electrons, ligand field symmetry, and manganese oxidation states of the photosynthetic water oxidizing complex: analysis of the S_2 state multiline EPR signals. *Inorg. Chem.* **35:** 3307-3319

Zimmermann JL, Rutherford AW (1986) Photoreductant-induced oxidation of Fe^{2+} in the electron acceptor complex of photosystem II. *Biochim. Biophys. Acta* **851:** 416-423

Zouni A, Witt HT, Kern J, Fromme P, Krauß N, Saenger W, Orth P (2001) Crystal structure of photosystem II from *Synechococcus elongatus* at 3.8 Å resolution. *Nature* **409:** 739-743

Lebenslauf

NAME	*Dmitriy Nikolaevich Shevela*
GEBURTSDATUM	30 December 1979
GEBURTSORT	Kaluga, Russland

AUSBILDUNG

1986 – 1997	Grundschule № 37 und Oberschule № 5 in Kaluga, Russland
Juni 1997	Abitur
1997 – 2002	Studium der Biologie an der Staatlichen Universität, Kaluga, Russland
Juni 2002	Diplom

ARBEITSVERHÄLTNISSE

Oktober 2002 – September 2004	Laboroberassistent im Institut für Fundamentale Biologische Fragestellungen, Puschino, Russland
Oktober 2004 – September 2005	Wissenschaftlicher Mitarbeiter im Labor für photosynthetische Wasseroxidation des Instituts für Fundamentale Biologische Fragestellungen, Puschino, Russland bei *Prof. Dr. V. Klimov*
Oktorber 2005 – April 2006	DAAD Stipendiat am Max-Planck-Institut für Bioanorganische Chemie im Projekt (A/05/00015), bei *Prof. Dr. J. Messinger*
seit Mai 2006	Stipendiat am Max-Planck Institut für Bioanorganische Chemie, Mülheim an der Ruhr bei *Prof. Dr. J. Messinger*

SONSTIGES

Mai 2007	Organisation des Photosynthese Workshops "Nord-West" am Max-Planck-Institut für Bioanorganische Chemie, Mülheim an der Ruhr
Juli 2007	Erhalt der Auszeichnung "Young Scientist-Best Poster", 14. internationale Photosythese Konferenz, Glasgow (Scotland)